PULSED MULTIPHOTON EXCITATION OF ATOMS

This thesis is submitted for the degree of
Doctor of Philosophy
in the University of London
and for the
Diploma of the Imperial College of Science and Technology
by

Mark Andrew Lauder

Abstract

This thesis reports a theoretical analysis of the intense-field excitation of multiphoton atomic resonances by pulsed, fluctuating laser fields.

A time-development operator technique is used to describe the excitation of three level atomic systems by laser pulses of arbitrary shape. The pulses are divided into small elements for which the time development is described using the first term in the Magnus expansion. When square pulses are described in this way, two photon excitation dressed state results, calculated previously, are recovered. These exhibit Rabi oscillations and population trapping. The system can be used to show the Stark splittings of the lower two levels by using the upper pulse as a probe. The atomic lineshapes are found to be modified considerably when the main pulse is altered in shape.

For a specific example of intense laser excitation of an atomic system, the resonant excitation of the 3868 cm^{-1} J=3 to 26558 cm^{-1} J=2 transition in uranium is considered. An experiment has been reported which measures the upper state population as a function of laser intensity. This data is re-analysed taking proper account of the atomic Doppler width, level degeneracies, the laser's temporal pulse shape and laser shot-to-shot intensity and frequency variations. The effects of laser phase-fluctuation bandwidth are also included.

It is known that windows of zero absorption occur in the photo-excitation of autoionising continuum resonances. A laser field can be used to induce resonances in continuum states, termed Laser Induced Continuum Structure (LICS). Recent experiments on the use of LICS to enhance photo-absorption have used intense, fluctuating laser fields. The effects of laser phase fluctuations are investigated paying particular attention to the Fano absorption profile. The Wiener-Lévy model is used to model the fluctuations and the effects of cross-correlation of the laser fields are included. Decay channels omitted in earlier work on LICS are now included and are found to modify the population trapping.

Contents

Chapter	Page
1 Overview	
.0 Introduction	5
.1 Plan of thesis chapters	7
2 Method of solution	
.0 Introduction	8
.1 Time development	9
.2 Forming the equation	13
.3 The solution	15
.4 References	17
3 Pulse shape effects in three level systems	
.0 Introduction	18
.1 Solving the three level system	20
.2 The temporal evolution of the three level system	24
.3 Populations as functions of detuning (Stark effects)	47
.4 Conclusions	61
.5 References	63
4 A realistic two level system	
.0 Introduction	66
.1 The experiment	68
.2 Modelling the atoms	70
.3 Modelling the laser field	77
.4 Combining the effects	85
.5 Results	89
.6 Conclusions	92
.A The Doppler profile integral	94
.B Fourier transform	97
.C Spectral profile of laser bandwidth in the PDM model	99
.7 References	103

5 Laser induced continuum structure
.0 Introduction 105
.1 Decay into a flat continuum 108
.2 The Fano eigenstates 113
.3 Trapping in LICS 120
.4 Conclusions 139
.A Product of principal parts 141
.B Trapped population 142
.5 References 144

6 Summary
.0 Conclusions 149
.1 Further work 151
.2 References 152

Acknowledgements 153

Publications
Resonant laser excitation of uranium with a pulsed laser
with P.T. Greenland
J. Phys. B 17 (1984) 3083-3090

Atomic beam velocity profiles
with P.T. Greenland and D. Wort
J. Phys. D, to be published

Making atoms transparent: trapped superpositions
with P.L. Knight, P.M. Radmore and B.J. Dalton
Acta Physica Austriaca 56 (1984) 4, 193-214

Chapter 1
Overview

1.0 Introduction

This theoretical thesis investigates some of the real processes involved in multiphoton excitation of atoms by pulsed lasers. Many previous works use idealised laser fields and atoms with flat, monochromatic pulses and simple two or three level atoms. Lately, more effort has been put into modelling real, rather than idealised, systems. Lasers are not monochromatic and bandwidth is introduced by various different processes. Neither have they got constant output powers. These effects complicate a theoretical analysis but should be included as they can have important consequences. They can be included in a general way by using numerical, rather than analytical, techniques. Described here is a numerical technique which can include the above processes, although in some cases, notably the bandwidth due to phase fluctuations, it is not obvious which model to include. Of course, the greater the number of processes included, the greater the computational problem. In some cases this is a limiting factor and may call for various simplifying assumptions to be made.

The processes that are dealt with affect both the exciting laser field and the excited atoms. The laser field has various parameters that are associated with it. In general the instantaneous mean frequency is a good parameter to specify, being useful and fairly well defined. However, this will most likely vary in time due to fluctuations in the optical cavity length caused by vibrations and heat fluctuations etc. This causes a frequency jitter which, in pulsed lasers, causes each pulse to have a different mean frequency. Other good parameters are the pulse length and shape. The effects that the shape has on excitation is one of the main topics and will be extensively covered. The differences between using CW and pulsed lasers, with perhaps fields with temporal envelopes approaching a Gaussian shape, are investigated showing that there is no 'equivalent' flat pulse for most processes. Associated with the mean frequency is the width of the spectral profile. This can be hard to quantify, or define, as the shape is also variable. Contributing to the single shot spectral profile is the transform width, which can be calculated from

the temporal profile, and phase fluctuation effects. As the temporal width is increased, ie the pulse is lengthened, so the spectral width decreases and the pulse becomes more monochromatic. The phase fluctuation bandwidth is caused by processes such as collisional broadening and natural decay lifetime bandwidth in the active atoms of the laser. The natural lifetime is generally much smaller than any other broadening processes and can be ignored. The collisional broadening is caused by collisions between a radiating atom and other bodies, such as walls and other atoms. This causes a shift in the energy levels giving rise to fluctuations in the frequency of the emitted radiation. One way of modelling this sort of process is to assume that the collision is instantaneous, and the only effect is to alter the phase in some jump-like stochastic way. This is the random telegraph signal approach. The model which is to be used in this thesis, when applied, is the phase diffusion model. In this the phase is assumed to perform a random walk, with the phase velocities being Gaussian white noise processes. The collisions are effectively continuous so that the phase is constantly varying in a well defined, but stochastic way. The amplitude of the field will generally fluctuate in a stochastic way so that for a pulsed laser the peak intensity of each pulse varies from shot to shot. This process can be averaged by assuming a distribution for the peak powers.

The irradiated systems generally have inhomogeneous broadenings associated with them, such as Doppler shifts and collisional broadening. These can be partially eliminated in the experimental technique, but can also be included in the theoretical model. Degenerate magnetic sub-levels and other interfering levels cause the simple Rabi oscillations, that can be predicted, to be partially, if not totally, destroyed.

All of these processes make it generally hard, if not impossible, to observe experimentally any effects predicted by theory. It is therefore necessary to be able to include these processes in the theory such that any effects still remaining can be found and then verified by experiment.

1.1 Plan of thesis chapters

In chapter two the physics of the time evolution of multi-photon processes is introduced. The method of solution, using a time development operator technique, is described along with the mathematics involved. The method is basically numerical so that many features can be included up to the limit of computer time available.

Chapter three applies this method to the solution of a three level system irradiated by a pulsed laser. The effects of the pulse shape on the temporal evolution and population trapping are extensively investigated. The effects of the motion of the atoms due to Doppler effects is calculated showing the differences between using co- and counter-propagating laser beams to excite the two transitions.

Chapter four is an extensive re-analysis of a previous experiment carried out in uranium. The re-analysis includes the pulse shape, shot to shot fluctuations in both the mean frequency and intensity, phase diffusion effects, Doppler effects and atomic sublevel degeneracy. New results are obtained for the values of the fitting parameters.

In chapter five the effects of a photoionisation continuum are introduced. Population trapping can occur if two bound states are coupled strongly to the continuum at the same point. This is due to the destructive interference of the amplitudes in a similar way to trapping in a three level system investigated in chapter three. Again the effects of pulse shape are investigated along with the important effects of the relative coherence of the exciting beams.

At many points during the thesis the numerical model is compared to exact analytical results obtainable for certain special sets of conditions. This is to give confidence in the results predicted when no such analytical result is possible.

Each chapter is comprised of sections with sub-sections etc. The equations and figures are numbered sequentially in each section, such that each equation is numbered "chapter.section,number" and each figure "chapter.section.roman numeral". When refered to in the text, if the chapter and section numbers are omitted then the current chapter and section are assumed. References and appendices are supplied with each chapter and are positioned at the end of each chapter. Three publications relevant to the work reported here are included at the end of the thesis.

CHAPTER 2

Method of solution

2.0 Introduction

In this chapter the basic formalism and method of solution is described. The systems being considered here are those such as an atom, with a few relevant bound states and maybe a continuum, interacting with a near resonant radiation field, usually the field from a laser. The method of solution is based upon the calculation of a Time Development Operator, generally time dependent, which is used to calculate the modified state of the system. The calculations are performed numerically and the results are compared to some exact analytical solutions obtainable under special circumstances. The method is then used to calculate solutions for which an analytical method can not be applied. This chapter describes the method of solution and forms the equations necessary for the following chapters.

2.1 Time development

The time development of a system can usually be written in the form

$$i\frac{d}{dt}|A(t)\rangle = T(t)|A(t)\rangle \qquad 2.1,1$$

where $|A(t)\rangle$ represents the state of the system. This can be considered to be a vector in an N dimensional Hilbert space. The Hilbert space may be an amplitude space or a space made up from any convenient combination of the amplitudes, eg the bilinear cross products. One of the postulates of quantum mechanics is that a system is completely described by its state vector in amplitude space. The dimension of the space depends upon the problem and can be infinite, such as when a continuum is considered, but is necessarily finite for numerical calculations. A problem involving a continuum can be reduced to a finite problem by analytical elimination, see for example Weisskopf and Wigner 1930 and Loudon 1983. This will, of course, reduce the amount of information that can be calculated about the system. In order to perform calculations a coordinate system is required within the Hilbert space. This is generally constructed from a set of energy eigenstates, usually the unperturbed states. Thus, under the action of a perturbation, in this case the laser field, the state vector is moved with respect to the chosen axes. The object is to find the position of the vector, as a function of time, with respect to these axes. This gives the amplitudes to be in each of the unperturbed states at a given time.

2.1.1 Time Development Operator

For this purpose it is convenient to calculate the Time Development Operator $U(t;t_o)$ which, given $|A(t_o)\rangle$, enables the calculation of $|A(t)\rangle$. This is defined from

$$U(t;t_o)|A(t_o)\rangle = |A(t)\rangle. \qquad 2.1,2$$

The operator $U(t;t_o)$ thus rotates the state vector $|A(t)\rangle$ with respect to the chosen coordinate system, and if it is not unitary it also alters its length. Substitution of this into equation 1 gives

$$i\frac{d}{dt}U(t;t_o)|A(t_o)\rangle = T(t)U(t;t_o)|A(t_o)\rangle. \qquad 2.1,3$$

This yields the equation for U,

$$i\frac{d}{dt}U(t;t_o) = T(t)U(t;t_o). \qquad 2.1,4$$

As T is generally time dependent, and does not commute with itself at different times, this has a non-trivial solution. The general solution is due to Magnus 1954 and can be found in Wille 1982.

$$U(t;t_o) = \exp\{W(t;t_o)\} \qquad 2.1,5$$

where

$$W(t;t_o) = -i\int_{t_o}^{t}dt_1T_1 - \frac{1}{2}\int_{t_o}^{t}dt_1\int_{t_o}^{t_1}dt_2[T_1,T_2]$$

$$+\frac{i}{6}\int_{t_o}^{t}dt_1\int_{t_o}^{t_1}dt_2\int_{t_o}^{t_2}dt_3\{[[T_1,T_2],T_3]+[[T_3,T_2],T_1]\}.... \qquad 2.1,6$$

and $T_i = T(t_i)$.

Assuming that W has been calculated it then becomes necessary to calculate $\exp\{W(t;t_o)\}$. This is non-trivial as all powers of W need to be known. However, if a transform is made to the diagonal representation, such that

$$X^{-1}\ W\ X = D \qquad 2.1,7$$

where D is the diagonal representation, then this can be used to substitute for W. Thus

$$U = \exp\{W\} = \exp\{X\ D\ X^{-1}\} \qquad 2.1,8$$

$$= X \exp(D) X^{-1} \qquad 2.1,9$$

as $X X^{-1} = 1$. The exponential of the diagonal representation D can be calculated easily as all the powers are known. In matrix representation the exponential of a diagonal matrix is just the diagonal matrix of the exponentials.

The calculation of W involves a complicated infinite series. Thus, either it must be truncated or approximated. If any of the commutator blocks, eg $[[T_1,T_2],T_3]$, are zero for all times then that term and all higher terms are zero. This is because the higher terms always contain the elements of the previous term commutated with T again. So the series self-truncates. This truncation only occurs for special forms of T. The most trivial case is when T is time independent. Under these circumstances the first order commutators, $[T_1,T_2]$, are zero for all times. The series therefore truncates leaving just the first term. In this case

$$W(t;t_o) = -i(t-t_o)T. \qquad 2.1,10$$

This is adequate for 'top-hat' perturbations, where T is the Hamiltonian and the Rotating Wave Approximation has been made, see section 3.1.1. However, the main object of this thesis is to show the effects of using pulsed perturbations which are not constant and in which some sort of approximation is required.

2.1.2 The Interaction representation

W is an expansion in $(t-t_o)(T-T_o)$ and converges more quickly if this quantity is small. Thus T must not vary much over the interval $t-t_o$. This can be achieved by careful selection of the coordinate system. It is often very advantageous to select a coordinate system that is rotating in the Hilbert space, such that with no perturbation the coordinates of the state vector are constant. This is called the Interaction representation. In this coordinate frame, under the action of the perturbation, the state vector varies only slowly and it is only necessary to take the first term in $W(t;t_o)$. The Interaction representation is found by making a coordinate transform, often

Unitary, within the Hilbert space. Thus

$$|A(t)\rangle \rightarrow |A'(t)\rangle = R(t)|A(t)\rangle. \qquad 2.1,11$$

This is substituted into equation 1 to obtain the transformation of the operator T.

$$i\frac{d}{dt}\{R^{-1}(t)|A'(t)\rangle\} = T(t)R^{-1}(t)|A'(t)\rangle \qquad 2.1,12$$

$$i\frac{d}{dt}R^{-1}(t)\,|A'(t)\rangle + iR^{-1}(t)\frac{d}{dt}|A'(t)\rangle = T(t)R^{-1}(t)|A'(t)\rangle \qquad 2.1,13$$

$$i\frac{d}{dt}|A'(t)\rangle = \{R(t)T(t)R^{-1}(t) - iR(t)\frac{d}{dt}R^{-1}(t)\}|A'(t)\rangle. \qquad 2.1,14$$

Therefore T transforms like

$$T(t) \rightarrow T'(t) = R(t)T(t)R^{-1}(t) - iR(t)\frac{d}{dt}R^{-1}(t). \qquad 2.1,15$$

A transform such as this can yield a T'(t) which varies slowly such that only the first term in the Magnus expansion need be used.

2.2 Forming the equation

Having given the method of solution, the means by which the initial equation is calculated must be shown. That is, what are T(t) and $|A(t)\rangle$ in equation 2.1,1?

2.2.1 Schrödinger's equation

An obvious example of an equation of the required type is Schrödinger's equation

$$i\hbar \frac{d}{dt} |\Psi(t)\rangle = H(t)|\Psi(t)\rangle. \qquad 2.2,1$$

This is already in the correct form to be solved by the above method. However, it is not always convenient to use it in this form. In some cases it is necessary to use a density matrix formalism, described in section 2.2.2. In equation 1 $|\Psi(t)\rangle$ is the state vector in the Hilbert space of the amplitudes and H(t) is the Hamiltonian. In order to perform calculations it is necessary to write down the state vector and the Hamiltonian in their matrix representation with respect to the chosen coordinate system. This is performed in section 3.3.1 of the next chapter, where a three level system is solved using this technique.

2.2.2 The density matrix

Some phenomena are very hard to model using the wavefunction approach. The most usual example of this inadequacy occurs when spontaneous emission <u>within</u> the system is allowed. Spontaneous emission of one level <u>out</u> of the system is included by making the energy levels complex. This is an adequate model for this type of decay. However, it is impossible to model repopulation of a level, equal to the decay of the upper level, ie no net loss or gain, and keep the equations linear [Smith 1978, Ackerhalt 1981]. The inclusion of this type of internal decay is only possible if the density matrix elements are used instead of the amplitudes. However, this has the disadvantage of increasing the size of the problem. The elements of the density matrix are given by

$$\rho_{ij} = a_i^* a_j \qquad 2.2,2$$

where a_i are the amplitudes. Thus, for a three level problem there are nine density matrix elements. The diagonal terms, ie ρ_{ii} are the populations to be in state $|i\rangle$ and the phenomenological decay is easy to model bacause populations decaying from state $|i\rangle$ to state $|j\rangle$ can be inserted by putting

$$\dot{\rho}_{ii} \rightarrow \dot{\rho}_{ii} - \Gamma\rho_{ii} \qquad 2.2,3a$$

$$\dot{\rho}_{jj} \rightarrow \dot{\rho}_{jj} + \Gamma\rho_{ii} \qquad 2.2,3b$$

where Γ is the decay constant. This obviously keeps the total population constant as

$$\sum_i \dot{\rho}_{ii} = 0. \qquad 2.2,4$$

Knowledge of the time dependence of the amplitudes a_i in terms of the other amplitudes is enough to be able to calculate the time dependence of ρ_{ij}. Differentiation of equation 2 yields

$$\dot{\rho}_{ij} = \dot{a}_i^* a_j + a_i^* \dot{a}_j. \qquad 2.2,5$$

Therefore the equation for the density matrix elements can be written in the same form as equation 1 and therefore solved using the method previously described. The use of the density matrix approach is dealt with in chapter five where it is applied to a two level system and a continuum. In this case the density matrix is used in order to average out some phase noise effects before the equations are solved.

2.3 The solution

In equation 2.1,1 it is assumed that the interaction T(t) is time dependent which means that the TDO, $U(t;t_o)$, is also time dependent. This time dependence is reduced by choosing a rotating frame such that the perturbation is only slowly varying. This means that only the first term in the Magnus expansion is required to calculate the TDO, so that

$$U(t;t_o) = \exp\{-i\int_{t_o}^{t} T'(t')dt'\} \qquad 2.3,1$$

Fig i shows an example of a Gaussian perturbation with its 'blocked' pulse of N = 20 blocks.

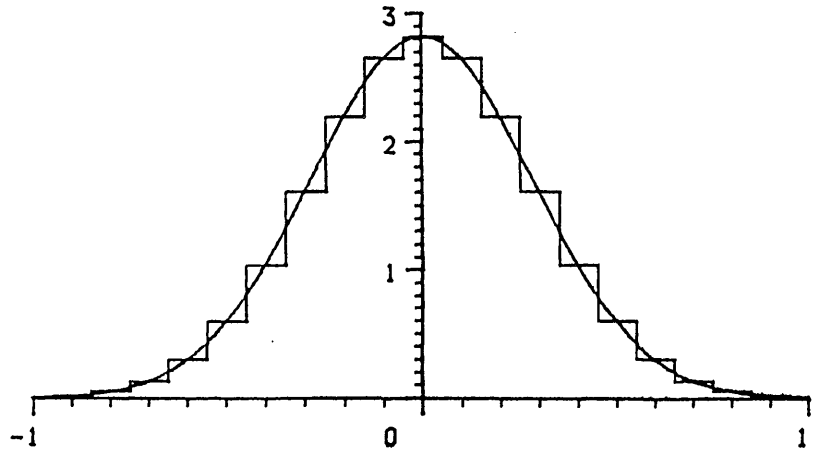


Fig 2.3.i

A Gaussian pulse and its 'blocked' equivalent, with 20 blocks.

The 'blocked' pulse is the actual perturbation used in the solution, and for increasing N provides a good approximation to the real pulse. The first term in the Magnus expansion is the average value of T'(t), over the interval t_o to t, multiplied by the time step, $t - t_o$. This approximation is equivalent to solving the equations using the blocked pulse, which can be done exactly as each block is time independent. The TDO is calculated for each block and is then used to obtain the state of the system at the end of that block, given the state at the end of the previous block. This procedure is continued until the end of the pulse is reached.

In the next chapter a three level system is solved, using the

Schrödinger equation, interacting with various pulse shapes, including a Gaussian pulse.

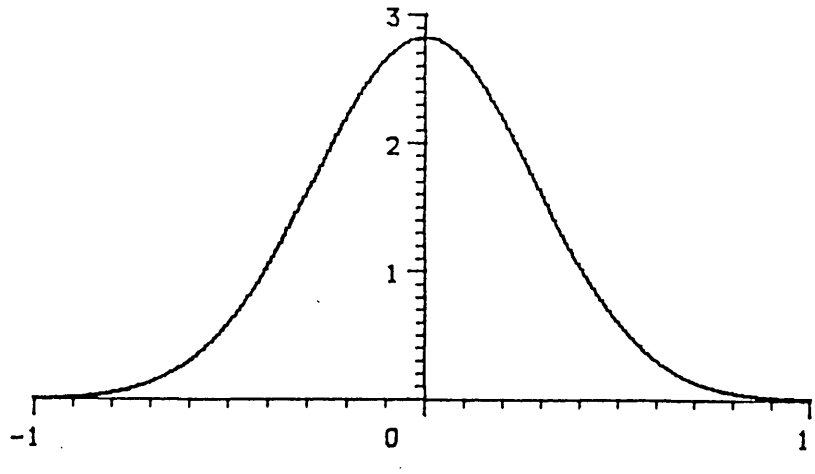


Fig 2.3.ii

A Gaussian 'blocked' pulse with 400 blocks.

In some of the examples as many as three or four hundred time steps are taken at which point the blocked pulse is hardly distinguishable from the real pulse, see fig ii.

The following chapters describe examples of the use of the previously described method when applied to two and three level systems and a two level system interacting with a continuum.

2.4 References

Ackerhalt J.R., 1981
Resonant laser excitation in a two level model: a non linear Schrödinger equation?
Opt. Lett. 6 (1981) 3, 136-138

Hindmarsh W.R., 1967
'Atomic Spectra'
Pergamon, Oxford, 1967

Loudon R., 1983
'The Quantum Theory of Light'
Clarendon Press, Oxford 1983

Magnus W., 1954
On the exponential solution of differential equations for a linear operator
Comm. in Pure and Appl. Maths 7 (1954) 649-673

Smith R.A., 1978
Excitation of transitions between atomic or molecular energy levels by monochromatic laser radiation
Proc. Roy. Soc. Lond. A 362 (1978) 1-12

Weisskopf V., Wigner E., 1930
Calculation of the natural linewidth on the basis of Dirac's theory of light
Z. Phys. 63 (1930) 54
translated in Hindmarsh 1967

Wille U., 1982
Non-perturbative study of rotationally induced inner-shell excitation
Z. Phys. A 308 (1982) 3

CHAPTER 3

Pulse shape effects in a three level system

3.0 Introduction

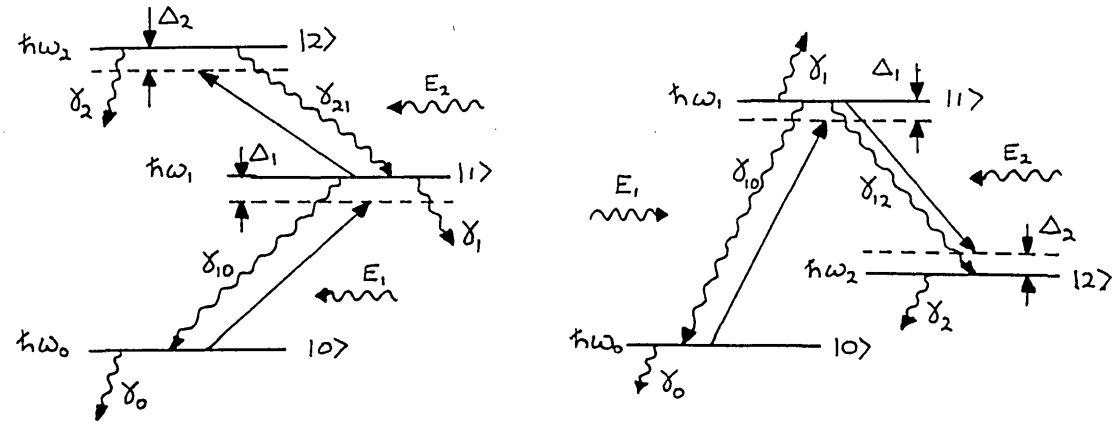
The previous chapter outlines the use of the Time Development Operator in the solution of systems under the effects of time dependent perturbations. In this chapter this method is applied to various three level systems in order to find the time development of the populations to be in each of the three levels. Experimentally the populations can be observed indirectly by looking at spontaneous decay from the required levels. The amount of radiation from this decay is proportional to the population in the decaying state. This allows the instantaneous populations to be determined. Alternatively the population in the excited state may be observed by monitoring photoionisation yield measurements. This is possible if only the population in the upper state is required, otherwise the ionisation yield includes the population from all of the higher states.

The three level system has been extensively studied, see for example Whitley and Stroud 1976, but mostly under the influence of constant perturbations or very special functional dependences, for example Thomas 1983 and references within. In this chapter the effects of pulse shape on the temporal evolution of the populations are calculated, numerically and/or analytically. Population trapping in three level systems has been both predicted, Radmore and Knight 1982 and Swain 1982, and observed, Gray, Whitley and Stroud 1978 and references within, and the effects of the pulse shape on trapping are investigated in section 3.2.1.3. Two-photon resonant excitation can be enhanced by the use of counter-propagating exciting beams in the presence of Doppler effects, see Hodgkinson and Wort 1981. Section 3.2.2 shows results using the TDO method for co- and counter-propagating beams and with flat and pulsed lasers. In section 3.3 important pulse shape effects are predicted in the observation of Stark splittings, where a two level system is excited by a pulsed laser and a probe pulse is used to excite the population in the combined atom/field states into a third level. Many experiments have been carried out on Stark, or Autler-Townes, effects, for example Gray and Stroud 1978, Delsart etal 1981 and Fisk etal 1984, but, again,

these are modelled using flat perturbations. Nayfeh and Nayfeh 1979 allow slowly varying pulses and give an analytical solution when the middle level is far off resonance whilst Greenland 1985 gives results for arbitrary pulse shape with a total envelope area of greater than 10π.

3.1 Solving the three level system

The time evolution and spectra of a general three level system, see fig i, can be described by a variety of methods. The specific method used depends upon the values of the parameters, such as the Rabi frequencies, detunings and decays, with certain sets allowing exact analytic solutions to be obtained.



a) the ladder system

b) the lambda system

Fig 3.1.i

The two configurations for a three level system.

Fig ia shows a ladder configuration whilst ib shows a lambda configuration. These are mathematically identical, apart from sign conventions, and so there is no need to differentiate between the two in any solution. Each transition is excited by a nearly resonant laser field which can have either a constant or slowly varying envelope. The conditions imposed upon the time-scales and other parameters are described for each particular method of solution. $|0\rangle$, $|1\rangle$ and $|2\rangle$ are the energy eigenstates of the unperturbed system, with energies $\hbar\omega_0$, $\hbar\omega_1$ and $\hbar\omega_2$ respectively. The lasers are detuned from the transition frequencies by amounts $\Delta_1 = \omega_1 - \omega_0 - \omega_{L1}$ and $\Delta_2 = \omega_2 - \omega_1 - \omega_{L2}$ which are assumed to be much less than the laser frequencies ω_{L1} and ω_{L2}. Damping can be introduced phenomenologically by the transformation of the energies from real to complex. This is an adequate model for effects which cause population loss from the system, γ_0, γ_1 and γ_2, such as ionisation, but is inadequate for decays within the system, γ_{10} and γ_{21}, such as spontaneous emission from, say, level 2 to 1. The former case can be modelled by keeping track of the three amplitudes

to be in each of the levels. The latter case requires the density matrix approach, where the nine bilinear cross products of the amplitudes need to be calculated. Obviously the former solution is preferable as it decreases the size of the problem; in this case it is of order three compared to the order nine density matrix. In this chapter the former solution will be used so that only external decays are allowed.

3.1.1 The Hamiltonian in the Schrödinger Picture

The method used in this chapter to describe the evolution of the three level system involves the calculation of the TDO for the amplitudes to be in each of the three unperturbed energy eigenstates. The initial equation used is simply Schrödinger's equation

$$H|\Psi\rangle = i\hbar \frac{d}{dt}|\Psi\rangle. \qquad 3.1,1$$

Thus the method used is that described in the previous chapter applied to the Hamiltonian and the state vector in amplitude space. The Hamiltonian for the three level system, with respect to the unperturbed energy eigenstates, can be written as

$$H = \begin{pmatrix} \hbar\omega_0 & -\underline{\mu}_{01}.\underline{E}_1 & 0 \\ -\underline{\mu}_{10}.\underline{E}_1 & \hbar\omega_1 & -\underline{\mu}_{12}.\underline{E}_2 \\ 0 & -\underline{\mu}_{21}.\underline{E}_2 & \hbar\omega_2 \end{pmatrix} \qquad 3.1,2$$

where $\underline{\mu}_{ij}$ is the dipole matrix element between states $|i\rangle$ and $|j\rangle$, thus $\underline{\mu}_{ij} = \langle i|\underline{\mu}|j\rangle$. There is no loss of generality in taking $\underline{\mu}$ to be real, so that $\underline{\mu}_{ij} = \underline{\mu}_{ji}$. It is assumed that the field $\underline{E}_1$, with frequency ω_{L1}, only couples states $|0\rangle$ and $|1\rangle$, and field $\underline{E}_2$, frequency ω_{L2}, only couples states $|1\rangle$ and $|2\rangle$. This is true if $|\omega_{L1} - \omega_{L2}| \gg 1/\tau$, where τ is the smallest time-scale of the problem. The interaction energy $-\underline{\mu}.\underline{E}$ is the energy of a dipole $\underline{\mu}$ in an electromagnetic field. The interaction with the magnetic field is ignored as it is several orders of magnitude less than that with the electric field. The ratio of the magnitudes of the interactions is given by the fine structure constant ~1/137 [Woodgate 1970]. The higher multipole terms can be ignored if the size of the system is

much less than the distance over which the field varies, which is just the wavelength. In the case of optical radiation and normal, non-Rydberg, atoms the wavelength is of the order of 500 nm, compared with the atomic size of about 1 nm. Phenomenological damping out of the system can be introduced by making the energies of the states complex. This introduces a decay out of each state proportional to the population in that state. The fields are assumed to have envelopes which vary much slower than the carrier frequencies. In this particular chapter none of the field parameters are allowed to vary stochastically. The field is given by $\underline{E}_i(t) = \underline{E}_i(t)\cos(\omega_{Li}t)$, where ω_{Li} is constant and $\underline{E}_i(t)$ is a sure function. The Hamiltonian can now be written as

$$H = \hbar \begin{pmatrix} \omega_o - i\frac{\underline{\gamma}_o}{2} & -\frac{\underline{\mu}_1 . \underline{E}_1}{\hbar}\cos(\omega_{L1}t) & 0 \\ -\frac{\underline{\mu}_1 . \underline{E}_1}{\hbar}\cos(\omega_{L1}t) & \omega_1 - i\frac{\underline{\gamma}_1}{2} & -\frac{\underline{\mu}_2 . \underline{E}_2}{\hbar}\cos(\omega_{L2}t) \\ 0 & -\frac{\underline{\mu}_2 . \underline{E}_2}{\hbar}\cos(\omega_{L2}t) & \omega_2 - i\frac{\underline{\gamma}_2}{2} \end{pmatrix} \qquad 3.1,3$$

where $\underline{\mu}_1 = \underline{\mu}_{o1}$ and $\underline{\mu}_2 = \underline{\mu}_{12}$. The Hamiltonian is now transformed to a rotating frame, following the previous chapter, using the transform

$$T = \begin{pmatrix} \exp(i\omega_{L1}t) & 0 & 0 \\ 0 & 1 & 0 \\ 0 & 0 & \exp(-i\omega_{L2}t) \end{pmatrix} . \qquad 3.1,4$$

Thus

$$H' = \hbar \begin{pmatrix} -i\frac{\underline{\gamma}_o}{2} & -\frac{\underline{\Omega}_1(t)}{2} & 0 \\ -\frac{\underline{\Omega}_1(t)}{2} & \Delta_1 - i\frac{\underline{\gamma}_1}{2} & -\frac{\underline{\Omega}_2(t)}{2} \\ 0 & -\frac{\underline{\Omega}_2(t)}{2} & (\Delta_1+\Delta_2) - i\frac{\underline{\gamma}_2}{2} \end{pmatrix} . \qquad 3.1,5$$

The Rotating Wave Approximation (RWA) has now been made, see for example Sargent, Scully and Lamb 1974. This allows the terms varying

at twice the optical frequency to be ignored as they average out after a few optical periods. The Rabi frequency [Allen and Eberly 1975] is introduced $\Omega_i(t) = \underline{\mu}_i.\underline{E}_i(t)/\hbar$. The transformation T is unitary, $TT^+ = T^+T = 1$, so the amplitudes, $C' = TC$, to be in the transformed eigenstates $T|i\rangle$ are only different to the original amplitudes by a phase factor. Thus the probabilities to be in the transformed states are the same as the old, $C'^+C' = C^+T^+TC = C^+C$.

3.2 The temporal evolution of the three level system.

This numerical method of solution can be used to calculate the evolution of the populations, as functions of time, for a general three level system.

3.2.1 Comparisons with other methods

As a means of checking the numerical results a few special cases are solved, using the most appropriate method, and compared with this general computational solution. Three special cases are considered. The first is a system in which both the fields are on resonance and none of the states can decay, but the fields have similar, slowly varying envelopes. The second method is a perturbative solution in which both fields are constant and have to be weak enough so that neither of the excited levels gain any appreciable population. The third is an analytic solution including detunings and decays in which the fields must be constant. However, the perturbative criterion that the fields must be weak is not required. This method is equivalent to the 'dressed states' model [Radmore and Knight 1982].

3.2.1.1 Analytical solution with no detuning or decay and similar field envelopes.

The Hamiltonian for this case is given by

$$H' = \Omega_1(t)\hbar/2 \begin{pmatrix} 0 & -1 & 0 \\ -1 & 0 & -a \\ 0 & -a & 0 \end{pmatrix} \qquad 3.2,1$$

where $\Omega_2(t) = a\Omega_1(t)$. This is exactly soluble, from equation 2.1,6, because the Hamiltonian commutes with itself at all times. This is because the time dependence $\Omega_1(t)$ can be factored out under the restriction that there are no decays and the fields are on resonance. The time development operator is then given by

$$U(t,t_o) = \exp\left\{ i\int_{t_o}^{t} \Omega_1(t')dt'/2 \begin{pmatrix} 0 & 1 & 0 \\ 1 & 0 & a \\ 0 & a & 0 \end{pmatrix} \right\}. \qquad 3.2,2$$

This is evaluated by calculating the eigenvalues, D_{ii}, and the eigenvectors, S_i, of the Hamiltonian. These are given by $H = SDS^{-1}$ or

$$\begin{pmatrix} 0 & 1 & 0 \\ 1 & 0 & a \\ 0 & a & 0 \end{pmatrix} = \begin{pmatrix} \frac{-a}{\sqrt{1}} & \frac{1}{\sqrt{21}} & \frac{1}{\sqrt{21}} \\ 0 & \frac{1}{\sqrt{2}} & \frac{-1}{\sqrt{2}} \\ \frac{1}{\sqrt{1}} & \frac{a}{\sqrt{21}} & \frac{a}{\sqrt{21}} \end{pmatrix} \begin{pmatrix} 0 & 0 & 0 \\ 0 & \sqrt{1} & 0 \\ 0 & 0 & -\sqrt{1} \end{pmatrix} \begin{pmatrix} \frac{-a}{\sqrt{1}} & 0 & \frac{1}{\sqrt{1}} \\ \frac{1}{\sqrt{21}} & \frac{1}{\sqrt{2}} & \frac{a}{\sqrt{21}} \\ \frac{1}{\sqrt{21}} & \frac{-1}{\sqrt{2}} & \frac{a}{\sqrt{21}} \end{pmatrix} \qquad 3.2,3$$

where $1 = 1+a^2$. S is the matrix of eigenvectors, S^{-1} its inverse and D the eigenvalues. So therefore

$$U(t,t_o) = S\exp\left\{i\frac{\theta(t)D}{\sqrt{1}}\right\}S^{-1} \qquad 3.2,4$$

where

$$\theta(t) = \int_{t_o}^{t} \Omega_1(t')dt'\frac{\sqrt{1}}{2}.$$

The pulse area is defined as $2\theta(t_{max})/\sqrt{1}$, and gives a measure of the strength of the pulse. Thus

$$U(t,t_o) = S\begin{pmatrix} 1 & 0 & 0 \\ 0 & \exp(i\theta(t)) & 0 \\ 0 & 0 & \exp(-i\theta(t)) \end{pmatrix} S^{-1} \qquad 3.2,5$$

$$= \begin{pmatrix} \frac{a^2}{1} + \frac{\cos(\theta(t))}{1} & \frac{i\sin(\theta(t))}{\sqrt{1}} & \frac{-a}{\sqrt{21}} + \frac{a\cos(\theta(t))}{1} \\ \frac{i\sin(\theta(t))}{\sqrt{1}} & \cos(\theta(t)) & \frac{ia\sin(\theta(t))}{\sqrt{1}} \\ \frac{-a}{1} + \frac{a\cos(\theta(t))}{1} & \frac{ia\sin(\theta(t))}{\sqrt{1}} & \frac{1}{1} + \frac{a^2\cos(\theta(t))}{1} \end{pmatrix} . \qquad 3.2,6$$

If the initial condition is that at $t = t_o$ all the population is in

the ground state, then

$$c'(t_o) = \begin{pmatrix} 1 \\ 0 \\ 0 \end{pmatrix}. \qquad 3.2,7$$

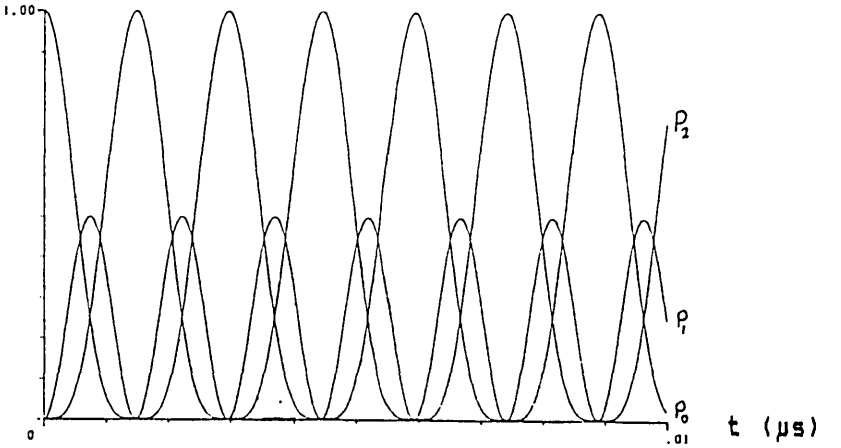
Therefore the populations are given by $P(t) = |c'(t)|^2$, so

$$P(t) = \begin{pmatrix} \left[\frac{a^2}{1} + \frac{\cos(\theta(t))}{1}\right]^2 \\ \frac{\sin^2(\theta(t))}{1} \\ \left[\frac{-a}{1} + \frac{a\cos(\theta(t))}{1}\right]^2 \end{pmatrix}. \qquad 3.2,8$$

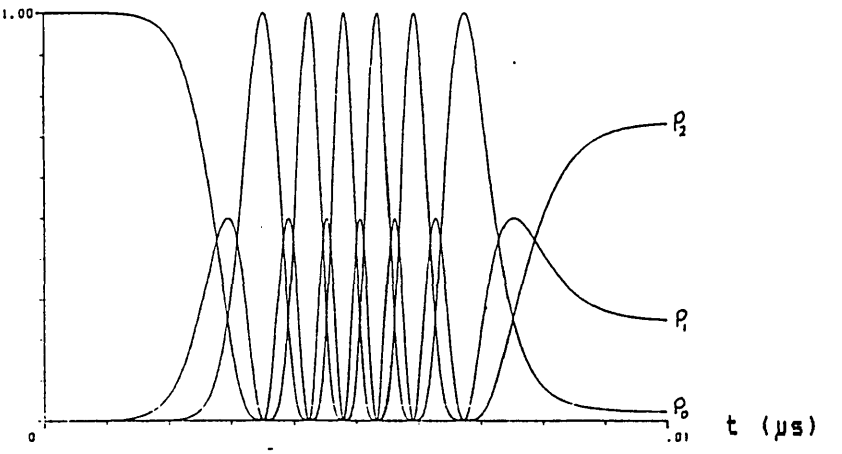
Fig ia shows the populations as functions of time for two flat pulses of equal strength, ie a = 1 and 1 = 2, and the pulse area $\Omega_1 t_{max}$ = 30 rads. The final populations are then

$$P(t) = \begin{pmatrix} \frac{(1 + \cos(\theta(t)))^2}{4} \\ \frac{\sin^2(\theta(t))}{2} \\ \frac{(1 - \cos(\theta(t)))^2}{4} \end{pmatrix} \sim \begin{pmatrix} 0.021 \\ 0.246 \\ 0.733 \end{pmatrix}. \qquad 3.2,9$$

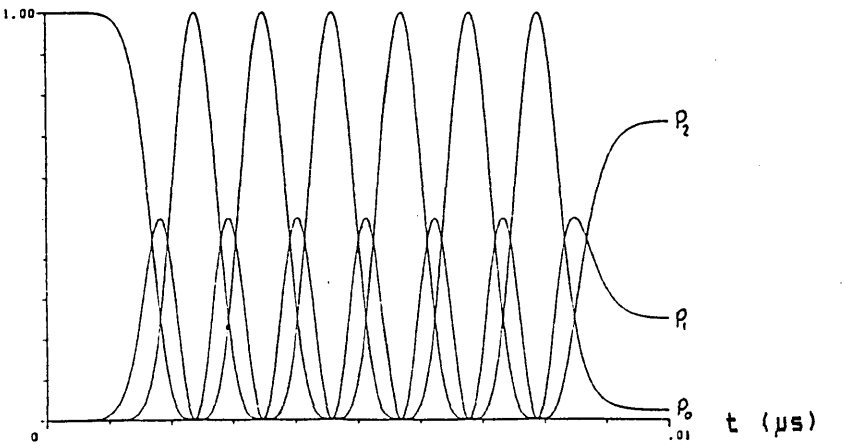
These results agree exactly with the numerical results. Figs ib and c show the numerical results for the evolution of the same system with a Gaussian pulse and with a pulse comprising a Gaussian rise and fall with a flat top. The pulses are all of the same area, 30 rads, and are shown in fig ii. The Gaussian pulse has a profile $\exp(-(t-t_p/2)^2/2\sigma_t^2)$, where the pulse is cut off at t = 0 and t_p. The width σ_t equals $t_p/5\sqrt{2}$ meaning that the pulse is cut off at $\exp(-25/4) \sim 0.002$ of the peak value. The flat topped Gaussian is flat between $t_p/5$ and $4t_p/5$, with a rise and fall qiven by $\exp(-(t-t_p/5)^2/2\sigma_t'^2)$ where $\sigma_t' = \sqrt{2}t_p/25$. The final populations for these two cases can be seen to be identical to the constant pulse case. This is due to the pairs of pulses having the same shapes. The



a) both pulses flat



b) both pulses Gaussian



c) both pulses flat-topped-Gaussian

Fig 3.2.i

Temporal evolution for different pulse shapes, all with area 30rads.

temporal evolutions are different because of the difference in the instantaneous Rabi frequencies. The maximum Rabi frequency of the Gaussian pulse is more than twice that of the average.

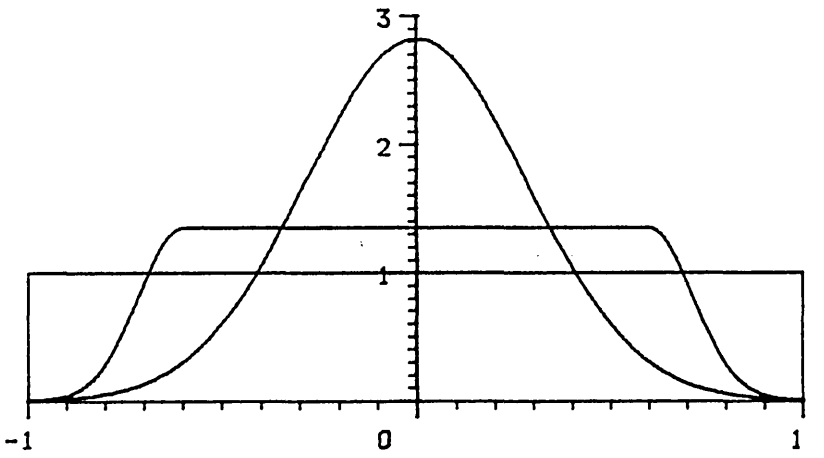


Fig 3.2.ii

The three pulse shapes: flat, Gaussian and flat-topped-Gaussian.

Thus at the beginning and the end of the pulse not much population transfer occurs, whilst at the peak the populations are evolving more rapidly to compensate. The dependence of the final populations on the pulse area alone is true only if there are no detunings or decays and the pulses are identical in shape. [Thomas 1983]

3.2.1.2 The perturbative solution

The second comparison is with the perturbative solution. This is valid for small pulse areas where $\Omega t \ll 1$. This condition means that there is no chance of either of the two upper levels gaining enough population to affect the rate of population transfer out of the ground state, assuming all the population starts in the ground state. The Hamiltonian in the rotating frame is given by

$$H' = \hbar \begin{pmatrix} 0 & -\frac{\Omega_1}{2} & 0 \\ -\frac{\Omega_1}{2} & \Delta_1 & -\frac{\Omega_2}{2} \\ 0 & -\frac{\Omega_2}{2} & \Delta_1+\Delta_2 \end{pmatrix} \qquad 3.2,10$$

where Ω_1 and Ω_2 are constant in time, $\gamma_o = 0$ and $\tilde{\Delta}_1 = \Delta_1 - i\gamma_1/2$ and $\tilde{\Delta}_2 = \Delta_2 - i(\gamma_2-\gamma_1)/2$. From Schrödinger's equation

$$i\hbar\frac{dC'}{dt} = H'C'. \qquad 3.2,11$$

Thus

$$\dot{c}_o = i\frac{\Omega_1}{2}c_i \ , \qquad 3.2,12a$$

$$\dot{c}_i = i\frac{\Omega_1}{2}c_o - i\tilde{\Delta}_1 c_i + i\frac{\Omega_2}{2}c_2 \qquad 3.2,12b$$

and

$$\dot{c}_2 = i\frac{\Omega_1}{2}c_i - i(\tilde{\Delta}_1+\tilde{\Delta}_2)c_2 \ . \qquad 3.2,12c$$

The perturbations are assumed weak enough so that the initial state, c_o, is never noticeably depleted. Thus $c_o = 1 \gg c_i, c_2$ for all time $t \ll 1/\Omega_1, \Omega_2$. This gives

$$\dot{c}_i = i\frac{\Omega_1}{2} - i\tilde{\Delta}_1 c_i \qquad 3.2,13$$

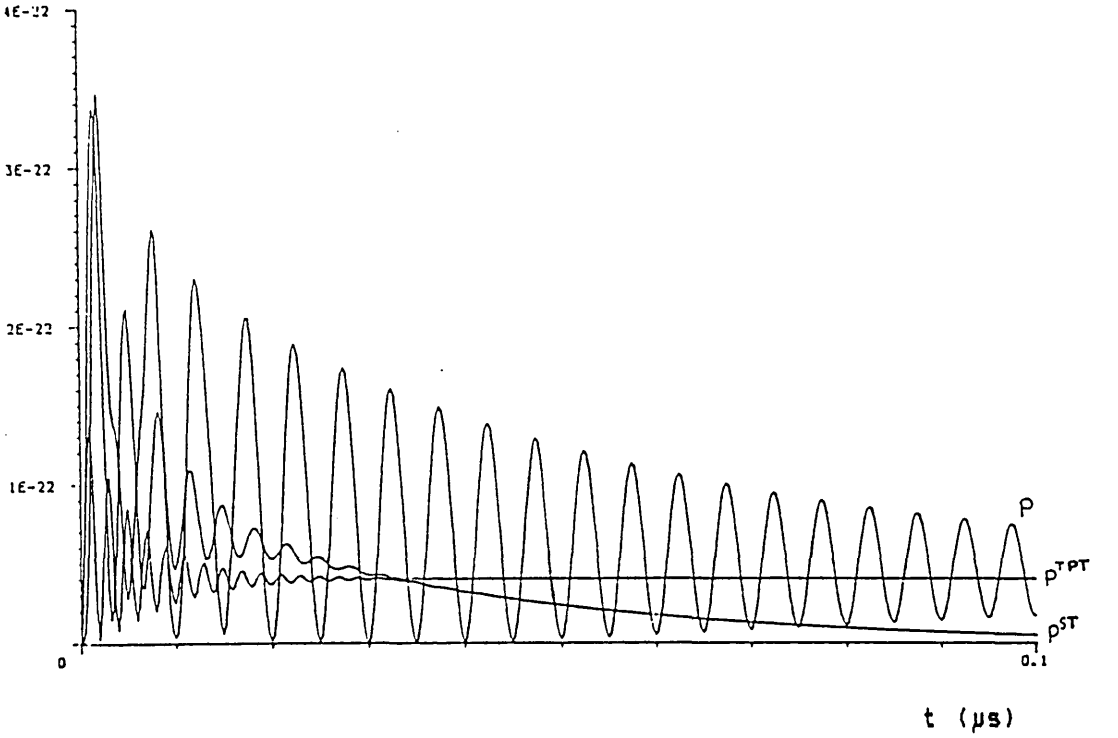
giving

$$c_i = \frac{\Omega_1}{2\tilde{\Delta}_1}(1 - \exp(-i\tilde{\Delta}_1 t)). \qquad 3.2,14$$

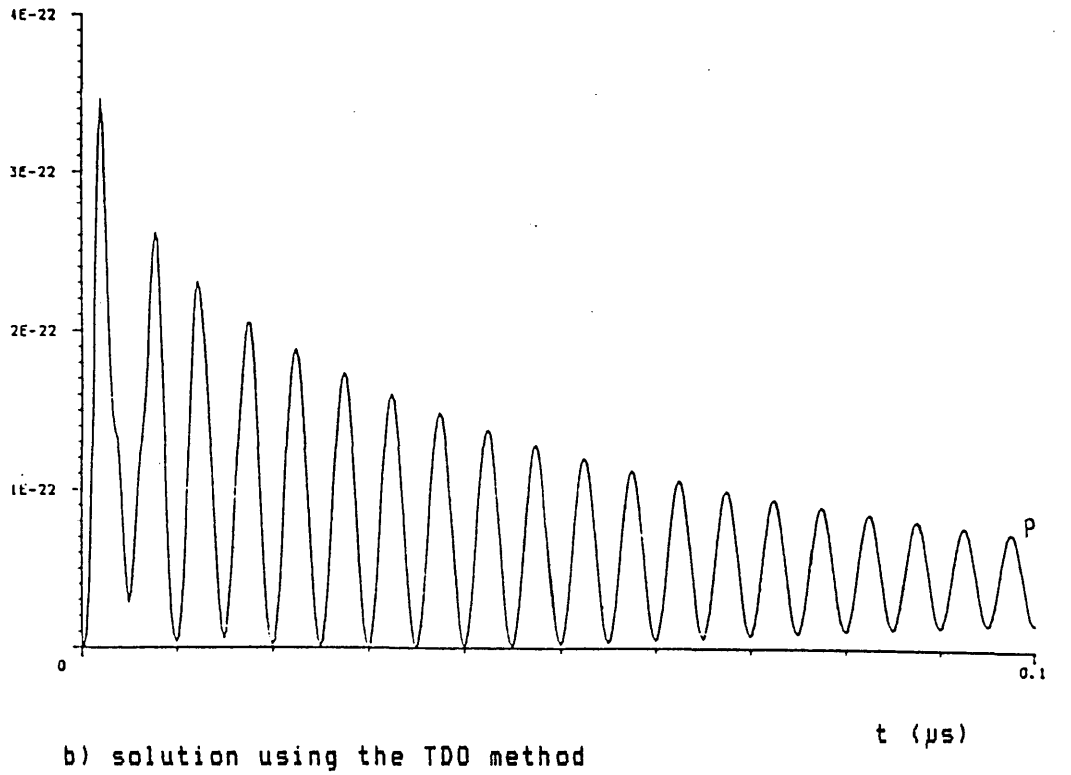
Therefore the probability to be in the middle state is given by $P_1 = |c_1\exp(-iE_1t/\hbar)|^2 = |c_1|^2 = |c_i|^2$, giving

$$P_1(t) = \frac{\Omega_1^2}{4(\Delta_1^2+\frac{\gamma_1^2}{4})}(1-2\exp(-\gamma_1 t/2)\cos(\Delta_1 t)+\exp(-\gamma_1 t)). \qquad 3.2,15$$

Note that the energy in the phase term is not complex and so



a) perturbative solution showing P, P^{TPT} and P^{ST}



b) solution using the TDO method

Fig 3.2.iii

Temporal solution using the perturbative approximation,

$\Omega_1 = \Omega_2 = 10^{-2}$ Mrads s^{-1}, $\Delta_1 = 200$ MHz, $\Delta_2 = 300$ MHz,

$\gamma_1 = 10\pi$ Mrads s^{-1} and $\gamma_2 = 100\pi$ Mrads s^{-1}.

additional damping is not introduced at this stage. Substituting equation 14 into equation 12c and making the perturbative approximation gives

$$\dot{c}_2 = \frac{i\Omega_1\Omega_2}{4\Delta_1}(1-\exp(-i\Delta_1 t)) - i(\Delta_1+\Delta_2)c_2 \qquad 3.2,16$$

giving

$$c_2 = \frac{\Omega_1\Omega_2}{4\Delta_1}\left[\frac{(1-\exp(-i(\Delta_1+\Delta_2)t))}{(\Delta_1+\Delta_2)} - \exp(-i\Delta_1 t)\frac{(1-\exp(-i\Delta_2 t))}{\Delta_2}\right] . \qquad 3.2,17$$

The first term in the square brackets depends upon the two photon detuning from the ground state $|0\rangle$. This is known as the two photon transition term where two photons are absorbed via a virtual middle state. The second term depends on the single photon detuning from the middle state $|1\rangle$ and is known as the stepwise transition term where a photon is absorbed when the system is in state $|1\rangle$. Due to the negative sign between them these two terms can interfere strongly to produce oscillations lasting much longer than the oscillations in each transition type. The population in the upper level, given by $|c_2|^2$ is shown in fig iiia along with the populations obtained by considering only the two photon transition P^{TPT}, and the stepwise transition P^{ST}.

$$P^{TPT} = \frac{\Omega_1^2\Omega_2^2(1-2\exp(-\gamma_2 t/2)\cos((\Delta_1+\Delta_2)t)+\exp(-\gamma_2 t))}{16(\Delta_1^2+\gamma_1^2/4)((\Delta_1+\Delta_2)^2+\gamma_2^2/4)} \qquad 3.2,18$$

$$P^{ST} = \frac{\Omega_1^2\Omega_2^2\exp(-\gamma_1 t)(1-2\exp(-(\gamma_2-\gamma_1)t/2)\cos(\Delta_2 t)+\exp(-(\gamma_2-\gamma_1)t))}{16(\Delta_1^2+\gamma_1^2/4)(\Delta_2^2+(\gamma_2-\gamma_1)^2/4)} . \qquad 3.2,19$$

The values used in the figure are $\Omega_1 = \Omega_2 = 10^{-2}$ Mrads s^{-1}, $\Delta_1 =$ 200 MHz, $\Delta_2 =$ 300 MHz, $\gamma_1 = 10\pi$ Mrads s^{-1} and $\gamma_2 = 100\pi$ Mrads s^{-1}. It can be seen that the oscillations in both the two photon transitions and the stepwise transitions die out in a time of the order of $2/\gamma_2$ and $2/(\gamma_2+\gamma_1)$ respectively. However, the oscillations in the real solution continue for a much longer time due to the interference between the two amplitudes. Fig iiib shows the results obtained using the TDO method. This yields an identical result to the perturbative

solution.

3.2.1.3 Dressed states method

The final comparison is with an analytic method involving the diagonalisation of the stationary Hamiltonian, see for example Radmore and Knight 1982 [RK], who use quantised fields in the Schrödinger picture and have a time independent Hamiltonian from the outset. In the semi-classical theory used here the equivalent Hamiltonian becomes stationary only after the RWA has been made and if the pulse envelopes are flat. As the system is a three level system the diagonalisation of the Hamiltonian involves the solution of a complex cubic to find the dressed state eigenenergies. This is soluble analytically and from these the eigenvectors (the dressed states) and inverse-eigenvectors can be formed enabling an exact solution to the problem to be found. In contrast to the perturbative solution, dealt with in the previous section, the Rabi frequencies can be strong enough, ie $\Omega_1 t \gtrsim 1$, to cause Rabi flopping between the states. Detunings and decays can be included with little added complication. As in the previous section the Hamiltonian can be written

$$H' = \hbar \begin{pmatrix} 0 & -\frac{\Omega_1}{2} & 0 \\ -\frac{\Omega_1}{2} & \tilde{\Delta}_1 & -\frac{\Omega_2}{2} \\ 0 & -\frac{\Omega_2}{2} & (\tilde{\Delta}_1+\tilde{\Delta}_2) \end{pmatrix} \qquad 3.2,20$$

where, as before, $\tilde{\Delta}_1 = \Delta_1 - i\gamma_1/2$, and $\tilde{\Delta}_2 = \Delta_2 - i(\gamma_2-\gamma_1)/2$. The energy eigenvalues, $\hbar\lambda_n$, are given by the solutions to the equation

$$\det (H' - \hbar I\lambda_n) = 0. \qquad 3.2,21$$

Thus the λ_n are given by the solutions to the cubic

$$\lambda^3 + \lambda^2(2\tilde{\Delta}_1+\tilde{\Delta}_2) + \lambda(\tilde{\Delta}_1\tilde{\Delta}-(\frac{\Omega_1^2+\Omega_2^2}{4})) + \frac{\Omega_1^2}{4}\tilde{\Delta} = 0 \qquad 3.2,22$$

where $\tilde{\Delta} = \tilde{\Delta}_1 + \tilde{\Delta}_2$. A cubic of the form

$$x^3 + Ax^2 + Bx + C = 0 \qquad 3.2,23$$

can be solved using the substitution

$$x = L + M\cos(N). \qquad 3.2,24$$

This yields

$$\cos^3(N)+\frac{(3L+A)}{M}\cos^2(N)+\frac{(3L^2+2AL+B)}{M^2}\cos(N)+\frac{(L^3+AL^2+BL+C)}{M^3} = 0. \qquad 3.2,25$$

This is equated with the identity

$$\cos^3(N) - \frac{3}{4}\cos(N) - \frac{\cos(3N)}{4} = 0 \qquad 3.2,26$$

resulting in the three equations

$$(3L + A)/M = 0 \ , \qquad 3.2,27a$$

$$3L^2 + 2AL + B = -3M^2/4 \qquad 3.2,27b$$

and

$$L^3 + AL^2 + BL + C = -M^3\cos(3N)/4 \qquad 3.2,27c$$

giving

$$L = -A/3 \ , \qquad 3.2,28a$$

$$M = \pm 2\sqrt{(A^2-3B)}\ /3 \qquad 3.2,28b$$

and

$$N = \frac{1}{3}\cos^{-1}\left[\frac{\pm(9AB-2A^3-27C)}{2(A^2-3B)^{3/2}}\right] . \qquad 3.2,28c$$

In this case

$$A = -(2\tilde{\Delta}_1 + \tilde{\Delta}_2) , \qquad 3.2,29a$$

$$B = (\tilde{\Delta}_1\tilde{\Delta}-(\Omega_1^2+\Omega_2^2)/4) \qquad 3.2,29b$$

and

$$C = \Omega_1^2\tilde{\Delta}/4. \qquad 3.2,29c$$

So the eigen-frequencies are given by

$$\lambda_n = \frac{(2\tilde{\Delta}_1+\tilde{\Delta}_2)}{3} + \frac{2}{3}\{\tilde{\Delta}_1^2 + \Delta_1\Delta_2+\tilde{\Delta}_2^2+\frac{3}{4}(\Omega_1^2+\Omega_2^2)\}^{1/2} \times$$

$$\cos\left\{\frac{1}{3}\cos^{-1}\left[\frac{\pm\left(-2\tilde{\Delta}_1^3-3\tilde{\Delta}_1^2\tilde{\Delta}_2+3\tilde{\Delta}_1\tilde{\Delta}_2^2+2\tilde{\Delta}_2^3 \;-\frac{9}{4}\left(\tilde{\Delta}_1\Omega_1^2+2\tilde{\Delta}_2\Omega_1^2-2\tilde{\Delta}_1\Omega_2^2-\tilde{\Delta}_2\Omega_2^2\right)\right)}{2\left(\tilde{\Delta}_1^2+\tilde{\Delta}_1\tilde{\Delta}_2+\tilde{\Delta}_2^2+\frac{3}{4}\left(\Omega_1^2+\Omega_2^2\right)\right)}\right]\right\} . \qquad 3.2,30$$

The eigenstates $|E_n\rangle$ are calculated from $H'|E_n\rangle = \hbar\lambda_n|E_n\rangle$ so that $(H' - \hbar\lambda_n I)|E_n\rangle = 0$, where the λ_n have already been chosen such that $\det(H' - \hbar\lambda_n I) = 0$, leading to non-trivial solutions for $|E_n\rangle$. The $|E_n\rangle$ are given by

$$|E_n\rangle = N_n \begin{pmatrix} \Omega_1(\lambda_n-\tilde{\Delta})/2 \\ -\lambda_n(\lambda_n-\tilde{\Delta}) \\ \Omega_1\lambda_n/2 \end{pmatrix} \qquad 3.2,31$$

where

$$N_n = \{|\lambda_n|^2\frac{\Omega_2^2}{4} + (|\lambda_n|^2+\frac{\Omega_1^2}{4})|\lambda_n - \tilde{\Delta}_1|^2\}^{-1/2} . \qquad 3.2,32$$

These are the 'dressed states' of the perturbed system with respect to

the eigenstates of the unperturbed system. The temporal evolution of the wave function is given by

$$|\Psi\rangle = \sum_{n=0}^{2} e_n \exp(-i\lambda_n t)|E_n\rangle \qquad 3.2,33$$

where e_n are time independent. The initial condition is that at time $t = 0$ all the population is in the ground state $|0\rangle$, so

$$\langle 0|\Psi(t=0)\rangle = 1, \qquad 3.2,34a$$

$$\langle 1|\Psi(t=0)\rangle = 0 \qquad 3.2,34b$$

and

$$\langle 2|\Psi(t=0)\rangle = 0 \qquad 3.2,34c$$

where the phase factor has been ignored as only the populations are being considered. Substituting from equations 31,32 and 33 yields the following

$$\langle 0|\Psi(t=0)\rangle = \sum_{n=0}^{2} e_n (1\ 0\ 0)|E_n\rangle N_n, \qquad 3.2,35a$$

$$\langle 1|\Psi(t=0)\rangle = \sum_{n=0}^{2} e_n (0\ 1\ 0)|E_n\rangle N_n \qquad 3.2,35b$$

and

$$\langle 2|\Psi(t=0)\rangle = \sum_{n=0}^{2} e_n (0\ 0\ 1)|E_n\rangle N_n \qquad 3.2,35c$$

giving

$$\begin{pmatrix} \frac{N_0\underline{\Omega}_1(\lambda_0-\bar{\Delta})}{2} & \frac{N_1\underline{\Omega}_1(\lambda_1-\bar{\Delta})}{2} & \frac{N_2\underline{\Omega}_1(\lambda_2-\bar{\Delta})}{2} \\ -N_0\lambda_0(\lambda_0-\bar{\Delta}) & -N_1\lambda_1(\lambda_1-\bar{\Delta}) & -N_2\lambda_2(\lambda_2-\bar{\Delta}) \\ \frac{N_0\underline{\Omega}_2\lambda_0}{2} & \frac{N_1\underline{\Omega}_2\lambda_1}{2} & \frac{N_2\underline{\Omega}_2\lambda_2}{2} \end{pmatrix} \begin{pmatrix} e_0 \\ e_1 \\ e_2 \end{pmatrix} = \begin{pmatrix} 1 \\ 0 \\ 0 \end{pmatrix}. \qquad 3.2,36$$

This can be inverted to give

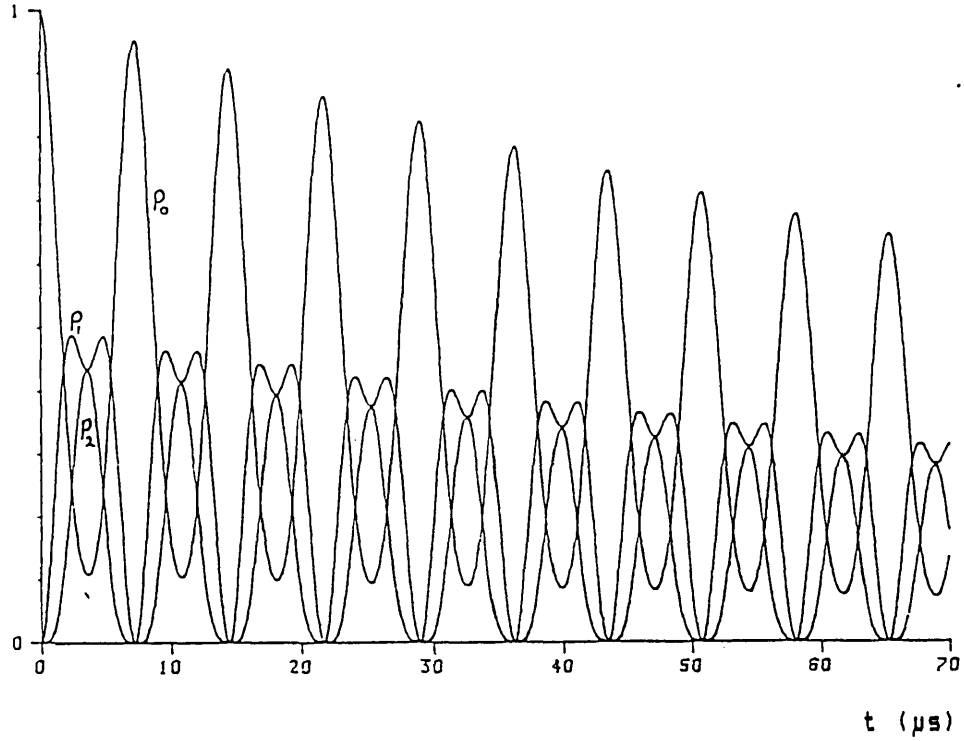


Fig 3.2.iv

TDO solution for comparison with the 'Dressed States' model,
$\Omega_1 = \Omega_2 = 1$ Mrads s^{-1}, $\Delta_1 = \Delta_2 = 1/4\pi$ MHz,
$\gamma_1 = 0.02$ Mrads s^{-1} and $\gamma_2 = 0$.

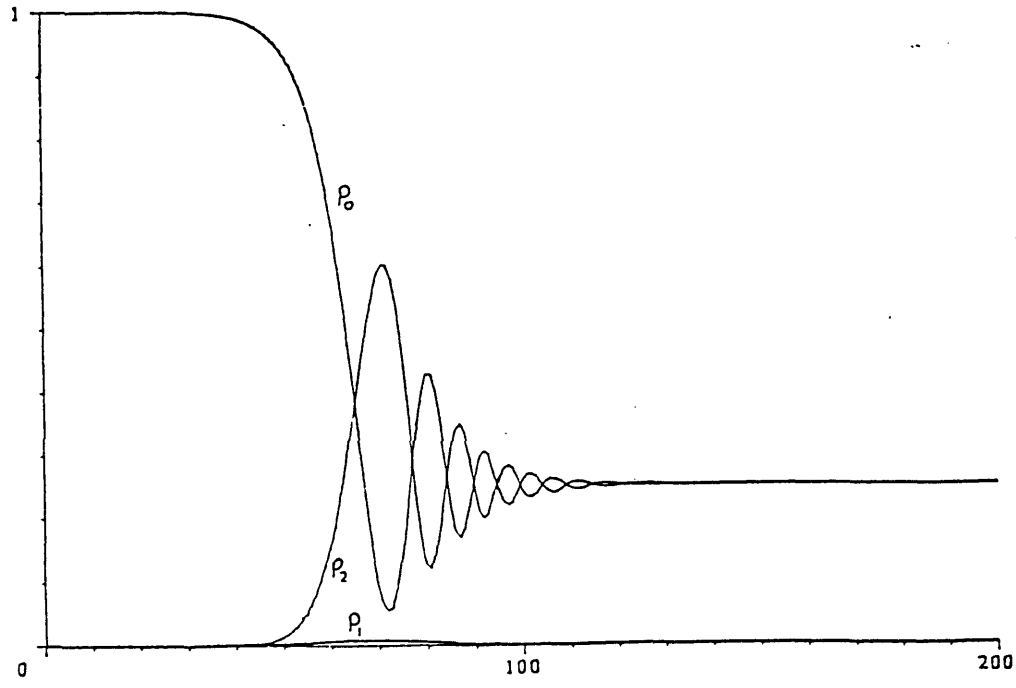


Fig 3.2.v

a) Population trapping with Gaussian pulses,
both areas = 200 rads, $\Delta_1 = -\Delta_2 = 5/2\pi$ MHz,
$\gamma_1 = 2$ Mrads s^{-1} and $\gamma_2 = 0$.

$$\begin{pmatrix} e_0 \\ e_1 \\ e_2 \end{pmatrix} = \begin{pmatrix} N_1N_2\lambda_1\lambda_2(\lambda_1-\lambda_2) \\ N_2N_0\lambda_2\lambda_0(\lambda_2-\lambda_0) \\ N_0N_1\lambda_0\lambda_1(\lambda_0-\lambda_1) \end{pmatrix} N \qquad 3.2,37$$

where

$$N = \frac{-2}{N_0N_1N_2\Omega_1\Omega\lambda_0\lambda_1\lambda_2}\left(\frac{\lambda_0}{\lambda_1}\frac{-\lambda_1}{\lambda_0}+\frac{\lambda_1}{\lambda_2}\frac{-\lambda_2}{\lambda_1}+\frac{\lambda_2}{\lambda_0}\frac{-\lambda_0}{\lambda_2}\right)^{-1} \qquad 3.2,38$$

The amplitudes c_n' to be in the unperturbed eigenstates $|n\rangle$ are given by $c_n' = \langle n|\Psi\rangle$. From equation 33 this can be written

$$c_n' = \sum_{n=0}^{2}\langle n|e_m\exp(-i\lambda_m t)|E_m\rangle \qquad 3.2,39$$

giving

$$c_0' = \frac{\Omega_1}{2}NN_0N_1N_2\left[\lambda_1\lambda_2\lambda_{12}e^{-i\hbar\lambda_0 t}(\lambda_0-\tilde{\Delta}) + \lambda_2\lambda_0\lambda_{20}e^{-i\hbar\lambda_1 t}(\lambda_1-\tilde{\Delta}) + \lambda_0\lambda_1\lambda_{01}e^{-i\hbar\lambda_2 t}(\lambda_2-\tilde{\Delta})\right], \qquad 3.2,40a$$

$$c_1' = -NN_0N_1N_2\lambda_0\lambda_1\lambda_2\left[\lambda_{12}e^{-i\hbar\lambda_0 t}(\lambda_0-\tilde{\Delta}) + \lambda_{20}e^{-i\hbar\lambda_1 t}(\lambda_1-\tilde{\Delta}) + \lambda_{01}e^{-i\hbar\lambda_2 t}(\lambda_2-\tilde{\Delta})\right] \qquad 3.2,40b$$

and

$$c_2' = \frac{\Omega_2}{2}NN_0N_1N_2\lambda_0\lambda_1\lambda_2\left[\lambda_{12}e^{-i\hbar\lambda_0 t} + \lambda_{20}e^{-i\hbar\lambda_1 t} + \lambda_{01}e^{-i\hbar\lambda_1 t}\right] \qquad 3.2,40c$$

where $\lambda_{ij} = \lambda_i - \lambda_j$. This is an exact solution, limited mainly by the RWA and the dipole approximation, for a three level system driven by nearly resonant optical laser fields of constant amplitude. Fig iv shows the evolution of the three levels, calculated using the TDO method, with the following parameters: $\Omega_1 = \Omega_2 = 1$ Mrad s^{-2}, $\Delta_1 = \Delta_2 = 1/4\pi$ MHz, $\gamma_1 = 0.02$ Mrads s^{-1} and $\gamma_2 = 0$. This is to be compared with the results of RK, who used the 'dressed states' method. After a small error in the results of RK was corrected, where the middle state population was doubly damped, the results were identical.

The ability of the TDO method to cope with shaped laser pulses, in

addition to detunings and decays, is used to generate fig va. Here the pulse areas are both 200 rads, $\Delta_1 = -\Delta_2 = 5/2\pi$ MHz, $\gamma_1 = 2$ Mrads s^{-1} and $\gamma_2 = 0$. This shows the effects of Gaussian, rather than flat, pulses on population trapping. This is to be compared with fig vb taken from RK, which shows the effect of having a two-photon resonant system with decay from the middle level. Under these circumstances population is trapped within the system, unable to decay via the one decay channel, even if the system is also one-photon resonant, see Radmore and Knight 1982. For the case where $\tilde{\Delta}_1 + \tilde{\Delta}_2 = 0$, ie two-photon resonance, the cubic for the dressed states eigenenergies reduces to a quadratic. Thus the eigenfrequencies are given by

$$\lambda_0 = 0, \qquad 3.2,41a$$

$$\lambda_1 = \frac{-\tilde{\Delta}_1 + \sqrt{\tilde{\Delta}_1^2 + \Omega_1^2 + \Omega_2^2}}{2} \qquad 3.2,41b$$

and

$$\lambda_2 = \frac{-\tilde{\Delta}_1 - \sqrt{\tilde{\Delta}_1^2 + \Omega_1^2 + \Omega_2^2}}{2}. \qquad 3.2,41c$$

The eigenstates are then given by

$$|E_0\rangle = \sqrt{(\Omega_1^2 + \Omega_2^2)}\begin{pmatrix} \Omega_2 \\ 0 \\ -\Omega_1 \end{pmatrix}, \qquad 3.2,42a$$

$$|E_1\rangle = \sqrt{(\Omega_1^2 + \Omega_2^2 + 4\lambda_1^2)}\begin{pmatrix} \Omega_1 \\ -2\lambda_1 \\ \Omega_2 \end{pmatrix} \qquad 3.2,42b$$

and

$$|E_2\rangle = \sqrt{(\Omega_1^2 + \Omega_2^2 + 4\lambda_2^2)}\begin{pmatrix} \Omega_1 \\ -2\lambda_2 \\ \Omega_2 \end{pmatrix}. \qquad 3.2,42c$$

As before, the initial condition that at time t equals zero all the population is in the ground state $|0\rangle$, is used to calculate the amplitudes, e_n, to be in the dressed states $|E_n\rangle$. Equation 36 becomes

$$\begin{pmatrix} N_o\Omega_2 & N_1\Omega_1 & N_2\Omega_1 \\ 0 & -2N_1\lambda_1 & -2N_2\lambda_2 \\ -N_o\Omega_1 & N_1\Omega_2 & N_2\Omega_2 \end{pmatrix} \begin{pmatrix} e_o \\ e_1 \\ e_2 \end{pmatrix} = \begin{pmatrix} 1 \\ 0 \\ 0 \end{pmatrix} \qquad 3.2,43$$

where

$$N_n = \sqrt{(\Omega_1^2 + \Omega_2^2 + 4\lambda_n^2)} \; . \qquad 3.2,44$$

This is inverted to obtain

$$\begin{pmatrix} e_o \\ e_1 \\ e_2 \end{pmatrix} = \begin{pmatrix} \dfrac{\Omega_2}{(\Omega_1^2+\Omega_2^2)^{1/2}} \\ \dfrac{-\Omega_2\lambda_2}{N_1(\Omega_1^2+\Omega_2^2)(\lambda_2-\lambda_1)} \\ \dfrac{\Omega_2\lambda_1}{N_2(\Omega_1^2+\Omega_2^2)(\lambda_2-\lambda_1)} \end{pmatrix} . \qquad 3.2,45$$

The wavefunction is then given by

$$|\Psi\rangle =$$

$$\frac{\Omega_2}{(\Omega_1+\Omega_2)} \left\{ \begin{pmatrix} \Omega_2 \\ 0 \\ -\Omega_1 \end{pmatrix} - \frac{1}{(\lambda_2-\lambda_1)} \frac{\lambda_2 \exp(-i\lambda_1 t)}{N_1^2} \begin{pmatrix} \Omega_1 \\ -2\lambda_1 \\ \Omega_2 \end{pmatrix} \frac{-\lambda_1 \exp(-i\lambda_2 t)}{N_2^2} \begin{pmatrix} \Omega_1 \\ -2\lambda_2 \\ \Omega_2 \end{pmatrix} \right\} . \qquad 3.2,46$$

Both of the non-zero eigenenergies, λ_1 and λ_2, have real parts which cause the exponentials to decay to zero for large t. Thus as $t \to \infty$ the wavefunction becomes

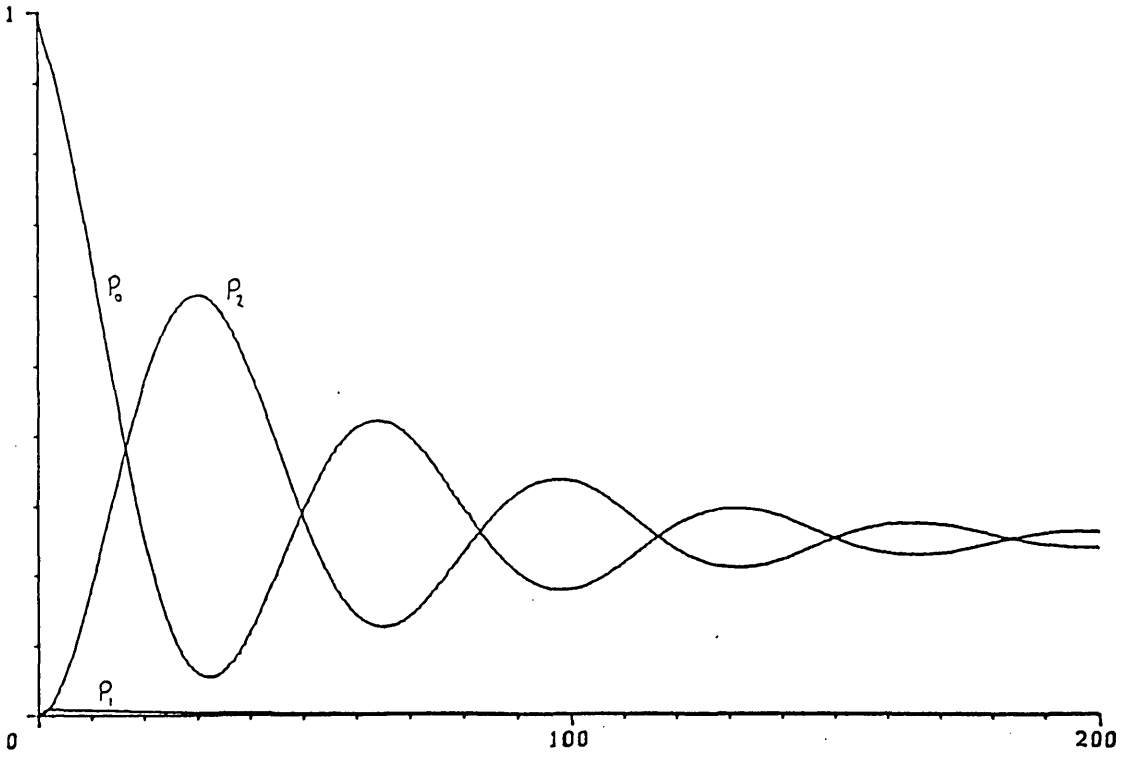


Fig 3.2.v

b) Population trapping with flat pulses, parameters as in a.

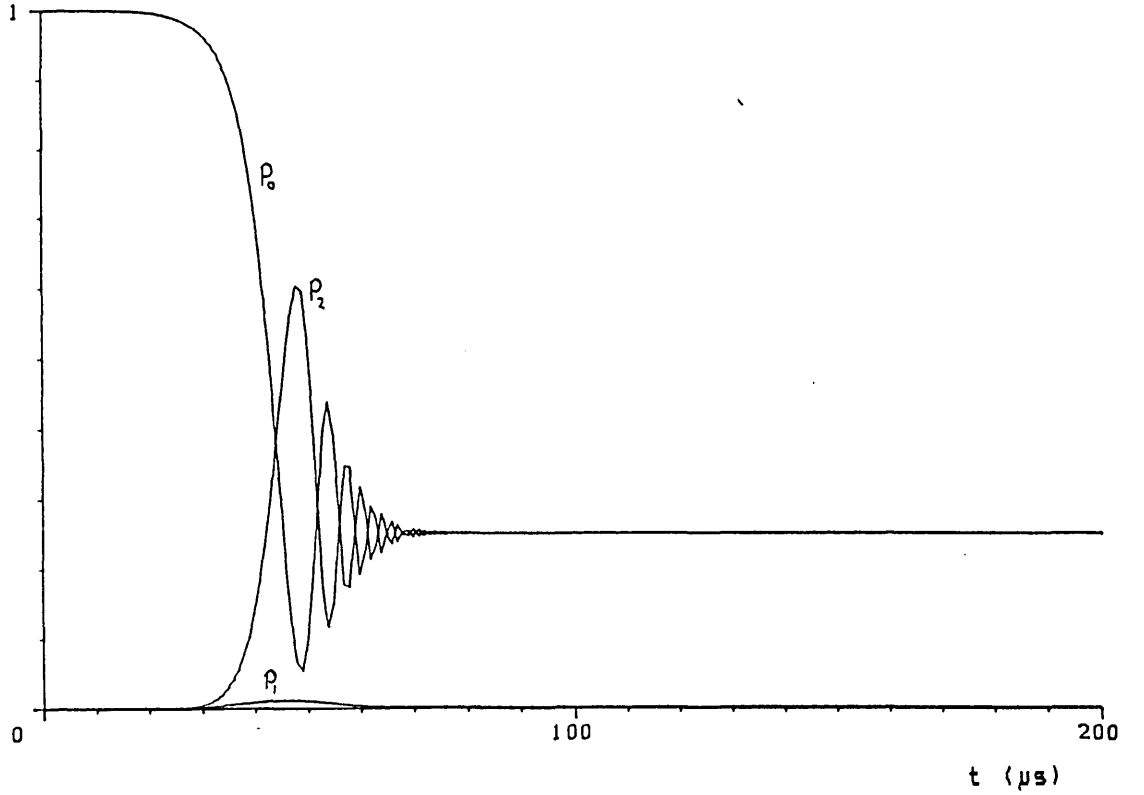


Fig 3.2.vi

Higher power Gaussian pulses causing equilibrium before pulse peaks, both areas = 800 rads, other parameters as in Fig 3.2.v.

$$|\Psi, t\to\infty\rangle = \Omega_2/(\Omega_1^2+\Omega_2^2)\begin{pmatrix}\Omega_2\\0\\-\Omega_1\end{pmatrix}. \qquad 3.2,47$$

The populations in the unperturbed states for large times are therefore

$$P_o = \frac{\Omega_2^4}{(\Omega_1^2+\Omega_2^2)^2}, \qquad 3.2,48a$$

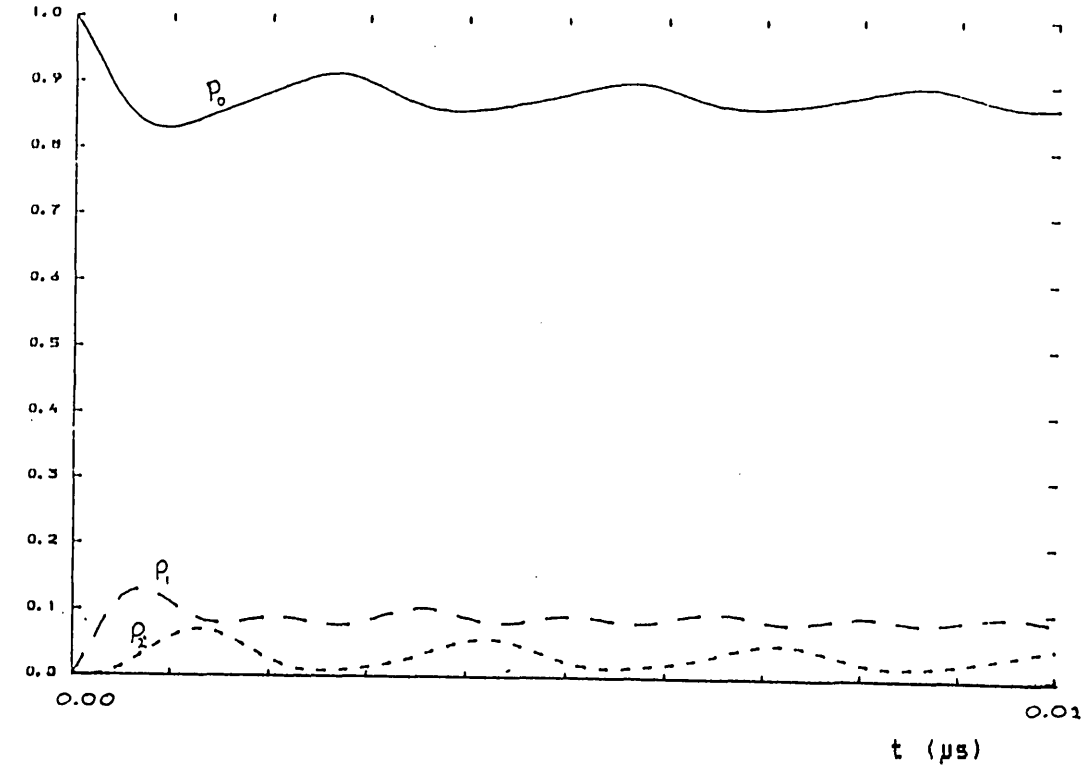
$$P_1 = 0 \qquad 3.2,48b$$

and

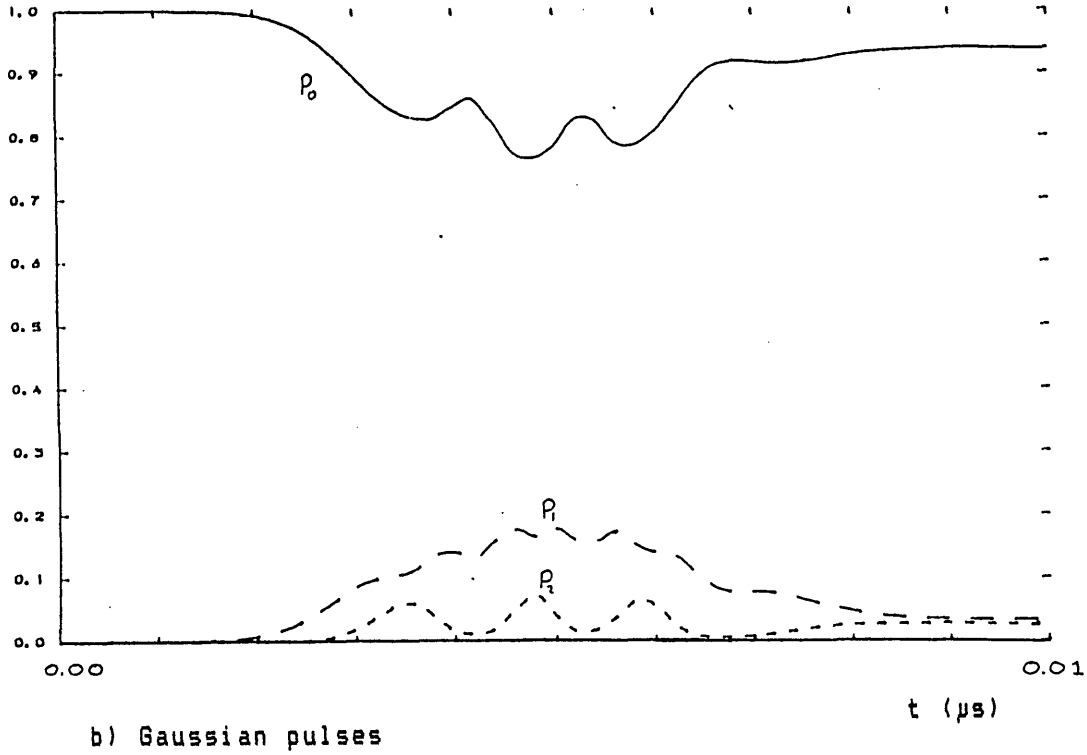
$$P_2 = \frac{\Omega_1^2\Omega_2^2}{(\Omega_1^2+\Omega_2^2)^2}. \qquad 3.2,48c$$

So for equal Rabi frequencies, $\Omega_1 = \Omega_2$, the final populations are $P_o = P_2 = 1/4$ and $P_1 = 0$, as seen in fig vb. In the Gaussian pulse case, the population trapping is still present, but as in previous cases, the temporal evolution is changed. Fig vi shows the result of increasing the Gaussian pulse areas to 800 rads. Equilibrium is reached earlier, even before the pulse has reached its peak. This shows that the populations have reached equilibrium with the fields. The fields are still varying but the final populations are dependent only on their relative size which remains constant.

There is very little reported experimental evidence of population trapping. This indicates that real effects, such as Doppler widths and bandwidths, tend to destroy the critical balance necessary for the trapping. Kaivola etal 1984 report trapping in a three-level system where two counter-propagating beams, from the same laser, are brought onto one- and two-photon resonance using a Doppler shift technique. An atomic beam of fast Ne^{20*} is excited with the two counter-propagating beams running collinearly, and the fluorescence from the middle level is observed as a function of the laser frequency and the atomic velocity. A dip in the flourescence spectrum is



a) Flat pulses

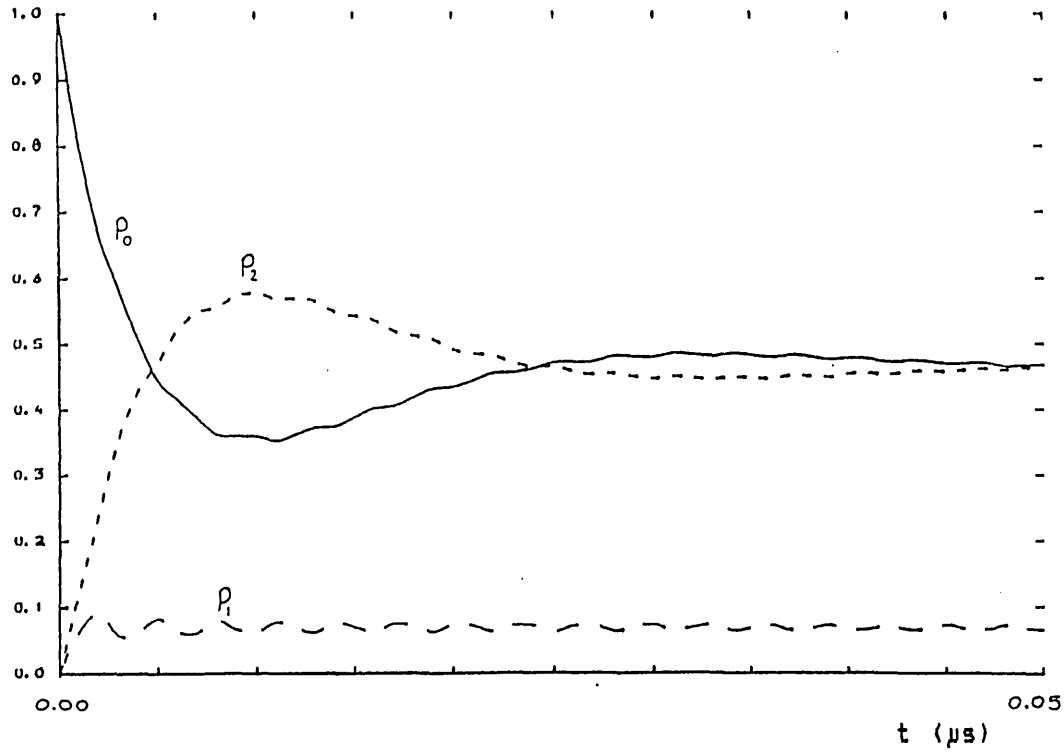


b) Gaussian pulses

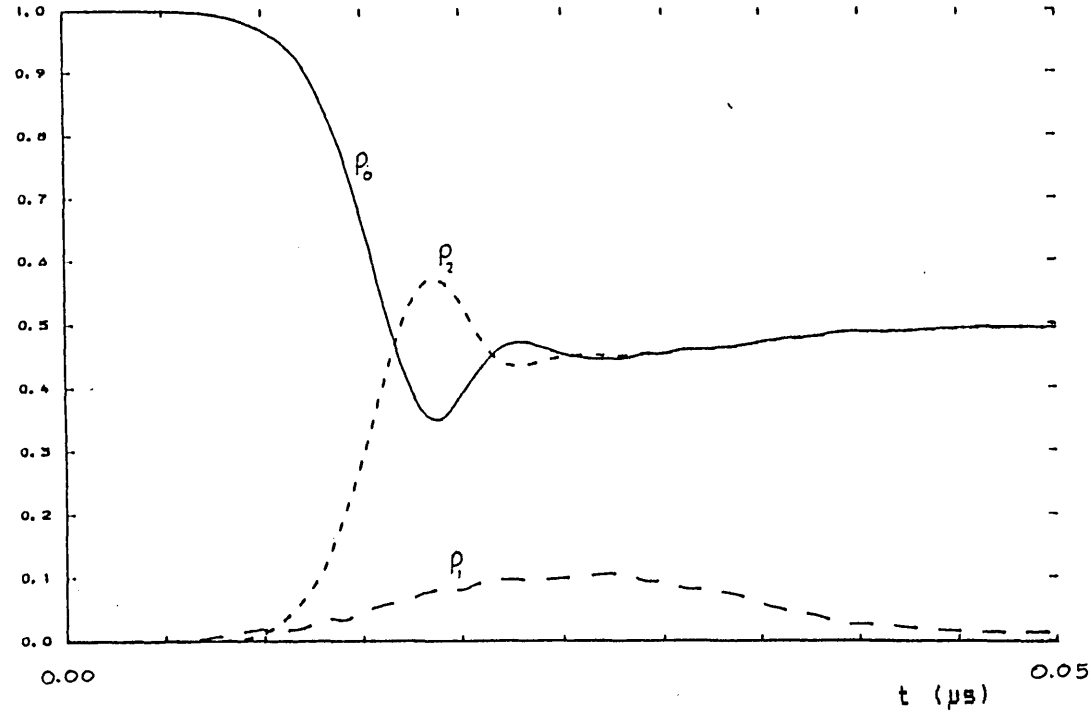
Fig 3.2.viii

Doppler effects for co-propagating pulses,

average Rabi frequencies = 3000 Mrads s^{-1}, Doppler widths = 2500 MHz.



a) Flat pulses



b) Gaussian pulses

Fig 3.2.ix

Doppler effects for counter-propagating pulses,
average Rabi frequencies = 3000 Mrads s^{-1}, Doppler widths = 2500 MHz.

observed close to two-photon resonance which can be interpreted as trapping. This experiment uses counter-propagating beams to reduce the Doppler distribution in a way described in the next section.

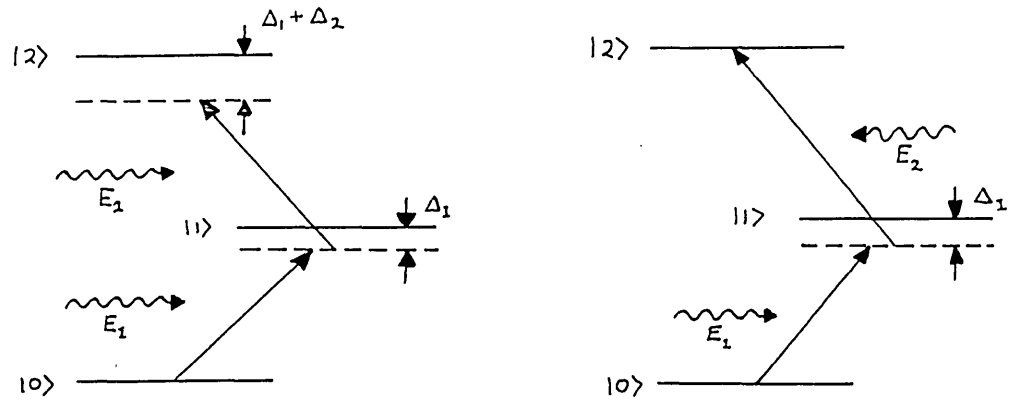
3.2.2 Doppler effects

So far the detunings have been considered to be well defined for the system. However, experimentally this is not usually the case. A system, such as an atom or molecule, irradiated by a laser is usually found to be moving with respect to the frame in which the frequency of the laser beam is measured. A set of such systems, in thermal equilibrium, have a velocity distribution which is given by the Boltzmann distribution. Thus the distribution of velocities parallel to the laser beam is given by a Gaussian distribution. An atom moving with velocity v in the direction of irradiation sees an extra detuning $\Delta = \nu v/c$, to first order in v/c which is considered small, where ν is the frequency of the laser beam. The average population distribution is then given by an integral over the individual populations weighted by the Boltzmann distribution. Thus

$$P_{o,1,2} = \sqrt{\frac{\pi}{2\sigma^2}} \int_{-\infty}^{\infty} P_{o,1,2}(\Delta) \exp(-\Delta^2/2\sigma^2) d\Delta \ . \qquad 3.2,49$$

For a three level system with two laser beams it is important to consider their relative directions. If the beams are co-propagating then the two-photon detuning of the upper level from the ground state is the sum of the two single-photon Doppler shifted detunings. If, however, the beams are counter-propagating then it is the difference. Thus, for a two-photon resonant system, where both transitions are equal, then the system remains on two-photon resonance, independent of the relative velocity of the system to the beams, provided that the beams are counter-propagating. Fig vii shows the effects of the shifts on an otherwise resonant system. Figs viiia and b show the temporal evolution of the three levels for two co-propagating flat pulses and Gaussian pulses respectively. The system becomes detuned from one- and two-photon resonance by the Doppler shifts so not much population transfer takes place. The Doppler width is σ = 2500 MHz, compared to the average Rabi frequencies of Ω = 3000 Mrads s^{-1}. Figs ixa and b show the same system for counter-propagating beams. The system is back

in two-photon resonance, but detuned from single-photon resonance, so population flops mainly between levels |0⟩ and |2⟩.



a) co-propagating beams b) counter-propagating beams

Fig 3.2.vii

The Doppler shifts caused by co- and counter-propagating beams.

An analytical solution to the case where the pulses are flat and counter-propagating is given in Hodgkinson and Briggs 1977, where the time averaged populations are calculated. The high frequency oscillation in the curves is the residual single-photon Rabi oscillation which is large due to the large effective detuning. The low frequency flop is similar to the effect seen in a two-photon resonant system with a far off resonance intermediate state. The two-photon Rabi frequency, using the widths as the effective detunings, is given by

$$\Omega_{TP} = \Omega_1\Omega_2/2\sigma \sim 45.6 \text{ MHz}. \qquad 3.2,50$$

This gives a two-photon oscillation period of around 0.02 μs. The decay of the oscillation is due to the dephasing of all the different oscillation frequencies due to the distribution in the detunings. In the case of the Gaussian counter-propagating pulses similar differences to the previous flat pulse cases are observed. There is a slow build up to the oscillations with a higher oscillation frequency as the pulses increase in amplitude. The higher instantaneous Rabi frequency of the Gaussian pulses near the peak causes the Doppler effects to be less noticeable, leading to more of an increase in the

middle state population. This is also apparent in the co-propagating example.

3.3 Populations as functions of detuning (Stark effects)

So far in this chapter the populations have only been observed as functions of time. It is also interesting to look at the final populations, after a known time, as functions of one or more of the other parameters. In this section the Stark splittings of the lower two levels are investigated by using the upper excitation as a probe to a much stronger lower interaction, see for example the reviews by Feneuille 1977 and Knight and Milonni 1980. The probe beam is scanned across a range of upper level, single-photon detunings and the upper state population is examined. As before, the TDO results can be compared to analytical methods for special sets of the parameters.

3.3.1 The probe approximation

For a three level system with no decays, no lower transition detuning and a very weak and constant upper level coupling a semi-analytical approximation is possible. The Hamiltonian is given by

$$H' = \hbar \begin{pmatrix} 0 & -\frac{\Omega_1(t)}{2} & 0 \\ -\frac{\Omega_1(t)}{2} & 0 & -\frac{\Omega_2}{2} \\ 0 & -\frac{\Omega_2}{2} & \Delta_2 \end{pmatrix} \qquad 3.3,1$$

where Ω_2 is a weak, ie $\Omega_2 t_{max} \ll 1$, and constant probe coupling. From Schrödinger's equation the amplitudes can be written

$$\dot{c}_o = i\frac{\Omega_1(t)}{2} c_i \ , \qquad 3.3,2a$$

$$\dot{c}_i = i\frac{\Omega_1(t)}{2} c_o + i\frac{\Omega_2}{2} c_2 \qquad 3.3,2b$$

and

$$\dot{c}_2 = i\frac{\Omega_2}{2} c_i - i\Delta_2 c_2 \ . \qquad 3.3,2c$$

Ω_2 is assumed to be much smaller than the peak of $\Omega_1(t)$, and so the amplitude c_2 is assumed to be much less than c_0 and c_1. Equation 2 then becomes

$$\dot{c}_0 = i\frac{\Omega_1(t)}{2}c_1 \ , \qquad 3.3,3a$$

$$\dot{c}_1 = i\frac{\Omega_1(t)}{2}c_0 \qquad 3.3,3b$$

and

$$\dot{c}_2 = i\frac{\Omega_2}{2}c_1 - i\Delta_2 c_2 \ . \qquad 3.3,3c$$

Equations 3a and b are just the equations for a strongly coupled, on resonance, two level system and have the solution, from equation 3.2,8 with a = 0 and 1 = 1,

$$c_0(t) = \cos(\theta(t)) \qquad 3.3,4a$$

and

$$c_1(t) = i\,\sin(\theta(t)) \qquad 3.3,4b$$

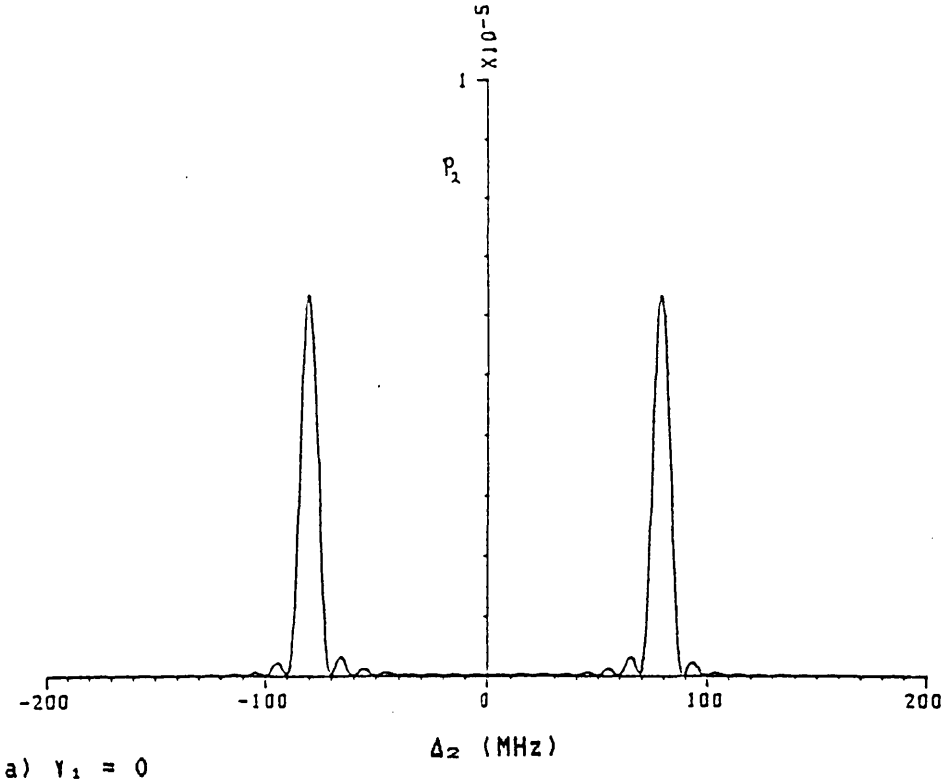
where

$$\theta(t) = \int_{t_0}^{t}\frac{\Omega_1}{2}(t')dt' \ . \qquad 3.3,5$$

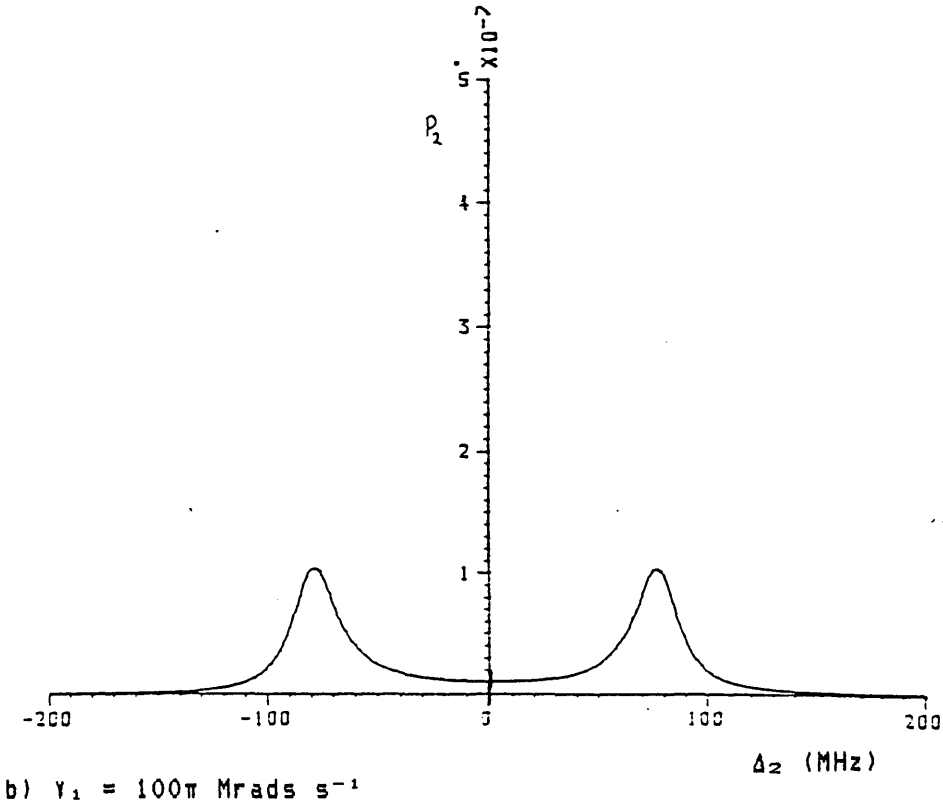
Thus

$$\dot{c}_2 = -\frac{\Omega_2}{2}\sin(\theta(t)) - i\Delta_2 c_2 \ . \qquad 3.3,6$$

This can be written as



a) $\gamma_1 = 0$



b) $\gamma_1 = 100\pi$ Mrads s^{-1}

Fig 3.3.i

Stark splittings for two flat pulses,

$\Omega_1 = 1000$ Mrads s^{-1}, $\Omega_2 = 0.1$ Mrads s^{-1},

$\Delta_1 = \gamma_2 = 0$ and $t = 0.1$ μs.

$$c_2'(t) = -\exp(-i\Delta_2 t)\frac{\Omega_2}{2}\int_{t_o}^{t}\exp(i\Delta_2 t')\sin(\theta(t'))dt' \quad . \qquad 3.3,7$$

For a flat pump pulse, switched on from t = 0 to t, this becomes

$$c_2' = i\frac{\Omega_2 t}{4}\exp(-i\Delta_2 t)\left[\exp(i\delta_1 t)\mathrm{sinc}(\delta_1 t)-\exp(-i\delta_2 t)\mathrm{sinc}(\delta_2 t)\right] \qquad 3.3,8$$

where $\mathrm{sinc}(x) = \sin(x)/x$, $\delta_1 = (\Omega_1+2\Delta_2)/4$ and $\delta_2 = (\Omega_1-2\Delta_2)/4$. If $\Omega \gg 1/t$ then the interference between the two sinc functions is negligible and so the probability can be written as

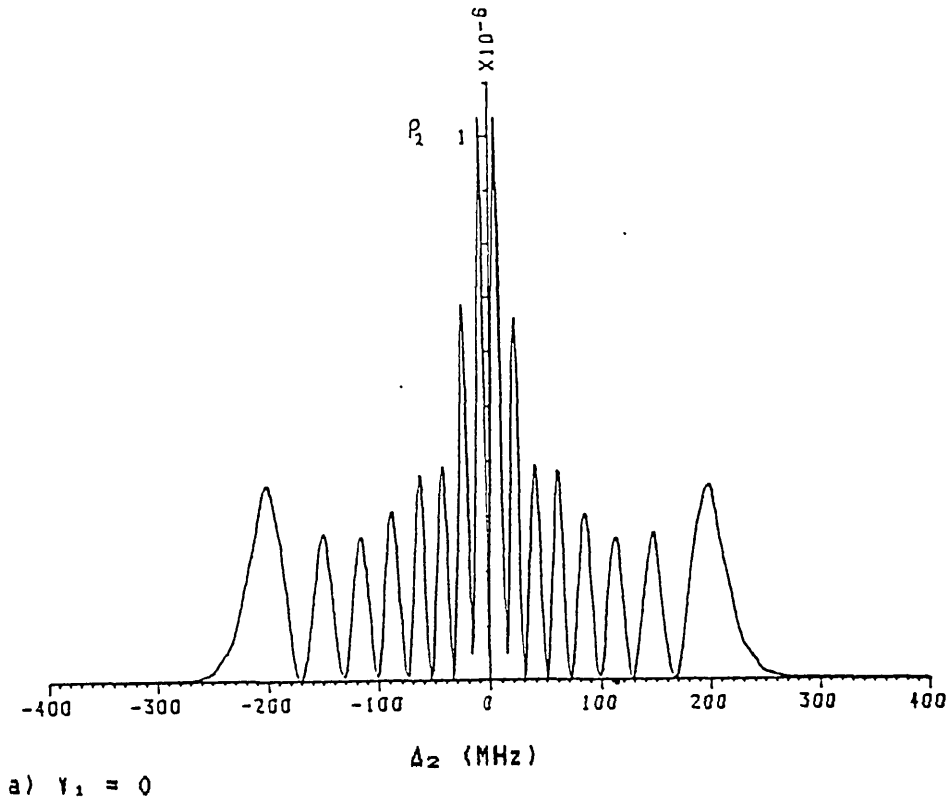
$$P_2(t) = |c_2'(t)|^2 = \left(\frac{\Omega_2 t}{16}\right)^2(\mathrm{sinc}^2(\delta_1 t)+\mathrm{sinc}^2(\delta_2 t)) \quad . \qquad 3.3,9$$

The two sinc squared functions are centred on $\Delta_2 = \pm\Omega_1/2$, ie separated by Ω_1, and are of width $\sim 1/t$. Fig ia shows the TDO solution for the case where $\Omega_1 = 1000$ Mrads s^{-1}, $\Omega_2 = 0.1$ Mrads s^{-1}, $\Delta_1 = \gamma_1 = \gamma_2 = 0$ and t = 0.1 μs. The ripples in between the two peaks are caused by the interference between the two terms in the amplitude of c_2'. Equation 9 predicts the correct positions and height of the peaks, $\sim \pm 80$ MHz and $6.25\ 10^{-6}$, but does not include the central interference ripples. Fig ib shows a more realistic result which includes some decay out of the middle level which, for $\gamma_1 = 100\pi$ Mrads s^{-1}, smooths out the ripples present in fig ia. A Gaussian pulse shape can also be included in equation 7 so that

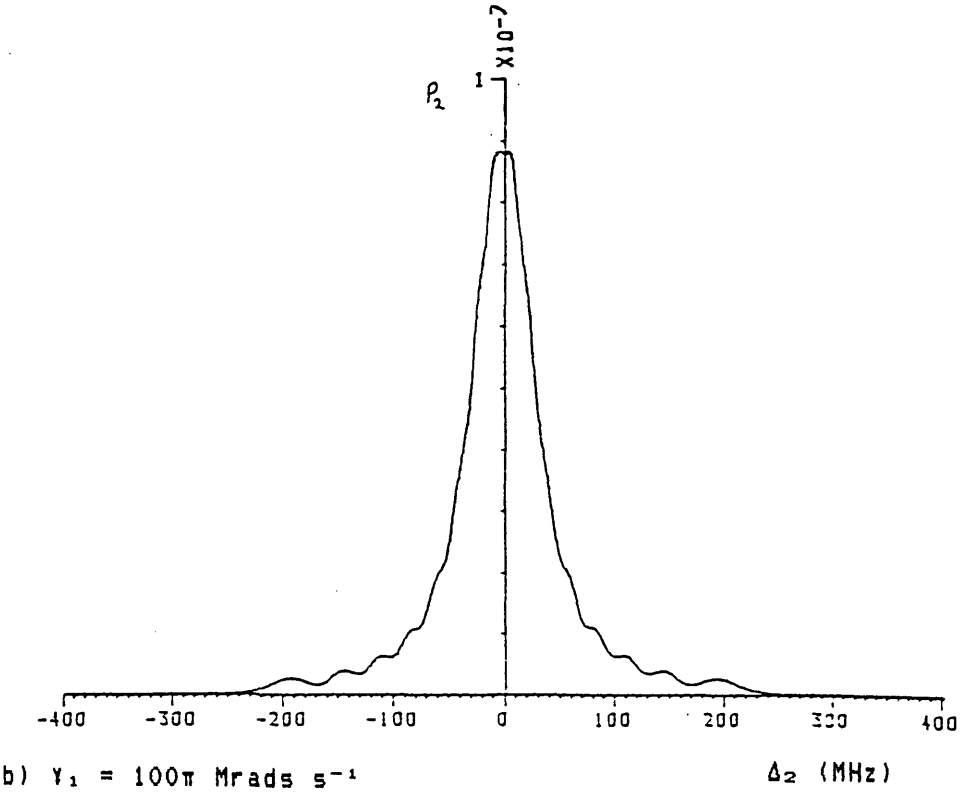
$$\theta(t) = \theta^\circ\int_{-\infty}^{t}\frac{\exp(-dt'/2\sigma^2)dt'}{\sqrt{2\pi}\sigma} = \frac{\theta^\circ}{4}(1+\mathrm{erf}(t/\sqrt{2}\sigma)) \qquad 3.3,10$$

which is normalised so that $\theta(t\to\infty) = \theta^\circ$. Substituting this into equation 7 gives

$$c_2'(t) = -\exp(-i\Delta_2 t)\frac{\Omega_2}{2}\int_{-\infty}^{t}\exp(i\Delta_2 t')\sin\{\frac{\theta^\circ}{2}(1+\mathrm{erf}(t'/\sqrt{2}\sigma))\}dt' \qquad 3.3,11$$



a) $\gamma_1 = 0$



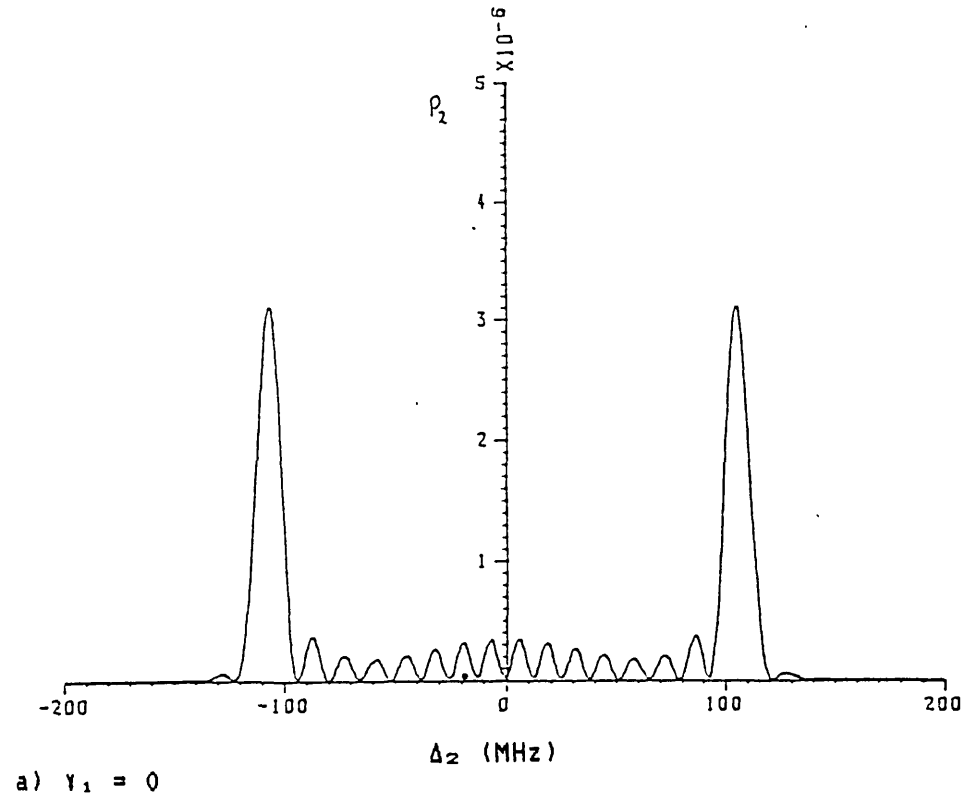
b) $\gamma_1 = 100\pi$ Mrads s^{-1}

Fig 3.3.ii

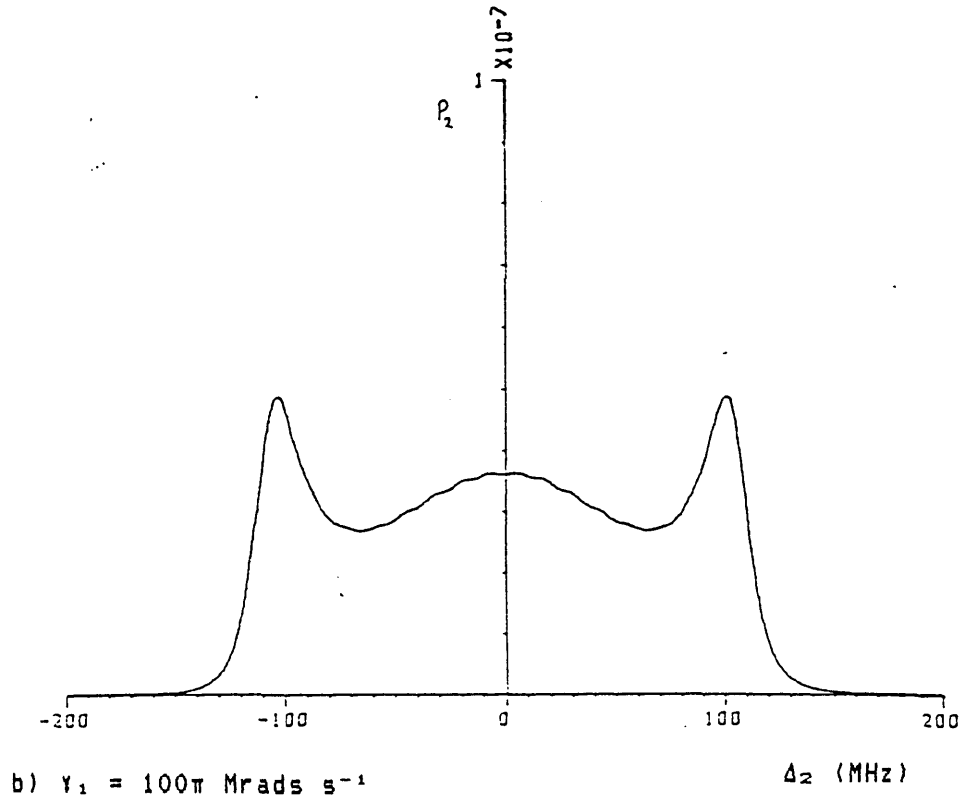
Stark splittings for Gaussian pump and flat probe,

$\Omega_1 = 1000$ Mrads s^{-1}, $\Omega_2 = 0.1$ Mrads s^{-1},

$\Delta_1 = \gamma_2 = 0$ and $t = 0.1$ μs.



a) $\gamma_1 = 0$



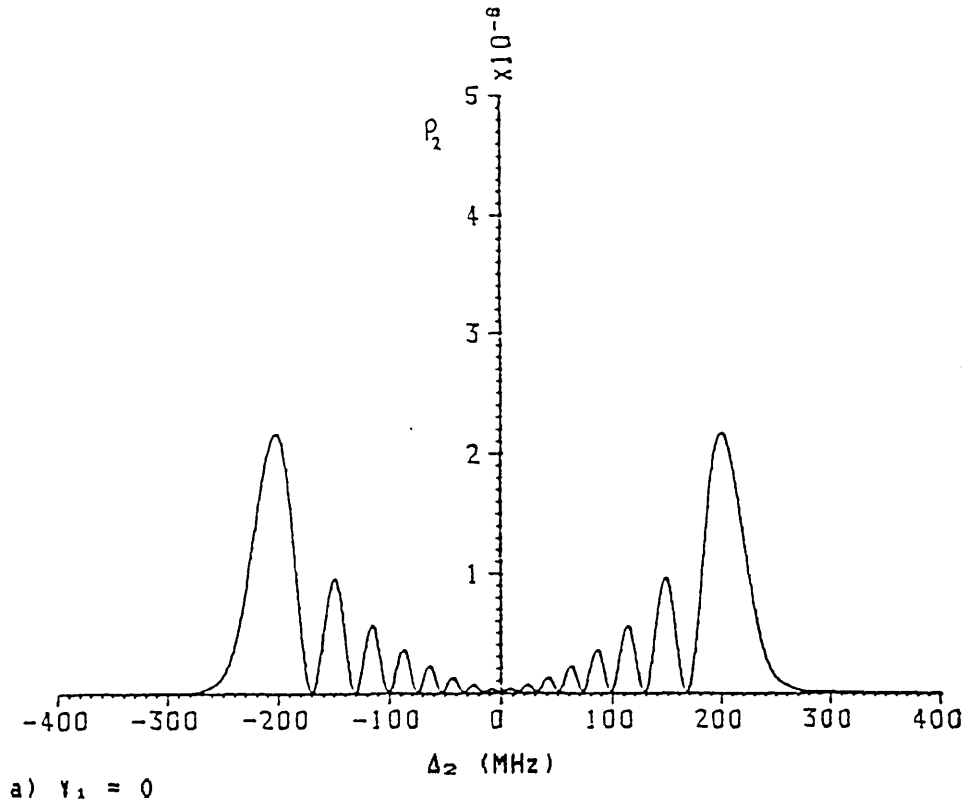
b) $\gamma_1 = 100\pi$ Mrads s^{-1}

Fig 3.3.iii

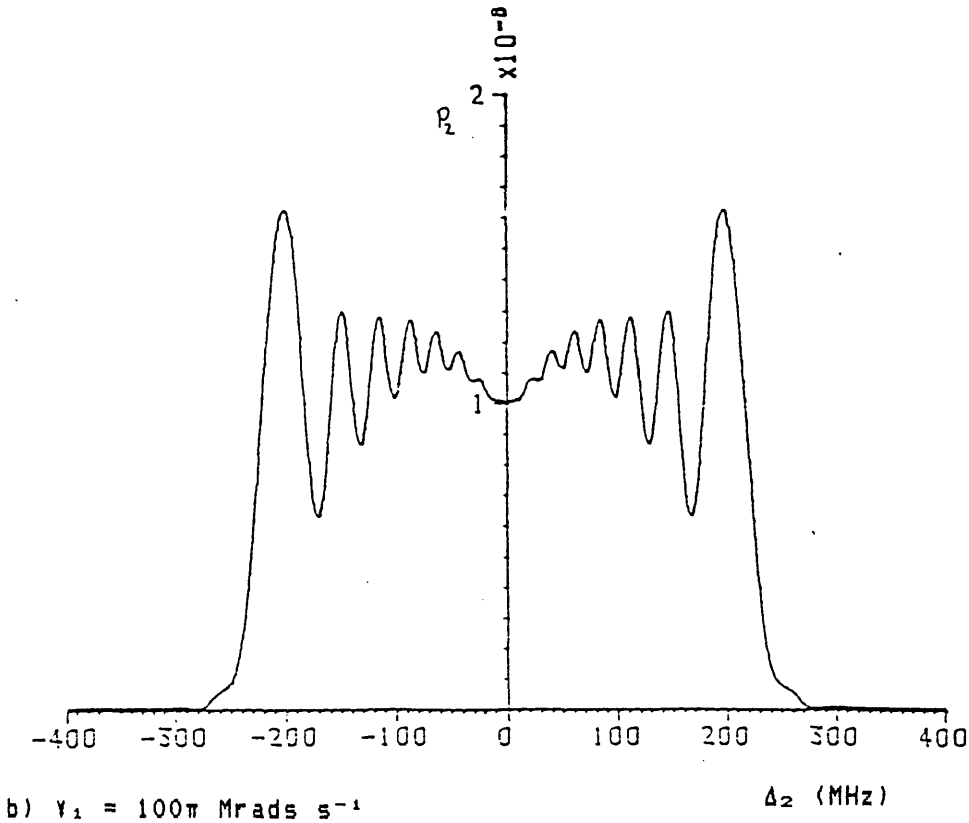
Stark splittings for F-T-G pump and flat probe,

$\Omega_1 = 1000$ Mrads s^{-1}, $\Omega_2 = 0.1$ Mrads s^{-1},

$\Delta_1 = \gamma_2 = 0$ and $t = 0.1$ μs.



a) $\gamma_1 = 0$



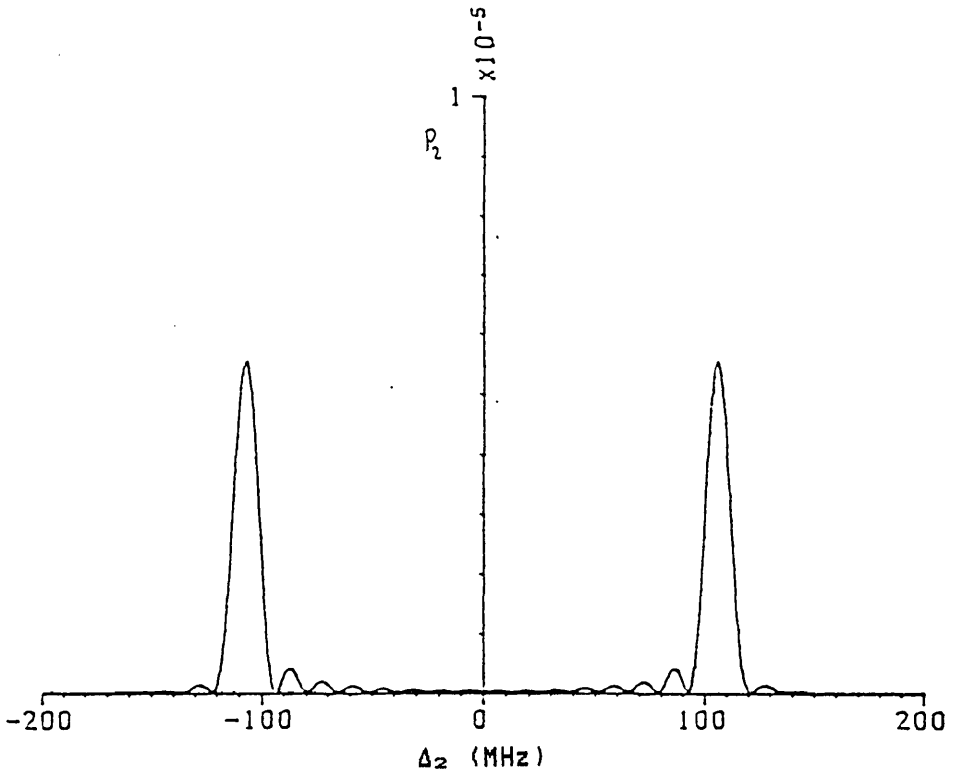
b) $\gamma_1 = 100\pi$ Mrads s^{-1}

Fig 3.3.iv

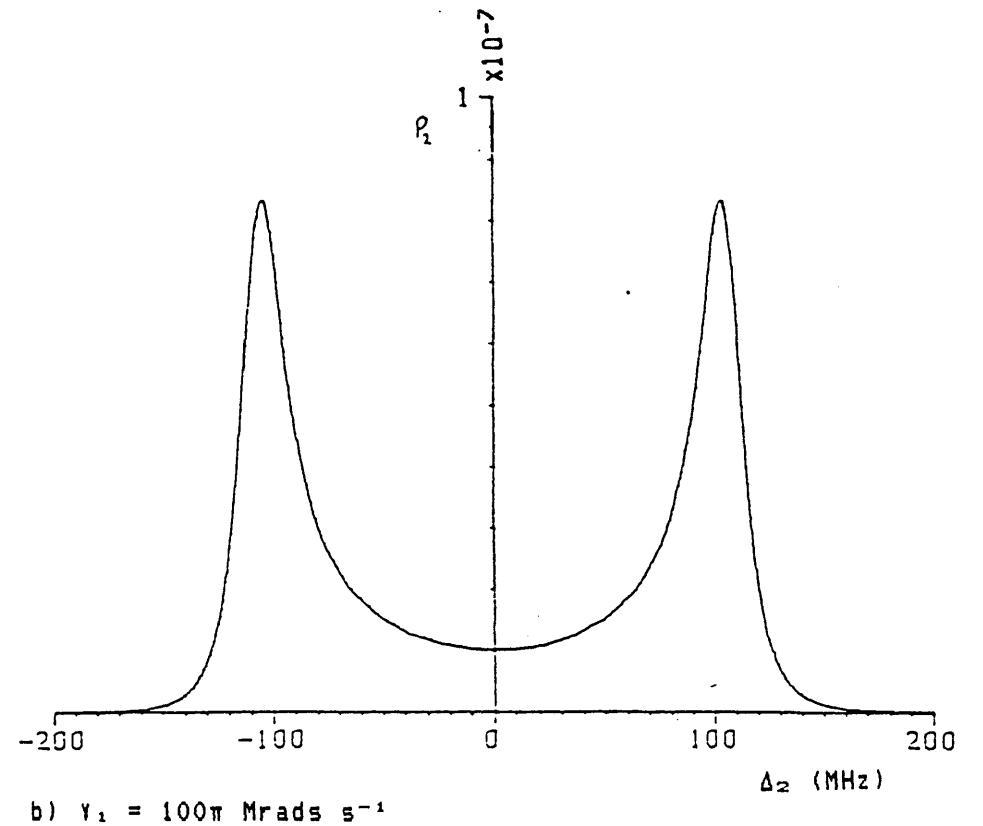
Stark splittings for two Gaussian pulses,

$\Omega_1 = 1000$ Mrads s^{-1}, $\Omega_2 = 0.1$ Mrads s^{-1},

$\Delta_1 = \gamma_2 = 0$ and $t = 0.1$ μs.



a) $\gamma_1 = 0$



b) $\gamma_1 = 100\pi$ Mrads s^{-1}

Fig 3.3.v

Stark splittings for two F-T-G pulses,

$\Omega_1 = 1000$ Mrads s^{-1}, $\Omega_2 = 0.1$ Mrads s^{-1},

$\Delta_1 = \gamma_2 = 0$ and $t = 0.1$ μs.

which can be solved numerically. This yields identical results to those in fig iia which shows the TDO results for a Gaussian pump pulse, of area $2\theta(t\rightarrow\infty) = 100$ rads as in fig ia, and a flat probe. The other parameters are as in fig ia. Fig iib shows these results with the same decay included as in fig ib. Figs iiia and b show the results for flat topped Gaussian pulses. With the Gaussian pump pulse the two outer peaks are separated by more than for the flat pulse case. The instantaneous Rabi frequency is changing and the results are a time average of the peaks as they move apart and then together again. The maximum separation is determined by the peak Rabi frequency, which for the Gaussian of area 100 rads is about 450 MHz. The oscillations in between the two peaks are caused as the pulse builds up and decays away. Including decay from the middle level totally destroys the Stark splitting effect and means that it would be unobservable for these parameters. The results for the flat topped Gaussian in figs iia and b show outer peaks, due to the long flat top, and small oscillations in between, due, again, to the rise and fall of the pulse. The width of the outer peaks is slightly more than for the flat pulse case as the pulse is effectively narrower by about 20%. In this case including decay from the middle level does not quite destroy the splittings. An asymptotic expansion solving equation 7 can be found in Greenland 1985. This paper also describes the Airy function nature of the oscillations between the main peaks for the cases in which the pump beam is resonant. All of the cases described so far have had a constant probe pulse. However, if good Stark splittings are required then it is advantageous to have the probe pulse of the same shape as the pump beam. Figs iva and b show the effect of having a Gaussian probe and a Gaussian pump. The Stark splitting becomes clearer and is even observable in the case where damping is included. This effect is caused by the probe probing the population in the middle level more when the pump beam is stronger, as they are now similar in shape. Thus a greater contribution to the upper state population occurs at a greater Stark splitting. Figs 3.3va and b show the same effect for flat topped Gaussian pulses. Again, the splittings are much more apparent than in the case where the probe is flat. It is therefore advantageous to have a probe of the same shape as, and coincident with, the pump beam if Stark splittings are to be observed.

If the pump beam is brought out of resonance with the lower

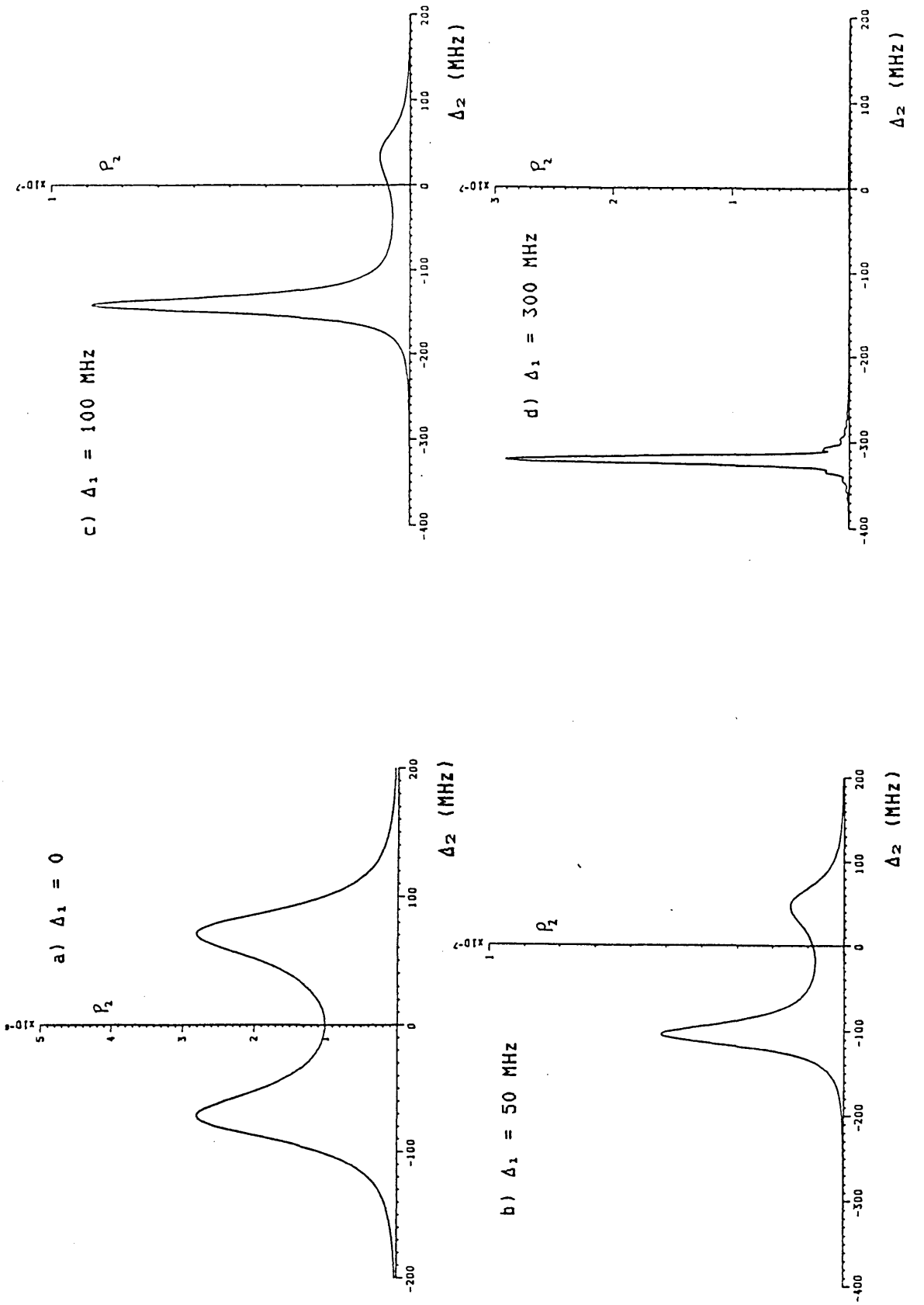


Fig 3.3.vi

Stark splittings for two flat pulses and an off resonance main beam,

Ω_1 = 1000 Mrads s^{-1}, Ω_2 = 0.1 Mrads s^{-1},

γ_1 = 200π Mrads s^{-1} and t = 0.1 μs.

transition frequency then the splittings are shifted and become asymmetric. This can be seen from figs via,b,c and d where the detuning, Δ_1, is given by 0, 50, 100 and 300 MHz respectively. The other parameters are γ_1 = 200π Mrads s^{-1}, Ω_1 = 1000 Mrads s^{-1}, Ω_2 = 0.1 Mrads s^{-1}, t_{max} = 0.1 μs and both the pulses are flat. Including a detuning, and/or decay, causes equations 3 to become

$$\dot{c}_ó = i\frac{\Omega_1}{2}(t)c_í \ , \qquad 3.3,12a$$

$$\dot{c}_í = i\frac{\Omega_1}{2}(t)c_ó - i\Delta_1 c_í \qquad 3.3,12b$$

and

$$\dot{c}_ź = i\frac{\Omega_2}{2}c_í - i(\Delta_1+\Delta_2)c_ź \qquad 3.3,12c$$

where, to enable an analytic solution, Ω_1 is restricted to being constant. These can be solved to give

$$c_í(t) = i\frac{\Omega_1}{\Omega_i}\exp(-i\frac{\Delta_1}{2}t)\sin(\frac{\Omega_i}{2}t) \qquad 3.3,13$$

where Ω_i is the off resonance Rabi frequency given by

$$\Omega_i = (\Omega_1^2 + \Delta_1^2)^{1/2}. \qquad 3.3,14$$

This is the solution for a flat pump pulse, off resonance by Δ_1, turning on at time t = 0. Substituting the new form for $c_í$ into equation 12c gives the solution for $c_ź$ as

$$c_ź(t) = -\exp(-i(\Delta_1+\Delta_2)t)\frac{\Omega_2\Omega_1}{2\Omega_i}\int_0^t \exp(i\frac{(\Delta_2+\Delta_1)}{2}t')\sin(\frac{\Omega_i}{2}t')dt' \qquad 3.3,15$$

$$= i\frac{\Omega_2 t}{4}\frac{\Omega_1}{\Omega_i}\exp(-i(\Delta_1+\Delta_2)t)\{\exp(i\delta_1 t)\mathrm{sinc}(\delta_1 t) - \exp(-i\delta_2 t)\mathrm{sinc}(\delta_2 t)\} \qquad 3.3,16$$

where

$$\delta_1 = \frac{(\Omega_i + 2\Delta_2 + \Delta_1)}{4} \qquad 3.3,17a$$

and

$$\delta_2 = \frac{(\Omega_i - 2\Delta_2 - \Delta_1)}{4} \; . \qquad 3.3,17b$$

For $\Omega_1 \gg 1/t$, and with Δ_1 real, ie with no decay, the population can be written

$$P_2(t) = \left(\frac{\Omega_2 t \Omega_1}{4\Omega_i}\right)^2 (\mathrm{sinc}^2(\delta_1 t) + \mathrm{sinc}^2(\delta_2 t)) \; . \qquad 3.3,18$$

These are two sinc squared functions, of the same height, centred on

$$\Delta_2 = \frac{(-\Delta_1 \pm \Omega_i)}{2} \; . \qquad 3.3,19$$

However, if there is also decay from the middle level the peaks are also altered in height to become asymmetric. Assuming, again, that $\Omega_1 \gg 1/t$ then the two terms are given by

$$P_2(t) = \left(\frac{\Omega_2 t \Omega_1}{4}\right)^2 \left|\frac{e^{-i(\Delta_1+\Delta_2)t}}{|\Omega_1'|^2}\right|^2 \left\{ \left|\frac{e^{2i\delta_1 t}-1}{2\delta_1 t}\right|^2 + \left|\frac{1-e^{-2i\delta_2 t}}{2\delta_2 t}\right|^2 \right\} \qquad 3.3,20$$

So the detuning causes a shift in the peaks whilst the decay is predominantly responsible for the asymmetry. In the limit that $\Omega_1 \ll \Delta_1$ then

$$\Omega_i \sim \Delta_1 , \qquad 3.3,21a$$

$$\delta_1 \sim \frac{(\Delta_1 + \Delta_2)}{2} \qquad 3.3,21b$$

and

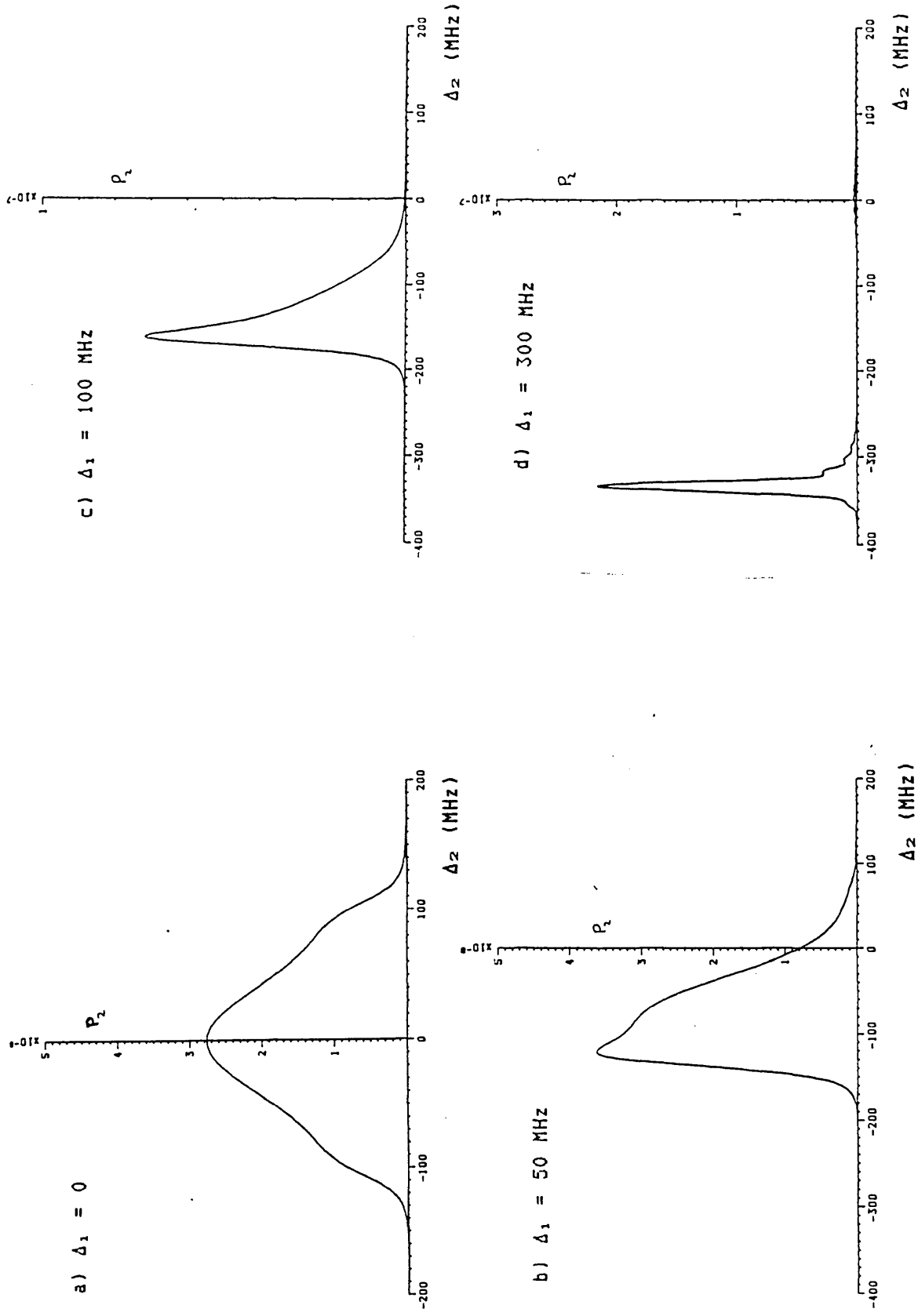


Fig 3.3.vii

Stark splittings for two F-T-G pulses and an off resonance main beam,

Ω_1 = 1000 Mrads s^{-1}, Ω_2 = 0.1 Mrads s^{-1},

γ_1 = 200π Mrads s^{-1} and t = 0.1 μs.

$$\delta_2 \sim -\frac{\Delta_2}{2} \qquad 3.3,21c$$

and equation 16 reduces to the wholly perturbative solution given in equation 3.2,17. Under these circumstances the resonances occur at $\Delta_2 = -\Delta_1$ and 0. $\Delta_2 = -\Delta_1$ corresponds to the two photon transition resonance and becomes less affected by the decay from the middle level as Δ_1 increases. $\Delta_2 = 0$ corresponds to the stepwise transition resonance and becomes relatively more and more depleted as Δ_1 increases causing the resonance to widen and diminish. Figs viia,b,c and d show the off resonance Stark splittings for two flat topped Gaussian pulses. Apart from the pulse shape, the parameters are as in fig vi. In this case the damping is too great to allow the Stark peaks to be observed.

Stark splittings have now been observed in experiments by many different groups. Picqué and Pinard 1976 use a sodium atomic beam with the $3^2S_{1/2}$, F=2 to $3^2P_{3/2}$, F=3 transition strongly excited and with a probe field scanning around the $5^2S_{1/2}$, F=2 level. The population in the $5^2S_{1/2}$ state, which decays to the 4P and 3P excited states, is monitored by the spontaneous emission of UV, at 330 nm, from the 4P state. Delsart and Keller 1976 investigate the dependence of the pump power on the splitting, showing the formation of the double peaks as the power of the saturating laser is increased. They saturate the $1S_5$ to $2P_4$ transition in neon with a CW dye laser and measure the transmission of a weak probe from a He-Ne laser tuned around the $2S_2$ level. Schuda, Stroud and Hercher 1974 observe the spectrum of resonantly scattered light at right angles to a sodium atomic beam. The F = 2 → 3 hyperfine component of the D_2 ($3^2S_{1/2}$, $3^2P_{3/2}$) line is strongly excited with a CW dye laser and the spectrum observed for various detunings. Hogan etal 1978 ionise the population in the $4D_{3/2}$ level of sodium to observe the Stark doublet formed by a saturating laser tuned to the $3S_{1/2} \rightarrow 3P_{1/2}$ transition in sodium vapour. They observe the symmetry of the two peaks as the lower transition laser is detuned from resonance. In each case the exciting pulses are formed sufficiently long such that any of the pulse shape effects described here are not observed.

3.4 Conclusions

This chapter shows some of the effects caused by the excitation of a three level system with pulsed lasers. The predominant features of a non-constant pulse envelope are the increases in both the transform bandwidth and peak power over flat pulses of the same area. The increase in bandwidth causes smaller, but wider, resonances whilst the variation in the Rabi frequency is responsible for the destruction of Stark splittings which depend upon the instantaneous Rabi frequency.

Various analytical models are compared to the computational solution giving good agreement for the special cases required. This gives confidence in the new phenomena predicted by the Time Development Operator method for the analytically insoluble cases.

The importance of the pulse area, as measured by the integral over all time of the Rabi frequency, in the calculation of the final population distribution is seen in equation 3.2,8. This is a more fundamental parameter than the total energy of the pulse which is proportional to the integral, over time, of the intensity, or Rabi frequency squared.

Clear advantages are seen in the excitation of the upper level by using counter-propagating beams if the system is influenced by Doppler effects, see section 3.2.2. Thus, even in an atomic beam, where the transverse Doppler widths are relatively small, a much larger upper state population is induced by exciting the two transitions with laser beams travelling in opposite directions. This reduces the two-photon detuning due to the Doppler effect although the single-photon detuning from the middle level remains unaltered.

Section 3.3 shows the advantage of using pump and probe laser pulses of the same shape, in order to see the Stark splittings of the lower levels, for cases where the pulses are not of constant amplitude. It also shows the effects of decay in broadening the Stark peaks such that for large decays the individual peaks are not resolvable.

Thus pulse shape effects are important in the bound/bound transitions investigated here. In most cases it is not sufficient to model experiments using 'equivalent' flat pulses if the rise and fall times are significant.

The bandwidth included in this chapter is due to the transform width of the pulse due to its temporal shape. Another temporal effect

is the bandwidth caused by fluctuations in the phase. In the next chapter the effects of this sort of bandwidth are investigated. These two sorts of bandwidth are fundamentally different because of the importance of the coherence of the exciting beam. Bandwidth caused by pulse shape does not affect the coherence, whilst phase fluctuation bandwidth is a measure of the incoherence. In the next chapter phase fluctuation bandwidth is included in the model as a temporal process along with the pulse shape.

3.5 References

Allen L., Eberly J.H., 1975
'Optical Resonance and Two-Level Atoms'
Wiley, New York, 1975

Delsart C., Keller J.C., 1976
Observation of the optical Autler-Townes splitting in neon gas with a cascade level scheme
J. Phys. B 9 (1976) 16, 2769-2775

Delsart C., Keller J.C., Kaftandjian V.P., 1981
Investigation of the dynamic Stark effect of a J=0 → J=1 optical transition
J. de Physique 42 (1981) 529-536

Feneuille S., 1977
Interaction of laser radiation with free atoms
Rep. on Prog. in Phys. 40 (1977) 11, 1257-1304
and references within

Fisk P.T.H., Bachor H.A., Sandeman R.J., 1984
Observation of the dynamic Stark effect in a J=0 → 1 → 0 three level Doppler free system
EGAS meeting Imperial College, London 1985; to be published

Gray H.R., Stroud C.R. Jr., 1978
Autler-Townes effect in double optical resonance
Opt. Comm. 25 (1978) 3, 359-362

Gray H.R., Whitley R.M., Stroud C.R. Jr., 1978
Coherent trapping of atomic population
Opt. Lett. 3 (1978) 218-220
and references within

Greenland P.T., 1985
The double optical resonance spectrum for arbitrary pulse shapes
J. Phys. B 18 (1985) 401-413

Hodgkinson D.P., Briggs J.S., 1977
Doppler free two photon absorption with a near resonant intermediate state
Opt. Comm. 22 (1977) 1, 45-48

Hodgkinson D.P., Wort D.J.H., 1981
Doppler-free two-photon excitation of U^{238}
J. Phys. B 14 (1981) 3891-3903

Hogan P.B., Smith S.J., Georges A.T., Lambropoulos P., 1978
A.C. Stark splitting in resonant multiphoton ionisation with broadband lasers
Phys. Rev. Lett. 41 (1978) 4, 229-232

Kaivola M., Bjerre N., Poulsen O., Javanainen J., 1984
Observation of population trapping in a two-photon resonant three-level atom
Opt. Comm. 49 (1984) 6, 418-422

Knight P.L., Milonni P.W., 1980
The Rabi frequency in optical spectra
Physics Reports 66 (1980) 2
and references within

Nayfeh M.H., Nayfeh A.H., 1979
Double resonance with pulsed fields
Phys. Rev A 19 (1979) 4, 1666-1672
and references within

Picqué J.L., Pinard J., 1976
Direct observation of the Autler-Townes effect in the optical range
J. Phys. B 9 (1976) 5, L77-L81

Radmore P.M., Knight P.L., 1982
Population trapping and dispersion in a three level system
J. Phys. B 15 (1982) 561-573

Sargent M, Scully M.O., Lamb W.E. Jr., 1974
'Laser Physics'
Addison-Wesley, New York, 1974

Schuda F., Stroud C.R. Jr., Hercher M., 1974
Observation of the resonant Stark effect at optical frequencies
J. Phys. B 7 (1974) 7, L198-L209

Swain S., 1982
Conditions for population trapping in a three level system
J. Phys. B 15 (1982) 3405-3412

Thomas G.F., 1983
Validity of the Rosen-Zener conjecture for Gaussian modulated beams
Phys. Rev. A 27 (1983) 5, 2744-2746

Whitley R.M., Stroud C.R. Jr., 1976
Double optical resonance
Phys. Rev. A 14 (1976) 4, 1498-1513

Woodgate G.K., 1970
'Elementary Atomic Structure'
McGraw-Hill, London, 1970

CHAPTER 4

A realistic two level system

4.0 Introduction

The understanding of the interaction of complex atoms with radiation is economically very important. The demand for efficient isotope separation methods in uranium is constantly increasing due to the rising demand for the isotopes for use in atomic reactors. The current separation methods, mainly diffusive and centrifugal, rely on the different masses of the isotopes. The relative masses are so close for the heavy atoms that these processes are very inefficient. The advantage of laser isotope separation, where the separation is due to the different electron energy levels, is in the selectivity. The method would not necessarily be 100% efficient in collecting all of the required species, but those that were collected would be almost pure. This is in contrast to the current methods where a sample is repeatedly processed until its overall purity has reached the required level. For these reasons it is very desirable to aquire as much knowledge of these complex atoms as is possible.

The previous chapter deals with the solutions of a three level system interacting with a simple pulsed laser field. These are idealised conditions where the laser has no bandwidth, apart from its transform width, and the transitions involved are non-degenerate.

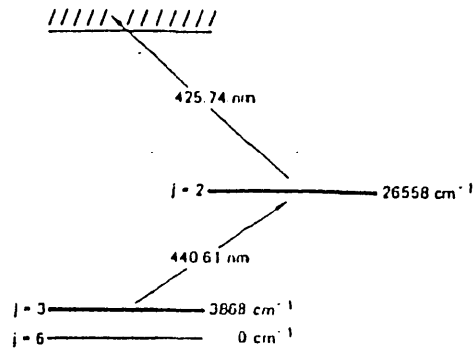


Fig 4.0.i

The uranium levels used in the experiment (taken from SHJR).

Unfortunately, these conditions are not always attainable in a real

experiment. This chapter deals with a simpler, two level system but includes many of the effects found in reality, such as magnetic sublevel degeneracy, Doppler effects and laser bandwidth, pulse shape and frequency fluctuations. Experiments have been done on simpler two level systems (see for example Grieneisen, Kurnit and Szöke 1971 and MacGillivray, Pegg and Standage 1978 where fluctuations in the frequency, intensity and phase of the pulse are unimportant or are ignored) in which the effects of the Rabi frequency can been seen. To determine whether such effects survive with more complex atoms and laser pulses an experiment to observe Rabi oscillations in a two level transition in uranium was carried out by Scarl, Hackel, Johnson and Rushford 1981 [SHJR] see fig i. This chapter attempts to model the effects found in this experiment, explaining in more detail the results in Lauder and Greenland 1984.

4.1 The Experiment

The sort of phenomena which need to be included result mainly from degrees of uncertainty in what is known about the laser and the irradiated system. Everything which is assigned a value, eg intensity, pulse length and detuning etc, has associated with it an uncertainty. Some of the uncertainties have well defined distributions and only complicate the theoretical analysis by forcing additional averaging. Other processes have unknown distributions and models have to be chosen and justified so that the distributions can be calculated.

In this experiment the uranium atoms have a velocity distribution and, because of the non-zero J values, magnetic sublevels. These lead to a detuning distribution because of the Doppler effect in the collimated atomic beam, and more than one Rabi frequency because of the different electric dipole moments between the magnetic sublevels. The laser field is pulsed and the shape has to be approximated. Shot to shot fluctuations in the laser pulse cause the intensity and mean detuning to vary. Phase fluctuations within a shot cause bandwidth in addition to the transform width. All these effects are to be modelled in this analysis.

The atomic effects, the variation in dipole matrix elements between the sublevels and the Doppler effect, are treated in sections 4.2.1 and 4.2.2. The laser effects, pulse shape, intensity fluctuations, frequency fluctuations and bandwidth, are treated in sections 4.3.1, 4.3.2, 4.3.3 and 4.3.4.

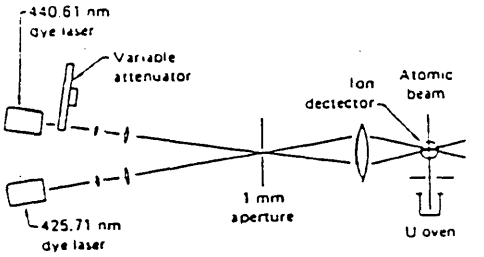


Fig 4.1.i
The experimental setup (taken from SHJR).

The experimental setup is shown in fig i. The atomic uranium beam is formed by two slits, 1 mm wide, 10 mm long and 20 mm apart, collimating the effusive output of a tungsten oven at 1750 K

containing a uranium rhenide source. The bisector of the 5° angle between the laser beams is perpendicular to the atomic beam, and intersects at a point where the atomic density is 10^9 cm^{-3}. Two pulsed dye lasers are used to irradiate the atomic beam. The 440.61 nm laser is used to excite the two level transition and is pumped by a Molectron nitrogen laser at a repetition rate of 19 Hz and with a pulse width of around 10 ns FWHM. Final tuning of the exciting laser is achieved by maximising the number of ions detected. The pulse is passed through a variable attenuator with density range 0 to 2, that is the output intensity is varied between a factor of 1 and 1/100 of the input intensity. Only the centre part of the beam is used so that the intensity is nearly uniform, within ±20%, over the interaction area.

The first laser pulse is followed by a second pulse at 425.74 nm which is used to ionise the atoms which are left in the upper of the two relevant states. This is a modified Molectron dye laser pumped by a second Molectron nitrogen laser. The intensity is 10^9 Wm^{-2} in a 5 ns pulse and saturates the transition from the 26558 cm^{-1} level to an autoionising level in the continuum. The ions are collected by a Galileo Channeltron electron multiplier producing 10^6 electrons per ion detected. This output pulse is averaged over the 10 μs that it takes the ions produced to be detected, and further averaged over 3 pulses by a box car averager. This is again averaged over a three minute period in which the variable attenuator rotates 30 times and the lasers pulse around 3500 times. Thus the ion current can be observed as a function of time. The time scale can be converted to an intensity scale by using the attenuator in conjunction with a linear photo-diode, which is then converted to an electric field scale. The final graphs are plots of the upper (26558 cm^{-1}) state population after the exciting pulse against the peak electric field of the pulse.

4.2 Modelling the atoms

In the experiment of Scarl et al the relevant levels in the uranium atom are the J=3 state at 3868 cm^{-1} and J=2 state at 26558 cm^{-1}. These are irradiated by a pulsed laser and later ionised, to an autoionising level in the continuum, using another pulsed laser. It is assumed that all the atoms left in the upper state after the exciting pulse are ionised so that the ion count corresponds exactly to the final upper state population. The aim of the experiment is to observe Rabi oscillations in a complex atom. This will manifest itself as an oscillation in the upper state population as a function of peak laser field. Rabi oscillations are usually observed as an oscillation in population of a level against time for a fixed Rabi frequency. In this case the population is observed at a fixed time, whilst varying the Rabi frequency by increasing the peak field.

Assuming thermal population of the levels in the oven then the ratio of the number of atoms in the ground state to the number in the excited state is given by $\exp(h(\nu_1-\nu_0)/kT):1$. For the levels involved, $\nu_1 = c/\lambda_1 = 7.97\ 10^{14}$ Hz, $\nu_0 = 1.16\ 10^{14}$ Hz, and a temperature of 1750 K this ratio is exp(17):1. Therefore the initial population in the excited state is assumed to be zero.

The ratio of the population in the true ground state to the population in the lower of the two resonant levels is 20:1. Thus only around 5% of the uranium atoms in the beam are used in the excitation. However, this is ample as ion detection is very sensitive. Population decay times are estimated to be of order 50 ns [Greenland 1985] and are therefore negligible when compared to the exciting pulse width of around 5 ns.

4.2.1 Magnetic sublevels

The non-zero J values lead to the levels having magnetic sublevels of equal energies, as the hyperfine structure is not present in U^{238} because of the symmetry of the nucleus. Thus the lower level, J=3, has seven and the upper level, J=2, five sublevels. The pulsed laser used is linearly polarised and so the transitions induced are $\Delta m = 0$ transitions, where m labels the sublevel. Thus the allowed transitions are as shown in fig i. The laser pulse duration is sufficiently short and the density of atoms sufficiently small such that collisional mixing between the sublevels can be ignored.

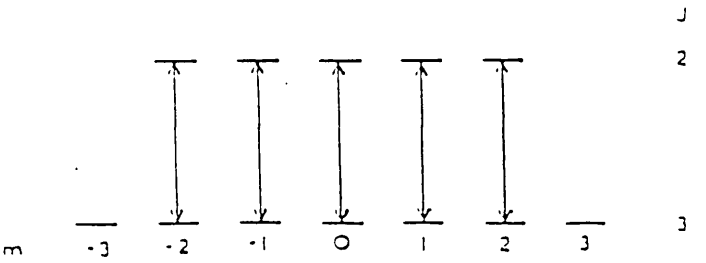


Fig 4.2.i

The allowed transitions for linearly polarised light.

The interaction time is around 5 ns and the beam density is around 10^{15} m^{-3}. The atomic velocity = $\sqrt{kT/m}$ = 2 10^{2} ms^{-1}. Thus in 5 ns the effective volume swept out is $2\pi r^2$ 10^{-6} $\sim 10^{-23}$ m^3. The dipole matrix element between the levels is dependent upon the magnitude of m for the transition. Thus it can be seen that, assuming all the lower sublevels are initially equally populated, 2/7 of the population can never be excited. Furthermore the transitions have different Rabi frequencies associated with them. This in itself leads to a more complex evolution due to the superposition of the different oscillation frequencies involved. This, however, is a simple effect to include in the model as the relative dipole matrix elements are well known [Condon and Shortley 1935]. If μ_o is the dipole matrix element for the m = 0 transition then the element for the m = ±1 transition is given by $\mu_1 = \mu_o\sqrt{8/9}$ and that for the m = ±2 is given by $\mu_2 = \mu_o\sqrt{5/9}$. The m = 0 dipole matrix element μ_o is one of the fitting parameters of the experiment.

4.2.2 Doppler widths

The atoms are in an atomic beam irradiated at approximately right angles by the laser beams. The transverse velocity distribution in the beam is large enough to cause a significant detuning distribution due to the Doppler effect. Knowledge of the geometry of the beam and the temperature of the oven allows a calculation of the detuning distribution, so that this can be included in the model. The temperature of the atoms in the oven is given to be 1750 K, the atoms are U^{238} and the collimating slits are 1 mm wide and 20 mm apart. The two lasers are incident on the beam such that the bisector of the 5°

angle between the two laser beams is normal to the atomic beam. Within the oven the velocity distribution is assumed to be a Boltzmann distribution. That is

$$P(v_x,v_y) = \frac{1}{2\pi\sigma_D^2}\exp\{-(v_x^2+v_y^2)/2\sigma_D^2\} \qquad 4.2,1$$

where $\sigma_D^2 = kT/m$.

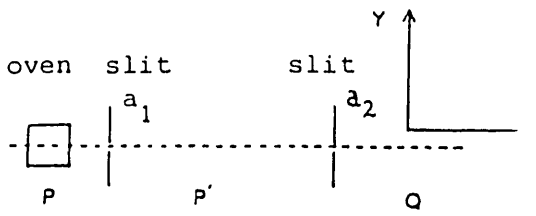


Fig 4.2.ii
The uranium beam collimator.

Only the x and y spatial components are considered, where x is the atomic beam axis and y is the direction of the laser beams, see fig ii. In the experiment the laser beams were each 2.5° away from the perpendicular to the atomic beam. This is assumed negligible and both lasers are assumed to be perpendicular to the beam, ie both along the y axis; for the effects of non-perpendicular observation angles see Greenland, Lauder and Wort 1985. Thus in the oven the distribution is given by $P(v_x,v_y)$. The flow into region P' is assumed to be effusive, that is the hole is small and the rate of escape of the atoms is small enough such that thermal equilibrium in the oven is not upset. The distribution in this region is weighted by v_x because the atoms with a larger v_x escape at a greater rate. Therefore

$$P'(v_x,v_y) = \frac{1}{\sqrt{2\pi}\,\sigma_D^3} v_x\exp\{-(v_x^2+v_y^2)/2\sigma_D^2\} \quad v_x>0. \qquad 4.2,2$$

The v_y dependence in region Q, after the second slit, is given by

$$Q(v_y)dv_y = \frac{1}{a_1}\int_{-\frac{a_1}{2}}^{\frac{a_1}{2}} dy \int_{v_x^{min}}^{v_x^{max}} dv_x \; P'(v_x, v_y)\; dv_y. \qquad 4.2,3$$

Where $v_x^{max}(y,v_y)$, $v_x^{min}(y,v_y)$ are the maximum and minimum values of v_x which will allow an atom at point y, in the first slit, with transverse velocity v_y to travel through the second slit. The slit width a_1 is restricted to $a_1 \ll a_2$ for ease of calculation. This includes the case that is required where $a_1 = a_2 = a$, and also another special case where $a_1 \to 0$, ie a pinhole source. Thus

$$v_x^{max} = \infty \qquad 4.2,4a$$

and

$$v_x^{min} = v_y\, L/(a_2/2 - y) \quad \text{for } v_y > 0 \qquad 4.2,4b$$

$$= |v_y| L/(a_2/2 + y) \quad \text{for } v_y < 0. \qquad 4.2,4c$$

So that

$$Q(v_y)dv_y = \frac{dv_y}{a_1}\int_{-\frac{a_1}{2}}^{\frac{a_1}{2}} dy \int_{\left(\frac{Lv_y}{\frac{a_2}{2}-y}\right)}^{\infty} dv_x \; P'(v_x, v_y) \quad v_y > 0 \qquad 4.2,5a$$

$$= \frac{dv_y}{a_1}\int_{-\frac{a_1}{2}}^{\frac{a_1}{2}} dy \int_{\left(\frac{L|v_y|}{\frac{a_2}{2}+y}\right)}^{\infty} dv_x \; P'(v_x, v_y) \quad v_y < 0. \qquad 4.2,5b$$

For $v_y < 0$ and if $y \to -y$ then the equations become identical provided that $v_y \to |v_y|$. Thus

$$Q(v_y)dv_y = \frac{dv_y}{a_1}\int_{-\frac{a_1}{2}}^{\frac{a_1}{2}} dy \int_{\left(\frac{L|v_y|}{\frac{a_2}{2}-y}\right)}^{\infty} dv_x \; P'(v_x, v_y). \qquad 4.2,6$$

Substituting for $P'(v_x,v_y)$ gives

$$Q(v_y)dv_y = \frac{P(v_y)dv_y}{a_1\sigma_D^2}\int_{-\frac{a_1}{2}}^{\frac{a_1}{2}}dy\int_{\frac{L|v_y|}{(\frac{a_2}{2}-y)}}^{\infty}dv_x\ v_x\exp(-v_x^2/2\sigma_D^2) \qquad 4.2,7$$

$$= \frac{P(v_y)dv_y}{a_1}\int_{-\frac{a_1}{2}}^{\frac{a_1}{2}}dy\ \exp\left\{\frac{-L^2|v_y|^2}{(a_2/2-y)^2 2\sigma_D^2}\right\}. \qquad 4.2,8$$

This is now not normalised as those atoms which do not pass through the second slit are lost. Appendix 4.A gives the normalisation and evaluation of the integral to give

$$Q(v_y)dv_y = a_1\frac{P(v_y)dv_y}{L(T_+-T_-)}\left\{\frac{(a_2+a_1)}{2}\exp(-\Sigma_+^2) - \frac{(a_2-a_1)}{2}\exp(-\Sigma_-^2)\right.$$
$$\left. + \sqrt{\frac{\pi}{2}}\frac{L|v_y|}{a_1\sigma\Delta}\left[\mathrm{erf}(\Sigma_+)-\mathrm{erf}(\Sigma_-)\right]\right\} \qquad 4.2,9$$

where

$$\Sigma_\pm = \frac{L|v_y|\sqrt{2}}{\sigma_D(a_2\pm a_1)} \qquad \text{and} \qquad T_\pm = \left\{1 + \left[\frac{a_2\pm a_1}{2L}\right]^2\right\}^{1/2}$$

For the case where $a_2 = a_1 = a$ then this reduces to

$$\underset{a1=a2=a}{Q(v_y)dv_y} = \frac{aP(v_y)dv_y}{L\{(1+(\frac{a}{L})^2)^{1/2}-1\}}\left\{\exp(-\Sigma^2) + \sqrt{\pi}\Sigma(\mathrm{erf}(\Sigma)-1)\right\} \qquad 4.2,10$$

where

$$\Sigma = \frac{L|v_y|}{\sqrt{2}\sigma_D a}.$$

For the case where $a_1 = 0$, $a_2 = a$ ie a pinhole source, then this reduces to

$$Q(v_y)dv_y \underset{a_1=0,a_2=a}{=} \frac{dv_y}{\sqrt{2\pi}\,\sigma_\Delta} \exp\left\{\frac{-v_y^2}{2\sigma_\Delta^2}\left(1+\frac{4L^2}{a^2}\right)\right\}\left\{\frac{2L}{a}\left[1+\frac{a^2}{4L^2}\right]^{1/2}\right\}. \qquad 4.2,11$$

This special case with a pinhole source is a known result [Corney 1977] and for a « L the widths are related by

$$\sigma_D \rightarrow \sigma_D' = a\sigma_D/2L.$$

A more extensive treatment allowing for non-zero observation angles can be found in Greenland, Lauder and Wort 1985. The transverse velocity gives rise to a frequency shift in the laser as seen by the atom. This leads to an additional detuning $\Delta\nu = \nu v/c$ to first order in v/c, where ν is the mean laser frequency. Thus the detuning distribution can be easily converted to a velocity distribution. For this transition ν is $6.81\ 10^{14}$ Hz and so Fig iii shows the theoretical transverse Doppler distribution, the pinhole approximation and the distribution measured in SHJR, all for the same geometry and oven temperature.

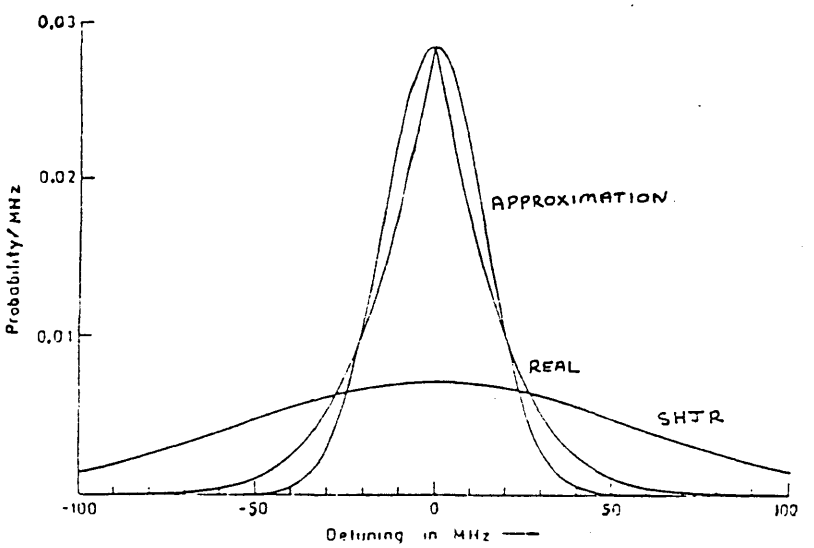


Fig 4.2.iii

The probability distributions for the transverse Doppler width of the relevant transition in the atoms in the atomic beam.

It can be seen that the point source cuts down the number of fast transverse atoms but that the FWHM of the equal slit case is actually

slightly smaller. The theoretical distribution of 16 MHz width, and the distribution quoted in SHJR of 56 MHz width, disagree by a factor of four. This inconsistency remains unresolved. The theory has been compared with other experimental studies of atomic transitions in atomic beams being driven by similar fields [Greenland, Lauder and Wort 1985] with good agreement. However the value of the Doppler width given in SHJR is used in these calculations, rather than the predicted width, as this is claimed to be the measured value. The authors in SHJR ignore the Doppler width in their analysis but it is included here as it has a considerable effect on the results.

To include these two effects in the model of the atom, a weighted sum over the different dipole moments of the m transitions and an integration weighted by the distribution must be carried out over the range of the Doppler detuning. These two effects are in principle easy to include as they just increase the amount of computation. The following section considers the uncertainties in the laser pulses.

4.3 Modelling the laser field

4.3.1 Pulse shape

The pulse shape is modelled as in previous chapters by dividing it into a number of blocks. Because of the number of other calculations involved, such as degeneracy sums and integrals over intensity, phase and detuning fluctuations, the number of blocks used can only be of the order of ten. However, this is considered to be an adequate representation of the Gaussian pulse shape for this analysis. In the experiment the ion count, giving the upper state population, is plotted against the peak laser field. The results are obtained from an average over a number of laser pulses and so any fluctuations in the peak intensity and mean frequency need to be modelled. Also, the laser has some bandwidth, in addition to the transform bandwidth, caused by random processes in the wavetrain. Collisions between the atoms in the laser amplifier medium and other disturbances cause the phase of the field to vary. This will cause the wavetrain to lose coherence and the bandwidth is therefore increased. The modelling of this loss of coherence is not easy as the exact process is not known.

4.3.2 Intensity fluctuations

Each pulse is assumed to be approximately Gaussian in shape, but with the peak intensity fluctuating from pulse to pulse. The fluctuation is, for want of a better approximation, assumed to follow Gaussian statistics.Thus if I is the peak intensity of a pulse and $\langle I \rangle$ is the mean peak intensity averaged over many pulses, then

$$P(I)dI \propto \exp\{-(I-\langle I \rangle)^2/2\sigma_I^2\}dI. \qquad 4.3,1$$

The pulses are passed through a variable attenuator and the ion count is plotted as a function of the mean field. It is assumed that the ratio $s = \sigma_I/\langle I \rangle$ remains constant for all attenuation values. This is true if the intensity fluctuations initiate from the laser, rather than being caused from a process within the attenuator. The value of s is not measured in the experiment but is used as a fitting parameter. The distribution P(I)dI can be normalised and converted to a distribution in terms of the on resonant Rabi frequency, where $I \propto \Omega_o^2$. It can then be included in the overall model by an averaging

integration

$$P(I)dI = \frac{2}{(1+\mathrm{erf}(1/s\sqrt{2}))}\frac{1}{\sqrt{2\pi}\,s\langle I\rangle}\exp\frac{-(I/\langle I\rangle-1)^2}{2s^2}\,dI. \qquad 4.3,2$$

As the intensity cannot become negative the normalising condition is just

$$\int_0^\infty P(I)dI = 1.$$

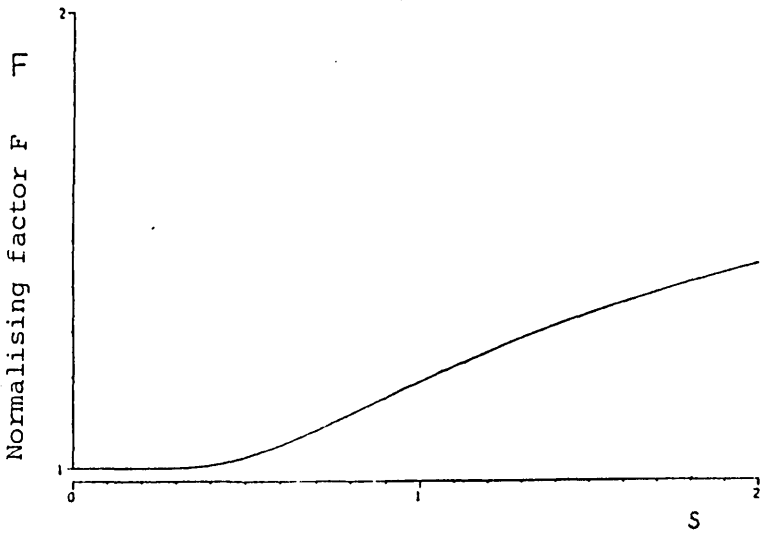


Fig 4.3.i

The normalisation factor, F, as a function of s.

In terms of the Rabi frequency the distribution is given by

$$P(\Omega_o)d\Omega_o = \frac{F}{\sqrt{2\pi}\,s}\exp\left\{\frac{-(\Omega_o^2/\langle\Omega_o^2\rangle-1)^2}{2s^2}\right\}\frac{d\Omega_o^2}{\langle\Omega_o^2\rangle} \qquad 4.3,3$$

where

$$F = 2/(1 + \mathrm{erf}(1/s\sqrt{2})).$$

The first factor F is ignored by the authors SHJR which is permissible if $s \lesssim 0.3$ (see fig i).However, the authors give the value of s to be $s = 0.7$ which leads to a value of $F = 1.08$. Although this is not large, the probability that the laser does not fire, which can be obtained by considering shots with the intensity $I < 0$, is given by $P(I<0) = (1-1/F)$ which for $F = 1.08$ leads to an estimated, large, fail rate of 8% in the laser firing. The value of s found in the present analysis is $s = 0.2$. This implies a fail rate of $< 10^{-4}\%$ which seems more realistic.

4.3.3 Frequency fluctuations

In modelling the atoms a frequency broadening term is to be included. This is caused by the Doppler effect and introduces a frequency shift in the laser pulse as observed by the atoms. To be added to this is the frequency jitter. This is a shift of each laser pulse around a mean frequency value. It is commonly observed and originates from effects such as unstable optical path lengths due to acoustic fluctuations. It is assumed to be a random shift and to follow Gaussian statistics. If $\Delta = \omega - \langle\omega\rangle$ then

$$P(\Delta)d\Delta = \exp\left\{-\frac{\Delta^2}{2\sigma_\Delta^2}\right\}\frac{d\Delta}{\sqrt{2\pi}\sigma_\Delta} . \qquad 4.3,4$$

It has already been shown that approximating the first slit to be a pinhole gives fairly good agreement with the exact condition in which the slits are equal. If this approximation is used then the calculations are simplified as the Doppler detuning distribution is Gaussian and therefore of the same type as the shot to shot detuning distribution. These can then be included in the same averaging integral with suitable modification of the width. That is, the new width is given by the sum in quadrature of the Doppler and frequency fluctuation widths. Thus

$$\sigma^2 = \sigma_D^2 + \sigma_\Delta^2 \qquad 4.3,5$$

where σ_D is now the width in frequency units rather than velocity.

4.3.4 Bandwidth

4.3.4.1 Causes of bandwidth

The shot to shot variation in mean frequency causes an increase in laser bandwidth as the bandwidth measurement takes place over numerous shots. Thus, so far, there are two causes of bandwidth. Firstly there is the transform bandwidth caused by the finite length of the pulse. The intensity profile is given to be Gaussian with width 2.13 ns. The field profile is therefore also Gaussian, with width $\sigma_t = \sqrt{2}\sigma_t^I$. The spectral and temporal widths of Gaussian intensity pulses are related by $2\sigma_t^I\sigma_\nu^I = 1$ rad (see appendix 4.B). Thus the transform limited width of the intensity spectrum is $\sigma_\nu^I = 1/(2 \times 2.13) = 235$ Mrad.s^{-1}. The measured width of the intensity spectrum is given to be 487 Mrad.s^{-1}. Thus the actual width is about twice the transform width. This means that extra bandwidth has to be included via shot to shot variations in frequency and in phase fluctuations within each pulse. The former process has already been dealt with, and being inhomogeneous is easy to add to the transform width. As both the transform and the inhomogenous broadening distributions are Gaussian, then they can be added in quadrature. Thus, ignoring phase fluctuations, the required shot to shot width is given by

$$(\sigma^I)^2 \text{ (measured)} = (\sigma_\Delta^I)^2 + (\sigma_\nu^I)^2 \qquad 4.3,6$$

where σ^I is the width of the power spectrum. For the shot to shot width $\sigma_\Delta = \sigma_\Delta^I$ as the mean frequency of the field and power spectra are the same. For the transform linewidth $\sigma_\nu = \sigma_\nu^I/\sqrt{2}$ from the relation $I \propto E^2$.

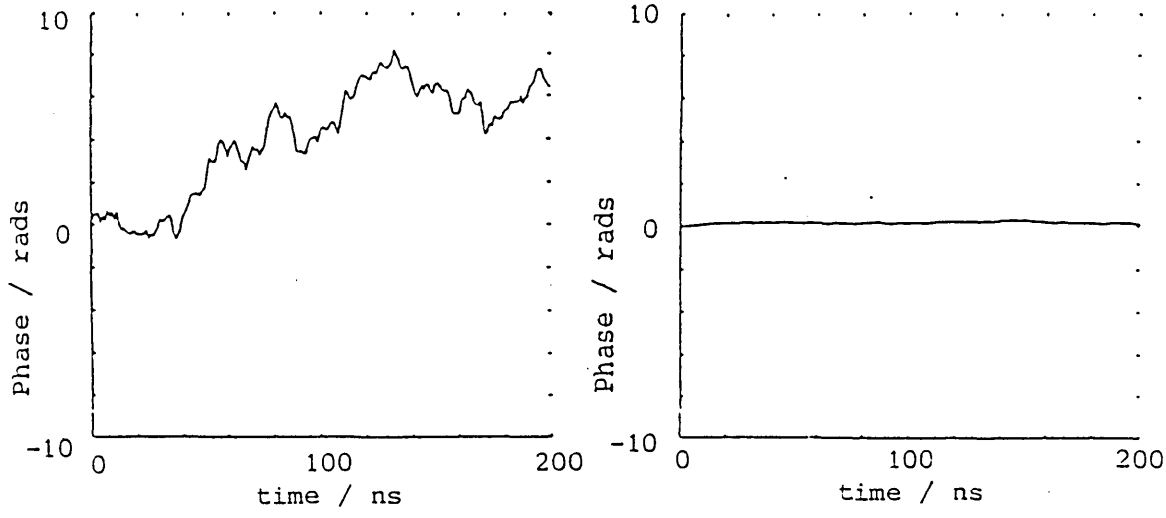
4.3.4.2 Phase fluctuations

There are, however, other important sources of broadening. These are due to fluctuations in the field during a pulse. The laser field can be given in the form

$$E(t) = E_o(t)\cos(\omega_L t + \phi) \qquad 4.3,7$$

where $E_o(t)$ is the envelope, ω_L the carrier frequency and ϕ the phase. If any of $E_o(t)$, ω_L or ϕ fluctuates stochastically then the power spectrum will aquire extra bandwidth, see for example Wax 1954. Here only fluctuations in the phase ϕ will be considered, that is ω_L is

constant for each pulse and $E_o(t)$ is a sure function. The form of fluctuations in ϕ, to be considered here, is given by the phase diffusion model (PDM). This is where the phase makes a random walk during the pulse and has been extensively studied [Wódkiewicz 1979].



a) a random walk b) an average over many random walks

Fig 4.3.iii

A random walk of the phase and the average over many of these.

Under many circumstances it is a good model for the laser lineshape near the centre of the power spectrum [Yeh and Eberly 1981, Swain 1982]. Figs iiia and b show a realisation of a random walk in the phase and an average over many of these realisations, giving zero. The third picture, fig iiic is a mean square average giving a graph of constant slope, the value of this slope is described shortly. This type of fluctuation results in a Lorentzian power spectrum of FWHM of, say, Σ_ϕ (see appendix 4.C). For this process the phase ϕ obeys the Langevin equation [Uhlenbeck and Ornstein 1930] in the limit that $\beta \to \infty$

$$\frac{d^2\phi}{dt^2} + \beta\frac{d\phi}{dt} = \beta F(t), \qquad 4.3,8$$

so that

$$\frac{d\phi}{dt} = F(t). \qquad 4.3,9$$

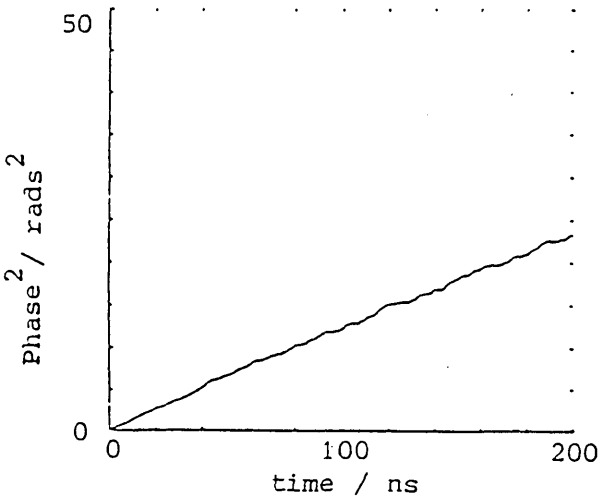


Fig 4.3.iiic

The mean sqare of the phase for Σ_ϕ = 120 MRads s^{-1}.

F(t) is a zero mean Gaussian white noise process such that

$$\langle F(t) \rangle = 0 \qquad 4.3,10a$$

and

$$\langle F(t)F(t') \rangle = \Sigma_\phi \delta(t-t') \qquad 4.3,10b$$

where $\langle\rangle$ indicates an ensemble average. From equation 9 $\phi(t)$ can be written explicitly as

$$\phi(t) = \int_0^t F(t')dt'. \qquad 4.3,11$$

Thus the mean square can be written as

$$\langle\phi(t)^2\rangle = \int_0^t dt' \int_0^t dt'' \; F(t')F(t''). \qquad 4.3,12$$

From equation 10b

$$\langle\phi(t)^2\rangle = \int_0^t dt' \int_0^t dt'' \; \Sigma_\phi \delta(t'-t'') \qquad 4.3,13$$

$$= \Sigma_\phi t. \qquad 4.3,14$$

Thus the slope of the mean square of the phase in fig iiic is just Σ_ϕ, the FWHM of the power spectrum. In the model the random walk of the phase with zero step length is replaced by one with a step length of one block. This is adequate provided that $\Sigma_\phi \ll 1/t_B$, where t_B is the length of one block of the pulse. The phase fluctuations have to, at most, increase the bandwidth of the pulse by a factor of two. Therefore Σ_ϕ is of the order of the transform width so it is required that $t_B \ll t_{pulse}$. Thus the number of blocks used to model the pulse shape (~10) is enough to model the phase fluctuations. Unfortunately the main problem in modelling the phase noise is in deciding the amount to include. The authors SHJR quote the measured bandwidth of the intensity pulse and give no indication of the weighting of the extra bandwidth as distributed between the shot to shot fluctuations and the phase noise. Whereas it is easy to sum the contributions from the shot to shot fluctuations and the transform bandwidth, as the widths add in quadrature, the phase noise having a Lorentzian distribution cannot be added in this way. The power spectrum is a Voigt profile, the convolution of a Gaussian with a Lorentzian profile.

$$P(\Delta)d\Delta = \frac{d\Delta\ \Sigma_\phi}{2\pi\sqrt{2\pi}(\sigma^I)^2} \int_{-\infty}^{\infty} d\Delta' \exp\left\{-\frac{(\Delta-\Delta')^2}{2(\sigma^I)^2}\right\} \frac{1}{\Delta'^2+\Sigma_\phi^2/4} \qquad 4.3,15$$

where

$$(\sigma^I)^2 = (\sigma_v^I)^2+(\sigma_\Delta^I)^2,$$

σ_{Δ}^{I} is the width of the Gaussian distribution of the shot to shot mean frequencies, σ_{ν}^{I} is the width of the Gaussian distributed intensity spectrum due to the transform width and Σ_{ϕ} is the FWHM of the Lorentzian distributed intensity spectrum due to the phase fluctuations. σ_{ν}^{I} can be calculated from the pulse temporal width, but the relation between Σ_{ϕ} and σ_{Δ}^{I} given the total spectral width is hard to calculate because of the Voigt profile. Minkowski and Bruck 1935 give an approximate relationship between the FWHM of the three distributions. The distribution observed by Scarl et al is assumed to have a Voigt profile and the width given is assumed to have been calculated from a FWMH measurement assuming a Gaussian profile. So Σ_{ϕ} and σ_{Δ}^{I} have to be chosen to add with σ_{ν}^{I} to give a Voigt profile of FWHM $\sqrt{8\ln 2}\,\sigma^{I}$(measured).

4.4 Combining the effects

The processes to be included in the model have now been described, and so now all that remains is to put them together. To summarise so far, the effects to be included are shot to shot fluctuations in intensity and frequency, different dipole strengths between the magnetic sublevels, extra detunings because of Doppler shifts, shaped pulses and stochastic phase fluctuations. Thus if $c_0(t)$ and $c_1(t)$ are the amplitudes to be in the lower and upper states respectively, then the upper state population, after the pulse, is given by

$$P_1 = |c_1(s,\sigma_\Delta,\Sigma_\phi,\mu_0)|^2$$

$$= \sum_{m=-3}^{3} \frac{1}{7} \int_0^\infty dI P(I) \int_{-\infty}^{\infty} d\Delta P(\Delta) \langle |c_1(\Delta,\mu_m,I,t\to\infty)|^2 \rangle \qquad 4.4,1$$

where m labels the magnetic sublevel, and s, σ_Δ, Σ_ϕ and μ_0 are the fitting parameters. Here $c_1(\Delta,\mu_m,I,t\to\infty)$ is found by stepping through the pulse using the time development operator as in previous chapters. The brackets $\langle\rangle$ indicate an average over the stochastic phase ϕ which leads to the extra bandwidth Σ_ϕ. As the pulse is divided into steps to model the pulse shape it is convenient to use these steps to model the stochastic variation in phase. Thus during each step the phase is given a new value using a routine that models a random walk dependent upon the extra bandwidth required. Calculating the upper state population in this way is computationally too lengthy to allow a least squares fit of the fitting parameters and so an approximation is also used.

4.4.1 Semi-analytical approximation

4.4.1.1 Substitution rule

The phase fluctuations are included explicitly by numerical averaging. This is so that different models can be used for the phase. However, for the particular model used so far, where the fluctuations in the phase are assumed to be a zero mean Gaussian white noise process, a substitution rule can be applied [Wódkiewicz 1979, Yeh and Eberly 1981]. This substitution converts the equations of motion for the density matrix with stochastic phase into corresponding equations

for the averaged density matrix elements with extra damping terms. All occurrences of $\pm i\dot{\phi}$ are replaced by $-\Sigma_\phi/2$.

4.4.1.2 Equivalent pulse

To simplify the calculations and therefore enable a least squares fit, the Gaussian pulse is approximated by a flat pulse and the stochastic averaging can then be achieved analytically using the above substitution. This rule only works for this particular model of laser noise and yields the following [Smith 1978]

$$\langle |c_1\langle \Delta, \mu_m, I, t\to\infty\rangle|^2\rangle = \{1 + \sum_{n=1}^{3}\lambda_n \exp(\gamma_n T)\} \qquad 4.4,2$$

where T is the length of the equivalent constant laser pulse. The γ_n are the three roots of the equation

$$\gamma\{(\gamma + \Sigma_\phi/2)^2 + \Delta^2\} + (\gamma + \Sigma_\phi/2)(\mu_m E_T)^2 = 0 \qquad 4.4,3$$

which is the secular equation of the matrix of coefficients in the equation for the density matrix. The λ_n are given by

$$\lambda_1 = ((\mu_m E_T)^2/2 - \gamma_2\gamma_3)/((\gamma_2 - \gamma_1)(\gamma_3 - \gamma_1)) \qquad 4.4,4$$

and cyclic permutations of the indices for λ_2 and λ_3. E_T is the effective field envelope of the flat pulse. T and E_T are obtained by requiring that the first three moments (0, 1 and 2) of the two pulses are identical for the field profiles. In the analysis by SHJR the first three moments of the intensity envelopes were equated. Previous chapters show that, in more idealised situations, it is the area of the field envelope that dominates in calculating the final populations. Thus if the Gaussian field envelope is given by

$$E^G(t) = E^G \exp(-t^2/2\sigma_t^2) \qquad 4.4,5a$$

and the constant field envelope is given by

$$E^C(t) = E_T\ , \quad -T/2 < t < T/2 \qquad 4.4,5b$$

$$= 0\ , \quad T/2 < |t| \qquad 4.4,5c$$

then

$$\int_{-\infty}^{\infty} E^{\Theta} \exp(-t^2/2\sigma_t^2)dt = \int_{-\frac{T}{2}}^{\frac{T}{2}} E_T dt \qquad 4.4,6a$$

and

$$\int_{-\infty}^{\infty} E^{\Theta} t^2 \exp(-t^2/2\sigma_t^2)dt = \int_{-\frac{T}{2}}^{\frac{T}{2}} E_T t^2 dt \qquad 4.4,6b$$

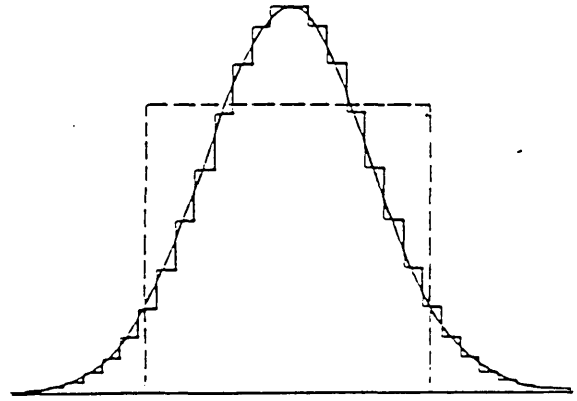


Fig 4.4.i

The real (Gaussian) pulse and the two approximations.

The first moment just centralises the pulses around t = 0. Equation 6a gives

$$E^{\Theta} \sigma_t \sqrt{2\pi} = TE_T \qquad 4.4,7a$$

and 6b gives

$$E^{\Theta} \sigma_t^3 \sqrt{2\pi} = T^3 E_T/12 \qquad 4.4,7b$$

so

$$T = 2\sqrt{3}\sigma_t = 2\sqrt{6}\sigma_t^{\,x} = 10.435 \text{ ns} \qquad 4.4,8a$$

$$E_T = \sqrt{\pi/6}\, E^{\Theta} \qquad 4.4,8b$$

Fig i shows the real Gaussian pulse shape, the stepped approximation to it, with 30 steps, and the equivalent square pulse. The method using the flat pulse approximation and the noise substitution rule is used to obtain a best fit to the data given in SHJR. Then the values are used in the full numerical model for comparison.

4.5 Results

Equation 4.4.i depends upon four fitting parameters. However, SHJR also measure the total bandwidth of the pulses, see table i. This fixes a relationship, although complex, between Σ_ϕ and σ_Δ. Thus the Lorentzian phase diffusion width Σ_ϕ, the Gaussian transform width $\sigma_\nu{}^I$ and the Gaussian inhomogeneous width $\sigma_\Delta{}^I$ should all add to give a Voigt profile of FWHM 182.5 MHz.

Pulse shape	Power Spectrum	Peak Power Density
Gaussian 5.02 ns FWHM	Gaussian? 182.5 MHz FWHM	1.55 10^8 Wm^{-2}

Table 4.5.i
The pulse data.

Fig i shows the data and analytical fit taken from SHJR.

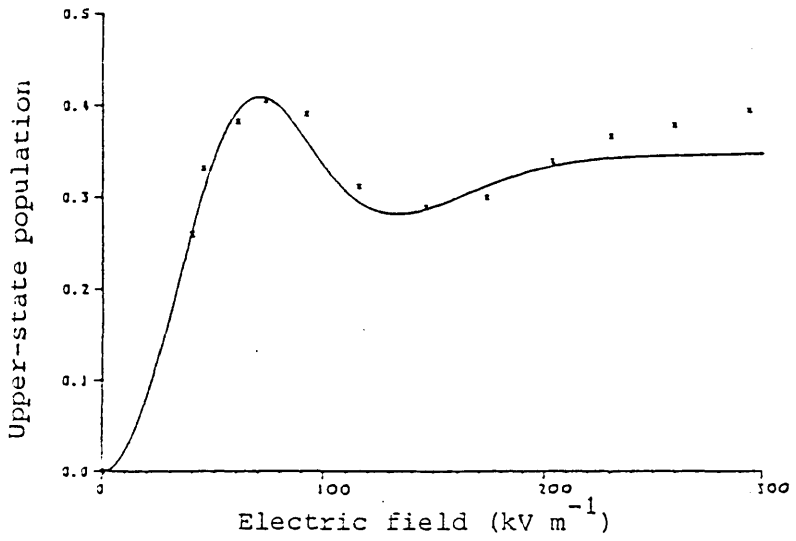


Fig 4.5.i
The experimental data and the analytical fit from SHJR.

There is no mention of how the absolute upper state population is obtained from the ion count and it is therefore assumed that the scale is not absolute. The best fits have therefore been normalised to the

peak of the data before the quality of the least squares fit is calculated. Two pairs of best fits are shown. Each pair comprises firstly, the semi-analytical fit, which is fitted using a least squares algorithm, and secondly, the full numerical solution using the same parameters. The semi-analytical solution uses the substitution rule to model the phase fluctuations and approximates the pulse shape to an equivalent square pulse. Fig ii shows fit 1 which includes the Doppler width. The parameters are shown in table ii. Q is the sum of the squares of the differences between the experimental and the semi-analytical fits and N is the factor by which the semi-analytical fit is multiplied to achieve normalisation to the peaks.

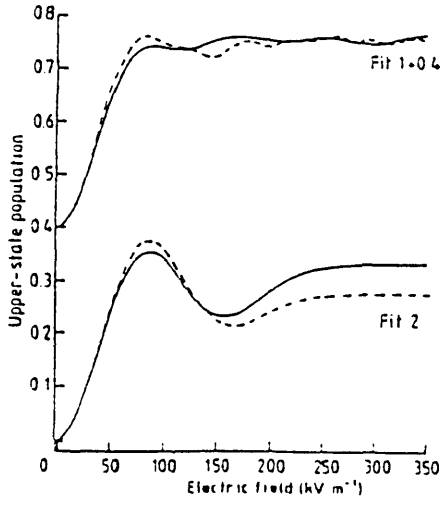


fig 4.5.ii

Best fit 1 includes Doppler width and phase fluctuations, whilst best fit 2 ignores both of these (solid line is semi-analytical, dashed is numerical).

Fit 2 in fig ii is a case in which the Doppler width is ignored and the bandwidths are taken to add linearly, with no phase fluctuations. These are essentially the same conditions as imposed by SHJR and the results are comparable. The values of z_o are different because in this work the moments of the field rather than the power envelopes are fitted. For zero bandwidth this implies

$$z_o\ (\text{SHJR}) = (2\pi/3)^{1/4} z_o\ (\text{this work}) \qquad 4.5.1$$

which is still approximately true for finite bandwidth.

	z_o(pm)	s	Σ_Φ(MHz)	σ_Δ(MHz)	Q	N
Fit 1	5.57	0.13	136	8	0.06	1.14
Fit 2	3.15	0.73	0	40	0.004	1.12

Table 4.5.ii

The values obtained for the fitting parameters.

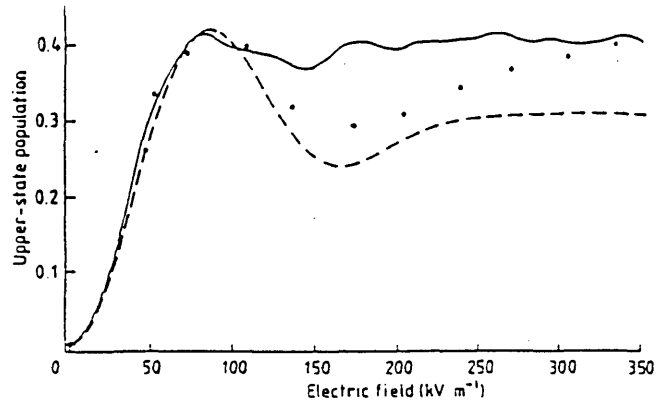


Fig 4.5.iii

Comparison of the best fits with the data.

Fig iii shows a comparison of the SHJR data, with the two semi-analytical best fits.

4.6 Conclusions

The best fit to the data given by SHJR has, from table 4.5.ii, z_o = 5.57 pm, Σ_ϕ = 136 MHz, σ_Δ = 8 MHz and s = 0.13. The error on these values is hard to estimate. However, values neer z_o = 4.5 pm, Σ_ϕ = 95 MHz and s = 0.23 also fit the data well, but give an incorrect measure of the laser bandwidth. These values give a total width of about 150 MHz compared to the required 182.5 MHz. If the discrepancy between these two sets of values is characteristic of the error then z_o = 5.6 ± 1 pm, Σ_ϕ = 130 ± 50 MHz, σ_Δ = 8 ± 8 MHz and s = 0.13 ± 0.1. The shot to shot fluctuations in detuning are essentially undetermined but must be less than about 30 MHz FWHM, or their effect on the fit would become important. It is worth commenting that, in future experiments of this type, it would be very useful to have an independent measure of the quantity s and, if possible, a better quantification of the laser bandwidth. That is, the intensity fluctuations should be measured explicitly to reduce the number of fitting parameters, and the distribution of the bandwidth between the homogeneous and inhomogeneous processes should be determined. This can be done by measuring the separation of the points of inflection, rather than the FWHM, of the laser lineshape. This allows the Lorentzian (homogeneous) and Gaussian (inhomogeneous) components to be deconvoluted simply [Stoneham 1972].

It has to be said that the fit achieved by this work does not appear to be as good as that of SHJR, but it is believed that the values obtained for the fitting parameters are more correct. The value of s in particular appears to be more realistic, implying a shot to shot fluctuation in intensity of around 30% FWHM, rather than the 165% fluctuation predicted by SHJR.

Finally, the semi-analytical model is seen to give a good representation of the numerical results, particularly for the case where the phase diffusion bandwidth is dominant. In this case equation 4.4,3 simplifies to a quadratic.

It is shown here that it is possible to include phase fluctuations as a temporal effect along with the pulse shape. This is important because in certain circumstances it is easier to model the noise in this way rather than analytically. The analytical substitution rule can only be applied for a very special noise process and requires the density matrix formalism. If the pulse shape needs modelling then

there is little extra work involved in including the laser noise. With more than three or four levels this extra work is less than the extra work required to perform the calculations with the density matrix.

In the next chapter a continuum is included in order to see if it has any of the properties already investigated in bound states. In this chapter Rabi oscillations are seen even with a degenerate two-level atom excited by a noisy laser, so is it possible to observe Rabi oscillations or population trapping if the bound states are strongly coupled into a continuum?

4.A The Doppler profile integral

Consider

$$I = \int_{A}^{B} dz \; \exp\{-b^2/(c-z)^2\}.$$

Put $x = 1/(c-z)$ so that $dx = dz/(c-z)^2$ substituting this yields

$$I = \int_{\frac{1}{c-A}}^{\frac{1}{c-B}} dx \; \exp\{-b^2x^2\}/x^2.$$

By partial integration using the substitutions

$$u = \exp\{-b^2x^2\} \quad \text{and} \quad dv = dx/x^2,$$

so that

$$du = -2b^2x \exp\{-b^2x^2\}dx \quad \text{and} \quad v = -1/x,$$

this becomes

$$I = \left[-\exp\{-b^2x^2\}/x\right]_{\frac{1}{c-A}}^{\frac{1}{c-B}} - 2b^2\int_{\frac{1}{c-A}}^{\frac{1}{c-B}} du \; \exp\{-b^2x^2\}$$

giving

$$I = (c-A)\exp\left\{\frac{-b^2}{(c-A)^2}\right\} - (c-B)\exp\left\{\frac{-b^2}{(c-B)^2}\right\} + \sqrt{\pi}b\left[-\mathrm{erf}\left\{\frac{b}{(c-A)}\right\} + \mathrm{erf}\left\{\frac{b}{(c-B)}\right\}\right].$$

Putting $b = L|v_y|/\sqrt{2}\sigma_D$, $c = a_2/2$, $A = -a_1/2$ and $B = a_1/2$ equation 4.2,8 becomes

$$I = \int_{-\frac{a_1}{2}}^{\frac{a_1}{2}} dz \; \exp\left\{\frac{-L^2|v_y|^2}{2\sigma_D^2(a_2/2-z)^2}\right\}$$

$$= \frac{(a_2+a_1)}{2}\exp\left\{\frac{-2L^2|v_y|^2}{\sigma_D^2(a_2+a_1)^2}\right\} - \frac{(a_2-a_1)}{2}\exp\left\{\frac{-2L^2|v_y|^2}{\sigma_D^2(a_2-a_1)^2}\right\}$$

$$+\sqrt{\frac{\pi}{2}}\frac{L|v_y|}{\sigma_D}\left[\operatorname{erf}\left\{\frac{\sqrt{2}L|v_y|}{\sigma_D(a_2+a_1)}\right\} - \operatorname{erf}\left\{\frac{\sqrt{2}L|v_y|}{\sigma_D(a_2-a_1)}\right\}\right].$$

Normalisation of $Q(v_y)dy$

In the region P' the distribution is normalised. However, due to the slit a_2 some of the atoms are stopped from reaching region Q. Therefore the new distribution in Q is not normalised. Put

$$N = \int_{-\infty}^{\infty} Q(v_y)\, dv_y$$

$$= \int_{-\infty}^{\infty} \frac{dv_y}{a_1\sigma_D\sqrt{2\pi}} \exp\left\{\frac{-|v_y|^2}{2\sigma_D^2}\right\} x$$

$$\left[\frac{(a_2+a_1)}{2}\exp\left\{\frac{-2L^2|v_y|^2}{\sigma_D^2(a_2+a_1)^2}\right\} - \frac{(a_2-a_1)}{2}\exp\left\{\frac{-2L^2|v_y|^2}{\sigma_D^2(a_2-a_1)^2}\right\}\right.$$

$$\left.+\sqrt{\frac{\pi}{2}}\frac{L|v_y|}{\sigma_D}\left[\operatorname{erf}\left\{\frac{\sqrt{2}L|v_y|}{\sigma_D(a_2+a_1)}\right\} - \operatorname{erf}\left\{\frac{\sqrt{2}L|v_y|}{\sigma_D(a_2-a_1)}\right\}\right]\right].$$

Consider

$$I = \int_{-\infty}^{\infty} \exp\{-a^2x^2\}\ |x|\ \operatorname{erf}\{b|x|\}\ dx$$

$$= 2\int_{o}^{\infty} \exp\{-a^2x^2\}\ x\ \operatorname{erf}\{bx\}\ dx.$$

This is integrated by parts with the substitutions

$$u = \operatorname{erf}(bx) \text{ and } dv = 2x\ \exp(-a^2x^2)\ dx$$

so that

$$du = 2b\ \exp(-b^2x^2)\ dx/\sqrt{\pi} \quad \text{and} \quad v = -\exp(-a^2x^2)\ /a^2$$

giving

$$I = -\left[\frac{\exp(-a^2x^2)\,\mathrm{erf}(bx)}{a^2}\right]_{x=0}^{\infty} + \frac{2b}{\sqrt{\pi}a^2}\int_0^{\infty}\exp(-(a^2+b^2)x^2)\,dx$$

So

$$I = \frac{b}{a^2\sqrt{a^2+b^2}}.$$

Thus the normalising factor N is given by

$$N = \frac{L}{a_1}\left\{\left[1 + \left[\frac{a_2+a_1}{2L}\right]^2\right]^{1/2} - \left[1 + \left[\frac{a_2-a_1}{2L}\right]^2\right]^{1/2}\right\}.$$

4.B Fourier Transform

The intensity goes like the square of the field, so that

$$I(t) \propto |E(t)|^2.$$

Let the field be a carrier wave of frequency ω_L, modulated in time by a Gaussian envelope of width σ_t. Thus the field E(t) is given by

$$E(t) = E_o \cos(\omega_L t) \exp(-t^2/2\sigma_t^2).$$

The Fourier transform of this is given by

$$E(\omega) = 1/\sqrt{2\pi} \int_{-\infty}^{\infty} dt E(t) \exp(i\omega t)$$

$$= E_o/2\sqrt{2\pi} \int_{\infty}^{\infty} dt \exp(-t^2/2\sigma_t^2 + i\Delta t)$$

where the counter-rotating term has been dropped, and $\Delta = \omega - \omega_L$. Thus

$$E(\omega) = E_o/2\sqrt{2\pi} \int_{-\infty}^{\infty} dt \exp(-(t/\sqrt{2}\sigma_t - i\Delta\sigma_t/\sqrt{2})^2 - \Delta^2\sigma_t^2/2).$$

Put $z = t/\sqrt{2}\sigma_t - i\Delta\sigma_t/\sqrt{2}$ so that $dz = dt/\sqrt{2}\sigma_t$. Then

$$E(\omega) = E_o\sigma_t/2\sqrt{2} \exp(-\Delta^2\sigma_t^2/2) \int_{-\infty - i\frac{\Delta\sigma_t}{\sqrt{2}}}^{\infty - i\frac{\Delta\sigma_t}{\sqrt{2}}} dz \exp(-z^2).$$

In the complex z plane the integral along the line AB, see fig 4.B.i, from $x = -\infty$ to $+\infty$ is required. There are no poles within ABCD except at $z \to -i\infty$, ie $\Delta \to \infty$, which is cancelled by the exponential outside the integral. Thus

$$\int_A^B = \int_A^D + \int_D^C + \int_C^B.$$

The integrals AD and BC are zero at infinity, thus

$$\int_A^B = \int_D^C = \sqrt{\pi}.$$

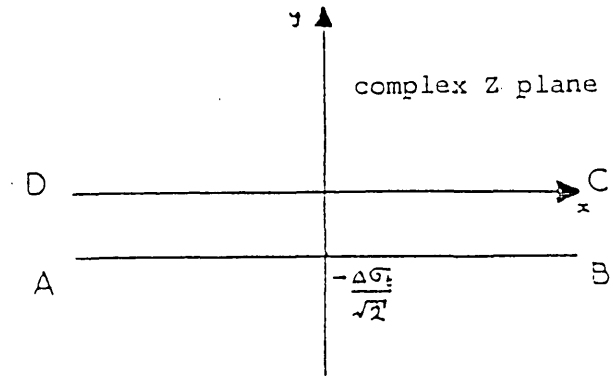


Fig 4.B.i

The complex Z plane for the transform integral.

So that

$$E(\omega) = \frac{E_o\sigma_t}{2} \exp(-\Delta^2\sigma_t^2/2) = E_o \exp(-\Delta^2/2\sigma_\Delta^2).$$

So for the Gaussian envelopes $\sigma_t\sigma_\Delta = 1$ rad, or for the intensity profiles $\sigma_t^I\sigma_\Delta^I = 1/2$ rad.

4.C Spectral Profile of Laser Bandwidth in the PDM Model

Within the RWA the laser field is given by

$$E(t) = E_o/2 \exp(i(\omega_o t + \phi(t)))$$

so that the Fourier transform is given by

$$E(\omega) = \frac{E_o}{2\sqrt{2\pi}} \int_{-\infty}^{\infty} \exp(-i\Delta t + i\phi(t))\, dt \ .$$

Now, $\phi(t)$ is given from the equation

$$\dot{\phi}(t) = F(t)$$

where $F(t)$ is a Gaussian white noise process with $\langle F(t) \rangle = 0$ and $\langle F(t)F(t') \rangle = \Sigma_\phi \delta(t-t')$. Integrating explicitly yields

$$\phi(t) = \int_o^t F(t_1) dt_1$$

where it is assumed, without loss of generality, that $\phi(t_o) = t_o = 0$. Thus

$$\langle \phi(t) \rangle = \int_o^t \langle F(t_1) \rangle dt_1 = 0$$

and

$$\langle \phi(t)\phi(t') \rangle = \int_o^t dt_1 \int_o^{t'} dt_2 \, \langle F(t_1)F(t_2) \rangle$$

$$= \Sigma_\phi \int_o^t dt_1 \int_o^{t'} dt_2 \, \delta(t_1 - t_2)$$

$$= \Sigma_\phi \min(t, t')$$

so that $\langle \phi(t)^2 \rangle = \Sigma_\phi t$.

Therefore

$$\langle \exp(i(\phi(t_1)-\phi(t_2))) \rangle = \langle 1+i(\phi(t_1)-\phi(t_2))-\frac{1}{2}(\phi(t_1)-\phi(t_2))^2+\ldots \rangle,$$

but

$$\langle \phi(t_1)-\phi(t_2) \rangle = 0$$

and

$$\langle (\phi(t_1)-\phi(t_2))^2 \rangle = \langle \phi(t_1)^2 \rangle + \langle \phi(t_2)^2 \rangle - 2\langle \phi(t_1)\phi(t_2) \rangle$$

$$= \Sigma_\phi |t_1-t_2|.$$

As F(t) is a Gaussian process then $\phi(t)$ and $\phi(t_1)-\phi(t_2)$ are also Gaussian processes, as they are linearly related. Therefore, all the odd order averaged products are zero, and all the even order averaged products are related by

$$\langle x^{2n} \rangle = \frac{(2n)!\langle x^2 \rangle^n}{2^n\, n!}.$$

This can be seen from the recursion relationship between the even moments of a Gaussian distribution. If

$$I_{2n} = \frac{1}{\sqrt{2\pi}\,\sigma} \int_{-\infty}^{\infty} x^{2n} \exp\left\{\frac{-x^2}{2\sigma^2}\right\} dx = \langle x^{2n} \rangle$$

then

$$I_{2n} = (2n-1)\sigma^2 I_{2(n-1)}$$

where $\langle x^2 \rangle = \sigma^2$,

so

$$I_{2n} = \sigma^{2n} I_o \, (2n-1)(2n-3)\ldots 3.1.$$

$I_o = 1$ and therefore

$$I_{2n} = \frac{(2n)!\langle x^2\rangle^n}{2^n n!} = \langle x^{2n}\rangle.$$

So by substitution in the expansion of the exponential it can be seen that

$$\langle \exp(i(\phi(t_1)-\phi(t_2)))\rangle = \exp(-\Sigma_\phi |t_1-t_2|/2).$$

Consider the Fourier transform of the intensity profile $I(t)$

$$\langle I(\omega)\rangle = \langle E(\omega)^* E(\omega)\rangle = \frac{|E_o|^2}{8\pi}\int_o^T dt_1 \int_o^T dt_2 \langle \exp(-i\Delta(t_1-t_2)+i(\phi(t_1)-\phi(t_2)))\rangle$$

$$= \frac{|E_o|^2}{8\pi}\int_o^T dt_1 \int_o^T dt_2 \langle \exp(-i\Delta(t_1-t_2)-\Sigma_\phi|t_1-t_2|/2)\rangle$$

Put $K = |E_o|^2/8\pi$ so that

$$\langle I(\omega)\rangle = K\int_o^T dt_1 \exp(-i\Delta t_1)\left\{\int_o^{t_1} dt_2 \exp\left(i\Delta t_2 - \frac{\Sigma_\phi}{2}(t_1-t_2)\right) + \int_{t_1}^T dt_2 \exp\left(-i\Delta t_2 - \frac{\Sigma_\phi}{2}(t_2-t_1)\right)\right\}$$

$$= K\int_o^T dt_1 \, \frac{[1 - \exp(-i\Delta t_1 - \Sigma_\phi t/2)]}{i\Delta + \Sigma_\phi/2}$$

$$+ \frac{[\exp(i\Delta(T-t_1)-\Sigma_\phi(T-t_1)/2) - 1]}{i\Delta - \Sigma_\phi/2}$$

$$= K\left[\frac{T}{i\Delta + \Sigma_\phi/2} - \frac{T}{i\Delta - \Sigma_\phi/2} + \frac{[\exp(-i\Delta T-\Sigma_\phi T/2) - 1]}{(i\Delta + \Sigma_\phi/2)^2}\right.$$

$$\left. - \exp(i\Delta T-\Sigma_\phi T/2)\frac{[\exp(-i\Delta T+\Sigma_\phi T/2) - 1]}{(i\Delta - \Sigma_\phi/2)^2}\right].$$

For $T\Sigma_\phi \gg 1$ then

$$\langle I(\omega)\rangle = K\left[\frac{T\Sigma_\phi}{\Delta^2+\Sigma_\phi^2/4} + \frac{2(\Sigma_\phi^2/4-\Delta^2)}{(\Delta^2+\Sigma_\phi^2/4)^2}\right],$$

for large T the first term will dominate giving the Lorentzian profile

$$\langle I(\omega)\rangle = \frac{|E_o|^2 T\Sigma_\phi}{8\pi}\,\frac{1}{(\Delta^2+\Sigma_\phi^2/4)}\,.$$

4.7 References

Condon E.U., Shortley G.H., 1935
'The Theory of Atomic Spectra'
University Press, Cambridge, rep 1964

Corney A., 1977
'Atomic and Laser Spectroscopy', pg. 268
Clarendon Press, Oxford, 1977

Greenland P.T., 1985
Private communication

Greenland P.T., Lauder M.A., Wort D., 1985
Atomic beam velocity profiles
J. Phys. D, to be published

Grieneisen H.P., Kurnit N.A., Szöke A., 1971
Flourescence induced by coherent optical pulses
Opt. Comm. 3 (1971) 4, 259-263

Jackson R.I., Swain S., 1982
The theory of non-Lorentzian laser bandshapes in atomic processes
J. Phys. B 15 (1982) 4375-4392

Lauder M.A., Greenland P.T., 1984
Resonant laser excitation of uranium with a pulsed laser
J. Phys. B 17 (1984) 3083-3090

MacGillivray W.R., Pegg D.T., Standage M.C., 1978
Observation of optical nutation effects in atoms
Opt. Comm. 25 (1978) 3, 355-358

Minkowski R., Bruck H., (1935)
Wahre und scheinbare Breite von Spektrallinien
Z. Phys. 95 (1935) 299-301

Scarl D, Hackel L.A., Johnson M.A., Rushford M.C., 1981
Observation of atomic coherence in laser excited uranium vapour
Phys. Rev. A 24 (1981) 2, 883

Smith R.A., 1978
Excitation of transitions between atomic or molecular energy levels by monochromatic laser radiation
Proc. Royal Soc. A 362 (1978) 1-12

Stoneham A.M., 1972
Linewidths in Gaussian and Lorentzian broadening
J. Phys. D 5 (1972) 670-672

Uhlenbeck G.E., Ornstein L.S., 1930
On the theory of Brownian motion
Phys. Rev. 36 (1930) 823, (rep in Wax 1954)

Wax N., 1954
'Noise and Stochastic Processes', (editor)
Dover Publications, New York, 1954

Wódkiewicz K., 1979
Stochastic incoherences of optical Bloch equations
Phys. Rev. A 19 (1979) 4, 1686-1696

Yeh J.J., Eberly J.H., 1981
Multiphoton ionization rate with a non-Lorentzian band shape laser
Phys. Rev. A 24 (1981) 2, 888-897

Chapter 5

Laser Induced Continuum Structure

5.0 Introduction

Ionisation is an important process in that it enables subsequent collection of the ionised species. Laser ionisation is especially important as the potential tuneability and low bandwidth of the lasers can mean high selectivity and excitation rates. These aspects are essential in Laser Isotope Separation (LIS) where a particular isotope can be preferentially ionised and subsequently separated by the application of a constant electric field. The selectivity depends upon the different electronic energy levels due to the difference in the structure of the nuclei. The different mass, spin and magnetic moment all have their effects on the energy levels even though they are usually small, see for example Woodgate 1970. This means that the difference between the energy levels of the isotopes is also usually small. In some cases the difference is less than the natural widths of the levels, making them practically indistinguishable. In other cases they are small compared with some of the homogeneous broadenings such as collisional and Doppler effects. Under these circumstances it is possible to arrange for these processes to have a reduced effect by decreasing the density and temperature, to reduce the collisional broadening, and by using collimated beams, to reduce Doppler effects. Once the levels are resolvable it is necessary to have a, preferably, tuneable laser of bandwidth small compared to the splitting in order to keep the levels resolved. Thus a set of isotopes can be ionised by selectively exciting the lower levels with a tuned, low bandwidth laser, and then ionised with a laser only capable of ionising the previously excited levels. However, in general the couplings from bound states to continuum, or ionised, states is small so that the final ionisation process is not very efficient. This is because of the small overlap between the wavefunctions. Continuum states are not bound to the nucleus, by definition, and therefore do not spend much time close to the nucleus. In a classical picture they have unclosed orbits and only come close to the nucleus on one pass. Bound states are continually 'orbiting' and thus interact with each other much more strongly. It is therefore important to investigate processes which can

increase the coupling between bound and continuum states.

Autoionising resonances [Fano 1961 and Beutler 1933 and 1935], where a bound state above the ionisation threshold is coupled to the continuum via the Coulomb interaction, have been investigated and it is known that these alter the coupling from other bound states to the continuum. These are, however, fixed in both position and shape and are therefore of limited use. On the other hand, another bound state coupled into the continuum with a laser field, can create identical structure but with the advantage that both the position and width of the resonance can be altered. The position is fixed by the frequency of the embedding laser and the width by its intensity. This process is termed Laser Induced Continuum Structure (LICS). Fig i shows an ideal separation scheme where three lasers are used to perform the selective ionisation.

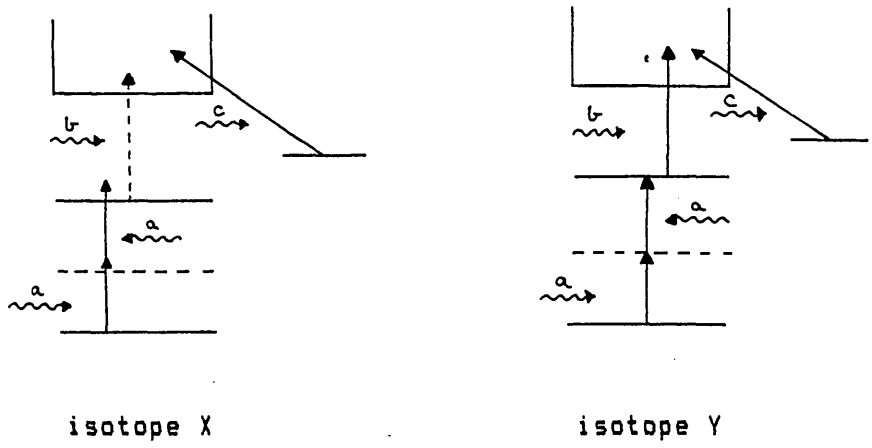


Fig 5.0.i
Selective enhanced ionisation of isotopes.

Laser a performs the selective excitation of isotope Y using a two-photon, counter-propagating Doppler free transition, see chapter three. Laser b then couples the excited state into the continuum, suitably modified by laser c, to produce the enhanced ionisation.

Autoionising states have been extensively examined both theoretically, notably Fano 1961, and experimentally, see for example the review by Collin 1977 and an early laser experiment using Mg_I by Bradley, Ewart, Nicholas, Shaw and Thompson 1973. Rzążewski and Eberly 1981 and 1983 and Lambropoulos and Zoller 1981 theoretically

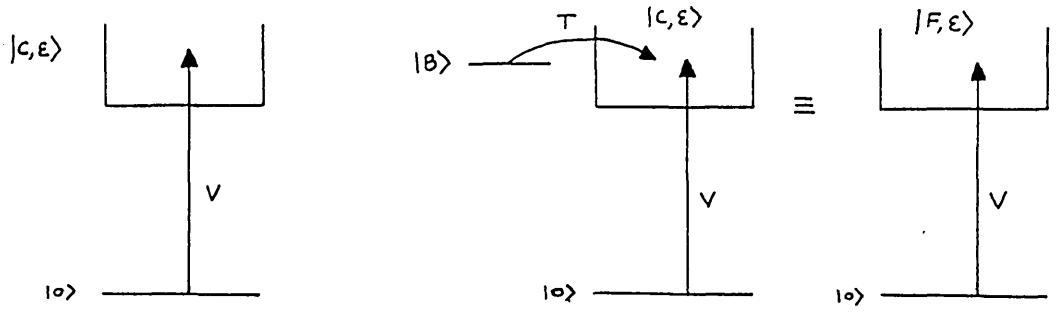
investigate the Fano profile as affected by the intensity of the probing laser, the Fano profile is only observed when the probe laser is weak. They also include some laser bandwidth effects. Alber and Zoller 1983a investigate a specific example of two-photon excitation, three-photon ionisation to an autoionising level, also for varying laser intensities. Armstrong and Wynne 1975 give a theoretical review of, and an experimental study of four-wave mixing with, autoionising resonances. Haus, Rzążewski and Eberly 1983 investigate the effects of inhomogeneous processes, such as Doppler profiles, where an average is taken over many systems.

Much theoretical work has been done on LICS, for example Armstrong, Beers and Feneuille 1975 who form the analogy between laser embedded states and autoionising states. Experimental evidence of LICS has been observed in a few experiments with Dimov etal 1982a/b and 1983 and Pavlov etal 1982 observing enhanced frequency tripling in sodium vapour and Hutchinson and Ness 1984 observing structure in xenon. Heller etal 1981 observe LICS in the continuum of caesium using a frequency doubled rhodamine B dye laser probing the structure induced by an Nd:YAG laser. They observe the the alteration of the polarisation of the probe field as a function of the two-photon detuning. Alber and Zoller 1983b propose an experiment to selectively induce structure into one of the continuum spin channels in the photoionisation of alkali atoms. Population trapping, where some of the population is not allowed to leave the bound states, in continuum processes has been theoretically studied by Coleman and Knight 1982, Greenland 1982, Coleman, Knight and Burnett 1982 and Knight, Lauder, Radmore and Dalton 1984. In the latter paper the effects of laser bandwidth and cross-correlations are investigated. Lecomte and Luc-Koenig re-interpret data from an experiment by Feneuille etal to show that stabilisation of some Stark states in rubidium is possibly an observation of population trapping of this type.

In this chapter the effects of pulse shape on the ionisation process is described, into both flat and modified continuum states, and the effects of laser bandwidths, due to pulse shape effects and coherence, is investigated.

5.1 Decay into a flat continuum

If there is a weak coupling from a bound state into the continuum then Fermi's Golden Rule gives a good approximation to the decay rate out of the bound state, see for example Cohen-Tannoudji etal 1977. If, however, the continuum is already coupled to another bound state then interference could occur between the different routes allowed.



a) a flat continuum b) an embedded state c) a Fano continuum

Fig 5.1.i
Decay into a flat continuum and a Fano continuum.

Fig ia shows a bound state |0⟩ coupled to the continuum |C,ε⟩ via an interaction V. For a weak interaction the decay out of state |0⟩ is just given by the Golden Rule rate

$$\Gamma = \frac{2\pi}{\hbar}\int_0^\infty d\varepsilon\, |\langle C,\varepsilon|V|0\rangle|^2 \delta(\varepsilon-\varepsilon_i)$$

$$= \frac{2\pi}{\hbar}|\langle C,\varepsilon_i|V|0\rangle|^2, \qquad 5.1,1$$

Section 5.1.1 shows that this is also true for strong V and also generalises the result to allow for time dependent V. Fig ib shows a situation in which another bound state, |B⟩, is coupled into the continuum, close to the original coupling V, by another interaction T. This interaction can be either Coulombic as in an autoionising level, or dipole as in LICS. This is treated in two ways. In section 5.2 it is assumed that V is weak and can thus be treated perturbatively so

that the Golden Rule can be applied. However, it is necessary to find the Fano wavefunction, $|F,\varepsilon\rangle$ [Fano 1961], which is the set of eigenstates of the bound state $|B\rangle$, the continuum state $|C,\varepsilon\rangle$ and the interaction between them. This is like a modified continuum as it also includes the bound state. Thus fig ib is equivalent to c. Section 5.3 makes a similar calculation in which it is assumed that both fields are strong such that the perturbative theory cannot be applied. In this section trapping is investigated where even though both states are coupled strongly into the continuum, and not directly to each other, population can be trapped in the bound states. This phenomenon is also investigated where the lasers are partially coherent both absolutely and relative to each other. The effects of pulse shape on the trapping is also investigated.

5.1.1 Decay into a continuum

Fig ia shows a bound state $|0\rangle$ coupled into a continuum $|C,\varepsilon\rangle$ via a coupling V. The wavefunction of the system is given by

$$|\psi,t\rangle = a_0(t) + \int_0^\infty d\varepsilon a_\varepsilon(t)|C,\varepsilon\rangle \qquad 5.1,2$$

where the $a_0(t)$ and $a_\varepsilon(t)$ are the amplitudes in the Schrödinger picture. The continuum states and the bound state have different units due to the normalisation used here. These states are normalised so that $\langle i|j\rangle = \delta_{ij}$ and $\langle C,\varepsilon_i|C,\varepsilon_j\rangle = \delta(\varepsilon_i-\varepsilon_j)$, thus the $|C,\varepsilon\rangle$ have units of inverse root energy. The amplitudes are similarly altered as it is required that $|a_\varepsilon(t)|^2$ is the population per unit energy at energy ε. From Schrödinger's equation the equations of motion for the amplitudes can be written as

$$i\dot{a}_0 = \omega_0 a_0 - \int_0^\infty d\varepsilon \Omega_{0\varepsilon}\cos(\omega_L t+\phi)a_\varepsilon \qquad 5.1,3a$$

and

$$i\dot{a}_\varepsilon = -\Omega_{\varepsilon 0}\cos(\omega_L t+\phi)a_0 + \omega_\varepsilon a_\varepsilon \qquad 5.1,3b$$

where the explicit time dependences are dropped for ease of notation. $\hbar\omega_0$ is the energy of the bound state $|0\rangle$ and $\hbar\omega = \varepsilon$, $\Omega_{0\varepsilon}$ is the Rabi frequency matrix element given by $\Omega_{0\varepsilon}(t) = \langle 0|V^\circ(t)|C,\varepsilon\rangle/\hbar$, where

$V^{o}(t)$ is the slowly varying envelope of the interaction $V(t)$, ω_L is the laser frequency and $\phi(t)$ is the slowly varying phase. Transforming to the interaction picture and making the RWA, as in chapter two, yields

$$i\dot{c}_o = -\int_o^\infty d\varepsilon \frac{\Omega_{o\varepsilon} c_\varepsilon \exp(i\phi - i\Delta_\varepsilon t)}{2} \qquad 5.1,4a$$

and

$$i\dot{c}_\varepsilon = -\frac{\Omega_{\varepsilon o} c_o \exp(-i\phi + i\Delta_\varepsilon t)}{2} \qquad 5.1,4b$$

where the transform used is $c_j = a_j \exp(i\omega_j t)$ and $\Delta_\varepsilon = \omega_\varepsilon - \omega_o - \omega_L$. Equation 4b is formally integrated with respect to time, taking $c_\varepsilon(t=0) = 0$ and $c_o(t=0) = 1$, ie all of the population is initially in the bound state. This is then substituted into equation 4a to eliminate the continuum amplitudes, giving an integro-differential equation for $c_o(t)$,

$$\dot{c}_o(t) = -\int_o^\infty d\varepsilon \int_o^t dt' \frac{\Omega_{o\varepsilon}(t)\Omega_{\varepsilon o}(t')}{4} \exp(-i\Delta_\varepsilon(t-t') + i(\phi(t)-\phi(t'))c_o(t). \qquad 5.1,5$$

Thus c_o depends upon its amplitude at all previous times, ie it is non-Markovian. It is not possible to proceed with this analytically unless the Markov approximation is made [Cohen-Tannoudji etal 1977 and Haken 1981] in which it is assumed that c_o only depends upon the current value of c_o. This is justified as follows; assume that the matrix elements $\Omega_{\varepsilon o}$ are only slowly dependent on ε and are of width $\sim \sigma$. The exponential term, $\exp(-i\Delta_\varepsilon(t-t'))$, is oscillatory in ε and of period $\sim 2\pi/(t-t')$. The $d\varepsilon$ integral is therefore zero unless this period is of the order of $\sigma/\hbar$. Thus the only contribution is made when $t-t' \lesssim 2\pi\hbar/\sigma$. In the Markov approximation $\Omega_{o\varepsilon}$ is assumed to be so flat in ε that $\sigma \to \infty$ and the only contribution is at $t = t'$. Hence equation 5 becomes

$$\dot{c}_o = -c_o\int_o^\infty d\varepsilon \frac{|\Omega_{o\varepsilon}|^2}{4}\int_o^t dt' \exp(-i\Delta_\varepsilon(t-t')). \qquad 5.1,6$$

The phase term is now lost. This is expected as the continuum has been assumed flat so that it does not matter where the bound state is tuned to, even if it is varying, as only the bound state population is required here. The dt' integral can be approximated by letting it run from $-\infty$ to t, as for $|t-t'| > 2\pi\hbar/\sigma$ the $d\varepsilon$ integral is zero. Thus, putting $T = t-t'$ the dt' integral becomes

$$\int_{-\infty}^t dt' \exp(-i\Delta_\varepsilon(t-t')) = \int_o^\infty dT \exp(-i\Delta_\varepsilon T) = -i\mathcal{P}(1/\Delta_\varepsilon) + \pi\delta(\Delta_\varepsilon). \qquad 5.1,7$$

This last part, in terms of the principal part and delta function, can be found in Cohen-Tannoudji etal 1977. So equation 6 becomes

$$\dot{c}_o = -\frac{c_o}{4}\int_o^\infty d\varepsilon |\Omega_{o\varepsilon}|^2 \{-i\,\mathcal{P}\frac{1}{\Delta_\varepsilon} + \pi\delta(\Delta_\varepsilon)\} \qquad 5.1,8$$

giving

$$\dot{c}_o = c_o\left\{i\mathcal{P}\int d\varepsilon \frac{|\Omega_{o\varepsilon}|^2}{4\Delta_\varepsilon} - \frac{\pi\hbar}{4}|\Omega_{o\varepsilon_1}|^2\right\} \qquad 5.1,9$$

where $\varepsilon_1 = \hbar(\omega_o+\omega_L)$ is the energy at which the laser plus bound state is tuned. The complex part contributes to the phase of c_o only, and therefore does not affect the population, causing an energy shift given by

$$\delta E = \hbar\mathcal{P}\int_o^\infty d\varepsilon \frac{|\Omega_{o\varepsilon}|^2}{4\Delta_\varepsilon}. \qquad 5.1,10$$

The real part, however, is a decay term due to the interaction with the continuum. The population in the bound state $|0\rangle$ is given by

$$P_o = |c_o|^2 = \exp(-\int_o^t \Gamma(t')dt') \qquad 5.1,11$$

where

$$\Gamma(t) = \frac{\pi\hbar}{2}|\Omega_{o\epsilon_1}(t)|^2. \qquad 5.1,12$$

This is the dynamic decay 'constant' for non-constant excitation pulses. For a constant interaction this is identical to the decay rate predicted by the Golden Rule as $V = \Omega\hbar/2$ due to the RWA. The Golden Rule predicts a constant rate of loss of population, and for very weak interactions this is approximately true, as the bound state does not get noticeably depleted. However, for strong interactions the rate decreases exponentially as the population decreases likewise. For interactions which are not constant the decay rate is simply proportional to the instantaneous intensity, ie $|\Omega_{o\epsilon}(t)|^2$, and the population remaining in the discrete state is obtained by integrating this loss.

This problem has been solved assuming that the continuum is structureless and the perturbative approximation has been shown to give correct results. In the next section a structured continuum is discussed where the structure is caused by an embedded bound state.

5.2 The Fano eigenstates

Figure 5.1.ib shows a bound state $|B\rangle$ embedded in the continuum $|C,\varepsilon\rangle$ by an interaction T. In order to solve for the decay of state $|0\rangle$ into this combination of bound and continuum states it is necessary to calculate the eigenstates which diagonalise the interaction T between them. These eigenstates are the Fano states, $|F,\varepsilon\rangle$, and are modified continuum states. The Fano states can be expanded in terms of the old states $|B\rangle$ and $|C,\varepsilon\rangle$ giving

$$|F,\varepsilon\rangle = b(\varepsilon)|B\rangle + \int_0^\infty d\varepsilon' c(\varepsilon,\varepsilon')|C,\varepsilon'\rangle. \qquad 5.2,1$$

The old states $|B\rangle$ and $|C,\varepsilon\rangle$ are eigenstates of the Hamiltonian H_o such that

$$H_o|B\rangle = E_B|B\rangle \qquad 5.2,2a$$

and

$$H_o|C,\varepsilon\rangle = \varepsilon|C,\varepsilon\rangle. \qquad 5.2,2b$$

The Fano states are eigenstates of the Hamiltonian including the interaction T, such that

$$H = H_o + T \qquad 5.2,3a$$

and

$$H|F,\varepsilon\rangle = \varepsilon|F,\varepsilon\rangle. \qquad 5.2,3b$$

Pre-multiplying equation 1 by $\langle B|H$ gives

$$(\varepsilon - E_B)b(\varepsilon) = \int_0^\infty d\varepsilon' c(\varepsilon,\varepsilon')T_{B\varepsilon'}. \qquad 5.2,4$$

where

$$T_{B\varepsilon'} = \langle B|T|C,\varepsilon'\rangle. \qquad 5.2,5$$

Pre-multiplying by $\langle C,\varepsilon'|H$ gives

$$(\varepsilon-\varepsilon')c(\varepsilon,\varepsilon') = b(\varepsilon)T_{\varepsilon\cdot B}. \qquad 5.2,6$$

This can be substituted into equation 4 to give an equation for $b(\varepsilon)$. However, there is a pole at $\varepsilon = \varepsilon'$ so that $1/(\varepsilon-\varepsilon')$ must be written in its principal and delta function parts giving

$$c(\varepsilon,\varepsilon') = b(\varepsilon)T_{\varepsilon\cdot B}\left\{\frac{P}{(\varepsilon-\varepsilon')} + z(\varepsilon)\delta(\varepsilon-\varepsilon')\right\} \qquad 5.2,7$$

where $z(\varepsilon)$ is to be determined. Substituting this into 4 gives

$$(\varepsilon-E_B)b(\varepsilon) = b(\varepsilon)\int_o^\infty d\varepsilon' |T_{B\varepsilon\cdot}|^2\left\{\frac{P}{(\varepsilon-\varepsilon')} + z(\varepsilon)\delta(\varepsilon-\varepsilon')\right\}. \qquad 5.2,8$$

In general $b(\varepsilon)$ is non-zero so that z is given by

$$z(\varepsilon) = \frac{(\varepsilon-E'_B(\varepsilon))}{|T_{B\varepsilon}|^2}, \qquad 5.2,9$$

where

$$E'_B(\varepsilon) = E_B + \int_o^\infty d\varepsilon' |T_{B\varepsilon\cdot}|^2 \frac{P}{(\varepsilon-\varepsilon')}. \qquad 5.2,10$$

Substituting equations 7 and 9 into 1 gives

$$|F,\varepsilon\rangle = b(\varepsilon)\left\{|B\rangle + \frac{[\varepsilon-E'_B(\varepsilon)]}{T_{B\varepsilon}}|C,\varepsilon\rangle + \int_o^\infty d\varepsilon' T_{\varepsilon\cdot B}\frac{P}{(\varepsilon-\varepsilon')}|C,\varepsilon'\rangle\right\}. \qquad 5.2,11$$

Finally the normalisation condition $\langle F,\varepsilon'|F,\varepsilon\rangle = \delta(\varepsilon-\varepsilon')$ is used to obtain $b(\varepsilon)$ so that

$$\delta(\varepsilon'-\varepsilon) = b^*(\varepsilon')b(\varepsilon)\left[1+\int_o^\infty d\varepsilon'' |T_{\varepsilon''B}|^2\left\{\frac{P}{(\varepsilon'-\varepsilon'')}+z(\varepsilon')\delta(\varepsilon'-\varepsilon'')\right\}\left\{\frac{P}{(\varepsilon-\varepsilon'')}+z(\varepsilon)\delta(\varepsilon-\varepsilon'')\right\}\right]. \qquad 5.2,12$$

This is complicated by the product of two principal parts and the treatment of this is dealt with in appendix 5.A which gives

$$|b(\varepsilon)|^2 = \frac{1}{|T_{\varepsilon B}|^2(\pi^2+z^2(\varepsilon))} \qquad 5.2,13a$$

$$= \frac{|T_{\varepsilon B}|^2}{\pi^2|T_{\varepsilon B}|^4+(\varepsilon-E'_B(\varepsilon))^2}. \qquad 5.2,13b$$

Thus, ignoring the overall phase

$$|F,\varepsilon\rangle = \frac{1}{[(\pi|T_{\varepsilon B}|^2)^2+(\varepsilon-E'_B(\varepsilon))^2]^{1/2}} X$$

$$\left[T_{B\varepsilon}|B\rangle+(\varepsilon-E'_B(\varepsilon))|C,\varepsilon\rangle+T_{B\varepsilon}\int_0^\infty d\varepsilon' T_{\varepsilon\cdot B}\frac{P}{(\varepsilon-\varepsilon')}|C,\varepsilon\rangle\right]. \qquad 5.2,14$$

Thus the old discrete state $|B\rangle$ is mixed with the continuum by T to produce a modified, or dressed, discrete state $|\Psi(\varepsilon)\rangle$, where

$$|\Psi(\varepsilon)\rangle = |B\rangle + \int_0^\infty d\varepsilon' T_{\varepsilon\cdot B}\frac{P}{(\varepsilon-\varepsilon')}|C,\varepsilon'\rangle, \qquad 5.2,15$$

so that

$$|F,e\rangle = \frac{1}{[(\pi|T_{\varepsilon B}|^2)^2+(\varepsilon-E'_B(\varepsilon))^2]^{1/2}}\left[T_{B\varepsilon}|\Psi(\varepsilon)\rangle+(\varepsilon-E'_B(\varepsilon))|C,\varepsilon\rangle\right]. \qquad 5.2,16$$

This new continuum is no longer flat in ε. $T_{\varepsilon B}$ is assumed, as in section 5.1.1, to be fairly constant in ε, as it just couples a bound state $|B\rangle$ to a flat continuum. Thus the old continuum is modified by a factor having a dispersive dependence on ε and the modified bound state $|\Psi(\varepsilon)\rangle$ has a square root Lorentzian factor, both centred on $\varepsilon = E'_B(\varepsilon)$. This state can now be probed by a weak interaction V from another bound state $|0\rangle$ and the Golden Rule used to calculate the rate of decay of the population initially in state $|0\rangle$. So

$$\Gamma_{OF} = \frac{2\pi}{\hbar}\int_0^\infty d\varepsilon\,\delta(\varepsilon-\varepsilon_i)\,|\langle 0|V|F,\varepsilon\rangle|^2, \qquad 5.2,17$$

giving

$$\Gamma_{OF} = \frac{\Gamma_{O\neq i}}{(\Gamma_{\neq i B}\hbar/2)^2+(\varepsilon_i-E'_B(\varepsilon_i))^2}\left\{\left(\frac{\Gamma_{B\neq i}\hbar}{2}\right)q(\varepsilon_i)+\varepsilon_i-E'_B(\varepsilon_i)\right\}, \qquad 5.2,18$$

where

$$\Gamma_{O\neq i} = \frac{2\pi}{\hbar}|V_{O\neq i}|^2 \qquad 5.2,19a$$

is the decay rate from $|0\rangle$ to the old continuum,

$$\Gamma_{B\neq i} = \frac{2\pi}{\hbar}|V_{B\neq i}|^2 \qquad 5.2,19b$$

is the decay rate of $|B\rangle$ into the old continuum and the Fano q parameter [Fano 1961], given by,

$$q(\varepsilon) = \frac{\langle 0|V|\Psi(\varepsilon)\rangle}{\langle 0|V|C,\varepsilon\rangle\pi T_{\neq B}} \qquad 5.2,19c$$

is the ratio of the transition probability into the modified bound state to that into the old continuum. So the ratio of the decay into the Fano continuum to the decay into the old continuum is given by

$$\frac{\Gamma_{OF}}{\Gamma_{O\neq i}} = \frac{|q(\varepsilon_i)+e(\varepsilon_i)|^2}{1+e^2(\varepsilon_i)} \qquad 5.2,20$$

where $e(\varepsilon)$ is a normalised detuning given by

$$e(\varepsilon) = \frac{2(\varepsilon-E'_B(\varepsilon))}{\hbar\Gamma_{B\neq}}. \qquad 5.2,21$$

Fig i, taken from Knight 1984, shows the ratio of the decay rates for various different values of q against the normalised detuning showing the famous Fano profile.

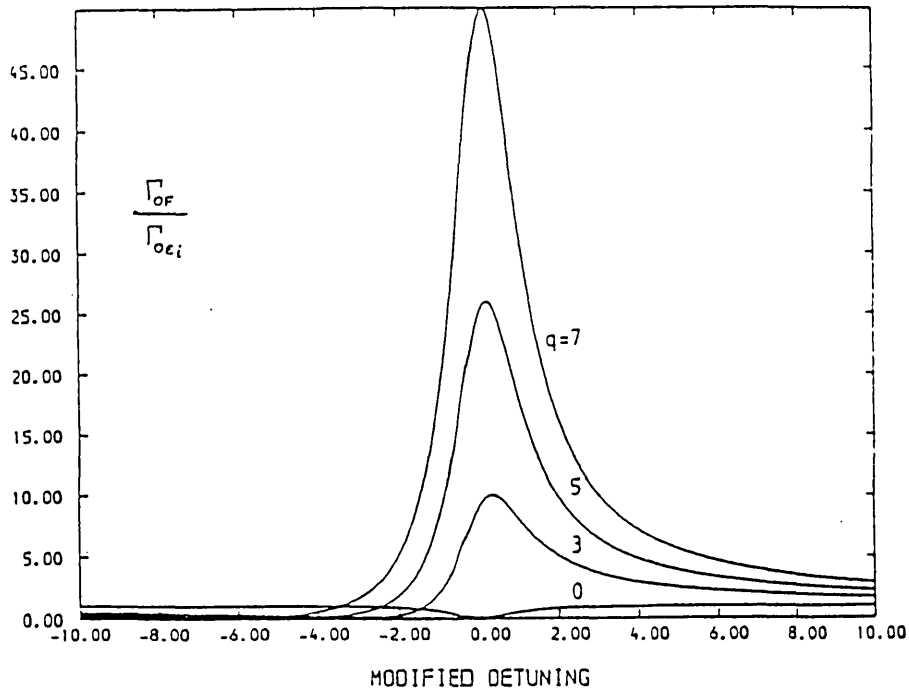


Fig 5.2.i

Enhancement in photoionisation rates to a Fano continuum as a function of dimensionless detuning.

For large q the coupling to the modified bound state is dominant giving an almost Lorentzian profile with a FWHM of 2. For low q the coupling to the old continuum dominates giving an asymmetric lineshape with a zero at e = -q where the two decay channels destructively interfere. The parameter q can be determined by finding the ratio of the peak heights, at e = 1/q, to the height at the large e limit. The ratio of these two heights is just $1 + q^2$. From equations 19c and 15 the Fano parameter can be expanded in terms of the original bound and continuum states, to give

$$q(\varepsilon) = \frac{\langle 0|V|B\rangle + \int d\varepsilon' T_{\varepsilon' \cdot B} P/(\varepsilon-\varepsilon') \langle 0|V|C,\varepsilon'\rangle}{\langle 0|V|C,\varepsilon\rangle \pi T_{\varepsilon B}} \qquad 5.2,22$$

Ordinarily, the coupling from $|0\rangle$, directly to the bound state $|B\rangle$ dominates over that to the continuum. However, under certain circumstances the coupling to the continuum can dominate. If the

interactions T and V are dipole interactions, that is both states $|0\rangle$ and $|B\rangle$ are coupled to the continuum by laser fields, then the coupling $\langle 0|V|B\rangle$ is not allowed by the dipole selection rule. This means that q is determined by the coupling $\langle 0|V|C,\varepsilon'\rangle$.

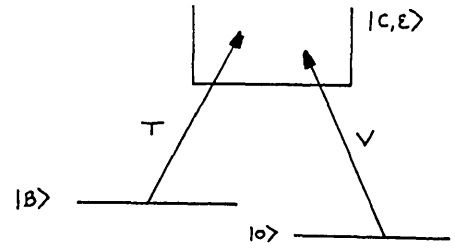


Fig 5.2.ii

Two lasers coupled into a continuum with no direct bound state coupling due to the dipole selection rule.

Fig ii shows this situation, where there is no transition allowed from $|0\rangle$ to $|B\rangle$ directly. This would appear to rule out the possibility of interference, and therefore a window, as there is only one path from $|0\rangle$ to the continuum. Under these circumstances the principal part term in q dominates and the two interfering paths are the two-photon direct and stepwise routes. This is then similar to the interference caused by these two routes in the three level system solved perturbatively in chapter three. As the T coupling is due to another laser then the structure is potentially adjustable in both position and width. The position is set by the laser frequency and the width by the intensity. For this case, where there is no single-photon coupling between the two bound states, the Fano q parameter is given by the ratio of the real to the imaginary part of the two-photon Rabi frequency between the two levels [Knight 1980, Milonni and Eberly 1978],

$$q(\varepsilon_i) = \int_0^\infty \frac{d\varepsilon' P/(\varepsilon_i-\varepsilon')\langle 0|V|C,\varepsilon'\rangle\langle C,\varepsilon'|T|B\rangle}{\pi\langle 0|V|C,\varepsilon_i\rangle\langle C,\varepsilon_i|T|B\rangle}, \qquad 5.2,23$$

where the continuum has caused the Rabi frequency to become complex

$$\Omega_{OB} = \lim_{X\to 0} \int_0^\infty \frac{d\varepsilon'\langle 0|V|C,\varepsilon'\rangle\langle C,\varepsilon'|T|B\rangle}{\varepsilon_i-\varepsilon'+iX}. \qquad 5.2,24$$

This can be split into its real and imaginary parts using, from, for example, Heitler 1954

$$\lim_{X\to 0^+} \frac{1}{x+iX} = P\left(\frac{1}{x}\right) - i\pi\delta(x). \qquad 5.2,25$$

This treatment is applicable to cases in which the probe interaction, V, is weak and does not alter the continuum structure. In the next section both interactions are allowed to be strong. This can be treated by dressing the two bound states to the continuum states as done by Coleman 1983, or by using the TDO method after eliminating the continuum. This latter method is used as it also allows the inclusion of pulse shapes which the dressed states model is unable to cope with.

5.3 Trapping in LICS

Fig i shows two bound states strongly coupled to a continuum. Here it is not applicable to talk of embedding and probe lasers as both cause structure in the continuum. The equations of motion for the two bound states include the continuum levels.

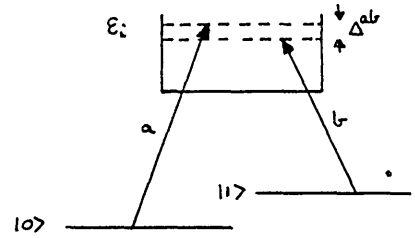


Fig 5.3.i
Two bound states strongly coupled to a continuum.

In order to find the populations in the bound states using the TDO method, the continuum must be eliminated. This is done as in section 5.1 using the Markov approximation in a similar way.

5.3.1 Pulse shape effects

The equations of motion for the amplitudes to be in the two bound states and the continuum are almost identical to those in section 5.1.1, and are written, in the Schrödinger picture, as

$$i\dot{a}_o(t) = \omega_o a_o(t) - \int_o^\infty d\varepsilon \Omega_{o\varepsilon}^a(t)\cos\{\omega_a t+\phi_a(t)\}a_\varepsilon(t)$$

$$-\int_o^\infty d\varepsilon \Omega_{o\varepsilon}^b(t)\cos\{\omega_b t+\phi_b(t)\}a_\varepsilon(t) \quad , \qquad 5.3,1a$$

$$i\dot{a}_1(t) = \omega_1 a_1(t) - \int_0^\infty d\varepsilon \Omega^a_{1\varepsilon}(t)\cos(\omega_a t+\phi_a(t))a_\varepsilon(t)$$

$$-\int_0^\infty d\varepsilon \Omega^b_{1\varepsilon}(t)\cos(\omega_b t+\phi_b(t))a_\varepsilon(t) \qquad 5.3,1b$$

and

$$i\dot{a}_\varepsilon(t) = \omega_\varepsilon a_\varepsilon(t) - a_0(t)[\Omega^a_{\varepsilon 0}(t)\cos(\omega_a t+\phi_a(t))+\Omega^b_{\varepsilon 0}(t)\cos(\omega_b t+\phi_b(t))]$$

$$-a_1(t)[\Omega^a_{\varepsilon 1}(t)\cos(\omega_a t+\phi_a(t))+\Omega^b_{\varepsilon 1}(t)\cos(\omega_b t+\phi_b(t))] \qquad 5.3,1c$$

where the scripts a and b denote the two lasers used, frequency ω_a and ω_b with phase $\phi_a(t)$ and $\phi_b(t)$ respectively. It is assumed, for the moment, that both lasers can ionise either of the bound states. These equations are transformed to the Interaction picture, using the transform $a_j \rightarrow c_j = a_j\exp(i\omega_j t)$; the cosine terms are split into the exponential representation and the detunings $\Delta^{1c} = \omega_\varepsilon - \omega_1 - \omega_c$ are substituted, giving

$$i\dot{c}_0(t) = -\int_0^\infty d\varepsilon c_\varepsilon(t)[\Omega^a_{0\varepsilon}(t)\exp(-i\Delta^{0a}t+i\phi_a(t))+\Omega^b_{0\varepsilon}(t)\exp(-i\Delta^{0b}t+i\phi_b(t))]/2, \qquad 5.3,2a$$

$$i\dot{c}_1(t) = -\int_0^\infty d\varepsilon c_\varepsilon(t)[\Omega^a_{1\varepsilon}(t)\exp(-i\Delta^{1a}t+i\phi_a(t))+\Omega^b_{1\varepsilon}(t)\exp(-i\Delta^{1b}t+i\phi_b(t))]/2 \qquad 5.3,2b$$

and

$$c_\varepsilon(t) =$$

$$i\int_0^t dt'\Big\{c_0(t')[\Omega^a_{\varepsilon 0}(t')\exp(i\Delta^{0a}t'-i\phi_a(t'))+\Omega^b_{\varepsilon 0}(t')\exp(i\Delta^{0b}t'-i\phi_b(t'))]$$

$$+ c_1(t')[\Omega^a_{\varepsilon 1}(t')\exp(i\Delta^{1a}t-i\phi_a(t))+\Omega^b_{1\varepsilon}(t)\exp(i\Delta^{1b}t-i\phi_b(t))]\Big\}/2$$

$$5.3,2c$$

where the RWA has been made and the last equation has been explicitly integrated to allow for subsequent substitution. Javanainen 1983 examines the validity of the RWA in bound/free transitions, concluding that the approximation is valid under the same circumstances as in bound/bound transitions.

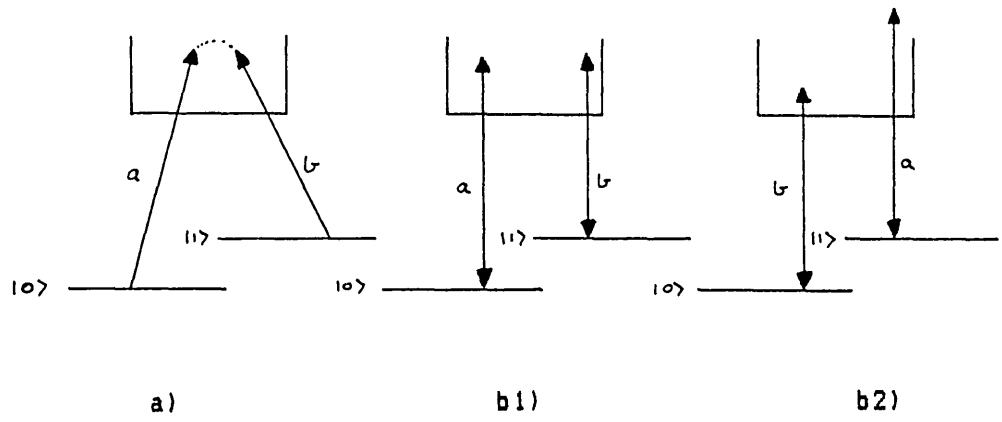


Fig 5.3.ii
The two-photon processes allowed.

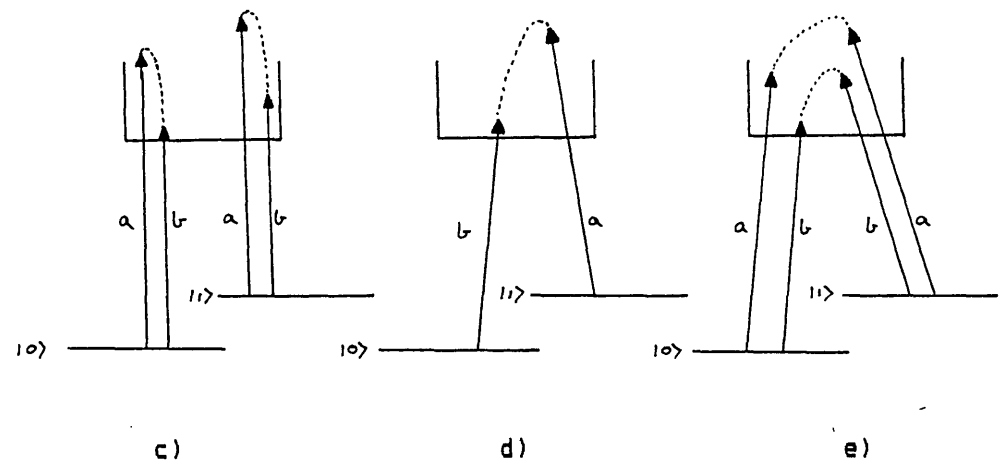


Fig 5.3.ii
The forbidden two-photon processes.

Figs iia and b show the two-photon transitions which are to be allowed. Figs c, d and e show those that that are to be forbidden. ω_a, ω_b and ω_0, ω_1 are sufficiently different that there is a negligible

coupling for the forbidden processes. This occurs if $|\omega_o-\omega_1|$ and $|\omega_a-\omega_b|$ are much greater than the inverse pulse width and the widths of the bound states due to other decay processes etc. The single-photon decays caused by either laser are still allowed for each state. Thus, substituting equation 2c into a and b and eliminating the forbidden transitions gives

$$\dot{c}_o(t) = -\frac{1}{4}\int_o^\infty d\varepsilon \int_o^t dt' \Big\{ c_o(t') \Big[\Omega^a_{o\varepsilon}(t)\Omega^a_{\varepsilon o}(t') \exp(-i\Delta^{oa}(t-t') + i(\phi_a(t)-\phi_a(t')) + \Omega^b_{o\varepsilon}(t)\Omega^b_{\varepsilon o}(t') \exp(-i\Delta^{ob}(t-t') + i(\phi_b(t)-\phi_b(t')) \Big] + c_1(t')\,\Omega^a_{o\varepsilon}(t)\Omega^b_{\varepsilon 1}(t') \exp(-i(\Delta^{oa}t - \Delta^{1b}t') + i(\phi_a(t)-\phi_b(t')) \Big\} \qquad 5.3,3a$$

and

$$\dot{c}_1(t) = -\frac{1}{4}\int_o^\infty d\varepsilon \int_o^t dt' \Big\{ c_1(t') \Big[\Omega^a_{1\varepsilon}(t)\Omega^a_{\varepsilon 1}(t') \exp(-i\Delta^{1a}(t-t') + i(\phi_a(t)-\phi_a(t')) + \Omega^b_{1\varepsilon}(t)\Omega^b_{\varepsilon 1}(t') \exp(-i\Delta^{1b}(t-t') + i(\phi_b(t)-\phi_b(t')) \Big] + c_o(t')\,\Omega^b_{1\varepsilon}(t)\Omega^a_{\varepsilon o}(t') \exp(-i(\Delta^{1b}t - \Delta^{oa}t') + i(\phi_b(t)-\phi_a(t')) \Big\} \qquad 5.3,3b$$

Now the Markov approximation is made in an identical way to that in section 5.1 giving

$$\dot{c}_o = c_o \Big\{ iP \int d\varepsilon \frac{|\Omega^a_{o\varepsilon}|^2}{4\Delta^{oa}} - \frac{\pi\hbar}{4}|\Omega^a_{o\varepsilon^{oa}}|^2 + iP \int d\varepsilon \frac{|\Omega^b_{o\varepsilon}|^2}{4\Delta^{ob}} - \frac{\pi\hbar}{4}|\Omega^b_{o\varepsilon^{ob}}|^2 \Big\} + \exp(i(\phi_a-\phi_b-\Delta^{ab}t))\,c_1 \Big\{ iP \int d\varepsilon \frac{\Omega^a_{o\varepsilon}\,\Omega^b_{\varepsilon 1}}{4\Delta_{\varepsilon\cdot}} - \frac{\pi\hbar}{4}\Omega^a_{o\varepsilon\cdot}\Omega^b_{\varepsilon\cdot 1} \Big\} \qquad 5.3,4a$$

and

$$\dot{c}_1 = c_1\left\{ iP\int d\varepsilon \frac{|\Omega^a_{1\varepsilon}|^2}{4\Delta^{1a}} - \frac{\pi\hbar}{4}|\Omega^a_{1\varepsilon^{1a}}|^2 \right.$$

$$\left. + iP\int d\varepsilon \frac{|\Omega^b_{1\varepsilon}|^2}{4\Delta^{1a}} - \frac{\pi\hbar}{4}|\Omega^b_{1\varepsilon^{1b}}|^2 \right\}$$

$$+ \exp(-i(\phi_a-\phi_b-\Delta^{ab}t))c_0\left\{ iP\int d\varepsilon \frac{\Omega^b_{1\varepsilon}\,\Omega^a_{\varepsilon 0}}{4\Delta_{\varepsilon\cdot}} - \frac{\pi\hbar}{4}\Omega^b_{1\varepsilon}\cdot\Omega^a_{\varepsilon\cdot 0}\right\} \qquad 5.3,4b$$

where

$$\Delta^{ab} = \Delta^{0a}-\Delta^{1b}, \qquad 5.3,5a$$

$$\varepsilon^{1c} = \hbar\Delta^{1c}, \qquad 5.3,5b$$

$$\varepsilon' = \hbar(\Delta^{0a}+\Delta^{1b})/2 \qquad 5.3,5c$$

and

$$\Omega^a_{0\varepsilon^{0a}}(t) \sim \Omega^a_{0\varepsilon\cdot}(t), \qquad 5.3,5d$$

$$\Omega^b_{1\varepsilon^{1b}}(t) \sim \Omega^b_{1\varepsilon\cdot}(t), \qquad 5.3,5e$$

as the continuum is assumed flat. In a similar way to that used in secction 5.1 the decays and energy shifts, due to the transistions in fig iib, for levels j = 0, 1 are written as

$$\Gamma_j(t) = \frac{\pi\hbar}{2}\left\{|\Omega^a_{j\varepsilon^{ja}}(t)|^2 + |\Omega^b_{j\varepsilon^{jb}}(t)|^2\right\}$$

$$= \Gamma^a_j(t) + \Gamma^b_j(t) \qquad 5.3,6a$$

and

$$\delta E_j(t) = \hbar P\int_0^\infty d\varepsilon\left\{\frac{|\Omega^a_{j\varepsilon}(t)|^2}{4\Delta^{ja}} + \frac{|\Omega^b_{j\varepsilon}(t)|^2}{4\Delta^{jb}}\right\}. \qquad 5.3,6b$$

The transition in fig iia leads to the decays and energy shifts given by

$$\Gamma(t) = \frac{\pi\hbar\Omega^a_{o\varepsilon}\cdot(t)\Omega^b_{\varepsilon\cdot 1}(t)}{2} \sim \sqrt{\Gamma^a_o(t)\Gamma^b_1(t)} \qquad 5.3,7a$$

and

$$\delta E(t) = \hbar P\int_0^\infty d\varepsilon\frac{\Omega^a_{o\varepsilon}(t)\Omega^b_{\varepsilon 1}(t)}{4\Delta_{\varepsilon\cdot}}. \qquad 5.3,7b$$

Equations 4a and b become

$$\begin{pmatrix} c\acute{o} \\ c\acute{i} \end{pmatrix} = -i\begin{pmatrix} -\frac{\delta E_o}{\hbar} - i\frac{\Gamma_o}{2} & -\frac{\Gamma}{2}(q+i) \\ -\frac{\Gamma}{2}(q+i) & -\frac{\delta E_1}{\hbar} - i\frac{\Gamma_1}{2} + \Delta^{ab} - (\dot\phi_a - \dot\phi_b) \end{pmatrix}\begin{pmatrix} c\acute{o} \\ c\acute{i} \end{pmatrix} \qquad 5.3,8$$

where the transform

$$\begin{pmatrix} c_o \\ c_1 \end{pmatrix} \to \begin{pmatrix} c\acute{o} \\ c\acute{i} \end{pmatrix} = \begin{pmatrix} 1 & 0 \\ 0 & \exp(i(\dot\phi_a - \dot\phi_b - \Delta^{ab})t) \end{pmatrix}\begin{pmatrix} c_o \\ c_1 \end{pmatrix} \qquad 5.3,9$$

is used to reduce the time dependence of the operator and put the equation into a form solvable by the TDO method. This is an Hermitian transform so that the populations in levels $|0\rangle$ and $|1\rangle$ are still given by $P_o = |c_o|^2 = |c\acute{o}|^2$ and $P_1 = |c_1|^2 = |c\acute{i}|^2$ respectively. The Fano q parameter is defined as in equation 5.1,19 remembering that the direct transition $|0\rangle$ to $|1\rangle$ is now forbidden, so that

$$q(\varepsilon) = \frac{\delta E(t)}{\hbar\Gamma(t)/2} \qquad 5.3,10$$

where the time dependences cancel leaving q time independent. In order to investigate the continuum structure explicitly, without the background radiation, the interactions in fig iib2 are forbidden so that $\Gamma_o^b = \Gamma_1^a = 0$. This means that laser a can only excite level $|0\rangle$ and laser b, level $|1\rangle$. For the moment it is assumed that the pulses are constant so that an analytical result can be obtained. This means that the energy Stark shifts can be ignored as they only cause a constant displacement in the energy levels. As the continuum is assumed flat this has no effect on the bound state populations. Equation 8 can now be written

$$\begin{pmatrix} \dot{c_o} \\ \dot{c_i} \end{pmatrix} = -i \begin{pmatrix} -i\frac{\Gamma_o}{2} & -\frac{\sqrt{\Gamma_o\Gamma_1}}{2}(q+i) \\ -\frac{\sqrt{\Gamma_o\Gamma_1}}{2}(q+i) & -i\frac{\Gamma_1}{2}+\Delta^{ab} \end{pmatrix} \begin{pmatrix} \dot{c_o} \\ \dot{c_i} \end{pmatrix} \qquad 5.3,11$$

where the phase terms have also been discarded so the lasers are assumed perfectly coherent. This is solved analytically to yield

$$\dot{c_o}(t) = \frac{\exp(\alpha t)}{2\beta}[(\beta+\alpha')\exp(\beta t) + (\beta-\alpha')\exp(-\beta t)] \qquad 5.3,12a$$

$$\dot{c_i}(t) = \frac{\sqrt{\Gamma_o\Gamma_1}}{4\beta}(1-iq)\exp(\alpha t)[\exp(\beta t) - \exp(-\beta t)] \qquad 5.3,12b$$

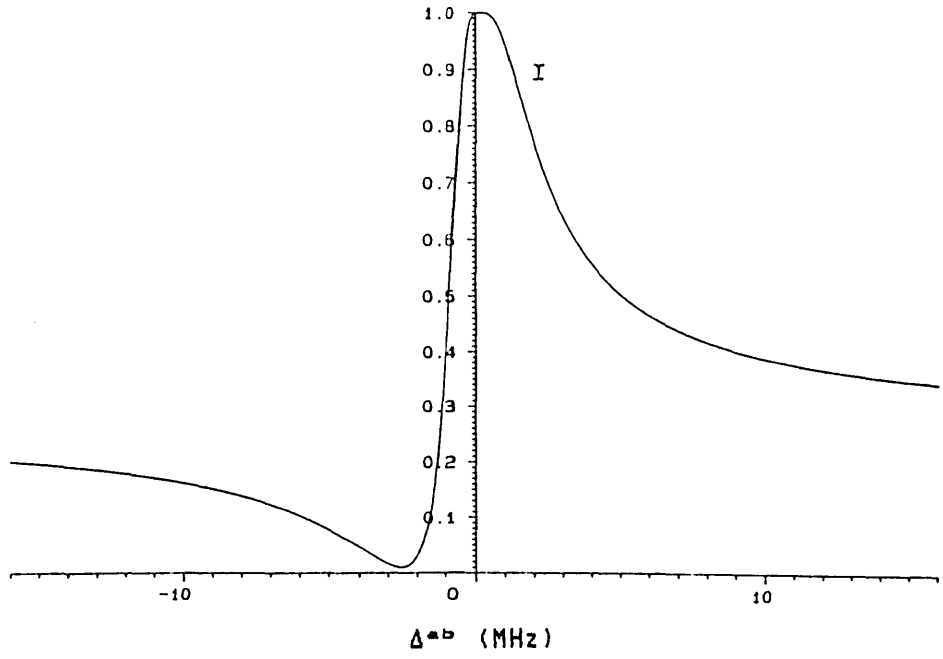
where

$$\alpha = -\frac{(\Gamma_o+\Gamma_1)}{4} - i\frac{\Delta^{ab}}{2}, \qquad 5.3,13a$$

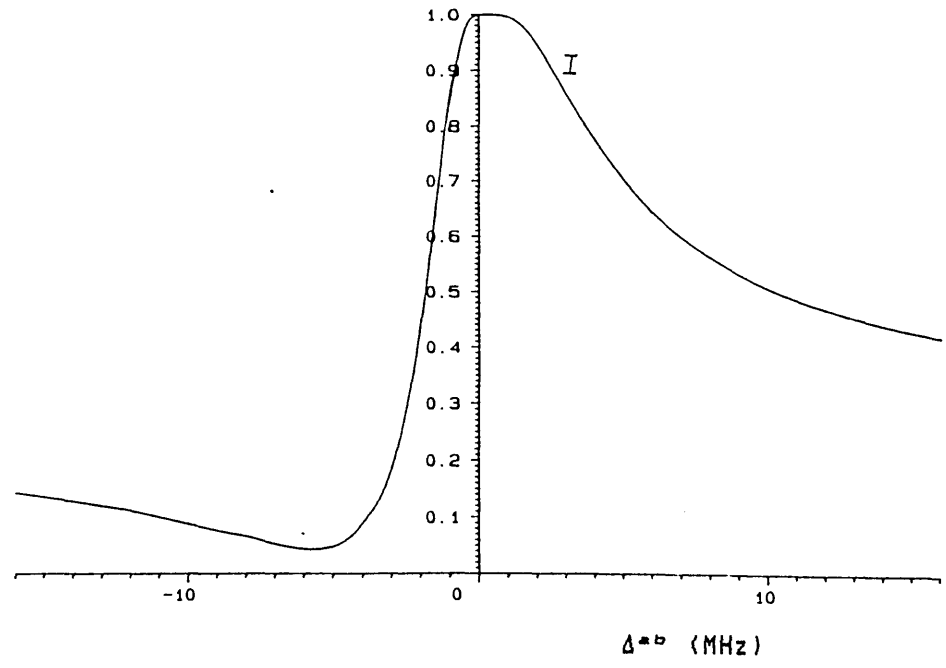
$$\alpha' = -\frac{(\Gamma_o-\Gamma_1)}{4} + i\frac{\Delta^{ab}}{2} \qquad 5.3,13b$$

and

$$\beta = \left\{\alpha'^2 + \frac{\Gamma_o\Gamma_1}{4}(1-iq)^2\right\}^{1/2}. \qquad 5.3,13c$$



a) both pulses flat



b) both pulses Gaussian

Fig 5.3.iii

The Fano profile for different pulse shapes,

Γ_o = 0.02π Mrads s^{-1}, Γ_1 = 2π Mrads s^{-1}, q = 5 and t = 5 μs.

This is the analytic result for the amplitudes to be in the bound states for two strong, flat laser pulses independently coupling two bound states into a flat continuum with a two-photon detuning Δ^{ab}. All the population is initially in state $|0\rangle$. No decay has been included which is not ionisation, so the number of ions produced is just

$$I(\Delta^{ab}) = 1 - |c_0|^2 - |c_1|^2. \qquad 5.3,14$$

5.3.1.1 Probed continuum structure.

Fig iiia shows the ions created, as a function of two-photon detuning, for a weak probe case (laser a is the probe) and flat pulses. The parameters used are $\Gamma_0 = 0.02\pi$ Mrads s^{-1}, $\Gamma_1 = 2\pi$ Mrads s^{-1}, $q = 5$, and the graphs are plotted at time $t = 5$ μs. This shows the traditional Fano lineshape with an ion enhancement and window. The ion yield at the window does not decrease all the way to zero as the probe laser is not infinitely small in amplitude and perturbs the continuum structure slightly. The positions of the window and peak are, from equations 5.2,20 and 21, at $\Delta^{ab} = -\Gamma_1 q/2$ and $\Gamma_1/2q$ rads s^{-1} respectively. Fig iiib shows the ionisation as a function of detuning where the pulses are Gaussian. For this the pulses are chosen to be of the same energy as those in the flat pulse case as it is the total energy that is the main factor in determining ionisation. Thus the integral over time of the <u>intensity</u> envelopes are equalised. This is in contrast to previous examples with pulse shapes where the field envelope areas have been equalised. This is due to the different processes involved in the population movement. In the bound/bound processes the phase is important which is present only in the field envelope. In bound/continuum transitions the phases are unimportant for flat continua and, from equation 5.1,11, the rate of decay is proportional to the energy. In fig iiib the minimum is partly destroyed as during the pulse evolution it moves because of its dependence on Γ_1, which is time dependent. This is similar to the effect that pulse shapes have on Stark shifts, as seen in chapter three, where the two peaks move during the course of the pulse. For the same reason the peak is much broader as the maximum intensity is about 2.8 times that of the flat pulse. This means the window moves from zero out to around 7 MHz and back during the evolution of the pulse. In modelling the flat pulses the Stark shifts of the bound

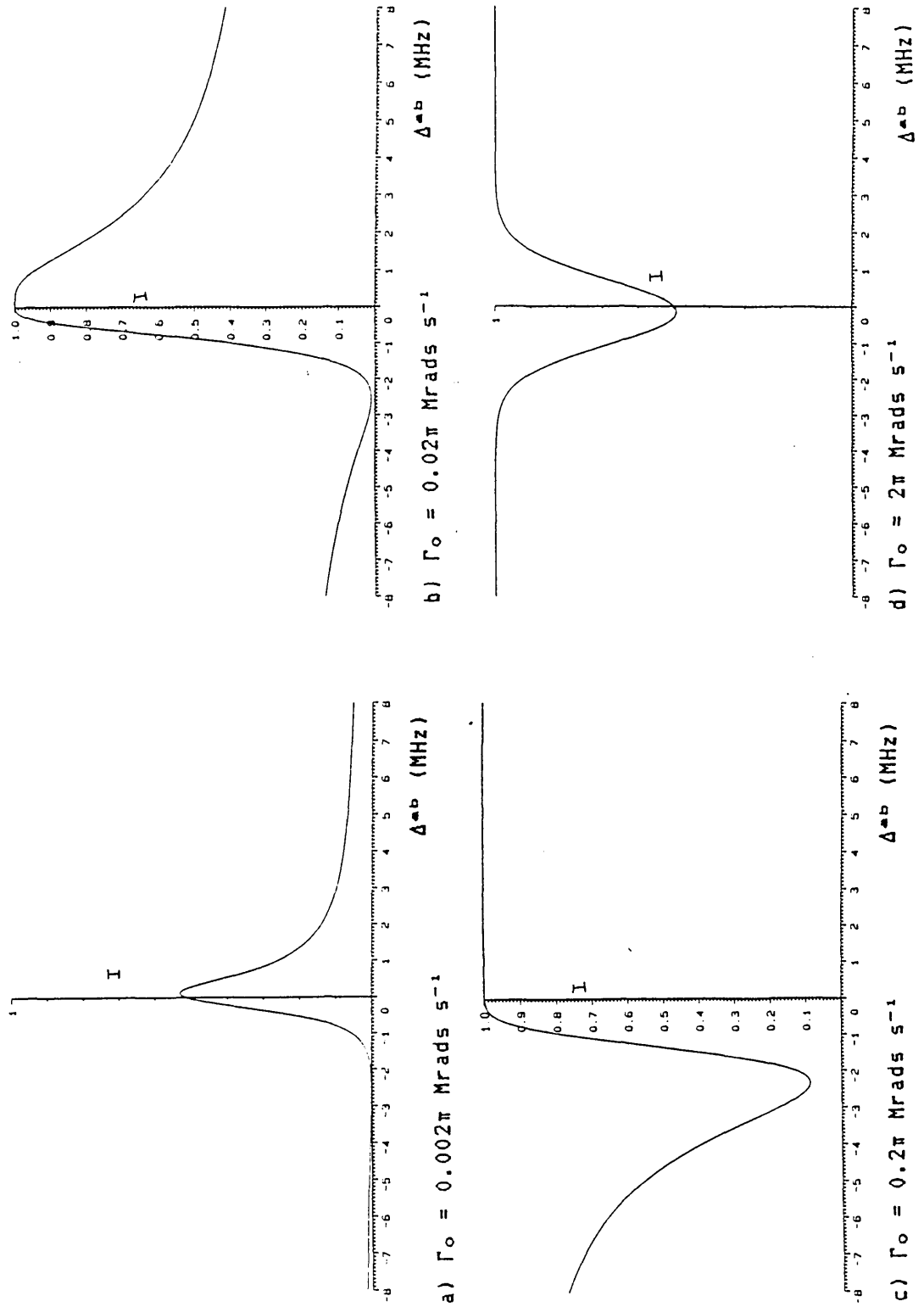


Fig 5.3.iv

The Fano profile as the probe power is increased with flat pulses, Γ_1 = 2π Mrads s^{-1}, q = 5 and t = 5 μs.

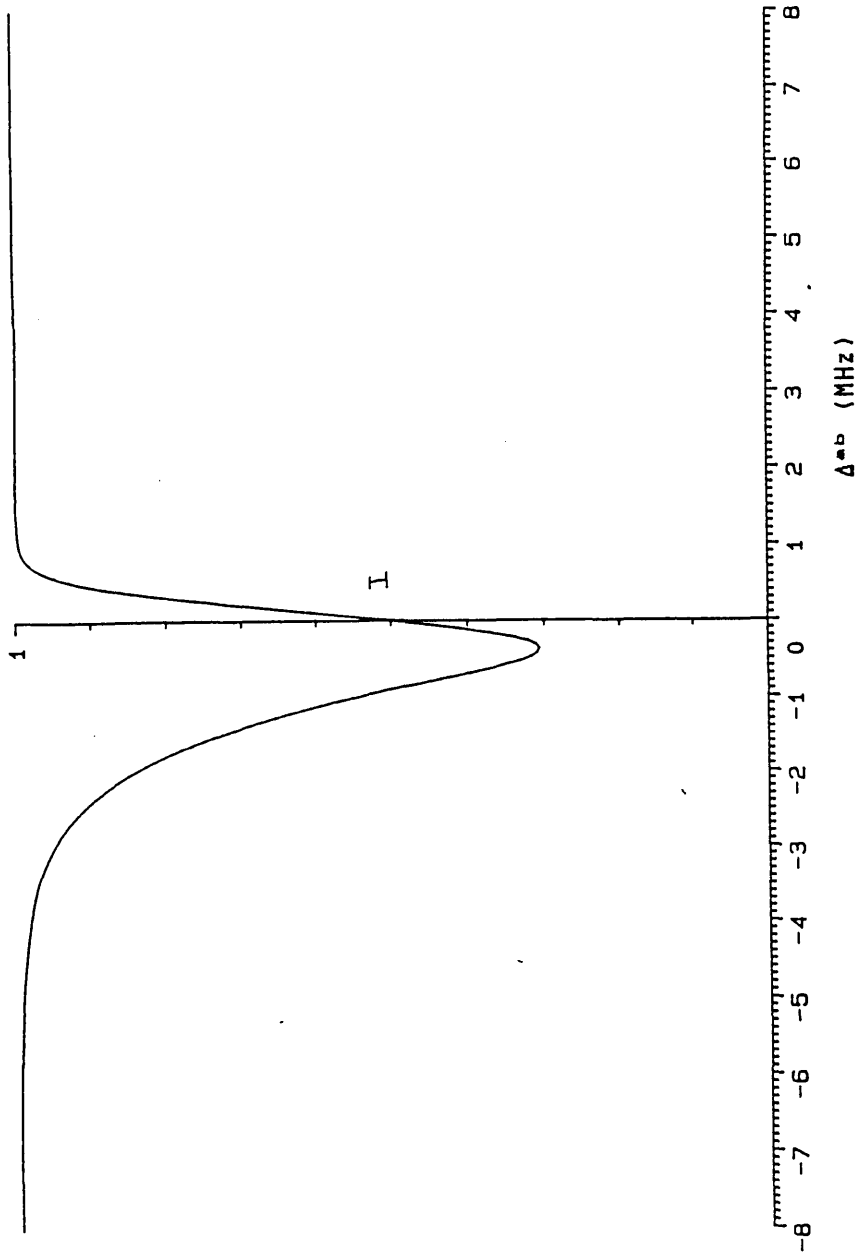


Fig 5.3.v

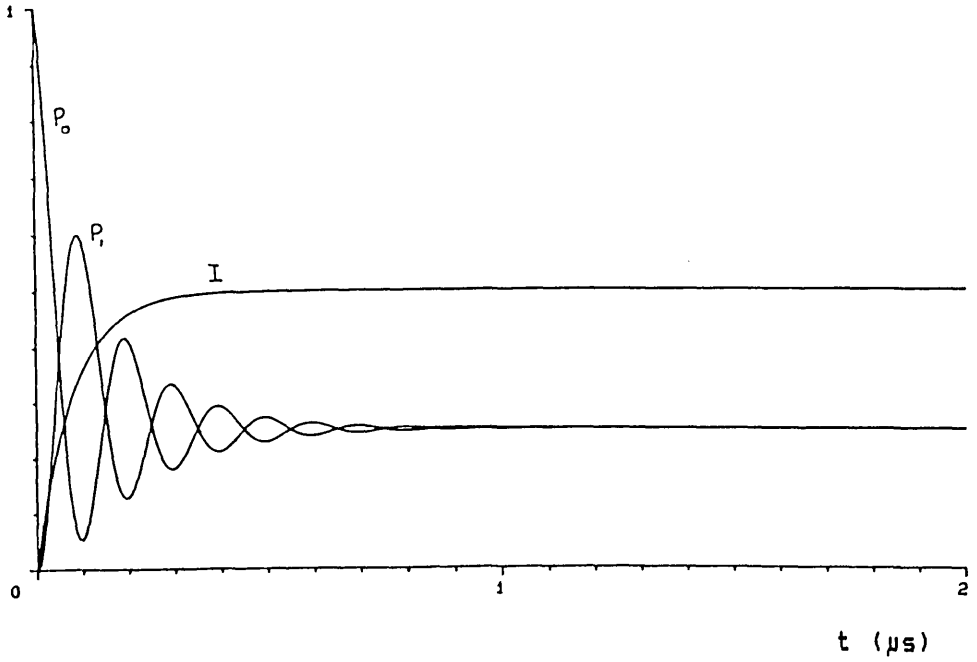
Strong couplings with Gaussian pulse shapes,

Γ_o = 2π Mrads s^{-1}, Γ_1 = 2π Mrads s^{-1}, q = 5 and t = 5 μs.

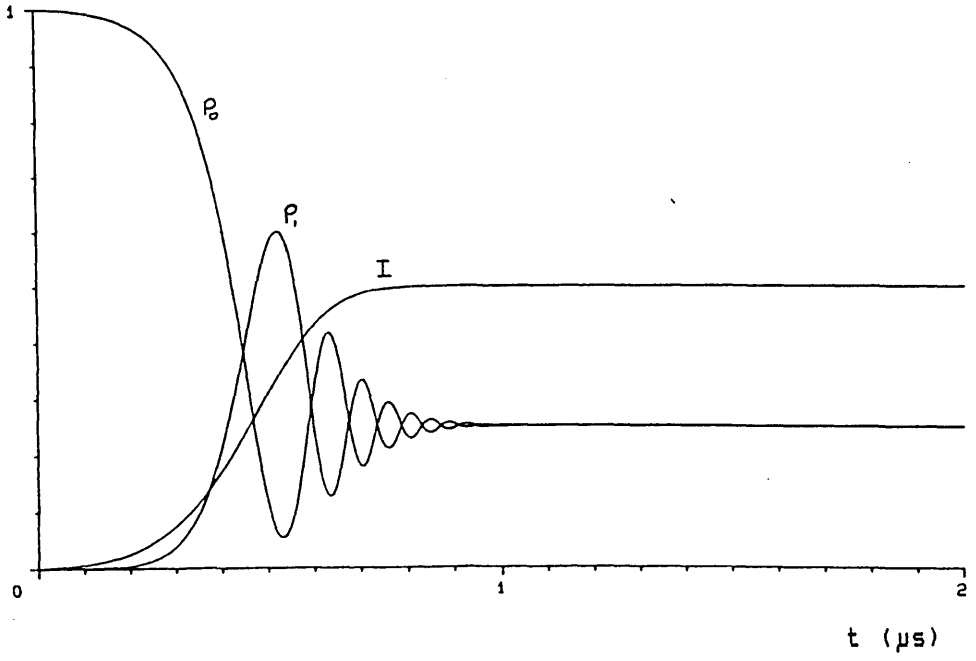
states, which are just constant energy shifts, are ignored. In the Gaussian pulse case it is incorrect to do this as the shifts are dependent upon intensity. However, in experiments performed with noble gases, [Ness 1984], these shifts are measured to be an order of magnitude less than the peak to window spacing, so they are not included here. These Stark shifts, however, could be very important as they cause the whole energy axis to move over the duration of the pulse. This has a greater averaging effect than that caused by the changing Γ's as the peak could be pushed over the dip at certain times. This means that this approximation has to be carefully validated before comparing to experimental results.

5.3.1.2 Strong fields and population trapping

The Fano profile is obtained when the probe laser is very weak, such that $\Gamma_o t \ll 1$. However, if the probe laser is increased in strength, until it is comparable with the embedding laser, the population trapping still occurs. Even for large times and strong couplings population remains trapped in the bound states, immune to photoionisation. For equal strength couplings this trapping occurs at two-photon resonance, $\Delta^{ab} = 0$. If the Stark shifts are included then real two-photon resonance occurs at some other value of Δ^{ab}. Figs iva,b,c and d show the destruction of the Fano profile as the intensity of the 'probing' laser is increased. In all cases $\Gamma_1 = 2\pi$ Mrads s^{-1}, $t = 5\ \mu s$ and $q = 5$. In a $\Gamma_o = 0.002\pi$ Mrads s^{-1} giving a Fano profile. b,c and d have $\gamma_o = 0.02\pi$, 0.2π and 2π Mrads s^{-1} respectively, showing that as γ_o is increased to become equal to γ_1 trapping still occurs. For equal gammas half the population is trapped. If the gammas are not equal then population trapping occurs at $\Delta = (\Gamma_o - \Gamma_1)q/2$ with $\Gamma_1^2/(\Gamma_o+\Gamma_1)^2$ of the population trapped in state $|0\rangle$ and $\Gamma_o\Gamma_1/(\Gamma_o+\Gamma_1)^2$ in $|1\rangle$. Thus the total population trapped is $\Gamma_1/(\Gamma_o+\Gamma_1)$ as shown in appendix 5.B, see Coleman and Knight 1982 and Beers etal 1975. Thus for very small Γ_o all the population is trapped at $\Delta^{ab} = -\Gamma_1 q/2$, the result obtained in the previous section. For equal gammas half the population is trapped at two-photon resonance. Fig v is the result of using Gaussian shaped laser pulses. This should be compared to fig ivd as, apart from the pulse shapes, the parameters are identical. Again, the energies of the pulses are equalised to calculate the correct peak intensity value, and the Stark shifts have been ignored. This shows that the evolution of the populations off



a) both pulses flat



b) both pulses Gaussian

Fig 5.3.vi

Population trapping with different pulse shapes,

$\Gamma_0 = 0.02\pi$ Mrads s^{-1}, $\Gamma_1 = 2\pi$ Mrads s^{-1}, $q = 5$ and $\Delta^{a,b} = 0$.

resonance appears to be slower than that for the 'equivalent' flat pulse case. On resonance the final populations are identical to the flat pulse case. This is for the same reason as that described in section 3.2.1.1 where the time dependence of the pulse shapes can be taken out of the TDO matrix, provided that the pulses are of the same shape and the system is on two-photon resonance. However, off resonance the final populations are different. This means that for unequal sized pulses, which implies that trapping occurs at non-zero Δ^{ab}, the predictions for the flat pulses case cannot be reliably used for pulsed excitations. Fig via shows the temporal evolution for two flat pulses, where $\Gamma_0 = \Gamma_1 = 2\pi$ Mrads s^{-1}, $q = 5$ and the system is two-photon resonant. This clearly shows trapping with equilibrium being reached whilst the pulses are still turned on, as shown in Coleman, Knight and Burnett 1982. Fig vib shows a similar situation with Gaussian pulses. Again, as in section 3.2.1.3, the final populations are identical to those with flat pulses, but the evolution is different due to the variation in instantaneous power. This trapping phenomenon should be compared to that seen in chapter three with three bound states, in which the intermediate state decays. In this chapter the intermediate state is replaced by a continuum with its own implicit decay. The amount of population trapped in the two remaining bound states is the same for both examples, for flat pulses only, as $\Gamma_1 \sim \Omega_1^2$, but in the case with the continuum, the lasers must be detuned for trapping to occur.

5.3.2 Coherence effects

The previous section shows the effects of having shaped laser pulses. This generally increases the transform bandwidth as the pulses are effectively narrower than the 'equivalent' flat pulses. However, the coherence of the fields is always maintained. This section shows the effect of incoherent lasers. Two extremes occur. Firstly the beams might be incoherent and totally uncorrelated as in two completely independent lasers. Or, secondly, the two lasers might be pumped by a single, incoherent pump in which case they might be very incoherent but mutually correlated. Of course anything in between could occur where the beams are only partially mutually coherent. Equation 8 gives the equation of motion for the amplitudes with the phase terms $\phi_a(t)$ and $\phi_b(t)$ included. In the previous section these are set to zero to

investigate the pulse shape effects. In this section these terms, with suitable assumptions about their nature, are included and dealt with analytically in order to investigate their effect on trapping. In order to achieve this the density matrix formalism is used as partially described in chapter two. This increases the computation required, needing a four by four time development operator. The reason for the use of the density matrix is that the quantities to be calculated are the populations. These are the absolute squares of the amplitudes. As a stochastic term is being included the amplitudes also become stochastic. The expectation value of the populations is not the same as the absolute square of the expectation value of the amplitudes. That is

$$\langle \rho_{ij} \rangle = \langle c_i c_j^* \rangle \neq \langle c_i \rangle \langle c_j^* \rangle . \qquad 5.3,15$$

This means that the quantities to be averaged have to be the density matrix elements and not the amplitudes. The density matrix elements are given by

$$\rho_{ij} = c_i c_j^* \qquad 5.3,16$$

so that

$$\dot{\rho}_{ij} = \dot{c}_i c_j^* + c_i \dot{c}_j^* . \qquad 5.3,17$$

Thus

$$\begin{pmatrix} \dot{\rho}_{oo} \\ \dot{\rho}_{o1} \\ \dot{\rho}_{1o} \\ \dot{\rho}_{11} \end{pmatrix} = -i \begin{pmatrix} -i\Gamma_o & \frac{\Gamma}{2}(q-i) & \frac{\Gamma}{2}(-q-i) & 0 \\ \frac{\Gamma}{2}(q-i) & -i\frac{(\Gamma_o+\Gamma_1)}{2} - \Delta^{ab} + (\dot{\phi}_a - \dot{\phi}_b) & 0 & \frac{\Gamma}{2}(-q-i) \\ \frac{\Gamma}{2}(-q-i) & 0 & -i\frac{(\Gamma_o+\Gamma_1)}{2} + \Delta^{ab} - (\dot{\phi}_a - \dot{\phi}_b) & \frac{\Gamma}{2}(q-i) \\ 0 & \frac{\Gamma}{2}(-q-i) & \frac{\Gamma}{2}(q-i) & -i\Gamma_1 \end{pmatrix} \begin{pmatrix} \rho_{oo} \\ \rho_{o1} \\ \rho_{1o} \\ \rho_{11} \end{pmatrix} \qquad 5.3,18$$

where the Stark shift terms have been discarded as in the previous section. The model used for the noise process in this case is the

Phase Diffusion Model (PDM), which assumes that the phases ϕ_a and ϕ_b make a random walk. For this process the 'velocities' $\dot{\phi}_a$ and $\dot{\phi}_b$ are both zero mean random variables with Gaussian statistics. It is shown in Wódkiewicz 1979 and Fox 1972 that an equation of this type can be transformed to yield an equation of motion for the stochastically averaged density matrix elements. An equation in the form

$$\dot{\rho} = [M_o + M_1 X(t)]\rho, \qquad 5.3,19$$

where M_o and M_1 are sure matrices and $X(t)$ is a stochastic variable with zero mean and Gaussian white noise statistics, can be written in terms of the expectation value of ρ thus

$$\langle\dot{\rho}\rangle = [M_o + M_1^2\gamma]\langle\rho\rangle. \qquad 5.3,20$$

$X(t)$ is given by its correlation functions and having Gaussian statistics is defined by the first two only. M_o and M_1 can be adjusted to guarantee that $X(t)$ has a zero mean, ie

$$\langle X(t)\rangle = 0, \qquad 5.3,21a$$

and the second order correlation function is given by

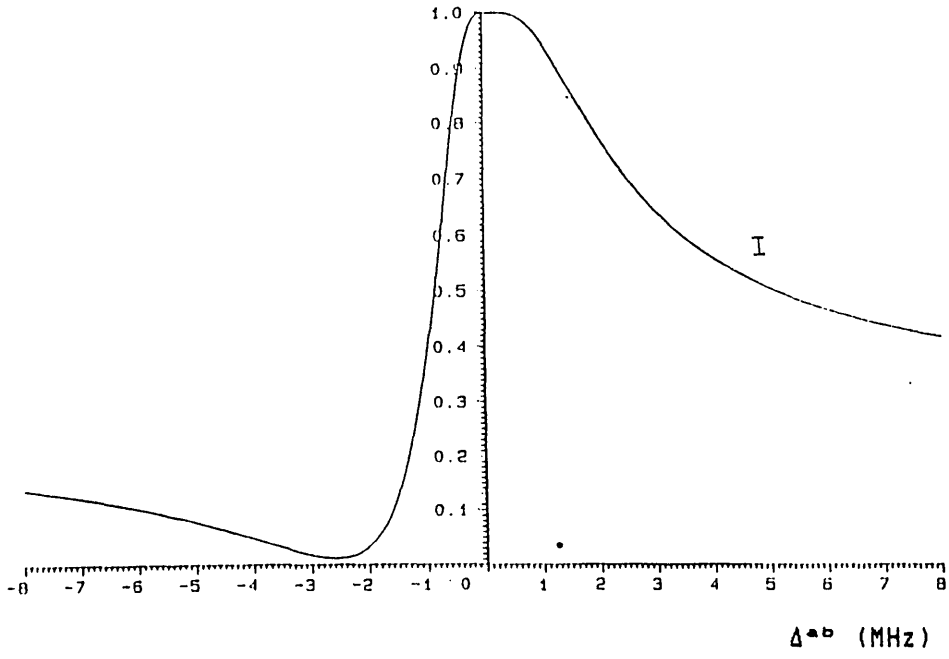
$$\langle X(t)X(t+\tau)\rangle = 2\gamma\delta(\tau). \qquad 5.3,21b$$

In this particular example $X(t) = \dot{\phi}_a(t)-\dot{\phi}_b(t)$, where both $\dot{\phi}_a$ and $\dot{\phi}_b$ are zero mean Gaussian white noise processes. Thus

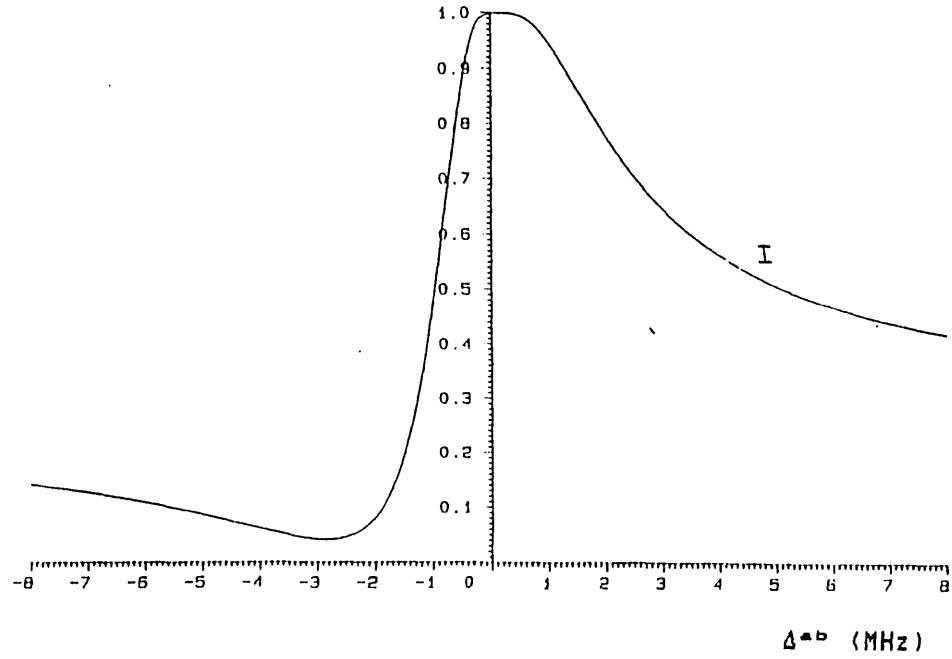
$$\langle X(t)X(t+\tau)\rangle = \langle(\dot{\phi}_a(t)-\dot{\phi}_b(t))(\dot{\phi}_a(t+\tau)\dot{\phi}_b(t+\tau)\rangle$$

$$= 2(\gamma_a+\gamma_b-2\gamma_{ab})\delta(\tau) = 2\gamma\delta(\tau), \qquad 5.3,22$$

where γ_c is the bandwidth of laser c and γ_{ab} is the cross spectral bandwidth of lasers a and b [Dalton and Knight 1982]. For total mutual correlation $\gamma = 0$ and for no mutual correlation $\gamma = \gamma_a+\gamma_b$. So equation 18 becomes



a) $\gamma = 0.01\pi$ Mrads s^{-1}



b) $\gamma = \pi/8$ Mrads s^{-1}

Fig 5.3.vii

The Fano profile with uncorrelated lasers,

$\Gamma_0 = 0.02\pi$ Mrads s^{-1}, $\Gamma_1 = 2\pi$ Mrads s^{-1}, $q = 5$ and $t = 5$ μs.

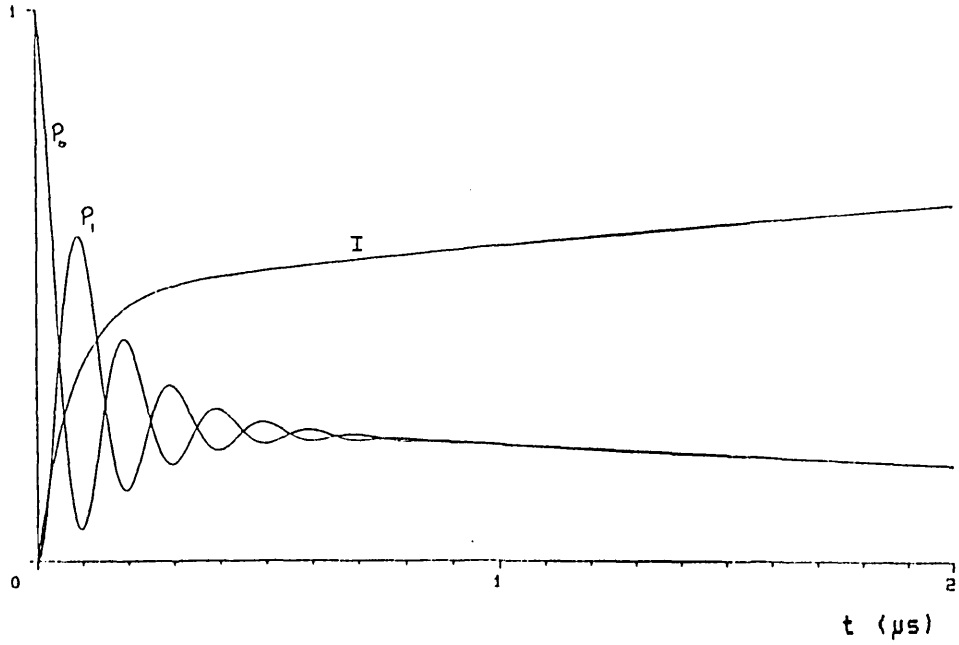


Fig 5.3.viii

Population trapping with uncorrelated lasers

$\Gamma_0 = \Gamma_1 = 2\pi$ Mrads s^{-1}, $q = 5$, $\Delta^{ab} = 0$ and $\gamma = \pi/8$ Mrads s^{-1}.

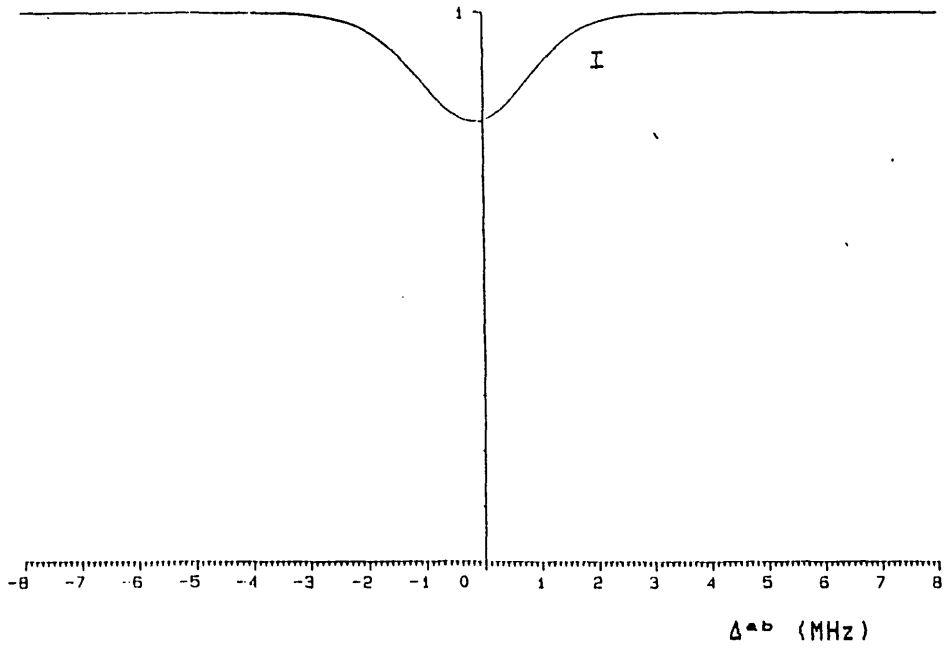


Fig 5.3.ix

Population trapping against detuning for uncorrelated lasers,

$\Gamma_0 = \Gamma_1 = 2\pi$ Mrads s^{-1}, $q = 5$, $\gamma = \pi/8$ Mrads s^{-1} and $t = 1$ and 5 μs.

$$\begin{pmatrix} \dot{\langle\rho_{oo}\rangle} \\ \dot{\langle\rho_{o1}\rangle} \\ \dot{\langle\rho_{1o}\rangle} \\ \dot{\langle\rho_{11}\rangle} \end{pmatrix} = -i \begin{pmatrix} -i\Gamma_o & \frac{\Gamma}{2}(q-i) & \frac{\Gamma}{2}(-q-i) & 0 \\ \frac{\Gamma}{2}(q-i) & -i\frac{(\Gamma_o+\Gamma_1)}{2} - \Delta^{ab} - i\gamma & 0 & \frac{\Gamma}{2}(-q-i) \\ \frac{\Gamma}{2}(-q-i) & 0 & -i\frac{(\Gamma_o+\Gamma_1)}{2} + \Delta^{ab} - i\gamma & \frac{\Gamma}{2}(q-i) \\ 0 & \frac{\Gamma}{2}(-q-i) & \frac{\Gamma}{2}(q-i) & -i\Gamma_1 \end{pmatrix} \begin{pmatrix} \langle\rho_{oo}\rangle \\ \langle\rho_{o1}\rangle \\ \langle\rho_{1o}\rangle \\ \langle\rho_{11}\rangle \end{pmatrix} \quad 5.3,23$$

where the angular brackets $\langle\rangle$ indicate a stochastic average over the phase fluctuations. This equation is now soluble using the TDO method. The populations in states $|0\rangle$ and $|1\rangle$ and the ion count are given by

$$P_o = \langle\rho_{oo}\rangle, \qquad 5.3,24a$$

$$P_1 = \langle\rho_{11}\rangle \qquad 5.3,24b$$

and

$$I = 1 - P_1 - P_o \qquad 5.3,24c$$

respectively. Fig viia, shows the effects of a small cross correlation bandwidth factor on the Fano minimum. In this example the parameters are the same as in fig iiia except that $\gamma = 0.01\pi$ Mrads s^{-1}. This has no great effect on the profile and even when γ is increased to $\pi/8$ Mrads s^{-1}, as in fig viib, there is only a small destruction of the minimum. When the probe pulse is increased the population trapping phenomenon is destroyed. This is as seen in figure viii which shows the effects of a bandwidth $\gamma = \pi/8$ Mrads s^{-1} on the evolution of the populations otherwise identical to fig vid. Fig ix shows the ionisation as a function of two-photon detuning for the same parameters. This clearly shows the increase in ionisation where trapping was once observed; compare to fig iva. Thus only the relative phases of the two exciting lasers are important in continuum excitation. The individual bandwidths have no effect when the continuum is assumed to be otherwise featureless.

5.4 Conclusions

This chapter shows some of the effects caused by pulse shapes and bandwidths when bound states are coupled to continuum states. The first section shows that the Fermi Golden Rule result, for a bound state coupled to a flat continuum, is basically correct, and generalises the result to include the pulse shape. The decay rate induced is proportional to the instantaneous intensity and is unaffected by any bandwidths. The next section examines the effects on the Fano profile, produced when a bound state is mixed strongly with the continuum whilst being probed from another bound state. It is shown that the profile is partially destroyed by both bandwidth and pulse shape effects. As the position of the peak and window are intensity dependent it is expected that during the course of a varying pulse the window moves as a function of two-photon detuning. This causes an averaging effect but still enables the window and resonance to be observed, even for Gaussian shaped pulses. Bandwidth effects are only apparent when there are phase fluctuations between the lasers. That is, both lasers can be incoherent but correlated and no effects are seen. This situation could occur if the two lasers are intrinsically coherent but both driven from the same incoherent laser. Population trapping occurs when the lasers are of similar coupling strengths. Unlike the trapping of chapter three, with three bound states, the two-photon detuning at which the trapping occurs depends upon the relative intensities. With three bound states trapping always occurs exactly on two-photon resonance. Cross correlation bandwidths destroy the trapping when they become comparable to the pulse ionisation rates. The introduction of pulse shapes complicates the trapping in a much greater way than for the three bound states type of trapping. It is shown in chapter three that the pulse shapes do not affect the final populations if there are no detunings or phenomenological decays. As the continuum trapping requires a two-photon detuning if the pulses are not identical in strength, the trapping disappears.

There are few experimental observations of LICS even though the above analysis shows that pulse shape and bandwidth do not totally destroy the effects. The most recent experimental evidence is from Hutchinson and Ness 1984 who observe some induced continuum structure in xenon. This experiment uses a two photon excitation, three photon

ionisation process to probe the continuum which is modified by another laser. The probe laser is kept fixed in frequency, because of the initial two-photon excitation process, and the embedding laser is scanned across the continuum. Fano-like resonances are observed which are intermediate between the probe resonances, with a window and a peak, and the equal field resonances, with just a window. The lasers used in the experiment are also pulsed, the exact shape is not known but is Gaussian-like, which, as they are of different coupling strengths, complicates any fitting of theory to data. The lasers are known to be noisy, with a bandwidth around ten times the transform width, but the cross spectral bandwidth is not known (both lasers are pumped from the same source). After the relative coupling strengths and cross spectral bandwidths are found it should be possible to model this experiment using the above procedure.

5.A Product of Principal parts

Consider the product of the two principal parts

$$P = \frac{P}{(\varepsilon'-\varepsilon'')} \frac{P}{(\varepsilon-\varepsilon'')} .$$

From Fano 1972 this can be written as

$$P = \frac{1}{(\varepsilon'-\varepsilon)}\left\{\frac{P}{(\varepsilon-\varepsilon'')} - \frac{P}{(\varepsilon'-\varepsilon'')}\right\} + \pi^2\delta(\varepsilon-\varepsilon'')\delta(\varepsilon'-\varepsilon''),$$

which has been properly resolved into its partial fraction and singular terms. Equation 5.2,12 thus becomes

$$\delta(\varepsilon'-\varepsilon) = b^*(\varepsilon')b(\varepsilon)\left\{1 + \int_0^\infty d\varepsilon''|T_{\varepsilon''B}|^2\left[\frac{1}{(\varepsilon'-\varepsilon)}\left(\frac{P}{(\varepsilon-\varepsilon'')} - \frac{P}{(\varepsilon'-\varepsilon'')}\right) + \pi^2\delta(\varepsilon-\varepsilon'')\delta(\varepsilon'-\varepsilon'')\right.\right.$$

$$+ z(\varepsilon)z(\varepsilon')\delta(\varepsilon'-\varepsilon'')\delta(\varepsilon-\varepsilon'')$$

$$\left.\left. + z(\varepsilon)\delta(\varepsilon-\varepsilon'')\frac{P}{(\varepsilon'-\varepsilon'')} + z(\varepsilon')\delta(\varepsilon'-\varepsilon'')\frac{P}{(\varepsilon-\varepsilon'')}\right]\right\}.$$

After some algebra this gives

$$\delta(\varepsilon'-\varepsilon) = b^*(\varepsilon')b(\varepsilon)|T_{\varepsilon B}|^2(\pi^2+z(\varepsilon)z(\varepsilon'))\delta(\varepsilon'-\varepsilon)$$

giving

$$|b(\varepsilon)|^2 = \frac{1}{|T_{\varepsilon B}|^2(\pi^2+z(\varepsilon)^2)} .$$

5.8 Trapped populations

From equations 5.3,12 population is trapped if the real part of $\beta+\alpha$ is zero. This is identical to requiring that the imaginary part of one of the dressed states energies, obtained by diagonalising equation 5.3,11, is zero, in a similar way to that described in chapter three. Thus, putting $\beta+\alpha = iE/2$, and requiring that E is real, places a restriction on the values that Δ^{ab} can take. From equations 5.3,13

$$iE = -\frac{(\Gamma_o+\Gamma_1)}{2} - i\Delta^{ab} + \left\{ \frac{(\Gamma_o-\Gamma_1)^2}{4} - (\Delta^{ab})^2 \right.$$

$$\left. -\Delta^{ab}(\Gamma_o-\Gamma_1) + \Gamma_o\Gamma_1(1-iq)^2 \right\}^{1/2} .$$

So that

$$\left[\frac{(\Gamma_o+\Gamma_1)}{2} + i(\Delta^{ab}+E) \right]^2 = \frac{(\Gamma_o+\Gamma_1)^2}{4}$$

$$- (\Delta^{ab})^2 - \Gamma_o\Gamma_1 q^2 - i\Delta^{ab}(\Gamma_o - \Gamma_1) - 2iq\Gamma_o\Gamma_1 .$$

Equating real and imaginary parts yields

$$E^2 + 2E\Delta^{ab} - \Gamma_o\Gamma_1 q^2 = 0$$

and

$$(\Gamma_o + \Gamma_1)E + 2\Gamma_o\Delta^{ab} + 2q\Gamma_o\Gamma_1 = 0.$$

The latter equation gives

$$E = -2\Gamma_o \frac{(q\Gamma_1+\Delta^{ab})}{(\Gamma_o+\Gamma_1)}$$

which is then substituted into the former equation to give a quadratic in Δ^{ab},

$$(\Delta^{ab})^2 - \Delta^{ab} q(\Gamma_o - \Gamma_1) + q^2 \frac{(\Gamma_o - \Gamma_1)^2}{4} = 0.$$

This has the solution

$$\Delta^{ab} = q\frac{(\Gamma_o - \Gamma_1)}{2} .$$

Substituting this into equations 5.3,12 and taking the limit of large time gives

$$c\acute{o}(t\to\infty) = \frac{\Gamma_1}{\Gamma_o+\Gamma_1}$$

and

$$c\acute{i}(t\to\infty) = \frac{\sqrt{\Gamma_o\Gamma_1}}{\Gamma_o+\Gamma_1} ,$$

so that the trapped populations are

$$P_o = \frac{\Gamma_1^2}{(\Gamma_o+\Gamma_1)^2}$$

and

$$P_1 = \frac{\Gamma_o\Gamma_1}{(\Gamma_o+\Gamma_1)^2} .$$

5.5 References

Alber G., Zoller P., 1983a
Harmonic generation and multiphoton ionization near an autoionizing resonance
Phys. Rev. A 27 (1983) 3, 1373-1388

Alber G., Zoller P., 1983b
Spin polarization by selective laser-induced interference
Phys. Rev. A 27 (1983) 3, 1713-1716

Armstrong L. Jr., Beers B.L., Feneuille S., 1975
Resonant multiphoton ionization via the Fano autoionization formalism
Phys. Rev. A 12 (1975). 5, 1903-1909

Armstrong J.A., Wynne J.J., 1975
The nonlinear optics of autoionizing resonances
in 'Nonlinear Spectroscopy' ed Bloembergen N. North Holland, 1977
and references within

Beers B.L., Armstrong L. Jr., 1975
Exact solution of a realistic model for two-photon ionization
Phys. Rev. A 12 (1975) 6, 2447-2454

Bradley D.J., Ewart P., Nicholas J.V., Shaw J.R.D., Thompson D.G., 1973
Photoionization from the selectively excited $3s3p\,^1P_1{}^\circ$ state to the $3p^2\,^1S_0$ autoionizing level of Mg_I
Phys. Rev. Lett. 31 (1973) 5, 263-266

Beutler H., 1933
Uber Absorptionsserien von Argon, Krypton und Xenon in Termen zwischen den beiden Ionisierungsgrenzen
Z. Phys. 86 (1933) 495

Beutler H., 1935
Uber Absorptionsspektren aus der Anregung innerer Elektronen
Z. Phys. 93 (1935) 177

Cohen-Tannoudji C., Diu B., Laloë F., 1977
'Quantum Mechanics, Vol. I'
Wiley, New York, 1977

Coleman P.E., Knight P.L., 1982
Population trapping in photoionisation to dressed continuum states
J. Phys. B 15 (1982) L235-241

Coleman P.E., Knight P.L., Burnett K., 1982
Laser-induced continuum structure in multiphoton ionisation
Opt. Comm. 42 (1982) 3, 171-178

Collin J.E., 1977
Autoionization in atomic and molecular physics
Endeavor 1 (1977) 122-128

Dalton B.J., Knight P.L., 1982
The effects of laser field fluctuations on coherent population trapping
J. Phys. B 15 (1982) 3997-4015

Dimov S.S., Pavlov L.I., Stamenov K.V., Altshuller G.B., 1983a
Nonlinear optical susceptibility measuremant at an autoionizing-like resonance in atoms
Opt. Quant. Electron. 15 (1983) 305-312

Dimov S.S., Pavlov L.I., Stamenov K.V., Heller Y.I., Popov A.K., 1983b
Laser-induced nonlinear resonances in the continuum at third-harmonic generation in Na vapor
Appl. Phys. B 30 (1983) 30, 35-40

Dimov S.S., Metchkov D.I., Pavlov L.I., Stamenov K.V., 1983
Laser-induced resonances in the continuum observed in optical frequency mixing in sodium vapor
Sov. J. Quant. Electron. 12 (1982) 5, 672-674

Fano U., 1961
Effect of configuration interaction on intensities and phase shifts
Phys. Rev. 124 (1961) 6, 1866-1878

Feneuille S., Liberman S., Luc-Koenig E., Pinard J., Taleb A., 1982
Field-induced stabilisation of Stark states in the rubidium atom
J. Phys. B 15 (1982) 1205

Fox R.F., 1972
Contributions to the theory of multiplicative stochastic processes
J. Math. Phys 13 (1972) 8, 1196-1207

Greenland P.T., 1982
Population trapping in the laser excitation of a realistic autoionising level
J. Phys. B 15 (1982) 3191-3198

Haken H., 1981
'Light', Vol. 1
North Holland, Amsterdam, 1981

Haus J.W., Rzążewski K., Eberly J.H., 1983
Laser-induced autoionization in an inhomogeneously broadened medium
Opt. Comm. 46 (1983) 3,4, 191-194

Heitler W., 1954
'The Quantum Theory of Light', third edition, pg. 69
Clarendon Press, Oxford, 1954

Heller Y.I, Lukinykh V.F., Popov A.K., Slabko V.V., 1981
Experimental evidence for a laser-induced autoionizing-like resonance in the continuum
Phys. Lett. A 82 (1981) 1, 4-6

Hutchinson M.H.R., Ness K.M.M., 1984
Laser induced autoionising states in xenon
International Quantum Electronics Conference, Arnheim, 1984

Javavainen J., 1983
The rotating wave approximation in bound-free transitions
J. Phys. B 16 (1983) 16, 1343-1361

Knight P.L., 1980
in 'Laser Physics', ed Walls D.F., Harvey J.D., pg. 63
Academic Press, Sidney, 1980

Knight P.L., 1984
Laser induced continuum structure
Comments At. Mol. Phys. 15 (1984) 4, 193-214
and references within

Knight P.L., Lauder M.A., Radmore P.M., Dalton B.J., 1984
Making atoms transparent: trapped superpositions
Acta Physica Austriaca 56 (1984) 103-117

Lambropoulos P., Zoller P., 1981
Autoionizing states in strong laser fields
Phys. Rev. A 24 (1981) 1, 379-397

Lecomte J.M., Luc-Koenig E., 1985
Exact stabilisation versus approximate stabilisation of a Stark state through ionising-channel interference
J. Phys. B 18 (1985) L357-L362

Milonni P.W., Eberly J.H., 1978
Temporal coherence in multiphoton absorption. Far off resonance intermediate states
J. Chem. Phys. 68 (1978) 1602

Ness K.M.M., 1985
Private communication

Pavlov L.I., Dimov S.S., Metchkov D.I., Mileva G.M., Stamenov K.V., Altshuller G.B., 1982
Efficient tunable tripler of optical frequency at an autoionizing-like resonance in a continuum
Phys. Lett. A 89 (1982) 9, 441-443

Rzążewski K., Eberly J.H., 1983
Photoexcitation of an autoionizing resonance in the presence of off-diagonal relaxation
Phys. Rev. A 27 (1983) 4, 2026-2042

Rzążewski K., Eberly J.H., 1981
Confluence of bound-free coherences in laser-induced autoionization
Phys. Rev. Lett. 47 (1981) 6, 408-412

Wódkiewicz K., 1979a
Exact solutions of some multiplicative stochastic processes
J. Math. Phys. 20 (1979) 1, 45-48

Wódkiewicz K., 1979b
Stochastic incoherences of optical Bloch equations
Phys. Rev. A 19 (1979) 19, 1686-1696

Woodgate 1970
'Elementary Atomic Structure'
McGraw-Hill, London, 1970

Chapter 6

Summary

6.0 Conclusions

This thesis is concerned with the effects of some of the real processes that occur in laser excitation of atomic transistions. The main theme is the effect that the pulse shape has on the temporal evolution of the excited system. Many high powered lasers operate in a pulsed mode where the temporal width of each pulse is of the same order as other time widths in the system. For these lasers it is essential, in most cases, to model the laser shape. Most of the cases dealt with here assume that the temporal shape of the pulse is Gaussian, or flat topped Gaussian. The method of solution presented here does not require any particular shape and those used have been chosen fairly arbitrarily, although in many cases they are a good approximation to real laser pulse shapes.

In chapter three an example of where the pulse shape is not important is given, when a three level system is being resonantly excited by two pulses of the same shape. This is, however, a fairly special case, as any detunings, Doppler widths or decays cause the shape to become important. This chapter also deals with an example where the pulse shapes are very important. This is in the observation of Stark effects. It is shown that, in order to see Stark splittings, the main pulse should be as flat as possible, in order to keep a constant splitting, and it is beneficial to have the probe of the same shape as the main pulse. Doppler effects are also investigated in this chapter, showing that for Doppler widths of the same order as the Rabi frequencies the relative directions of the two exciting beams becomes very important [Hodgkinson and Briggs 1977]. Thus, if the object is to excite the upper of the three levels, it is highly advantageous to have the beams counter-propagating. This produces a temporal evolution much like a damped two-photon excitation. The evolution is damped as the two-photon Rabi frequency depends on the detuning from the middle state. This is assumed to have a Boltzmann distribution, as the Doppler detuning is proportional to the velocity, and so there is an infinite sum of Rabi frequencies which causes a damping effect. Population trapping [Radmore and Knight 1982] is investigated with

shaped pulses showing that trapping still exists. This is because of the requirement that the fields be on two-photon resonance. One of the main conclusions from this chapter is the importance of the pulse area, the integral over time of the Rabi frequency, in determining the effect on the irradiated system. Thus, two pulses of different shape have similar effects if their pulse areas are equal. They only have identical effects if there are no detunings or decays etc. This is a more important parameter than the pulse energy.

In chapter four an experiment performed by Scarl, Hackel, Johnson and Rushford 1981 is re-modeled, and shot to shot phase and intensity fluctuations, Doppler and sublevel degeneracy effects are included. It is felt that the values obtained for the fitting parameters are more accurate than those found by SHJR, even though the actual fit of the theory to the experimental data does not appear to be as good.

In chapter five the continuum is explicitly investigated. A flat continuum when coupled to a bound state causes a decay out of the bound state proportional to the instantaneous intensity of the coupling. This is an example where the energy of the pulse is more fundamental than the pulse area, which is more important in bound/bound transitions. If the continuum is not flat, such as when a bound state, or autoionising state, is coupled into the continuum close by, then windows or population trapping phenomena are evident. The Fano profile is investigated [Fano 1961], where an autoionising state is probed from another level, when the probe laser is increased in strength. The effects of pulse shape are also investigated and are shown to partially destroy the windows in most circumstances. This is because the position of the window is intensity-dependent and thus moves during the course of a non-constant pulse. However, when the pulses, probe and embedding, are of equal coupling strength the trapping occurs when the pulses are two-photon resonant [Coleman and Knight 1982]. If the Stark shifts of the bound states are negligible then this allows the trapping to become independent of pulse shape, and depend only on the energy of the couplings. Phase fluctuations are shown to be important only when the lasers are mutually incoherent [Knight, Lauder, Radmore and Dalton 1984], causing dephasing and destruction of the trapping.

6.1 Further work

Only preliminary results for population trapping with LICS and pulsed lasers are reported here, and much more work can be done on this subject. It is shown in chapter five that for unequal pulse strengths trapping occurs off resonance. In chapter three populations calculated for constant excitations can only be used for pulsed excitations if the system is resonant. Thus, the pulse shape is important in LICS trapping. The experiment by Hutchinson and Ness 1984 involves pulse shapes, coherence effects and a continuum. This is the subject which will continue to be investigated as both the theory and experiment are at early stages.

6.2 References

Coleman P.E., Knight P.L., 1982
Population trapping in photoionisation to dressed continuum states
J. Phys. B 15 (1982) L235-L241

Fano U., 1961
Effect of configuration interaction on intensities and phase shifts
Phys. Rev. 124 (1961) 6, 1866-1978

Hodgkinson D.P., Briggs J.S., 1977
Doppler free two photon absorption with a near resonant intermediate state
Opt. Comm. 22 (1977) 1, 45-48

Hutchinson M.H.R., Ness K.M.M., (1984)
Laser induced autoioninising states in xenon
International Quantum Electronics Conference, Anaheim, 1984

Knight P.L., Lauder M.A., Radmore P.M., Dalton B.J., 1984
Making atoms transparent: trapped superpositions
Acta Physica Austriaca 56 (1984) 103-117

Radmore P.M., Knight P.L., 1982
Population trapping and dispersion in a three level system
J. Phys. B 15 (1982) 561-573

Scarl D., Hackel L.A., Johnson M.A., Rushford M.C., 1981
Observation of atomic coherence in laser excited uranium vapor
Phys. Rev. A 24 (1981) 2, 883

Acknowledgements

I gratefully acknowledge the enourmous amounts of help and advice given by both my college supervisor, Dr. P.L. Knight, and my CASE supervisor, Dr. P.T. Greenland. I would also like to take this opportunity to thank the members of the laser theory group at Imperial college, headed by Prof. G.H.C. New, including J.N.E, P.M.R, J.M.C. and C.P.

I am pleased to acknowledge the financial support of the SERC and UKAEA Harwell, who also provided excellent computing facilities in their status as collaborating establishment.

TP.1071

ATOMIC BEAM VELOCITY DISTRIBUTIONS

P.T. Greenland and M.A. Lauder

Abstract

We examine the Doppler profile of a collimated effusive atomic beam, for two situations of experimental interest. First, we show that there is an advantage in making the source and collimating slit of comparable size. Secondly we discuss the distribution along a line of sight which is not normal to the beam axis. We compare the predictions with some preliminary experiments.

Theoretical Physics Division
AERE Harwell

August 1984

HL84/3034

I. Introduction

We consider particles effusing from an oven through a slit of width a_1, collimated by a second slit of width a_2 ($> a_1$) at a distance L. The geometry is shown in figure 1. This is the usual method of producing a collimated atomic beam. We wish to calculate the velocity distribution of the particles in the beam along a line of sight which makes and angle ϕ with the axis of the beam. Apart from special cases this problem does not appear to have received much attention in the literature*. However the precision obtainable with modern lasers implies that the Doppler motion of the collimated beam may be the largest source of line broadening in high resolution spectroscopy, and it is therefore important to treat it properly.

In section II we derive the general expression for the distribution. This involves an integral which can only be evaluated in terms of simple functions for two limiting cases; first for all lines of sight, provided the slit in the oven (a_1) is very much smaller than the collimating slit (a_2), and secondly, for arbitrary slit sizes, provided the direction of observation is normal to the beam axis. Both these cases are met in practice, and they are discussed in sections III and IV. Some comparison with experiment is made in section V, and conclusions are drawn in section VI.

II. The Velocity Profile

It is convenient to work in polar coordinates. The velocity distribution for those atoms effusing out of the oven at point y and moving with speed v at angle θ to the beam axis is (Ramsey 1956)

---

*After this work was completed our attention was drawn to Minkowski and Bruck (1935) who have derived our equation 10. We thank Dr. Woodgate for drawing our attention to this work.

$$P(y,\theta,v)dy\ d\theta\ dv = N\ v^3 e^{-v^2/2\sigma^2}\ \cos\theta\ dy\ d\theta\ dv \qquad (1)$$

where N is the normalization, which need not be explicitly given. At atom moving in this way has a line of sight component v_L given by

$$v_L = v\ \sin(\phi-\theta) \qquad (2)$$

where the geometry is shown in figure 2. Normal viewing corresponds to $\phi=0$.

In order for an atom starting at y to pass through the second set of slits we must have

$$\theta_{min}(y) < \theta < \theta_{max}(y) \qquad (3)$$

where $\tan\theta_{max} = (\frac{1}{2}a_2 - y)/L$ and $\tan\theta_{min} = -(\frac{1}{2}a_2 + y)/L$. However this is not the only restriction on θ. The effusion velocity v is always positive, and therefore equation 2 implies that

$$\theta_{min} < \theta < \min(\phi, \theta_{max}) \quad \text{for } v_L > 0 \qquad (4a)$$

and

$$\phi < \theta < \theta_{max} \quad \text{for } v_L < 0 \qquad (4b)$$

There is no negative component of velocity unless $\phi < \theta_{max}$. Putting this together gives an expression for $P_L(v_L,\phi)$ the normalized line of slight velocity distribution at angle ϕ. After some manipulation it may be written

$$P_L(v_L,\phi) = \{\theta(v_L) \int_{-a_{1/2}}^{a_{1/2}} dy \int_{\max(0,\phi-\theta_{max}(y))}^{\phi-\theta_{min}(y)} (\cos\phi \frac{\cos\chi}{\sin^3\chi} + \frac{\sin\phi}{\sin^2\chi}) e^{-v_L^2/2\sigma^2\sin^2\chi} d\chi$$

$$+ \theta(-v_L) \int_{-a_{1/2}}^{a_{1/2}} dy\ \theta(\theta_{max}(y)-\phi) \int_{o}^{(\theta_{max}(y)-\phi)} (\cos\phi \frac{\cos\chi}{\sin^3\chi} - \frac{\sin\phi}{\sin^2\chi}) e^{-v_L^2/2\sigma^2\sin^2\chi} d\chi \}/R \qquad (5)$$

where

$$R = \sqrt{2\pi}\,\sigma^3\{[\frac{(a_1+a_2)^2}{4} + L^2]^{\frac{1}{2}} - [\frac{(a_2-a_1)^2}{4} + L^2]^{\frac{1}{2}}\} \qquad (6)$$

(It is a surprising fact that although $P_L(v_L,\phi)$ cannot be obtained in closed form $\int_o^\infty dv_L\ P_L(v_L,\phi)$ can be. It is, of course, independent of ϕ since it represents the total number of atoms observed and this does not depend upon the direction of observation).

This expression was derived on the assumption that $0 < \phi < \pi/2$. However it is easy to show that $P_L(-v_L,-\phi) = -P(v_L,\phi)$ and therefore equation 5 can be used for the whole range $-\pi/2 < \phi < \pi/2$. Unfortunately the integrals cannot, in general, be expressed in terms of simple functions. We therefore consider two special cases.

III. Pinhole Source

If $a_1 << a_2$ then we may let $a_1 \to 0$ in equation 5. This is the pinhole source approximation. Under this condition the integral in equation 5 can be performed (for all ϕ). The limit of equation 6 as $a_1 \to 0$ must also be taken. The final result is

$$P_p(v_L,\phi) = \frac{1}{\sqrt{2\pi}\,\sigma\,\sin\alpha}\{\cos\phi[(e^{-\frac{v_L^2}{2\sigma^2\sin^2(\alpha+\phi)}} - e^{-\frac{v_L^2}{2\sigma^2\sin^2\lambda}})\Theta(v_L)$$

$$+ [1-\Theta(v_L)]\Theta(\alpha-\phi)\, e^{-\frac{v_L^2}{2\sigma^2\sin^2(\alpha-\phi)}}]$$

$$+ \sqrt{\frac{\pi}{2}}\,\frac{|v_L|}{\sigma}\, e^{-\frac{v_L^2}{2\sigma^2}}\sin\phi[(\mathrm{erfc}(\frac{|v_L|\cot(\alpha+\phi)}{\sqrt{2}\,\sigma}) - \mathrm{erfc}(\frac{|v_L|\cot\lambda}{\sqrt{2}\,\sigma}))\Theta(v_L)$$

$$- [1-\Theta(v_L)]\Theta(\alpha-\phi)\mathrm{erfc}(\frac{|v_L|\cot(\alpha-\phi)}{\sqrt{2}\,\sigma})]\} \qquad (7)$$

where $\lambda = \max(0,\phi-\alpha)$ and α is defined as $\alpha = \tan^{-1}\frac{a_2}{2L}$, ie α is the half angle subtended by the collimating slit at the source.

In many cases one is interested in the situation that ϕ is very small; that is, one is attempting to view the beam normally. In this case it is a good approximation to ignore the terms in $\sin\phi$, and take

$$P_p(v_L,\phi<<1) \approx \frac{1}{\sqrt{2\pi}\,\sigma\,\sin\alpha}\, e^{-\frac{v_L^2}{2\sigma^2\sin^2(\alpha+\phi)}} \qquad v_L > 0$$

$$\approx \frac{1}{\sqrt{2\pi}\,\sigma\sin\alpha}\, e^{-\frac{v_L^2}{2\sigma^2\sin^2(\alpha-\phi)}} \qquad v_L < 0 \qquad (8)$$

where we assume that $\phi < \alpha$. We see that the distribution is asymmetric, with a 'steep' side for $v_L < 0$ corresponding to a Gaussian full width half

maximum (FWHM) $\sqrt{8\ln 2}\,\sigma \sin(\alpha-\phi)$, and a 'shallow' side corresponding to a Gaussian FWHM $\sqrt{8\ln 2}\,\sigma \sin(\alpha+\phi)$. Overall the FWHM is therefore $\sqrt{8\ln 2}\sigma \sin\alpha\cos\phi \approx$

$$W \approx \sqrt{8\ln 2}\,\sigma \sin\alpha$$

since $\phi \ll 1$. Thus, the principle effect of viewing at a small angle to the beam is to distort the shoulders rather than to move the peak. If α is also small so that it is possible to have $\alpha < \phi \ll 1$, then there is a range of observation angles for which the above discussion does not apply, and one has

$$P_p(v_L \;\; \alpha < \phi \ll 1) \approx \frac{1}{\sqrt{2\pi}\sigma \sin\alpha} \left(e^{-\frac{v_L^2}{2\sigma^2 \sin^2(\alpha+\phi)}} - e^{-\frac{v_L^2}{2\sigma^2 \sin^2(\phi-\alpha)}} \right) \quad v_L > 0 \tag{9}$$

In this case, not only is the distribution asymmetric, but the peak is shifted from $v_L = 0$. Indeed no negative velocities are observed. We shall return to this point in section V. We now consider the other case in which equation 5 can be further reduced.

IV. Two Slit Collimation

If we limit ourselves to normal viewing ($\phi = 0$) then the integrations over slit width and angle can be performed in terms of known functions, to give (taking v to be the velocity normal to the beam direction)

$$P_s(v,a_1,a_2) = |v| e^{-v^2/2\sigma^2} \frac{\{\Gamma(-\frac{1}{2}, \frac{v^2}{2\sigma^2 S^2}) - \Gamma(-\frac{1}{2}, \frac{v^2}{2\sigma^2 T^2})\}}{4\sqrt{\pi}\,\sigma^2\{(1+S^2)^{\frac{1}{2}} - (1+T^2)^{\frac{1}{2}}\}} \quad (10)$$

where $\Gamma(-\frac{1}{2},x)$ is an incomplete gamma function and

$$S = \frac{a_1 + a_2}{2L} \; ; \; T = \frac{a_2 - a_1}{2L}$$

This distribution has some remarkable features. First putting $a_1 = a_2 = a$ gives

$$P_s(v,a,a,) = \frac{|v| e^{-v^2/2\sigma^2} \Gamma(-\frac{1}{2}, \frac{v^2 L^2}{2\sigma^2 a^2})}{4\sqrt{\pi}\,\sigma^2(1+a^2/L^2)^{\frac{1}{2}}} \quad (11)$$

Surprisingly if FWHM is taken as a criterion of beam collimation this distribution is <u>narrower</u> than the Gaussian which would be obtained by letting $a_1 \to 0$. That is, collimation with two equally sized slits is better than collimation with a pinhole and a slit.

The value of $P_s(o,a_1,a_2)$ is easily obtained as

$$P_s(0,a_1a_2) = \frac{a_1}{\sqrt{2\pi}\sigma\,[(1+S^2)^{\frac{1}{2}} - (1+T^2)^{\frac{1}{2}}]L} \quad (12)$$

It is straightforward to show that for a pinhole ($a_1 \to o$) and $L >> a_2$

$$P_s(0,0,a_2) \to \frac{1}{\sqrt{2\pi}\,\sigma} \frac{2L}{a_2}\left(1 + \frac{a_2^2}{8L^2}\right) \text{ whereas } P_s(0,a_2,a_2) \to \frac{1}{\sqrt{2\pi}\sigma} \frac{2L}{a_2}\left(1 + \frac{a_2^2}{2L^2}\right).$$

Thus not only is the distribution narrower, but the probability of finding slow atoms is comparable in the two cases. (Notice that since the flux will be larger for the equal slit case, the absolute number of slow atoms will be larger). Finally we must consider the behaviour as $v \to \infty$. We find

$$P_s(v \to \infty,\ a_1,a_2) \to \frac{e^{-v^2/2\sigma^2(\frac{1+S^2}{S^2})}}{\sqrt{2\pi}\left[(1+S^2)^{\frac{1}{2}}-(1+T^2)^{\frac{1}{2}}\right]} \frac{\sigma S^3}{v}\left(1-\frac{T^3}{S^3}\right) e^{-\frac{v^2 a_1 L^3(3a_2^2-a_1^2)}{2\sigma^2(a_2^2-a_1^2)^2}} \tag{13a}$$

The pinhole limit is

$$P_s(v\to 0,0,a_2) \to \frac{1}{\sqrt{2\pi}\sigma\ \varepsilon} e^{-v^2/2\varepsilon^2} \tag{13b}$$

with $$\varepsilon = a_2\sigma/(4L^2 + a_2^2)^{\frac{1}{2}}$$

The exponential term in brackets in equation 13a will be negligable unless $a_1 << a_2$. (For $a_1 = a_2$ it is exactly zero). If $a_1 << a_2$ then we have

$$P_s(v,a_1,a_2) \approx \frac{e^{-v^2/2\sigma^2(\frac{1+S^2}{S^2})}}{\sqrt{2\pi}\left[(1+S^2)^{\frac{1}{2}}-(1+T^2)^{\frac{1}{2}}\right]} \frac{\sigma S^3}{v}\left[1-e^{-\frac{24a_1L^3v^2}{\sigma^2 a_2^4}}\right] \tag{14}$$

which implies that the second term is only negligible for

$$\frac{v}{(2^{\frac{1}{2}}\sigma\ a_2/2L)} >> \frac{a_2}{2\sqrt{3}(a_1L)^{\frac{1}{2}}} \tag{15}$$

We have written equation 15 in this way because the LHS is the velocity in units of the e folding width of the collimated beam. Equation 15 therefore provides some limit on the use of the pinhole approximation in the wings of the distribution. If equation 15 is satisfied the 2nd term in brackets in equation 13a is negligible, and the pinhole asymptotic form, (equation 13b) is not obtained.

In summary a beam collimated by two slits of finite width has a more complicated velocity profile than the pinhole case. There is an 'umbral' region, where the collimation is better than is achieved by a pinhole source, and a 'penumbral' where the collimation is worse (see fig. 3). Equation 15 gives some indication of where the transition between these two regions lies. We now turn to the experimental situation.

V. Experiment

In figure 4 we plot the velocity distribution for typical experimental parameters. It is clear that the pinhole approximation is valid (to the plotting accuracy) over a wide range of oven slit sizes. Thus equation 7 can be used for viewing at non-normal incidence, even for moderate oven slit sizes. Unfortunately, the only experiments available so far have been performed with a laser with 65 ~ 83 MHz (FWHM) jitter. Provided this is much less than the expected Doppler width it is unimportant, but for a highly collimated beam it can be critical. The precision of the present experiments does not warrant an elaborate least squares fitting procedure; we are content to demonstrate that the observed profiles are consistent with the assumed geometry.

Figure 5a shows the Doppler profile obtained with an oven slit of 1mm, a collimating slit of 10mm and a slit separation of 15mm. Ignoring both the laser jitter and the possibility of non-normal observation the fit to the profile in figure 5a implies a FWHM Doppler profile for the oven of

982 MHz*. This in turn implies an oven temperature of 1753°K which is lower than expected. The design temperature of the oven is 2000°C. The possibility that atoms in the edge of the atomic beam are not observed for some geometric reason must be considered. An oven temperature of 2000°C coupled with a measured FWHM of 309 MHz is consistent with a geometry which only allows the central 86% of the collimated beam to be observed. We are not able to explain the discrepancy between theory and experiment in the wings of the distribution.

Figure 5b shows the profile obtained with an oven slit of 1mm, a collmating slit of 3mm and a slit separation of 17.5 mm. Also shown is the Doppler profile obtained in a cold cathode lamp. It is instantly clear that the Doppler profile is not only asymmetric, but also that its peak is shifted from the position given by the lamp. Furthermore, the expected Doppler width is comparable with the width of the laser jitter. the resultant profile is then a convolution of both distributions, ie

$$P_{obs}(v,\phi) = \int dx\ P_L(v-x)\ P_D(x,\phi) \qquad (16)$$

where P_L is the distribution of laser frequencies and P_D the Doppler distribution in the beam (observed at angle ϕ). The measured distribution is consistent with the following data: viewing angle $\phi = 5°$, oven temperature T = 2000°C and P_L the laser frequency jitter is a Gaussian, FWHM = 83 MHz (standard deviation σ_L). Under these conditions P_P is approximately zero for $v < 0$ and Gaussian $\sigma_D = \sigma_{oven} \sin(2\phi)$ for $v > 0$ (σ_D is the standard deviation for the final distribution, σ_{oven} the standard deviation for the oven). The convolution integral P_{obs} gives

---

*The Doppler profile is given in terms of detuning from line centre. This of course reflects the velocity distribution along the line of sight.

$$P_{obs} \sim e^{\frac{-v^2}{2(\sigma_D^2 + \sigma_L^2)}} \left[1 - \frac{1}{2}\,\mathrm{erfc}\left(\frac{\sigma_D}{\sigma_L}\,\frac{v}{\sqrt{2\sigma_D^2 + 2\sigma_L^2}}\right)\right] \qquad (17)$$

which has a shift of ~ 46 MHz and FWHM of 134 MHz. The theoretical and experimental distributions are compared in figure 5.

VI. Conclusions

It is unfortunate that only some preliminary experimental profiles taken with a noisy laser are available. This has prevented a precise comparison between theory and experiment. Nevertheless three important results emerge from the study. First, and most importantly, the two slit distribution is narrower than the pinhole and slit distribution. Thus it is possible to improve count rates, and collimation by increasing the size of the slit in the oven wall. Secondly, the pinhole approximation implies that there is a critical angle α. Observation within this angle results in all velocities being observed, whereas observation outside the critical angle result in only positive velocities. For viewing angle $\phi \ll 1$ the major effect of non-normal observation within the critical angle is to distort the distribution, without altering its peak position. Thirdly observation of this distorted distribution with a laser of finite bandwidth leads to a shift in the peak position. We believe that the second and third of these effects have been observed. The first effect has not yet been seen.

References

Minkowski, R., Bruck, H., 1935 Z.Phys. 95 274.

Ramsey N.F. 1956 'Molecular Beams' Oxford University Press (Oxford).

Figure Captions

Figure 1 The collimating slits.

Figure 2 The geometry of the emerging beam. The probability of an atom emerging from point y with velocity v, in direction θ is given in equation 1. The line of sight angle is ϕ.

Figure 3 The 'umbral' and 'penumbral' regions. The whole width of slit a_1 contributes slow atoms to the umbral region. The penumbral region contains fast atoms.

Figure 4 The velocity distribution for typical experimental parameters. What is plotted is the distribution of $u = v/\sqrt{2}\sigma$ where σ is the standard deviation of the distribution in the oven. Each distribution is labelled by the values of a_1, a_2 and L. It is clear that the Gaussian form appropriate for $a_1 \to o$ is quickly reached.

Figure 5 Comparison between the experimental and theoretical distributions discussed in the text. A tracing of the original oscilliscope photograph and a comparison between this data and experiment is shown on a more convenient scale.

(a) The data for a_1 = 1mm, a_2 = 10mm, L=15mm, σ_{oven} = 417 MHz

(b) The data for a_1 = 1mm, a_2 = 3mm, L=17.5mm, σ_{oven} = 475 MHz and a viewing angle of 5°. This distribution has been convoluted with the Gaussian distribution of the laser jitter (FWHM = 83 MHz).

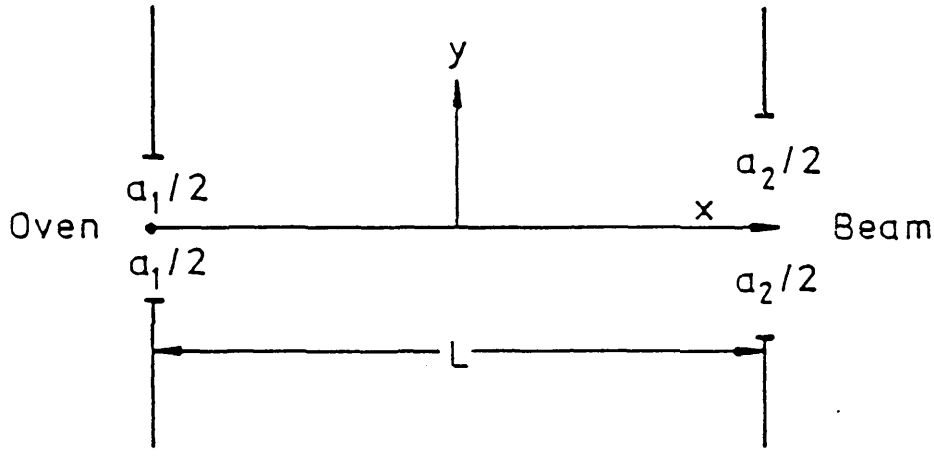


FIG. 1.

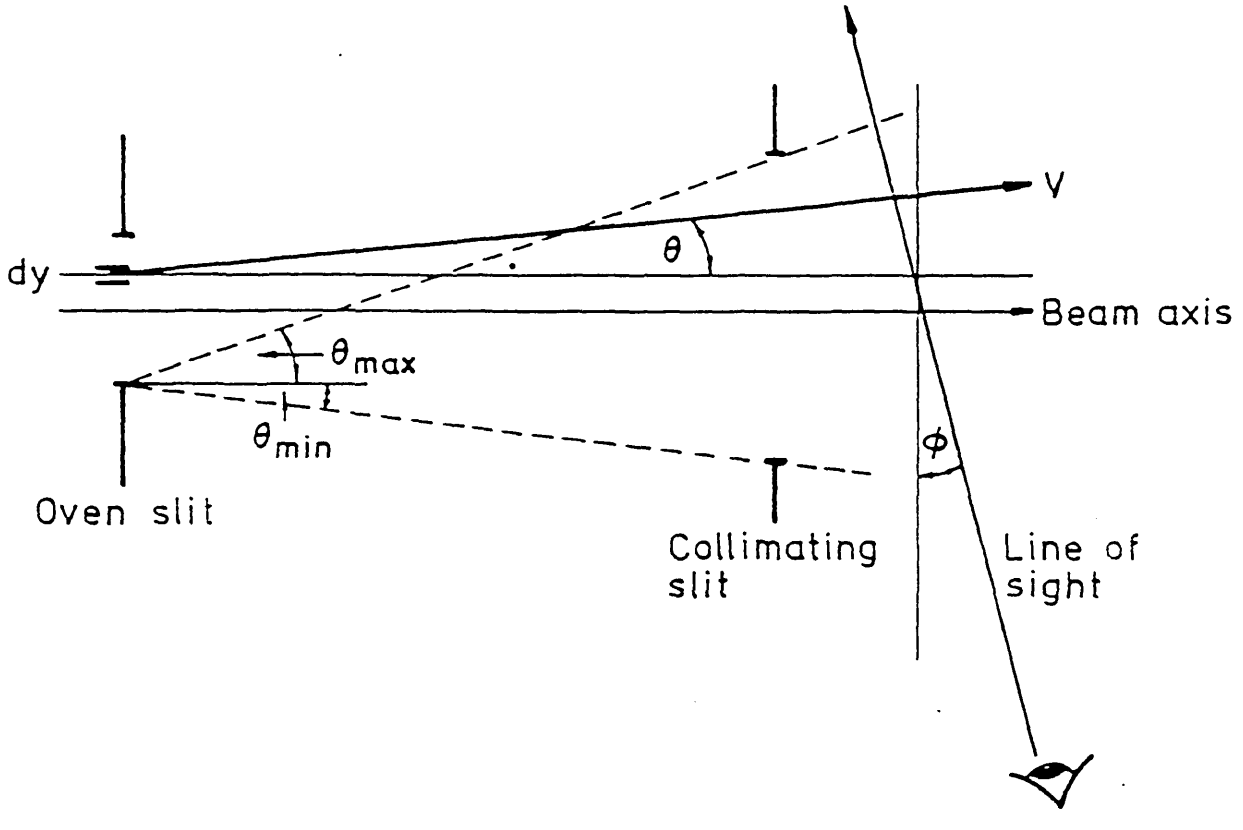

V
dy
θ
Beam axis
θmax
θmin
Oven slit
Collimating slit
Line of sight
φ

FIG. 2.

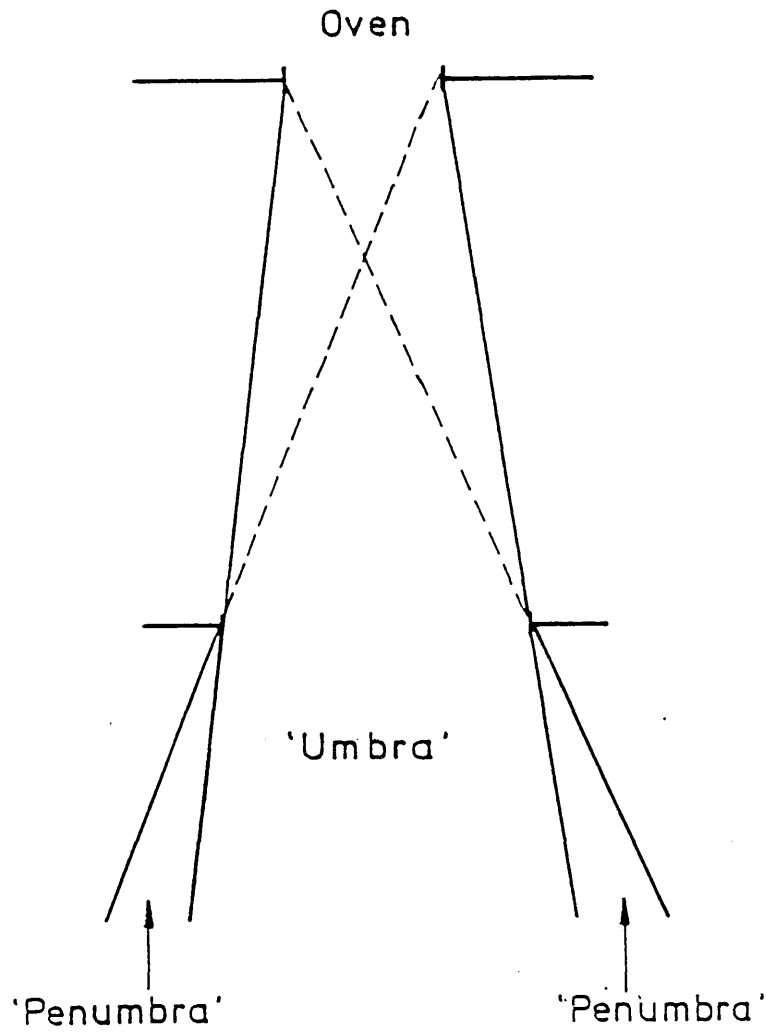


FIG. 3.

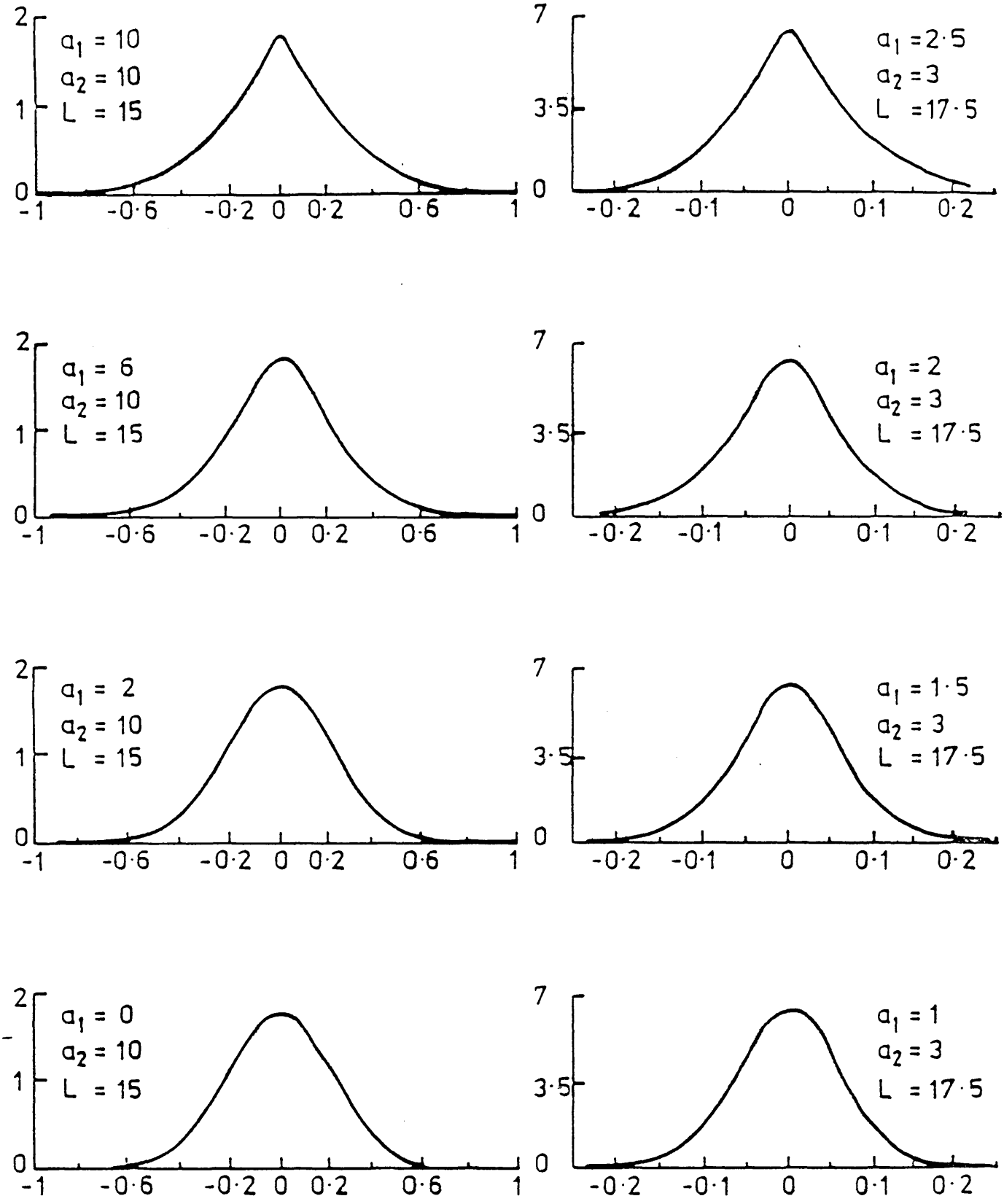

$a_1 = 10$
$a_2 = 10$
$L = 15$
$a_1 = 2{\cdot}5$
$a_2 = 3$
$L = 17{\cdot}5$
$a_1 = 6$
$a_2 = 10$
$L = 15$
$a_1 = 2$
$a_2 = 3$
$L = 17{\cdot}5$
$a_1 = 2$
$a_2 = 10$
$L = 15$
$a_1 = 1{\cdot}5$
$a_2 = 3$
$L = 17{\cdot}5$
$a_1 = 0$
$a_2 = 10$
$L = 15$
$a_1 = 1$
$a_2 = 3$
$L = 17{\cdot}5$
2
1
0
7
3·5
-1
-0·6
-0·2
0
0·2
0·6
1
-0·2
-0·1
0·1
0·2

FIG. 4.

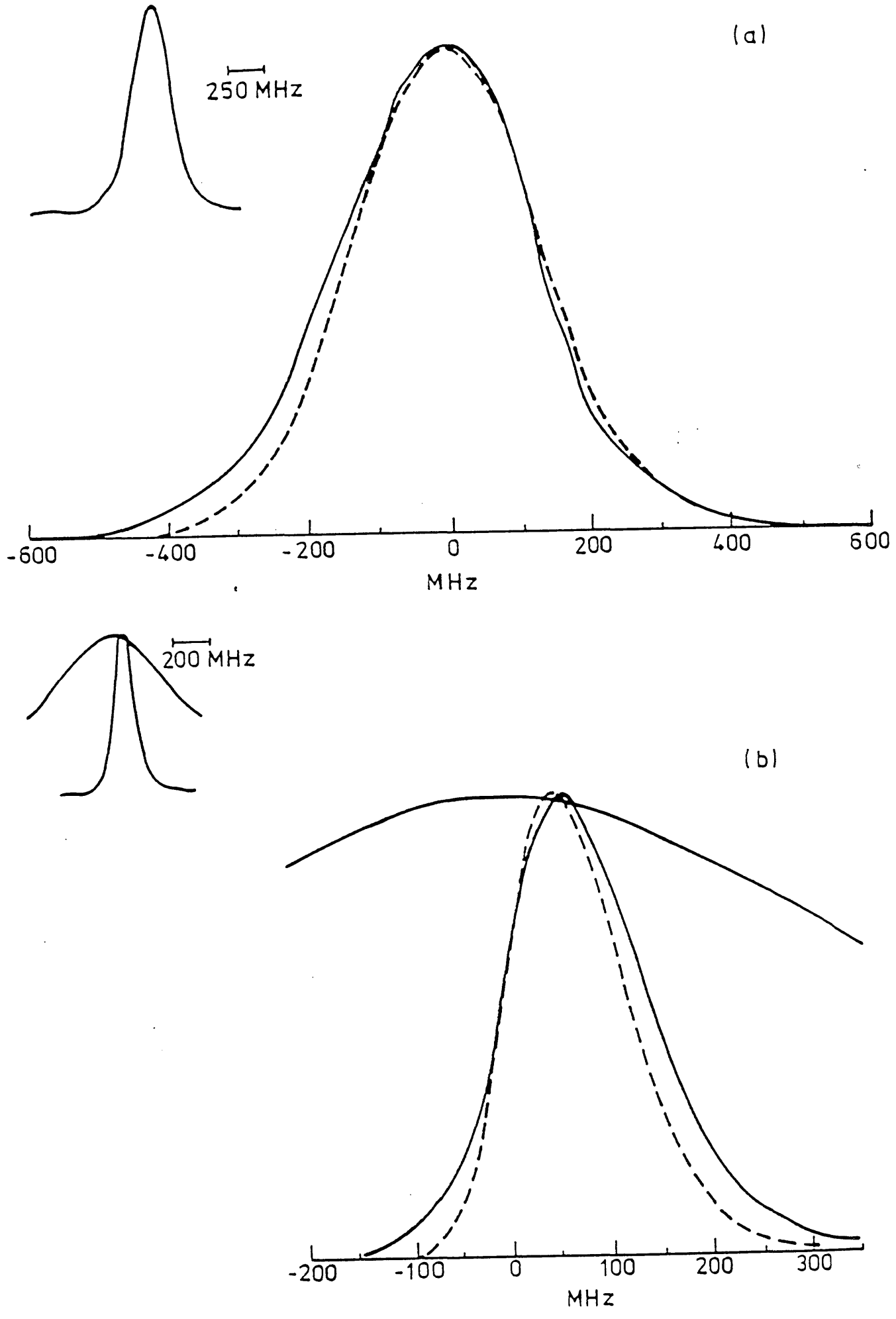

(a)
250 MHz
-600
-400
-200
0
200
400
600
MHz
200 MHz
(b)
-200
-100
0
100
200
300
MHz

FIG.5.

J. Phys. B: At. Mol. Phys. 17 (1984) 3083–3090. Printed in Great Britain

Resonant laser excitation of uranium with a pulsed laser

M A Lauder† and P T Greenland

Theoretical Physics Division, AERE Harwell, Didcot, Oxon, England

Received 3 December 1983, in final form 26 March 1984

Abstract. We consider the resonant excitation of the 3868 cm^{-1} $J=3$ to 26 558 cm^{-1} $J=2$ transition in uranium. An experiment has already been done by Scarl *et al* which measures the upper-state population as a function of laser intensity. We re-analyse these data taking proper account of the laser's temporal pulse shape. The effect of the laser bandwidth is also included in a novel way. We find a fit to the data which gives different values for the physical parameters from those found by Scarl *et al*. We draw some general conclusions for experiments of this type.

1. Introduction

In a recent experiment Scarl *et al* (1981) have considered the resonant excitation of the 3868 cm^{-1} $J=3$ to 26 558 cm^{-1} $J=2$ levels of uranium. They used a nitrogen-laser-pumped dye laser of fixed frequency and pulse length to excite the 26 558 cm^{-1} level. This state was then ionised through an autoionising level by a second N_2 pumped laser. The ion signal, and hence 26 558 cm^{-1} state population, was measured as a function of exciting laser intensity. The experimental results show clear evidence of Rabi oscillations as a function of field intensity.

Scarl *et al* (1981) analysed their data by making a series of approximations. They assumed, first, that the laser's true Gaussian temporal pulse shape can be replaced by an equivalent constant pulse, and, secondly, that the laser bandwidth can be represented by an effective detuning. They then obtained a good fit to their data in terms of two parameters, z_0, the reduced dipole matrix element for the transition, and s, the width of the distribution of shot-to-shot laser intensity fluctuation.

The purpose of this paper is to re-analyse their data using a more realistic description of the laser. Because they use a pulsed laser, and average over many shots we must take account of both incoherence due to the variation between different laser shots, and incoherence whose source is a stochastic fluctuation during the course of a single shot. The effect of the pulse envelope must also be correctly included. An important result of the analysis is that by fitting the data of Scarl *et al* we are able to determine what part of the measured power spectral bandwidth is due to a variation in shot-to-shot laser frequency and what component arises from a genuine stochastic broadening of the single-shot laser linewidth. In analogy to the terminology used in discussing atomic line shapes we call the former source of broadening inhomogeneous, and the latter homogeneous.

† Optics Section, Imperial College of Science and Technology, Prince Consort Road, London SW7, England.

0022-3700/84/153083+08$02.25 © 1984 The Institute of Physics

So far as we are aware, this is the first time that an analysis of laser-induced Rabi oscillations including all these effects has been done. Further, since our results are different from those of Scarl *et al* it seems worthwhile to present this analyis.

In § 2 we discuss pulse shape effects. Fortunately the stochastic processes which give rise to the laser bandwidth can be treated within the same theoretical framework. In § 3 the sources of inhomogeneous broadening will be considered. These include shot-to-shot fluctuations, both in laser frequency and intensity, and the broadening due to the residual Doppler width of the atomic beam.

When all the effects are included the solutions described in § 2 take too long to form the basis of a least-squares fit. Section 4, therefore, describes an analytic approximation which we use to extract values for z_0, s, etc, from the experimental data. The exact results of § 2 are then used to compare theory and experiment in § 5, and are somewhat different from those found by Scarl *et al.* The source of these differences is discussed, and some conclusions drawn, in § 6.

2. Upper-state populations with pulsed lasers

The equation of motion of a two level atom excited by a near-resonant pulsed laser with field envelope $\boldsymbol{E}(t)$ can be written (Sargent *et al* 1974)

$$\mathrm{i}\begin{pmatrix}\dot{c}_1(t)\\ \dot{c}_2(t)\end{pmatrix}=\begin{pmatrix}0 & \frac{1}{2}V(t)\\ \frac{1}{2}V^*(t) & \Delta\end{pmatrix}\begin{pmatrix}c_1(t)\\ c_2(t)\end{pmatrix} \tag{1}$$

with

$$V(t)=\boldsymbol{d}\cdot\boldsymbol{E}(t)/\hbar$$

where $\boldsymbol{d}$ is the atomic dipole matrix element and Δ the laser detuning. $c_n(t)$ is the time-dependent occupation amplitude of level n ($=1, 2$), and the rotating-wave approximation has been made, implying that the time development of the field envelope is much slower than the laser's optical period. The solution to equation (1) is well known under the circumstance that $V(t)$ is time independent, and can be written

$$\begin{pmatrix}c_1(t)\\ c_2(t)\end{pmatrix}=\left[\exp\frac{1}{\mathrm{i}}\begin{pmatrix}0 & \frac{1}{2}V\\ \frac{1}{2}V^* & \Delta\end{pmatrix}t\right]\begin{pmatrix}c_1(0)\\ c_2(0)\end{pmatrix} \tag{2}$$

where the initial conditions $c_1(0)$ and $c_2(0)$ must be specified. If $V(t)$ is time dependent, this is no longer true. However we can take advantage of the fact that equation (2) provides an approximate solution for small t and write, (with a slight, but obvious change of notation)

$$\begin{pmatrix}c_1(t+\delta t)\\ c_2(t+\delta t)\end{pmatrix}=\left[\exp\frac{1}{\mathrm{i}}\begin{pmatrix}0 & \frac{1}{2}V(t)\\ \frac{1}{2}V^*(t) & \Delta\end{pmatrix}\delta t\right]\begin{pmatrix}c_1(t)\\ c_2(t)\end{pmatrix}. \tag{3}$$

Thus by dividing the pulse into sections and using (3) to propagate the solution in time we are able to solve (1). The exponential in equation (3) is actually the first term in the Magnus solution to equation (1) (Wilcox 1967). The requirement that (3) be an adequate approximation is that the second term in the Magnus expansion should be small in comparison with the first. This implies that δt must be chosen so that

$$V(t)\gg\frac{\mathrm{d}V}{\mathrm{d}t}\delta t \tag{4}$$

which is often a less severe requirement than the perturbative criterion $V\delta t \ll 1$. Figure 1 shows the pulse envelope and our approximation to it. It may be worth remarking that our technique gives the exact solution to the stepped pulse. Provided (4) is satisfied this is an acceptable approximation to the real pulse.

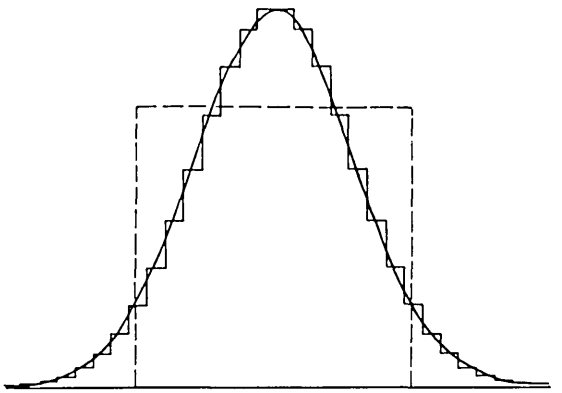


Figure 1. How the pulse is divided. The true Gaussian shape (full curve) is approximated by the stepped pulse for the numerical calculations. The equivalent flat pulse used in the analytical calculations is shown as a broken line.

We have written $V(t)$ as a complex function in (1). If we take

$$V(t) = V_0(t)\exp(i\phi(t)) \tag{5}$$

and assume that ϕ satisfies the stochastic equation

$$\frac{d^2\phi}{dt^2} + \beta\frac{d\phi}{dt} = \beta F(t) \tag{6}$$

where F is a Gaussian white-noise driving force, so that

$$\langle F(t+\tau)F(t)\rangle = W\delta(\tau) \tag{7}$$

then the effect of the stochastic phase ϕ is to give the laser a bandwidth. If $\beta \gg 1/\tau_0$ where τ_0 is the pulse length, $\phi(t)$ is a Wiener–Levy process and this bandwidth will be Lorentzian, with full width at half maximum of W. Realisations of $\phi(t)$ are easy to generate from (6) since the differential equation can be solved explicitly (Wax 1954). Each realisation appears as a time-dependent phase, and introduces no essential difficulties in the solution of (1). In general terms, the time scale for variation in the phase is given by the reciprocal of the bandwidth. In all cases we consider, this is comparable to the pulse length, and therefore the pulse partitioning shown in figure 1 is also adequate for the time dependence of the phase. An average over a large number of realisations of the stochastic phase reproduces the phase diffusion model of laser bandwidth. In fact, the number of extra calculations for this averaging is not very large, since integrals over inhomogeneous broadenings must be done. If each contribution to the numerical quadrature is calculated with a separate realisation of ϕ, the bandwidth is adequately reproduced.

3. Inhomogeneous broadening and intensity fluctuations

We consider three sources of inhomogeneous broadening. First, shot-to-shot fluctuations in the laser intensity of exactly the type considered by Scarl *et al* are included. Secondly we assume that there is a shot-to-shot variation in laser frequency. This variation contributes to the measured bandwidth. The transverse Doppler motion of the atoms must also be included. Scarl *et al* give a value of 56 MHz for the variance σ_D^2 of the Doppler width.

We follow Scarl *et al* and assume that the shot-to-shot intensity distribution is Gaussian, with mean intensity $\langle I\rangle$ and width given by $\sigma_I = s\langle I\rangle$. Here s is a fitting parameter. Explicitly the distribution of intensity I is

$$P_I(I) = \frac{2}{[1+\mathrm{erf}(1/s\sqrt{2})]}\frac{1}{\sqrt{2\pi}\sigma_I}\exp\left(-\frac{(I/\langle I\rangle - 1)^2}{2s^2}\right). \tag{8}$$

Scarl *et al* assume that the normalisation factor $2/(1+\mathrm{erf}(1/s\sqrt{2}))$ can be approximated by unity. For their value of $s = 0.7$ this introduces an error of $\simeq 8\%$. Although this is not large, a concommitant prediction is that $s = 0.7$ implies that the laser fails to fire once in twelve shots.

Secondly we include a shot-to-shot fluctuation in laser frequency. We assume that the laser frequency fluctuates around the atomic resonance frequency to give any particular shot a detuning Δ. For lack of any other information we assume that this detuning is Gaussian distributed with variance σ_s^2. This adds in quadrature to the Doppler width, so that the total inhomogeneous detuning is distributed as

$$P_\Delta(\Delta) = \frac{1}{\sqrt{2\pi}\sigma_\Delta}\exp(-\Delta^2/2\sigma_\Delta^2) \tag{9}$$

with $\sigma_\Delta^2 = \sigma_s^2 + \sigma_D^2$.

This determines the ion signal in terms of four parameters.

4. An analytic model

We have the four fitting parameters z_0, W, σ_s and s. The observed ion signal N is given by

$$N(z_0, W, \sigma_\Delta, s) = \int \mathrm{d}I \int \mathrm{d}\Delta P_I(I) P_\Delta(\Delta)\overline{\langle |c_2(z_0, W, \Delta, I, t\to\infty)|^2\rangle} \tag{10}$$

where the important arguments of the amplitude c_2 have been indicated. The brackets $\langle\ \rangle$ indicate that an average over realisations of the stochastic phase $\phi(t)$ must be made and the bar implies that $|c_2|^2$ must also be averaged over the degeneracy of the initial level. Since plane-polarised laser light was used this produces no difficulty because the magnetic substates of the initial level are completely decoupled from each other. Although the procedure described in § 2 is entirely tractable for determining the 'exact' value of N given its arguments, it is too difficult to use to extract values of these arguments from a least-squares fit to the experimental data. The source of the trouble is the calculation of $\langle |c_2|^2\rangle$. Consequently we make use of the well known substitution rule for the Wiener–Levy process (Wodkiewicz 1979) which enables us to

write (Smith 1978)

$$\langle|c_2^m|^2\rangle = \frac{1}{2}\left(1 + \sum_{n=1}^{3} \lambda_n \exp(\mu_n T)\right) \tag{11}$$

under the assumption that the true Gaussian pulse can be approximated by a constant pulse of effective length T. In equation (11) μ_n are the roots of the cubic

$$\mu[(\mu + \tfrac{1}{2}W)^2 + \Delta^2] + (\mu + \tfrac{1}{2}W)V_m^2 = 0 \tag{12a}$$

and

$$\lambda_1 = \frac{\frac{1}{2}V_m^2 - \mu_2\mu_3}{(\mu_2 - \mu_1)(\mu_3 - \mu_1)} \tag{12b}$$

with cyclic permutation of the indices for λ_2, λ_3. Finally

$$V_m = C_m E_{\text{eff}} z_0 \tag{13}$$

C_m is the (Clebsch–Gordan) coefficient which determines the fraction of the transition strength taken by the magnetic sublevel m. Thus

$$\overline{\langle|c_2|^2\rangle} = \tfrac{1}{7}\sum_{m=-3}^{3} \langle|c_2^m|^2\rangle. \tag{14}$$

We determine T and E_{eff} by the requirement that the first three moments (0, 1, 2) of the *field* envelope are identical for the Gaussian and equivalent constant pulse. This is in contrast to Scarl *et al* who require that the first three moments of the *power* envelope are identical. Our method has the advantage that the analytic and numerical results agree exactly for zero detuning and laser bandwidth. This would not be the case had we used the moments of the power envelope. We get

$$T = 2\sqrt{6}\sigma_p = 10.435 \text{ ns} \tag{15a}$$

$$E_{\text{eff}} = \sqrt{\pi/6}E_0 \tag{15b}$$

where σ_p is the standard deviation of the power envelope (2.13 ns) and E_0 is the laser's peak electric field. This procedure is sufficiently simple that equation (14) can be used as a basis for a least-squares fit. However it is only useful if the approximations (equation (15)) are not serious. Figure 2 shows a comparison between the analytic approximation and the true numerical result for selected values of the fitting parameters. The agreement is quite good in cases where the bandwidth results from phase diffusion, but not nearly so good in cases where the bandwidth has an inhomogeneous source. Fortunately we find overall the best fit corresponds to the former case.

5. Results

Equation (10) depends upon four parameters. However Scarl *et al* also measure the total bandwidth (see table 1). This fixes a relationship between W and σ_s. Unfortunately the way in which the bandwidths add is not simple. Nevertheless, the result of convoluting a Gaussian and Lorentzian lineshape is the well known Voigt profile (see, e.g., Sobel'man 1972). We require that the Lorentzian phase diffusion width, the Gaussian transform width and the Gaussian inhomogeneous width (σ_s) should all add to give a Voigt profile FWHM 182.5 MHz. The best fit then implies that the FWHM of

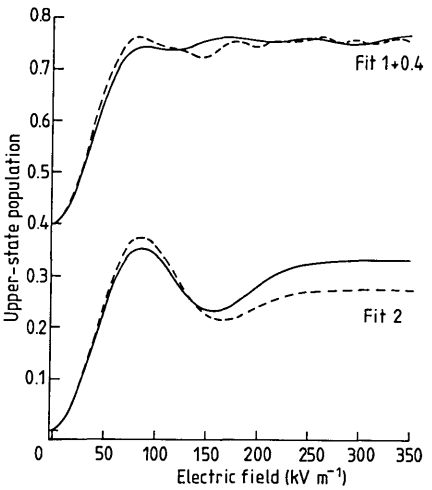


Figure. 2. Comparison between the analytic (full curve) and numerical (broken curve) results for the two fits listed in table 2. For clarity of display 0.4 has been added to the results for fit 1. The abscissa is the peak electric field (in $kV\,m^{-1}$) given by the laser.

Table 1. The experimental parameters.

Pulse shape	Power spectrum	Peak power density
Gaussian 5.02 ns FWHM	Gaussian? 182.5 MHz FWHM	$1.55\times10^{8}\ W\,m^{-2}$

the phase diffusion width should be 136 MHz. The corresponding value of σ_s is 8 MHz and the other parameters are tabulated in table 2 (fit 1).

In order to compare with the procedure of Scarl *et al* we also consider the situation in which all the bandwidths add linearly and the Doppler width is ignored. A least-squares fit to the data gives fit 2 of table 2. This is essentially the result given by Scarl *et al.* We get a somewhat different value for z_0 because we have fitted moments of the field envelope rather than power envelope. For the zero bandwidth case we would find that this implies

$$z_0(\text{Scarl } et\ al) = (\tfrac{2}{3}\pi)^{1/4} z_0\ (\text{this work}) \tag{16}$$

which is still approximately true for the finite bandwidth case. Figure 3 shows the two fits, normalised to the experimental data. This is an unusual way of presenting theory;

Table 2. The two fits discussed in the text, where the parameters z_0, W, σ_s and s are defined. Σ is the sum of the squares of the difference between the theoretical fit and experimental points.

	z_0 (pm)	W (MHz)	σ_s (MHz)	s	Σ
Fit 1	5.57	136	8	0.13	0.06
Fit 2	3.15	0	40	0.73	0.004

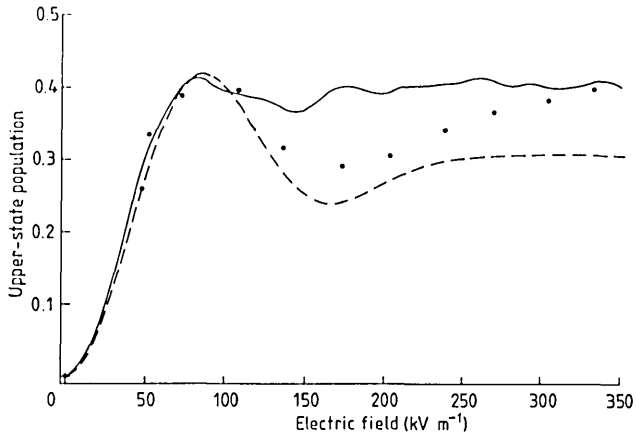


Figure 3. Comparison between the two fits and experiment. The experimental points are from Scarl *et al* (1981). The two fits are normalised to experiment at the peak, so that what is actually plotted is $N \times$(theoretical result). The values of N are: fit 1 (——), $N = 1.14$; fit 2 (- - - -), $N = 1.12$. For these results approximately 16 realisations of the phase have been used for each point in the inhomogeneous integrations (see § 2). Once again, the abscissa is the peak electric field of the laser.

normally one would normalise the experiment to the theory if the experimental measurements are not absolute. Scarl *et al* do not say if their experimental data are absolute and we do not assume so. The procedure adopted in figure 3 then displays both fits on an equal footing†.

6. Conclusions

The best values consistent with the data given by Scarl *et al* are $z_0 = 5.57$ pm, $W = 136$ MHz and $\sigma_s = 8$ MHz, $s = 0.13$. Under these conditions the standard deviation per point of the analytic fit is approximately 0.07. The error on the fitting parameters is more difficult to estimate. However we find that values near $z_0 \simeq 4.5$, $W = 95$, $s = 0.23$ also fit the data well, (but are inconsistent with the measured bandwidth of the laser, giving a total width of about 150 MHz). If we assume that the discrepancy between these values, and our recommended values is characteristic of the error we get: $z_0 = 5.57 \pm 1.0$ pm, $W = 136 \pm 45$ MHz, $\sigma_s = 8 \pm 8$ MHz, $s = 0.13 \pm 0.1$. (The shot to shot fluctuations in detuning are essentially undetermined but less than about 30 MHz FWHM, or their effect on the fit would be important.)

A few points are worth highlighting. First, an independent measurement of the value of s would be very valuable if experiments of this type are repeated. Indeed the explicit form of the distribution of shot-to-shot intensity fluctuation should, if possible, be determined. In some circumstances this may not be very difficult (Wort 1983). Secondly a better characterisation of the measured laser bandwidth would be desirable. If the overall lineshape is indeed a Voigt profile then the separation of the points of inflection, rather than the FWHM enables the Lorentzian and Gaussian components to be deconvoluted simply (Stoneham 1972).

† In the figure caption we give the ratio of experiment to theory.

Thirdly, we may remark that although our recommended values fit the data less well than the values given by Scarl *et al* we believe that they are more correct. The value of s in particular appears to be realistic, implying a shot-to-shot fluctuation in intensity of about 30% FWHM about the mean, rather than the 165% fluctuation required by Scarl *et al.*

Finally, the analytic model described in § 4 gives a good representation of the numerical results, particularly in the case where the phase diffusion bandwidth is dominant. It is especially convenient for this case, since equation (12*a*) reduces to a quadratic, for zero detuning.

Acknowledgments

One of us (MAL) acknowledges the receipt of an SERC CASE award in conjunction with AERE Harwell. We have had useful conversations with A M Lane, D Wort and A M Stoneham of AERE Harwell.

References

Sargent M, Scully M O and Lamb W E 1974 *Laser Physics* (Reading, MA: Addison Wesley)
Scarl D, Hackel L A, Johnson M A and Rushford M C 1981 *Phys. Rev.* A **24** 883
Smith R A 1978 *Proc. R. Soc.* A **362** 1
Sobel'man I I 1972 *An Introduction to the Theory of Atomic Spectra* transl. T F J Le Vierge (Braunschweig: Pergamon) p 382
Stoneham A M 1972 *J. Phys. D: Appl. Phys.* **5** 670
Wax N (ed) 1954 *Selected Papers on Noise and Stochastic Processes* (New York: Dover)
Wilcox R M 1967 *J. Math. Phys.* **8** 962
Wodkiewicz K 1979 *Phys. Rev.* A **19** 1686
Wort D J H 1983 private communication

Acta Physica Austriaca 56, 103–117 (1984)

Acta Physica Austriaca

© by Springer-Verlag 1984

Making Atoms Transparent: Trapped Superpositions*

By

P. L. Knight[1], M. A. Lauder[1], P. M. Radmore[1], and B. J. Dalton[2]

[1] Optics Section, Blackett Laboratory, Imperial College, London, England

[2] Physics Department, University of Queensland, St. Lucia, Australia

With 8 Figures

(Received June 6, 1984)

Summary

Population initially in a discrete state which is coupled to a smooth continuum is usually lost by an irreversible decay. The question arises: can we turn off this decay using coherent superposition states to make the atoms transparent to perturbations? We discuss examples of such "population trapping" in laser-induced continuum structure and multichannel multiphoton ionization. We also examine the stability of trapped states when light field amplitudes and phases fluctuate.

1. Introduction

Population initially in a discrete state $|0\rangle$ which is coupled to a smooth continuum $|E\rangle$ by an interaction V_{0E} is usually lost by an irreversible decay at a rate

$$\Gamma_0 = \frac{2\pi}{\hbar} \sum_E |V_{0E}|^2 \, \delta(E - E_0). \tag{1.1}$$

The question arises: can we turn off this decay? In this article we discuss the use of coherent superposition states to turn off decay channels and to make the atoms transparent to perturbations.

We first consider the three-level lamda system shown in Fig. 1 in which a laser field of frequency ω_a and amplitude E_a excites a transition from 0 to 1, while another laser field of frequency ω_b and amplitude E_b excites a transition from the other ground state 2 to the common

* Invited lecture presented at the seminar on "Fundamentals of Quantum Optics", in Obergurgl, Austria, 1984.

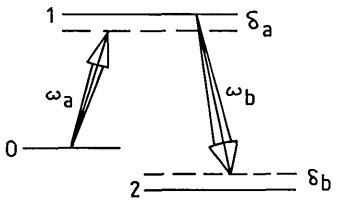


Fig. 1. Excitation of three level system by two laser fields

excited state 1. When the fields are two-photon resonant ($\delta_a = \delta_b$), the coherent superposition excited by approximately equal Rabi frequency interactions ($\Omega_a = d_{01}E_a/\hbar$, $\Omega_b = d_{12}E_b/\hbar$)

$$\psi(t) \simeq \frac{1}{\sqrt{2}}(\exp[-i\omega_0 t]|0\rangle - \exp[-i\omega_2 t]|2\rangle) \tag{1.2}$$

is trapped, immune to photo-excitation [1–22]. The excitation rate R is, from Fermi's Golden Rule

$$R \simeq \frac{2\pi}{\hbar}|\langle\psi(t)|\underline{d}\cdot(\underline{E}_a + \underline{E}_b)|1\rangle|^2 \simeq 0. \tag{1.3}$$

The atom is transparent simply because the fields induce equal but opposite sign transition moments. This is the origin of the so-called "dark-line resonances" observed by Orriols and others [2–6, 13]. The coherent superposition responsible for this population trapping is extremely sensitive to the degree of mutual coherence between the two laser fields E_a and E_b. Unless the two fields are critically cross-correlated so that instantaneous frequency fluctuations preserve two-photon resonance, the superposition slowly dephases and absorbs radiation [15–18].

It has been known for many years that windows of zero absorption occur in the photo-excitation of autoionizing resonances [23]. Such windows are caused by interference between different quantum mechanical paths to the same final state [24] and certainly fall into the category of coherence-induced transparencies. Indeed the zeros of absorption are derived from cancelling transition moments as above. Autoionizing resonances are fairly immutable and un-tunable, being created by configuration mixing. A laser field can induce resonances in continuum states which behave much as tunable autoionizing resonances of adjustable width [25, 26]. These produce not only resonant enhancements and excitation windows but also some interesting power-broadening and AC Stark splitting effects which are the intense field manifestation of the low field destructive interference [27–36].

A convenient language in which to describe continuum coupling is the Fano theory of autoionization [24]. We have used this to discuss the

properties of laser-induced continuum structure (LICS). In this article where we are interested in the role of laser fluctuations, we work instead in terms of the undressed states 0 and 1. We do, however, retain much of the descriptive language of Fano theory, especially in the use of a Fano q-parameter.

Theoretical activity on LICS and autoionizing resonances in strong fields in the last two years has far outstripped experimental work [37–40]. The coherence effects responsible for LICS are very sensitive to laser fluctuations and especially to the cross-correlations between probe and dressing lasers [15–18]. A great deal of theoretical work on the effects of stochastic incoherences and spontaneous decay on the continuum structure excitation has been reported [41–50], almost all of this on autoionizing resonances. Much of this work, especially that on radiative decay from an autoionizing state to a non-laser field driven lower state can be accounted for by the simple and obvious substitution of a complex energy for the energy of the continuum resonance [51]. Inhomogeneous broadening has been discussed by Haus *et al.* [52]; the effect of further continuum absorptions by Andryushin and others [53–55]; the rotating wave approximation by Javanainen [56]. The curiously asymmetric AC Stark splitting and saturation properties of strongly-excited continuum resonances affect up-conversion; harmonic generation ionization losses can be minimized by exploiting the population trapping phenomenon [57, 58].

2. ICS Model and Master Equation Derivation

In our model of the effects of laser fluctuations on LICS, the atom has two discrete states $|0\rangle$, $|1\rangle$ and a continuum of states $|f\rangle$ (see Fig. 2)

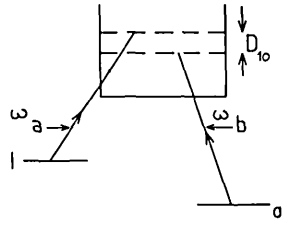


Fig. 2. Excitation of LICS by two laser fields

of opposite parity to $|0\rangle$, $|1\rangle$. The atom, initially in the ground state $|0\rangle$, interacts with two single mode laser fields a, b of angular frequencies ω_a, ω_b, polarizations $\underline{\epsilon}_a$, $\underline{\epsilon}_b$ and which are initially in coherent states $|\alpha_a\rangle$, $|\alpha_b\rangle$. By convention $\omega_b > \omega_a$, the transition frequency $\omega_{10} > 0$,

and the frequencies ω_a, ω_b are assumed to be sufficiently large that photoionization processes from the states $|1\rangle$, $|0\rangle$ respectively, to continuum states $|f\rangle$ well above threshold are possible. The laser frequencies will be taken to satisfy approximately the condition of two-photon (Raman) resonance $\omega_a + \omega_0 \simeq \omega_b + \omega_1$. We write $\alpha_c = \bar{n}_c^{1/2} \exp(-i\pi/2)$, $(c = a, b)$, where $\bar{n}_c$ is the mean number of photons of frequency ω_c $(c = a, b)$. Ignoring laser fluctuations for the present, the contributions from the two laser modes to the corresponding classical electric fields at the atom are given by $\mathscr{E}_{0c}\,\hat{\underline{\epsilon}}_c \cos \omega_c t$, where $\mathscr{E}_{0c} = 2(\hbar\omega_c/2\epsilon_0)^{1/2} \times$ $\times (\bar{n}_c/V)^{1/2}$ and where V is the volume the radiation field occupies. We take $\bar{n}_c/V$ to be finite whilst $\bar{n}_c \to \infty$, $V \to \infty$. Spontaneous emission processes are ignored. Laser-induced transitions between different continuum states are also ignored. Interactions between the atom and the laser modes are treated in the electric dipole approximation. The nonzero matrix elements of the electric dipole operator $\underline{\mu}$ which connect discrete and continuum states only, are assumed real.

The part of the overall system of most interest to us here is the coupled laser-discrete atomic state system. Accordingly, the total Hamiltonian (ignoring laser fluctuations) will be written as

$$H = H^S + H^B + V \tag{2.1a}$$

where

$$H^S = \sum_{i=0,1} \sum_{n_a, n_b} (\hbar\omega_i + (n_a + \tfrac{1}{2})\hbar\omega_a + (n_b + \tfrac{1}{2})\hbar\omega_b) \times |in_a n_b\rangle\langle in_a n_b|, \tag{2.1b}$$

$$H^B = \sum_{f} \sum_{n_a n_b} (\hbar\omega_f + (n_a + \tfrac{1}{2})\hbar\omega_a + (n_b + \tfrac{1}{2})\hbar\omega_b) \times |fn_a n_b\rangle\langle fn_a n_b|, \tag{2.1c}$$

and

$$V = -(\underline{\mu} \cdot \underline{E}_a + \underline{\mu} \cdot \underline{E}_b) \tag{2.1d}$$

with

$$\underline{E}_c = i(\hbar\omega_c/2\epsilon_0 V)^{1/2} \hat{\underline{\epsilon}}_c (a_c - a_c^+), \qquad c = a, b. \tag{2.1e}$$

The uncoupled energy eigenstates are $|in_a n_b\rangle \equiv |i\rangle|n_a\rangle|n_b\rangle$ and $|fn_a n_b\rangle$ $\equiv |f\rangle|n_a\rangle|n_b\rangle$, where $|n\rangle$ are number states for the mode involved. The Hamiltonians H^S, H^B describe the free discrete atomic state-laser mode system and continuum atomic state-laser mode system. The interaction V couples the two separate subsystems.

As in our previous work [15, 16], laser fluctuations are treated via a generalized Wiener-Levy phase-diffusion model in which the laser spectrum is considered to be Lorentzian. A stochastic term is added to

the Hamiltonian in the form

$$H_{\text{stoch}} = \hbar\mu_a(t)a_a^+a_a + \hbar\mu_b(t)a_b^+a_b \tag{2.2}$$

where $\mu_a(t)$, $\mu_b(t)$ are zero-mean Gaussian-Markoff processes which are delta-function correlated and which represent stochastic frequency fluctuations. Thus

$$\langle\mu_c(t)\mu_d(t')\rangle = 2\Delta_{cd}\,\delta(t-t'), \qquad c,d = a,b, \tag{2.3a}$$

$$\langle\mu_c(t')\rangle = 0. \tag{2.3b}$$

The quantities Δ_{aa}, Δ_{bb} ($\geqslant 0$) are the bandwidths of the two lasers and the quantity Δ_{ab} ($= \Delta_{ba}$) is the cross-spectral bandwidth ($\Delta_{ab}^2 \leqslant \Delta_{aa}\cdot\Delta_{bb}$) which describes correlations between the phase fluctuations of the two lasers.

The time-independent Liouville equation for the stochastically-averaged density matrix elements [16, 59] ($k, l = 0, 1, f$) are

$$\frac{d}{dt}\sigma_{kn_an_b;lm_am_b} = -\frac{i}{\hbar}[H^S + H^B + V, \sigma]_{kn_an_b;lm_am_b} - \Delta(n_a - m_a, n_b - m_b)\sigma_{kn_an_b;lm_am_b} \tag{2.4a}$$

where

$$\Delta(p_a, p_b) = \Delta_{aa}p_a^2 + \Delta_{bb}p_b^2 + 2\Delta_{ab}p_ap_b\,. \tag{2.4b}$$

The second (non-Hermitian) term in (2.4a) represents the effect of laser fluctuations.

Master equations for the density matrix elements $\sigma_{in_an_b,jm_am_b}$ ($i,j = 0, 1$) describing the discrete atomic state-laser mode subsystem can be obtained using projection operator methods developed by one of us [60]. The unperturbed Liouville operator will be given as the sum of $[H^S + H^B, \ldots]$ and the non-Hermitian system Liouville operator representing laser fluctuations. The system-reservoir matrix elements are

$$\begin{aligned} v_{in_an_b;fk_ak_b} &= -\frac{1}{\hbar}\langle in_an_b\,|(\underline{\mu}\cdot\underline{E}_a + \underline{\mu}\cdot\underline{E}_b)|fk_ak_b\rangle \\ &\approx -\tfrac{1}{2}\xi_{if}^a(\delta_{k_a,n_a+1} - \delta_{k_a,n_a-1})\delta_{k_b,n_b} \\ &\quad -\tfrac{1}{2}\xi_{if}^b(\delta_{k_b,n_b+1} - \delta_{k_b,n_b-1})\delta_{k_a,n_a} \end{aligned} \tag{2.5a}$$

where the (real) bound-continuum Rabi frequencies are given by

$$\xi_{if}^c = \langle i\,|\underline{\mu}\cdot\hat{\underline{\epsilon}}_c|f\rangle\mathcal{E}_{0c}/\hbar. \tag{2.5b}$$

In deriving (2.5) we assume that all n_ak_a, n_ak_b of interest are close to $\bar{n}_a$, $\bar{n}_b$ respectively, which follows from the proportionately negligible

spread of photon numbers associated with fields in coherent states with large $\bar{n}_c$.

In view of the slow variation of the above matrix elements with continuum energy $\hbar\omega_f$, it follows that the Markoff approximation is valid in the evaluation of relaxation elements. We then find that the stochastically averaged discrete-atomic-states-laser modes density matrix elements satisfy the master equations ($ijlm = 0, 1$):

$$\frac{d}{dt}\sigma_{in_an_b;jm_am_b} = -i\{\omega_{ij} + (n_a - m_a)\omega_a + (n_b - m_b)\omega_b - i\Delta(n_a - m_a, n_b - m_b)\}\sigma_{in_an_b;jm_am_b} + \sum_{lr_ar_b} \Gamma_{in_an_b,jm_am_b;lr_ar_b,mS_aS_b}\sigma_{lr_ar_b;mS_aS_b} \quad (2.6a)$$

where the weak coupling Markovian relaxation matrix elements are

$$\Gamma_{in_an_b,jm_am_b;lr_ar_b,mS_aS_b} = -i\sum_{fk_ak_b}\left(\frac{v_{in_an_b,fk_ak_b}v^*_{lr_ar_b,fk_ak_b}}{\omega_{lf} + (r_a - k_a)\omega_a + (r_b - k_b)\omega_b + i\epsilon}\delta_{jm}\delta_{m_aS_a}\delta_{m_bS_b} + \frac{v^*_{jm_am_b,fk_ak_b}v_{mS_aS_b,fk_ak_b}}{\omega_{fm} + (k_a - S_a)\omega_a + (k_b - S_b)\omega_b + i\epsilon}\delta_{il}\delta_{n_ar_a}\delta_{n_bS_b}\right). \quad (2.6b)$$

These can be further simplified by using the secular, or rotating-wave approximation of the second kind [61]. This restricts terms in the sum in Eq. (2.6b) to those for which $\omega_{lm} + (r_a - S_a)\omega_a + (r_b - S_b)\omega_b \simeq \simeq \omega_{ij} + (n_a - m_a)\omega_a + (n_b - m_b)\omega_b$. In the present work we also assume that ω_{10} does not approximately equal $2\omega_a$, so that the possible direct two-photon resonant transition $|0\rangle + 2\omega_a \rightarrow |1\rangle$ via the virtual continuum states $|f\rangle$ is not treated here.

The evaluation of the relaxation constants is tedious, if straightforward. The present restriction to laser frequencies approximately satisfying the two-photon resonance condition $(\omega_a + \omega_0) \simeq (\omega_b + \omega)$ enables us to inter-relate many of the relaxation constants. The relaxation constants ultimately involve the following quantities (a) γ_i^c ($c = a, b$; $i = 0, 1$), the rate constant for the ionization of state $|i\rangle$ due to laser c (proportional to the intensity I_c of laser c), (b) δ_{10}^c ($c = a, b$) the Stark shift of transition frequency ω_{10} due to laser c (also proportional to I_c) and (c) ϵ^{ab} and γ^{ab} which specify off-diagonal relaxations or complex two-photon Rabi frequencies [29, 30], (both ϵ^{ab}, γ^{ab} are proportional to $\sqrt{I_aI_b}$). Explicitly,

$$\gamma_i^c = \frac{\pi}{2} \sum_f (\xi_{if}^c)^2 \, \delta(\omega_{fi} - \omega_c)$$

$$= \frac{\pi}{2} \rho(\omega_f = \omega_i + \omega_c)(\xi_{if}^c)^2, \tag{2.7a}$$

$$\delta_{10}^c = -\frac{1}{4} \sum_f (\xi_{1f}^c)^2 \left(\frac{P}{\omega_{f1} + \omega_c} + \frac{P}{\omega_{f1} - \omega_c} \right)$$

$$+ \frac{1}{4} \sum_f (\xi_{0f}^c)^2 \left(\frac{P}{\omega_{f0} + \omega_c} + \frac{P}{\omega_{f0} - \omega_c} \right)$$

$$= -\frac{1}{4} \int d\omega_f \, \rho(\omega_f)(\xi_{1f}^c)^2 \left(\frac{P}{\omega_{f1} + \omega_c} + \frac{P}{\omega_{f1} - \omega_c} \right)$$

$$+ \frac{1}{4} \int d\omega_f \, \rho(\omega_f)(\xi_{0f}^c)^2 \left(\frac{P}{\omega_{f0} + \omega_c} + \frac{P}{\omega_{f0} - \omega_c} \right), \tag{2.7b}$$

$$\epsilon^{ab} = \frac{1}{4} \sum_f \xi_{0f}^a \xi_{1f}^b \left(\frac{P}{\omega_{f1} + \omega_b} + \frac{P}{\omega_{f1} - \omega_a} \right)$$

$$\approx \frac{1}{4} \sum_f \xi_{0f}^a \xi_{1f}^b \left(\frac{P}{\omega_{f0} + \omega_a} + \frac{P}{\omega_{f0} - \omega_b} \right)$$

$$= \frac{1}{4} \int d\omega_f \, \rho(\omega_f) \xi_{0f}^a \xi_{1f}^b \left(\frac{P}{\omega_{f1} + \omega_b} + \frac{P}{\omega_{f1} - \omega_a} \right), \tag{2.7c}$$

$$\gamma^{ab} = \frac{\pi}{2} \sum_f \xi_{1f}^a \xi_{0f}^b \, \delta(\omega_{f1} - \omega_a)$$

$$\approx \frac{\pi}{2} \sum_f \xi_{1f}^a \xi_{0f}^b \, \delta(\omega_{f0} - \omega_b)$$

$$\approx \frac{\pi}{2} \rho \left(\omega_f = \begin{Bmatrix} \omega_0 + \omega_a \\ \omega_1 + \omega_b \end{Bmatrix} \right) \xi_{1f}^a \xi_{0f}^b, \tag{2.7d}$$

$$(\gamma^{ab})^2 \approx \gamma_1^a \gamma_0^b. \tag{2.7e}$$

Note that the Stark shift δ_{10}^c ($c = a, b$) contains both resonant and anti-resonant contributions; $\rho(\omega_f)$ is the continuum density of states.

The effective Fano q-parameter is defined by

$$q \equiv \epsilon^{ab} / (\tfrac{1}{2} \gamma^{ab}) \tag{2.8}$$

and plays a dominant role in the physics of LICS. We again note the presence of counter-rotating terms in q through ϵ^{ab}. Alber and Zoller [62] have found such counter-rotating terms can be important when the

Raman-like coupling responsible for ϵ^{ab} contains contributions from low-lying discrete states; such low-lying states contribute as intermediate states to ϵ^{ab} but because they are discrete do not contribute to the continuum loss γ^{ab} and can only enhance $|q|$.

If the density matrix elements in (2.6) are written as $\sigma_{in_an_b;j\overline{n_a+p_a},\overline{n_b+p_b}}$ it can be seen easily that the sets of equations involve coefficients that do not depend upon n_a, n_b. They break up into coupled sets, the $(n_an_bp_ap_b)$ set containing elements $\sigma_{\alpha\beta}$, where $\alpha = 0\, n_a n_b;\ 1\,\overline{n_a+1}\,\overline{n_b-1}$, $\beta = 0\,\overline{n_a+p_a}\,\overline{n_b+p_b};\ 1\,\overline{n_a+p_a+1}\,\overline{n_b+p_b-1}$. This corresponds to the coupling of states $|0 n_a n_b\rangle$ and $|1\,\overline{n_a+1}\,\overline{n_b-1}\rangle$ via the continuum states $|f\, n_a\, \overline{n_b-1}\rangle$. The coupled density matrix elements can be written in the form

$$\sigma_{ij}(p_ap_b) \times c(n_an_b). \tag{2.9}$$

For example $\sigma_{0n_an_b;1\overline{n_a+p_a+1},\overline{n_b+p_b-1}} = \sigma_{01}(p_ap_b) \times c(n_an_b)$. The initial conditions along with the choice of $\sigma_{00}(p_ap_b) = \exp[i(\frac{1}{2}p_a\pi + \frac{1}{2}p_b\pi)]$ leads to

$$\sigma_{ij}(p_ap_b;\, t=0) = 0, \qquad i,j \neq 0,0, \tag{2.10a}$$

$$c(n_a, n_b) = |\langle n_a|\alpha_a\rangle|^2 \cdot |\langle n_b|\alpha_b\rangle|^2. \tag{2.10b}$$

The atomic factors $\sigma_{ij}(p_ap_b)$ then satisfy the optical Bloch equations (2.11):

$$\frac{d}{dt}\begin{bmatrix}\sigma_{00}\\ \sigma_{01}\\ \sigma_{10}\\ \sigma_{11}\end{bmatrix} = -i\begin{bmatrix} A_{00,00} & (q-i)\frac{1}{2}\sqrt{\gamma_1^a\gamma_0^b} & (-q-i)\frac{1}{2}\sqrt{\gamma_1^a\gamma_0^b} & 0\\ (q-i)\frac{1}{2}\sqrt{\gamma_1^a\gamma_0^b} & A_{01,01} & 0 & (-q-i)\frac{1}{2}\sqrt{\gamma_1^a\gamma_0^b}\\ (-q-i)\frac{1}{2}\sqrt{\gamma_1^a\gamma_0^b} & 0 & A_{10,10} & (q-i)\frac{1}{2}\sqrt{\gamma_1^a\gamma_0^b}\\ 0 & (-q-i)\frac{1}{2}\sqrt{\gamma_1^a\gamma_0^b} & (q-i)\frac{1}{2}\sqrt{\gamma_1^a\gamma_0^b} & A_{11,11}\end{bmatrix}\begin{bmatrix}\sigma_{00}\\ \sigma_{01}\\ \sigma_{10}\\ \sigma_{11}\end{bmatrix} \tag{2.11}$$

where

$$A_{00,00} = -(\Omega(p_ap_b) + i\Delta(p_ap_b) + i(\gamma_0^a + \gamma_0^b)), \tag{2.11a}$$

$$A_{01,01} = -\left(\Omega(p_ap_b) + i\Delta(p_a+1, p_b-1) + \delta_{10} + \frac{i}{2}(\gamma_1^a + \gamma_0^a + \gamma_1^b + \gamma_0^b)\right), \tag{2.11b}$$

$$A_{10,10} = -\left(\Omega(p_ap_b) + i\Delta(p_a-1, p_b+1) - \delta_{10} + \frac{i}{2}(\gamma_1^a + \gamma_0^a + \gamma_1^b + \gamma_0^b)\right), \tag{2.11c}$$

$$A_{11,11} = -(\Omega(p_ap_b) + i\Delta(p_a, p_b) + i(\gamma_1^a + \gamma_1^b)). \tag{2.11d}$$

The quantity $\Omega(p_ap_b)$ and the Stark-shifted detuning are defined by

$$\Omega(p_a p_b) = p_a \omega_a + p_b \omega_b, \tag{2.12a}$$

$$\delta_{10} = (\omega_1 + \omega_a - \omega_0 - \omega_b) + \delta_{10}^a + \delta_{10}^b. \tag{2.12b}$$

The condition for two-photon resonance will therefore be $\delta_{10} = 0$. The above Bloch equations allow for $|0\, n_a\, n_b\rangle \to |f\, \overline{n_a - 1}\, n_b\rangle$ and $|1\, n_a\, n_b\rangle \to |f\, n_a\, \overline{n_b - 1}\rangle$ ionization decay channels ignored in previous work.

We solve the Bloch equations (2.11) in terms of the right (Y_i) and left (Z_i) eigenvectors of the matrix A in Eq. (2.11). We write (2.11) as

$$\frac{d}{dt} X = -iAX \tag{2.13}$$

where the elements ($X_1 = \sigma_{00}(0, 0)$ etc.) are

$$X = \begin{pmatrix} X_1 \\ X_2 \\ X_3 \\ X_4 \end{pmatrix}$$

so that $AY_i = \lambda_i Y_i$ and $A^{\mathrm{T}} Z_i = \lambda_i Z_i$ (where T denotes transpose). We check that orthogonalization $Z_i^{\mathrm{T}} Y_j = \delta_{ij}$ and find

$$X_i(t) = \sum_{jk} Z_{ji} X_k(0) \exp(-i\lambda_j t)\, Y_{jk} \tag{2.14}$$

with initial condition

$$X(0) = \begin{pmatrix} 1 \\ 0 \\ 0 \\ 0 \end{pmatrix}. \tag{2.15}$$

The populations $X_1 = \sigma_{00}$ ($p_a = p_b = 0$), $X_4 = \sigma_{11}$ ($p_a = p_b = 0$) are of interest to us here. In Fig. 3 we plot the time-evolution of the populations of the discrete states 0 and 1, $X_1(t)$ and $X_4(t)$ and the ion probability $P_I = 1 - X_1(t) - X_4(t)$ versus time. We have taken as input values those of Fig. 3 of Ref. [30] [$\gamma_1^a = 2\pi$, $\gamma_1^b = 0$, $\gamma_0^a = 0$, $q = 5$, $\gamma_0^b = 2\pi$, $\delta_{10} = 0$] but with an uncorrelated laser bandwidth factor

$$\Delta = \Delta_{aa} + \Delta_{bb} - 2\Delta_{ab} = \pi/8.$$

Whereas when $\Delta = 0$, half the population is asymptotically trapped in a non-interacting superposition state, in the non-zero laser bandwidth case we see that the trapping state asymptotically decays away. We have systematically explored the effects of the relevant parameters in Eq. (2.11) and will present these results at length elsewhere.

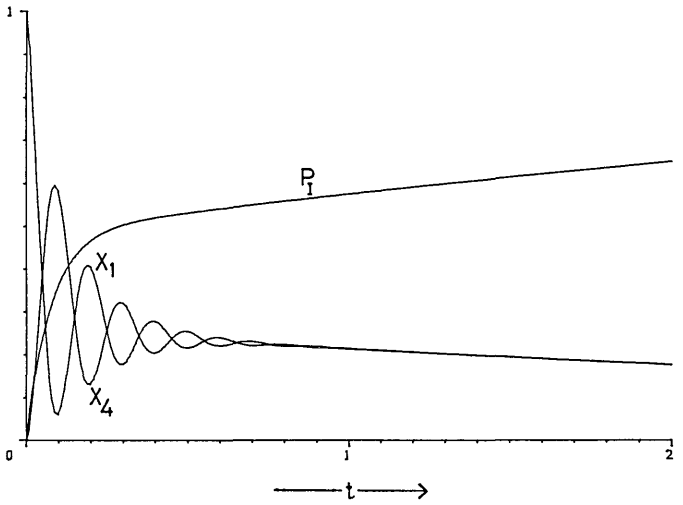


Fig. 3. Time development of bound populations X_1 and X_4 of states 0 and 1 and ion probability $1 - X_1 - X_4 = P_I$ excited by uncorrelated laser fields with parameters given in the text

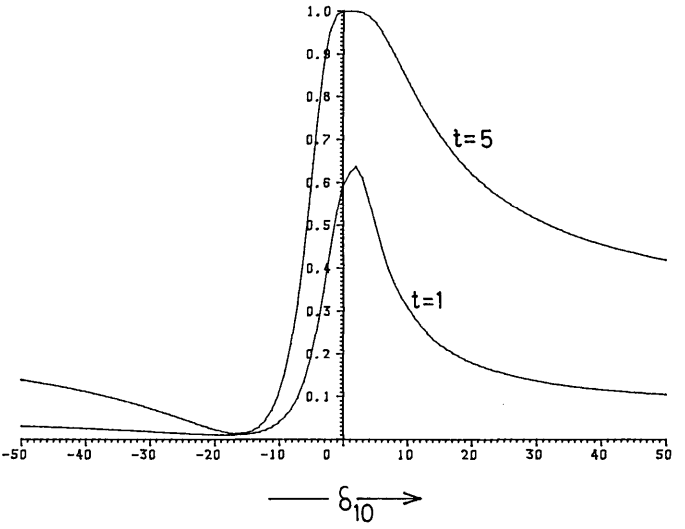


Fig. 4. Dependence of ion probability P_I on detuning δ_{10} for weak probe field at times $t = 1$ and $t = 5$, other values given in text

In Fig. 4 we plot the ionization probability P_I versus detuning δ_{10} for two different times, $t = 1$ and $t = 5$, for an intense dressing interaction

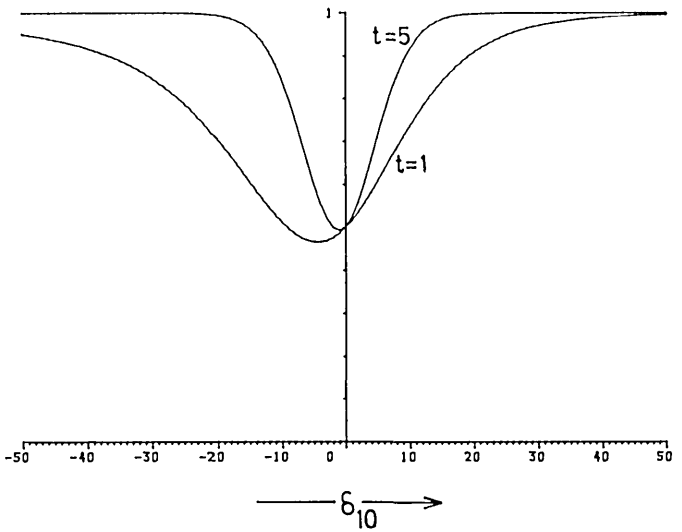


Fig. 5. Dependence of ion probability P_I on detuning δ_{10} for strong coherent probe field at times $t = 1$ and $t = 5$, other values given in text

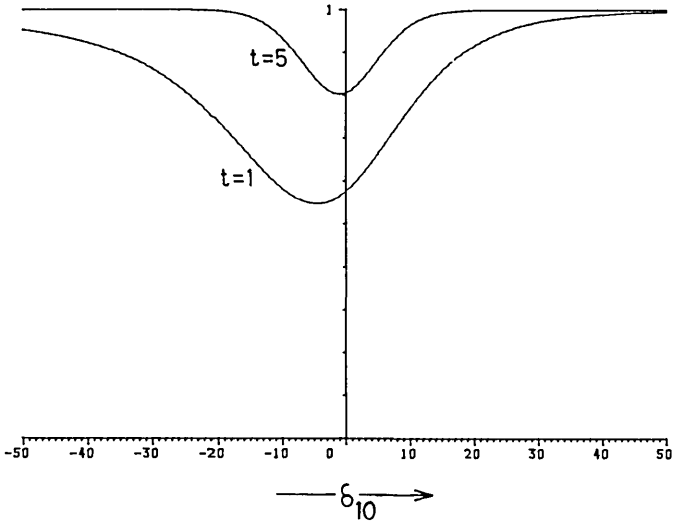


Fig. 6. As Fig. 5 but with uncorrelated laser fields

but weak probe interaction, so that a Fano profile is generated with a window of small absorption and a large resonant peak. In Fig. 4, we have chosen $\gamma_1^a = 2\pi$, $\gamma_1^b = 0$, $\gamma_0^b = 0.01 \times 2\pi$, $\gamma_0^a = 0$, $q = 5$, and a very small

laser bandwidth factor $\Delta = 0.005 \times 2\pi$. We note that the small Δ has hardly affected the Fano lineshape; increasing Δ does begin to destroy the Fano minimum although it is comparatively insensitive to Δ. This is not true when the "probe" field becomes as large as the dressing. In Fig. 5 we choose a strong, coherent probe and dressing interaction with $\gamma_1^a = 2\pi$, $\gamma_1^b = 0$, $\gamma_0^b = 2\pi$, $\gamma_0^a = 0$, $q = 5$, $\Delta = 0$ and see the unusual window behaviour replacing the Fano lineshape of Fig. 4 [30]; when the bandwidth factor is increased to $\Delta = \pi/8$, retaining $\gamma_1^a = 2\pi$, $\gamma_1^b = 0$, $\gamma_0^b = 2\pi$, $\gamma_0^a = 0$ and $q = 5$, we see a rapid decay of the window commensurate with the decay of the nearly-trapped superposition shown in Fig. 3. Experimental work on the effect of laser bandwidths on LICS has yet to be reported.

3. Population Trapping in Two-Channel Two-Photon Ionization

The population trapping mechanism in LICS involves a state of zero width and non-zero energy. The lambda system population trapping involves a state of zero width but at a zero energy. We have recently investigated the general problem of two-channel two-photon ionization in which *both* mechanisms contribute [63]. In Fig. 7 we show the level

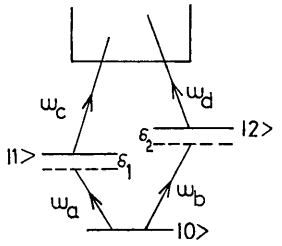


Fig. 7. Level scheme for two-channel two-photon ionization

scheme appropriate, in which a ground-state $|0\rangle$ can be excited by a laser frequency ω_a to state $|1\rangle$ or by frequency ω_b to state $|2\rangle$. Both (intermediate) states $|1\rangle$ and $|2\rangle$ are coupled to a common photoionization continuum. Note that the upper part of the level scheme involves LICS transitions. We have solved the equations of motion for each of the states using Fourier transform methods, and find that the dynamics is governed by three dressed state eigen-energies. Population trapping occurs when one or more of these dressed states has a vanishing width (i.e. decouples from the continuum). In Fig. 8 we plot a representative trio of eigen-energies $\tilde{E}_k$ as a function of the detuning of ω_a from ω_{10}. We have plotted $\mathrm{Re}\,\tilde{E}_k \pm \frac{1}{2}\,\mathrm{Im}\,\tilde{E}_k$ to indicate the width, with input

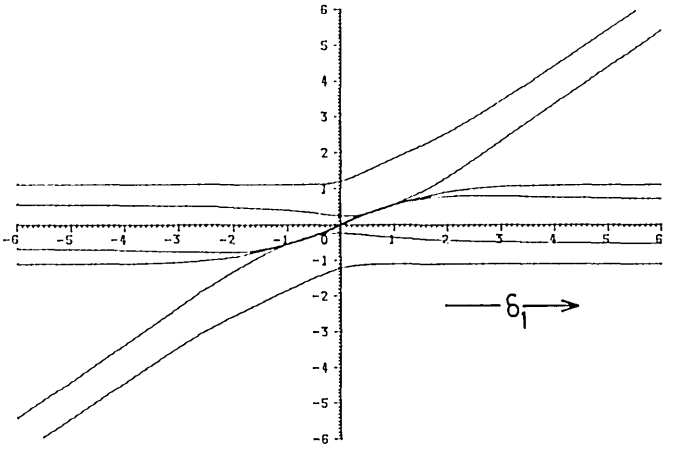


Fig. 8. Dressed state eigen-energies and widths as a function of detuning δ_1 in two-channel two-photon ionization with parameters given in text

parameters $0 \rightarrow 1$ and $0 \rightarrow 2$ Rabi frequencies 0.75 and 1.0, the photo-ionization rates from 1 and 2 being 1.0, a zero q-parameter and a resonant $0 \rightarrow 2$ excitation. Note the vanishing widths at the resonance anticrossings. We have discussed the general conditions for trapping in this system at length elsewhere [63].

Acknowledgements

This work was supported by the UK SERC, the Nuffield Foundation, the British Council, the Royal Society and NATO under grant number 0482/82.

References

[1] Whitley, R. M., Stroud, C. R., jr.: Phys. Rev. **A14**, 1498 (1976).
[2] Alzetta, G., Gozzini, A., Moi, L., Orriols, G.: Nuovo Cim. **B36**, 5 (1976).
[3] Arimondo, E., Orriols, G.: Nuovo Cim. Lett. **17**, 333 (1976).
[4] Gray, H. R., Whitley, R. M., Stroud, C. R., jr.: Opt. Lett. **3**, 218 (1978).
[5] Orriols, G.: Nuovo Cim. **B53**, 1 (1979).
[6] Alzetta, G., Moi, L., Orriols, G.: Nuovo Cim. **B52**, 209 (1979).
[7] Stettler, J. D., Bowden, C. M., Witriol, N. M., Eberly, J. H.: Phys. Lett. **73A**, 171 (1979).
[8] Agarwal, G. S., Jha, S. S.: J. Phys. **B12**, 2655 (1979).
[9] Hioe, F. T., Eberly, J. H.: Phys. Rev. Lett. **47**, 838 (1981).
[10] Chang, C. S., Schlier, R.: Phys. Rev. **A21**, 872 (1980).
[11] Kancheva, L., Pushkarov, D., Rashev, S.: J. Phys. **B14**, 573 (1981).
[12] Radmore, P. M., Knight, P. L.: J. Phys. **B15**, 561 (1982).
[13] Thomas, J. E., Hemmer, P. R., Ezekiel, S., Leiby, C. C., jr., Picard, R. H., Willis, C. R.: Phys. Rev. Lett. **48**, 867 (1982).

[14] Cardimona, D. A., Raymer, M. G., Stroud, C. R., jr.: J. Phys. **B15**, 55 (1982).
[15] Dalton, B. J., Knight, P. L.: Opt. Commun. **42**, 411 (1982).
[16] Dalton, B. J., Knight, P. L.: J. Phys. **B15**, 3997 (1982).
[17] Swain, S.: J. Phys. **B15**, 3405 (1982).
[18] Dalton, B. J., Knight, P. L.: Proc. 3rd New Zealand Symposium on Laser Physics (Walls, D. F., Harvey, J. D., eds.). Berlin-Heidelberg-New York: Springer 1983.
[19] Knight, P. L.: in: Coherence and Quantum Optics (Mandel, L., Wolf, E., eds.). New York: Plenum 1984.
[20] Kyrola, E.: to be published.
[21] Deng, Z.: Opt. Commun. **48**, 284 (1983).
[22] Radmore, P. M.: Phys. Rev. **A26**, 2252 (1982).
[23] Beutler, H.: Z. Physik **86**, 495 (1933); **93**, 177 (1935).
[24] Fano, U.: Phys. Rev. **124**, 1866 (1961).
[25] Armstrong, L., jr., Beers, B. L., Feneuille, S.: Phys. Rev. **A12**, 1903 (1975).
[26] See also Pert, G. J.: IEEE J. Qu. El. **QE8**, 623 (1972).
[27] Beers, B. L., Armstrong, L., jr.: Phys. Rev. **A12**, 2447 (1975).
[28] Armstrong, L., jr., Theodosiou, C. E., Wall, M. J.: Phys. Rev. **A18**, 2538 (1978).
[29] Coleman, P. E., Knight, P. L.: J. Phys. **B15**, L235 (1982); J. Phys. **B15**, 1957 (1982).
[30] Coleman, P. E., Knight, P. L., Burnett, K.: Opt. Commun. **42**, 171 (1982).
[31] Lambropoulos, P.: Appl. Opt. **19**, 3926 (1980).
[32] Lambropoulos, P., Zoller, P.: Phys. Rev. **A24**, 379 (1981).
[33] Rzazewski, K., Eberly, J. H.: Phys. Rev. Lett. **47**, 408 (1981).
[34] Greenland, P. T.: J. Phys. **B15**, 3191 (1982).
[35] Kim, Y. S., Lambropoulos, P.: Phys. Rev. Lett. **49**, 1698 (1982).
[36] Rzazewski, K., Eberly, J. H.: Phys. Rev. **A27**, 2026 (1983).
[37] Heller, Y. I., Lukinykh, V. F., Popov, A. K., Slabko, V. V.: Phys. Lett. **82A**, 4 (1981).
[38] Pavlov, L. I., Dimov, S. S., Metchkov, D. I., Mileva, G. M., Stamenov, K. V., Altshuller, G. B.: Phys. Lett. **89A**, 441 (1982).
[39] Dimov, S. S., Pavlov, L. I., Stamenov, K. V., Heller, Y. I., Popov, A. K.: Appl. Phys. **B30**, 35 (1983).
[40] Dimov, S. S., Pavlov, L. I., Stamenov, K. V., Altshuller, G. B.: Opt. and Quant. Elect. **15**, 305 (1983).
[41] Agarwal, G. S., Haan, S. L., Burnett, K., Cooper, J.: Phys. Rev. Lett. **48**, 1164 (1982).
[42] Eberly, J. H., Rzazewski, K., Agassi, D.: Phys. Rev. Lett. **49**, 693 (1982).
[43] Agarwal, G. S., Haan, S. L., Burnett, K., Cooper, J.: Phys. Rev. **A26**, 2277 (1982); Agassi, D., Rzazewski, K., Eberly, J. H.: Phys. Rev. **A28**, 3648 (1983).
[44] Agarwal, G. S., Agassi, D.: Phys. Rev. **A27**, 2254 (1983).
[45] Lewenstein, M., Haus, J. W., Rzazewski, K.: Phys. Rev. Lett. **50**, 417 (1983).
[46] Agarwal, G. S., Haan, S. L., Cooper, J.: Phys. Rev. (in press).
[47] Crance, M., Armstrong, L., jr.: J. Phys. **B15**, 3199 (1982).
[48] Haan, S. L., Agarwal, G. S.: in: Spectral Lineshapes, Vol. 2 (Burnett, K., ed.), p. 1013. Berlin: de Gruyter 1983.
[49] Haan, S. L., Cooper, J.: Phys. Rev. A (in press).

[50] Haus, J. W., Lewenstein, M., Rzazewski, K.: in press.
[51] Ben-Aryeh, A., Knight, P. L.: unpublished.
[52] Haus, J. W., Rzazewski, K., Eberly, J. H.: Opt. Commun. **46**, 191 (1983).
[53] Andryushin, A. I., Fedorov, M. V., Kazakov, A. E.: J. Phys. **B15**, 2851 (1982).
[54] Bialynicka-Birula, Z.: Phys. Rev. **A28**, 836 (1983).
[55] Bialynicka-Birula, Z.: J. Phys. **B16**, 4351 (1983).
[56] Javanainen, J.: J. Phys. **B16**, 1343 (1983).
[57] Alber, G., Zoller, P.: Phys. Rev. **A27**, 1373 (1983).
[58] Crance, M., Armstrong, L., jr.: J. Phys. **B15**, 4637 (1982).
[59] Agarwal, G. S.: Phys. Rev. **A18**, 1490 (1978).
[60] Dalton, B. J.: J. Phys. **A15**, 2157 (1982); ibid. **15**, 2177 (1982); J. Phys. **A15**, 553 (1982).
[61] Cohen-Tannoudji, C.: in: Frontiers in Laser Spectroscopy, Vol. 1 (Balian, R., Haroche, S., Liberman, S., eds.). Amsterdam: North-Holland 1977.
[62] Alber, G., Zoller, P.: Phys. Rev. **A27**, 1713 (1983).
[63] Radmore, P. M., Knight, P. L.: Phys. Lett. **102A**, 180 (1984).